Functionalisation of Biomaterials with Bone Sialoprotein for Joint and Bone Replacement

Dissertation
zur Erlangung des Grades

"Doktor der Naturwissenschaften"

im Promotionsfach Pharmazie

am Fachbereich Chemie, Pharmazie und Geowissenschaften
der Johannes Gutenberg-Universität
in Mainz

Anja Klein

Mainz, 2017

Dekan:

1. Gutachter:

2. Gutachter:

Datum der mündlichen Prüfung: 17. April 2018

What lies behind us and what lies before us
are tiny matters compared to what lies within us.

Ralph Waldo Emerson

Zusammenfassung

Biomaterialien werden im Bereich der Orthopädie und Unfallchirurgie unter anderem in Form von Endoprothesen, Osteosynthesematerialien oder als Knochenersatz eingesetzt. Mangelnde Osseointegration von Implantaten und die Suche nach einem adäquaten Ersatz für die als Goldstandard geltende autologe Knochentransplantation sind zentrale Herausforderungen, denen sich die Biomaterialforschung stellen muss. Das Extrazellularmatrixprotein Bone sialoprotein (BSP) spielt eine wichtige Rolle bei der Knochenbildung und Knochenmineralisation. Daher beschäftigt sich diese Arbeit mit der Prüfung der Möglichkeit der Biomaterialfunktionalisierung mit rekombinant hergestelltem BSP und anschließender Evaluierung dieser Materialien für den Knochen- beziehungsweise Gelenkersatz.

Zu Beginn wurde der Effekt von BSP auf murine bzw. humane Zellen einzeln, ohne Trägermaterial untersucht. Neben der Überprüfung auf Zytotoxizität wurde die Mineralisierungsfähigkeit und Alkalische Phosphatase Aktivität analysiert. Zentraler Bestandteil der Arbeit war die Etablierung einer BSP Beschichtung von drei verschiedenen Trägermaterialien - Titan, Calciumphosphat-Zement sowie Kollagen. Die BSP-Beschichtung wurde qualitativ (Fluoreszenzmikroskopie) und quantitativ (Röntgenphotoelektronenspektroskopie, Immunoassay) überprüft. Die biologischen Auswirkungen wurden anhand von Viabilitäts-, Morphologie-, Genexpressions- und Angiogenese-Untersuchungen mit primären humanen Osteoblasten respektive humanen Endothelzellen charakterisiert. Abschließend erfolgte die Evaluierung *in vivo* mit BSP beschichteten Calciumphosphat-Zementen an einem etablierten Maus Kalotten-Bohrlochdefektmodell (desmale Ossifikation) und einem Ratten Femurkondylen-Bohrlochdefektmodell (endochondrale Ossifikation).

Die Ergebnisse zeigen, dass BSP nicht zytotoxisch wirkt. Durch Zugabe von BSP wird die Aktivität der Alkalischen Phosphatase in den Knochenzellen und die Knochenmineralisierung gefördert. BSP kann erfolgreich an verschiedene Trägermaterialien gekoppelt werden. Nach Oberflächenaktivierung kann BSP sowohl adsorptiv als auch kovalent an Titan gekoppelt werden. Bei den Zementen zeigt die adsorptive Funktionalisierung bereits gute Ergebnisse. *In vitro* stellt sich der Einfluss auf die Genexpression von humanen Osteoblasten, insbesondere auf die Marker RUNX2 und SP7 nach 4 Tagen als zentraler Effekt heraus. Neben der Förderung der Genexpression führt die BSP-Zugabe zu vermehrten Zell-Aussprossungen im Angiogenese-Assay. Bei beiden *in vivo* Versuchen gibt es hinsichtlich der Menge an neu gebildeten Knochen keine signifikanten Unterschiede zwischen unbeschichteten und BSP beschichteten Materialien. Dennoch weist die Behandlung mit BSP-beschichteten Materialien tendenziell mehr Knochenwachstum auf im Vergleich zur Behandlung mit unbeschichteten Calciumphosphat-Zementen. Dieser Trend wird insbesondere durch histologische Färbungen bestätigt.

Insgesamt konnte gezeigt werden, dass BSP *in vitro* die Osteoblastendifferenzierung fördert, sowie einen angiogenesefördernden Effekt aufweist. Diese Effekte führten jedoch *in vivo* nur zu tendenziell verbesserter Knochenbildung. Die unzureichende Signifikanz *in vivo* wirft weitere Fragen auf, da bereits unbeschichtete Calciumphosphat-Zemente die Knochenbildung unter-

stützen. Dessen ungeachtet stellt die BSP Funktionalisierung aufgrund der aussichtsreichen *in vitro* Ergebnisse und histologischen Befunde für andere, nicht-osteoinduktive Materialien weiterhin eine Option dar. Diese sollte jedoch erst in weiteren Studien untersucht werden.

Abstract

In orthopaedics and trauma surgery, biomaterials are frequently applied as endoprostheses, osteosyntheses or bone substitutes. Lack of implant osseointegration and the search for a suitable alternative for the gold standard of autogenous bone grafting are main challenges in biomaterial research. In order to improve existing biomaterials, this work focuses on the approach of biomaterial functionalisation with the extracellular matrix (ECM) protein bone sialoprotein (BSP), which plays an important role during bone formation and mineralisation. The aim of this work was to evaluate biomaterial functionalisation with the recombinant manufactured BSP for bone and joint replacement.

First, the effect of BSP on cells was examined separately, without any carrier materials. Tests for cytotoxicity, mineralisation capability and alkaline phophatase activity were conducted in cell cultures. Moreover, the establishment of BSP functionalisation procedures for three different biomaterials - titanium, calcium phosphate cement (CPC) and collagen - was a central element of this work. BSP coatings were evaluated both qualitatively (fluorescence microscopy) and quantitatively (x-ray photoelectron spectroscopy, immuno assay). Biological effects on primary human osteoblasts and human endothelial cells were characterised by investigations of cell viability, cell morphology, gene expression and angiogenesis assays. Finally, a proof of concept was performed *in vivo* using an established calvarial defect model (desmal ossification) in mice and a femoral condyle defect model (endochondral ossification) in rats.

The results demonstrate that BSP is not cytotoxic and enhances mineralisation as well as alkaline phosphatase activity in cell cultures. BSP functionalisation has been achieved on different carrier materials. Physisorption or covalent coupling techniques via silanes are most promising for titanium. However, surface activation of titanium is required prior to any coating method. Physisorption has been shown to be an effective method for BSP coating of CPCs. *In vitro*, employing primary human osteoblasts, significant effects were observed after four days, mainly in gene marker expression of RUNX2 and SP7. Besides up-regulation of osteogenic markers, BSP functionalisation results in a significantly increased angiogenetic sprouting demonstrated in angiogenesis assays. *In vivo*, however, in both models, no significant differences have been observed in bone formation between BSP-coated and uncoated materials. Nevertheless, the implantation of BSP-coated materials displays a trend to enhance bone formation, which is supported by histological results.

In summary, BSP enhances osteogenic differentiation and angiogenesis *in vitro*. Those effects results *in vivo* only towards a trend of improved bone formation. These effects raise further questions as uncoated CPCs alone support bone formation. Nevertheless, due to promising *in vitro* and histological results, BSP functionalisation may be an option for refining non-osteoinductive biomaterials.

Contents

Abbreviations

ALP	alkaline phosphatase
AB	antibody
APTES	3-aminopropyltriethoxysilane
B2M	β-2-microglobulin
BACT	β-actin
BCIP	5-bromo-4-chloro-3-indolyl phosphate
BIC	bone-implant contact
BMP-7	bone morphogenetic protein-7
BSA	bovine serum albumin
BSP	bone sialoprotein
BV/TV	bone volume/total volume
C	carbon
CDHA	calcium deficient hydroxy apatite
CLSM	confocal laser scanning microscope
CHO	Chinese hamster ovary
Col1	collagen 1
CPC	calcium phosphate cement
CSD	critical size defect
CSL	cumulative sprouting length
DCP	dicalcium phosphate
DMEM	Dulbecco's modified eagle medium
DMSO	dimethylsulfoxide
EBM	endothelial cell basal medium
ECM	extracellular matrix
EDTA	ethylenediaminetetraacetic acid

ELISA enzyme-linked immunosorbent assay

EtOH ethanol

FCS foetal calf serum

FGF fibroblast growth factor

GA glutaraldehyde

GAPDH glyceraldehyde-3-phosphate dehydrogenase

GFP green fluorescent protein

HA hydroxyapatite

HMBS hydroxymethylbilane synthase

HE haematoxylin-eosin

hOB human osteoblast

HPRT-1 hypoxanthine phosphoribosyl-transferase 1

HRP horseradish peroxidase

HUVEC human umbilical vein endothelial cell

IHC immunohistochemistry

IPA isopropyl alcohol

KDR kinase insert domain receptor

MCAM melanoma cell adhesion molecule

MEM minimal essential medium

MGT Masson-Goldner trichrome

MSC mesenchymal stem cell

MTT 3-(4,5-dimethylthiazol-2-yl)-2,5-diphenyltetrazolium bromide

N nitrogen

NBT nitro blue tetrazolium

O oxygen

OPN osteopontin

PBS phosphate-buffered saline

PECAM	platelet endothelial cell adhesion molecule-1
PLGA	poly(lactic-co-glycolic) acid
pNP	p-nitrophenyl
pNPP	p-nitrophenylphosphate
PS	penicillin/streptomycin
PFA	paraformaldehyde
RNA	ribonucleic acid
ROI	region of interest
rpm	revolutions per minute
RUNX2	runt-related transcription factor-2
RT	reverse transcriptase
rt	room temperature
qPCR	real-time quantitative polymerase chain reaction
SEM	scanning-electron microscope
Si	silicon
SIBLING	small integrin-binding ligand N-linked glycoprotein
SPARC	osteonectin
SP7	osterix
T	Technovit®
TAE	TRIS - acetic acid - EDTA
TCP	tricalcium phosphate
Ti	titanium
TB	toluidine blue
TRIS	tris(hydroxymethyl)aminomethane
ULAP	ultra-low-attachment plate
VEGF	vascular endothelial growth factor
vWF	von Willebrand factor

XPS x-ray photoelectron spectroscopy

μCT micro-computed tomography

ZDBC zinc dibutyldithiocarbamate

ZDEC zinc diethyldithiocarbamate

1 Introduction

1.1 Biomaterials

The term *biomaterial* does not describe a living material, even if the word *bio* is derived from the Old Greek word *bios*, which means life. Indeed, the word describes the connection of a material with a living system. According to the International Union of Pure and Applied Chemistry (IUPAC), it is defined as a 'material exploited in contact with living tissues, organisms, or microorganisms' [1]. A more detailed definition was determined by the European Society of Biomaterials (ESB) during the 2nd ESB Consensus Conference 1991. They defined it as a:

> *Material intended to interface with biological systems to evaluate, treat, augment or replace any tissue, organ or function of the body* [2].

In this definition, the focus is more concentrated on the application of biomaterials. One main part is their medical use such as in stents, catheters, heart valves, hip and knee joints or dental implants [3]. A deeper look into biomaterials used in orthopaedics and trauma surgery as well as their requirements follows in the next section.

1.1.1 Biomaterials in orthopaedics and trauma surgery

In orthopaedics and trauma surgery, biomaterials are most commonly used for fixation and stabilisation in osteosyntheses as well as for bone or joint replacement. Over the last few years, the use of biomaterials has increased rapidly, as seen in Fig. 1.1. Particularly, the use of alloplastic materials for bone replacement has rapidly increased, the number of cases is more than 2.5-fold higher than 10 years earlier (2005: 8,539 vs. 2015: 22,389), along with only a slight increase in bone grafting (2005: 76,401 vs. 2015: 83,497). Therefore, the proportional amount of synthetic bone replacement materials has increased from 10.1 % to 20.1 % during this period. The number of cases of osteosyntheses has doubled during the same time (2005: 60,911 vs. 2015: 128,742). Moreover, there has been an increase in the number of cases of hip (2005: 194,453 vs. 2015: 227,293) and knee (2005: 128,932 vs. 2015: 173,304) endoprotheses. The number of revision surgeries (hip from 30,658 to 35,290; knee from 16,111 to 24,747) has further increased, notwithstanding new developments during the last few years [4]. With regard to an ageing society, the number of cases may rise further due to degenerative diseases such as arthritis, arthrosis or osteoporosis [5].

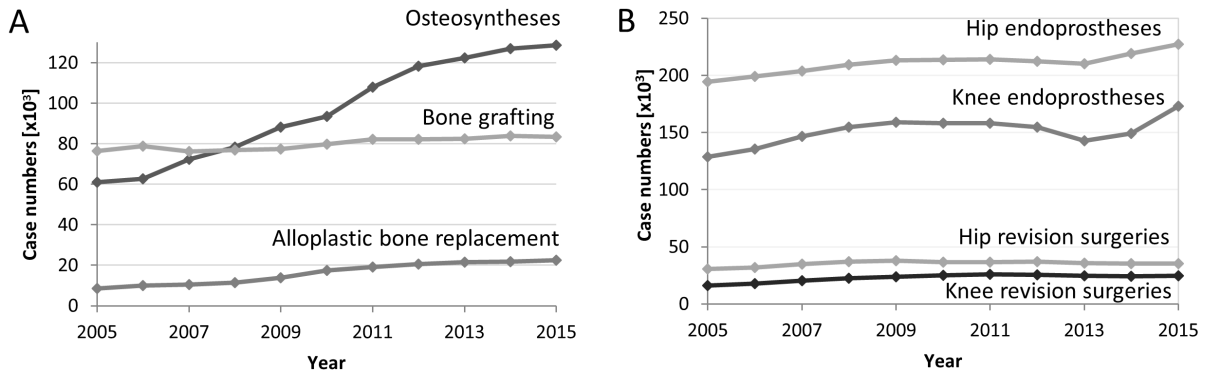

Fig. 1.1: Selected case numbers in orthopaedics and trauma surgery from 2005 to 2015 in Germany. A displays osteosyntheses, bone grafting and the use of alloplastic materials for bone replacement surgeries; B displays the development of hip and knee endoprostheses. The numbers were taken from the yearly DRG-report published by the Federal Statistical Office [4].

Complicated fractures frequently require stabilisation via nails, wires, screws or plates. However, those osteosyntheses are not sufficient in some cases. The treatment of large bone defects or non-unions, which occur after severe traumata, accidents or cancer, is still a challenge. Even autogenous bone grafts - the actual gold standard for the treatment of large-sized defects - have its limitations. Biological safety is more a problem of allogenic or xenogenic bone grafts. Main problems of the gold standard are donor-site morbidity and the need of a secondary operation. Other problems of bone grafts deal with size restriction. Suitable and large-sized bone grafts are often limited [6, 7, 8]. Biomaterials are one approach closing this gap. The increasing use of alloplastic materials during the last few years confirms the need for synthetic bone substitute materials. Requirements for these materials are more precisely explained in the next section. Besides the need for bone replacement due to severe trauma, the ageing society increasingly fights against loss of joint functions. Promising developments of joint prostheses began in the late 1950s with Charnley's total hip prostheses [9, 10]. At present, endoprostheses last ideally for 15 or more years. However, revision surgeries and implant failure occur due to inflammation processes, fibrous encapsulation or micro-motions. Low wear or corrosion resistance may lead to systemic reactions and hypersensitivity, low fracture toughness to mechanical failure or stress shielding effect [5]. Therefore, the main focus concentrates on enhancing osseointegration at the bone-implant interface, besides the choice of high-quality material characteristics [11]. The next section specifies the particular requirements for the application of biomaterials as endoprostheses or bone substitute materials.

1.1.2 Biomaterials: Classification and requirements

Biomaterials can be classified in several ways. According to their origin, they can be divided into biological or synthetical. From the perspective of materials, they are categorised into metals, ceramics, polymers or composites, which compose of a minimum of two different materials. A further possibility is classification by use (short-term use in contrast to long-term use) or behaviour (biostable versus biodegradable) [12, 13, 14, 15]. Their division into three

different generations takes place due to their biocompatibility. Bioinert materials belong to the first generation of biomaterials in contrast to bioactive or bioresorbable materials belonging to the second generation. In the third generation both, bioactive and bioresorbable properties are combined to achieve materials that activate cells or special functions [15, 16]. Even though the first generation was termed as bioinert, no biomaterial is really inert - it will ever cause a body reaction [3, 17]. Therefore, instead of bioinert, the term biocompatibility has become important as the main condition for biomaterials. It is, as defined by Williams, 'the ability of a material to perform with an appropriate host response in a specific application' [2] this means that the implant does not cause any toxic, inflammatory, immune or allergic reaction. Biocompatibility is further dependent on the site of implantation, function and implant size as well as implant duration [17, 18]. Requirements for biomaterials depend mainly on their further use or application. By way of example, a short-term implant must be bioinert, while the focus of long-term implants lie on osseointegration for endoprostheses as well as complete resorption for bone replacement materials. Therefore, the requirements are separately listed for both applications.

Mechanical properties play a decisive role for joint replacement materials. With regard to load-bearing applications, such materials have to be mechanically stable as well as corrosion and wear-resistant. Low corrosion- or wear-resistance can lead to debris that can accumulate and cause inflammation or allergic reactions. Further important properties concern the modulus, fatigue strength, bio-functionality and osseointegration. Any mismatch of bone and implant modulus can lead to irregular load transfer, followed by bone resorption and implant loosening in the long run - this is also described as stress shielding effect [19, 20]. Osseointegration, which 'means a direct [...] contact between living bone and implant' is one essential requirement for long-term applications [21]. Formation of fibrous tissue hinders osseointegration and leads frequently to implant failure. The property of osseointegration also plays a crucial role for bone substitute materials. Pore sizes between 100 and 200 µm are considered optimal for osseointegration [5]. Osteogenic, osteoinductive, osteoconductive and osteopromotive properties are essential biological characteristics for bone substitute materials. Osteogenic materials contain living bone cells for new bone formation, osteoconductive materials serve as support for cells to adhere, osteoinductive describes the ability to attract bone cells and induce differentiation and osteopromotive materials allow guided tissue regeneration. Bioresorbable or biodegradable bone substitutes are preferable. The long-term aim is the complete transformation of bone substitute materials into endogenous bone [22, 23]. A more detailed view of the properties of the three examples used in this work follows in the next section.

1.1.3 Titanium: A metallic biomaterial

One of the most used implant materials is titanium, particularly for dental implants, osteosyntheses or endoprostheses. The main advantage of metallic biomaterials is mechanical stability, which makes it suitable for load-bearing applications. Further representatives of metallic biomaterials are stainless steel, cobalt or magnesium and its alloys [24, 25]. Pure titanium,

Ti-6Al-4V and Ti-6Al-7Nb are most common for medical applications [14, 15]. Commercial pure titanium (CP Ti) exists in different grades dependent on their oxygen contents. For the following experiments, CP Ti grade 4 were used. Grade 4 includes the highest oxygen proportion (up to 0.4 %) and the best tensile as well as yield strength [3]. Besides its high strength, titanium is characterised by a low density, high corrosion-resistance, bioinertness and it is non-degradable. Biocompatibility of titanium is favoured by its ability of passive oxide layer formation [5, 20]. Nevertheless, implant failure happens mainly due to poor osseointegration, which leads to micro-motions and further to aseptic loosening. Surface modifications or coatings are an option for enhancing osseointegration [26, 27].

1.1.4 Calcium phosphates

Defined by their properties or manufacturing process, calcium phosphates are ordered into ceramics, sintered by high temperatures, or cements that harden during contact with liquids like body fluids [28, 29]. Besides calcium phosphate ceramics, there are ceramics based on aluminium and bioglass ceramics. Cements based on the polymer PMMA (poly(methyl methacrylate)) are most common used besides CPCs [25]. Calcium phosphates are bioactive as well as biodegradable. These properties are dependent on the Ca/P ratio, purity and crystalline structure [30]. Calcium phosphates are osteoconductive and, in some cases, also osteoinductive [31]. CPCs are composed of a CPC powder, which consists mainly of more than two distinct calcium phosphates, and a liquid solution. Even if there exist multiple calcium phosphates, the product after the setting reaction is either brushite (dicalcium phosphate dihydrate, DCPC) or apatite (hydroxyapatite (HA) or calcium deficient hydroxy apatite (CDHA)) [28, 30]. Due to the low setting temperatures, CPCs are suitable for drug delivery [32]. Moreover, the injectability of CPC pastes allow adaptablity to the defects size or they are printable with regard of modern technologies. 3D-printing allows the production of scaffolds with specified sizes and interconnecting pores [33]. Micro- and macro-porosity are crucial factors for tissue and implant interactions [24].

1.1.5 Collagen: A natural polymer

Collagen is not only the most frequent protein in humans [34], it is also a natural representative of the class of polymers. Besides natural polymers like gelatin, fibrin, hyaluronic acid, cellulose, pullulan or chitosan, there exist also synthetic representatives (polyethylene, polyvinylchloride, poly(lactic-co-glycolic) acid (PLGA), ...) [25]. Collagen is biocompatible, biodegradable and it has low immunogenicity [35]. Moreover, it is an ideal host for drugs, proteins or nanoparticles. Modifications via crosslinking influence biodegradability and make collagen an applicable drug delivery system [35, 36]. Owing to its superior cell compatibility, collagen is a versatile tool for *in vitro* studies of cell adhesion, growth, differentiation or migration, cell-cell interactions and for evaluation of angiogenetic potential [34, 35]. Collagen has high tensile strength, but only weak mechanical strength - this limits certain applications (e.g. load-bearing applications).

Nevertheless, wound healing, bone regeneration, ophthalmics and pharma are a few examples of the numerous fields where collagen has become an integral part [37, 38, 39].

1.2 Functionalisation of biomaterials

In biomaterial research, surface functionalisation attracted a lot of greater attention in the last few decades along with the focus on the materials. Implant integration with the surrounding bone is pivotal for the success of implantation [5].

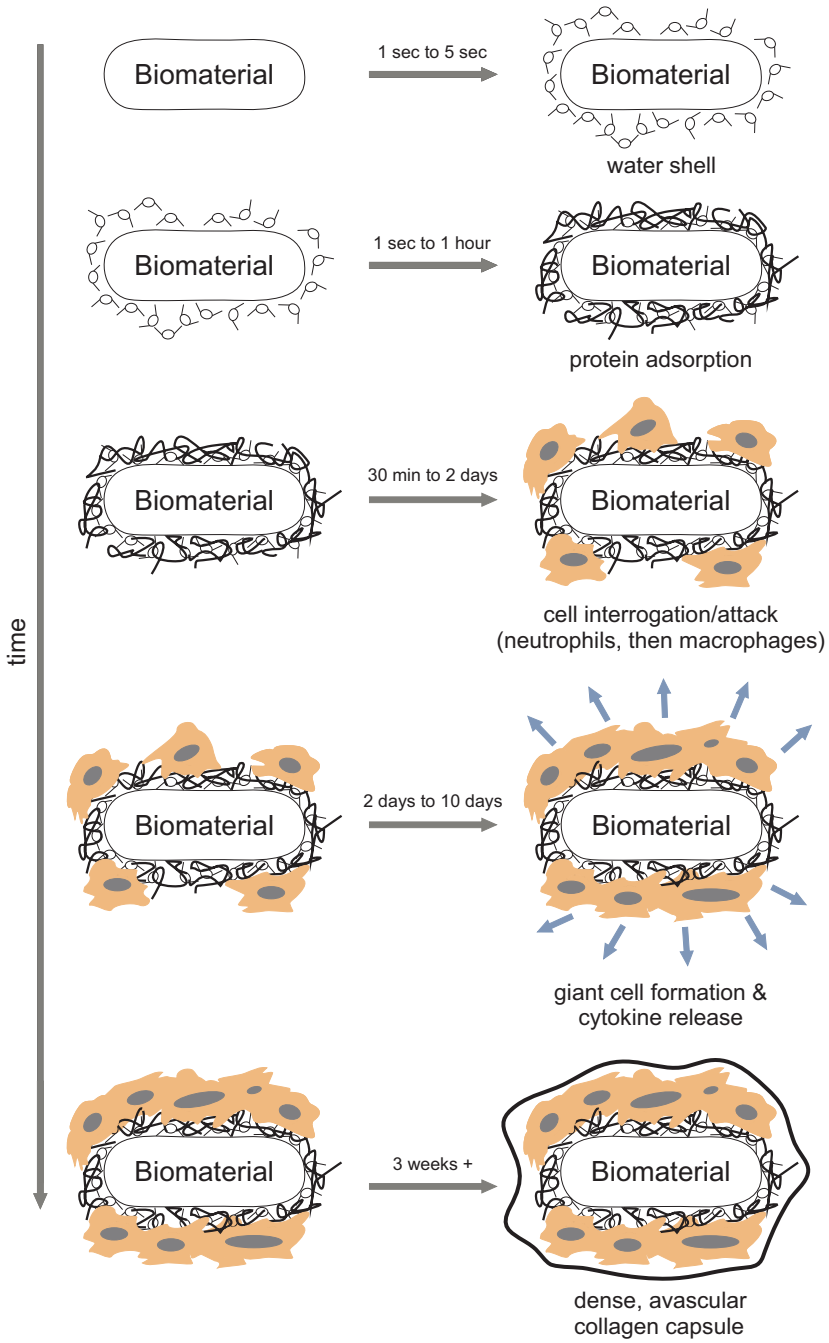

Fig. 1.2: Overview of the body reaction after implantation. Accumulation of water and proteins attracts cell attachment. Adheared cells form networks and release cytokines. Formation of a fibrous capsule due to inadequate implant integration might resulting in later complications. The figure was created with Corel Draw according to Ratner et al. [3].

Instead of creating new materials, the approach of biomaterial functionalisation is based on the modification of proven materials. Regarding the three different generations of biomaterials, the aim is to create bioactive materials with special functions [40]. Prior to any modification procedure, it is recommended that biomaterial and tissue interactions be explained in detail (Fig. 1.2). The first stage after implantation is the contact with water molecules, which envelope the implant and build a water shell whithin seconds. This step is followed by protein adsorption from blood or the surrounding tissue - this occurs within the first few hours [3, 40, 41]. However, the initially adsorbed proteins can desorb as well. Smaller adsorbed proteins can frequently be replaced by larger proteins with a higher surface affinity. This *surface enrichment* is also termed as the *Vroman effect* [40, 42, 43]. Cell-surface interactions are determined by the protein composition. The cells adhere, migrate and differentiate; moreover, they send signals to surrounding tissues. In an ideal case, the biomaterial is in direct contact with the living tissue. But, most commonly, the implant is surrounded by fibrous tissue, which needs to be prevented, among others, via biomaterial functionalisation [3, 17]. Numerous options exist to modify surfaces via mechanical (grinding, blasting, ...), chemical (acidic treatment, biochemical via covalent coupling, ...) or physical (plasma treatment) procedures [11, 17, 44]. Here the focus is on biomaterial functionalisation with bioactive molecules - this can be achieved via physical (adsorption, entrapment) and chemical (covalent bonding) modifications (see Fig. 1.3) [45].

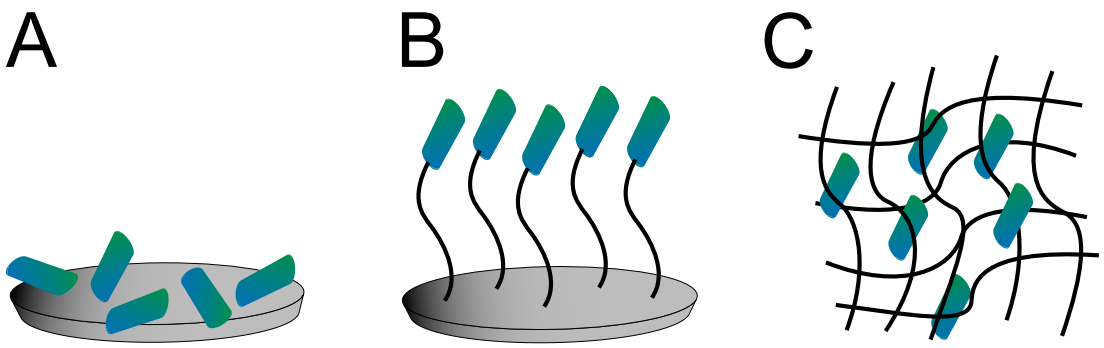

Fig. 1.3: Strategies for biomaterial functionalisation. A - Adsorption, B - Covalent bonding, C - Entrapment. The figure was created with Corel Draw according to Maia et al. [45].

Adsorption or physisorption is a simple coating method. The material is dipped into or coated with a solution containing the bioactive molecule. However, besides adsorption processes, there also exist desorption processes. Together with this uncontrolled release, which may result in undesired side-effects, there cannot be a control regarding the arrangement of molecules [46, 47, 48]. Molecule immobilisation via covalent coupling techniques is a method to influence the orientation of molecules at the surface. Several studies have postulated a similar protein activity after coupling compared to the activity of soluble forms [49, 50, 51]. The protein is tightly bound to the surface and therefore no protein release will occur. Functional groups - e.g. hydroxyl groups of the titanium oxide layer - serve as foundation for coupling of selected linkers (glutaraldehyde, carbodiimide, silanes, ...); this in turn, facilitates protein coupling

via the proteins' amino- or carboxy group [45, 40]. Protein entrapment during the process of preparation is a suitable method for collagen gels or ink formulations for 3D-printing. A uniform protein distribution and a release dependent on the tissue-material interaction are advantages of this method [46, 52].

1.3 Bone sialoprotein

Bone is a composite of the ECM and bone cells. Bone cells include osteoblasts, osteoclasts, bone lining cells and osteocytes [53].
The extracellular matrix consists of an organic and an inorganic phase. The inorganic phase comprises mainly calcium and hydroxyapatite, while collagen I, proteoglycans and non-collagenous proteins, such as bone sialoprotein, ostocalcin, osteonectin, thrombospondin and osteopontin belong to the organic phase [53, 54].
Bone sialoprotein is expressed by osteoblasts, osteocytes, osteoclasts, odontoblasts, cementoblasts or hypertropic cartilage cells [55, 56]. This protein belongs, besides osteopontin and dentin-sialoprotein, to the small integrin-binding ligand N-linked glycoprotein (SIBLING) family. As expressed in their name, they interact with integrins over a special motif. The combination of the three aminoacids - arginine, glycine and aspartic acid, better known as the RGD-motif, is responsible for integrin binding and several effects like cell adhesion and cell differentiation [56, 57, 58, 59]. Besides the RGD-motif, the BSP structure contains tyrosine-rich regions, which effects cell adhesion [55], a collagen-binding sequence and glutamine acid regions [55]. Fig. 1.4 displays the BSP structure more clearly.

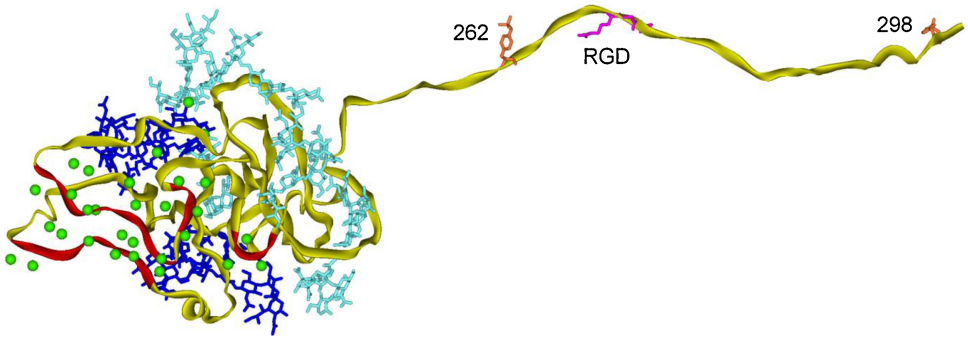

Fig. 1.4: Model of bone sialoprotein. Reprinted from Vincent et al. [55] with permission from Elsevier.

BSP effects osteoblast differentiation via integrin ($\alpha_v\beta_3$) interaction [56, 57, 59, 60]. Being bind to this receptor leads to the activation of the MAPK (mitogen-activated protein kinase) pathway. Downstream, the extracellular-signal regulated kinase ERK will be activated - this, in turn effects expression of AP-1, osterix (SP7) and runt-related transcription factor-2 (RUNX2) [61, 62]. An overview of this process is presented in Fig. 1.5.

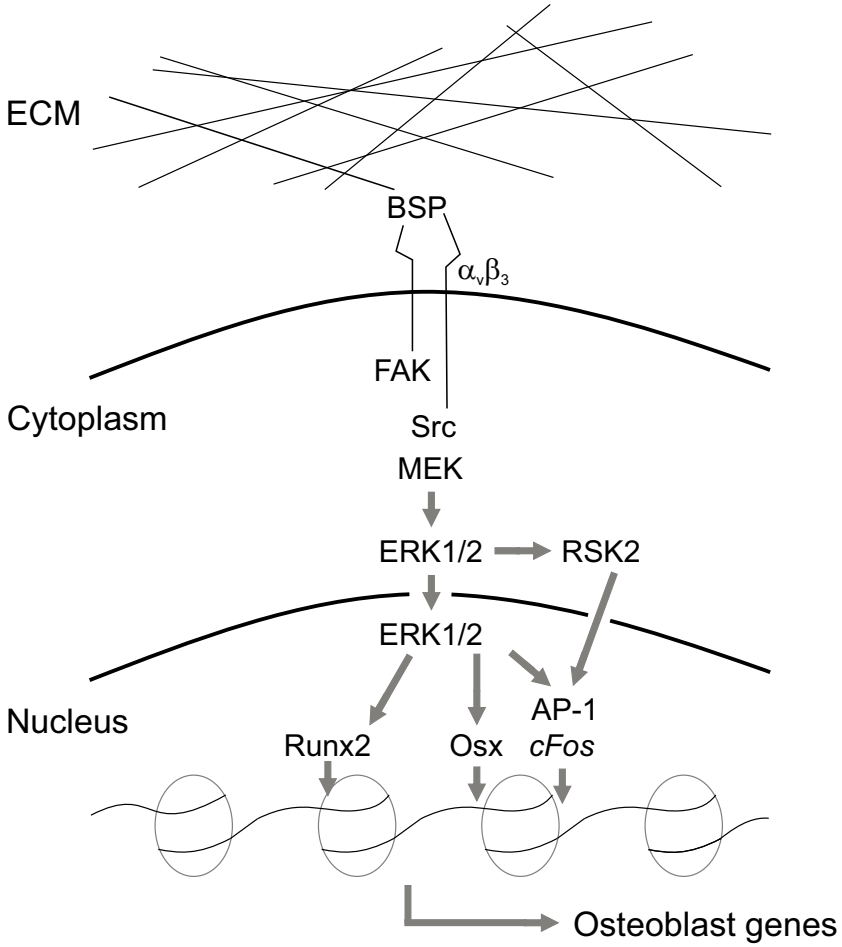

Fig. 1.5: BSP binding to integrin receptors activates the MAPK-pathway and affects the transcription factors Runx2, Osx/SP7 and AP-1. FAK - focal adhesion kinase, MEK - mitogen-activated protein kinase kinase, ERK1/2 - extracellular-regulated kinase, RSK2 - ribosomal S6 kinase. The figure was created with Corel Draw according to Gordon et al. [61].

BSP plays further a decisive role in HA nucleation [63, 64]. The importance of BSP becomes apparent in case of BSP deficiency. Lack of BSP (e.g. BSP knockout) impairs bone formation processes. This resulted in shorter as well as hypomineralised bones [65, 66, 67, 68]. All those functions make BSP an ideal candidate for biomaterial functionalisation.

1.4 Investigation models for bone regeneration

Bone regeneration is a very complex process with multiple factors involved [69, 70, 71, 72]. Therefore, *in vivo* tests are mandatory. Nevertheless, prior *in vitro* tests are valuable to gain a first impression of cytocompatibility as well as further effects.

1.4.1 *In vitro* models

For evaluation of biomaterials or substances with regard to bone regeneration, several *in vitro* tests are ready for selection. A main standard test is the MTT assay for cytotoxicity determination. This routine test is precisely regulated in DIN ISO norm 10993 for the biological

evaluation of medical devices. Examinations concerning osteogenic characteristics play, besides cytotoxicity, a decisive role. Osteogenic activity is mainly examined due to the alkaline phosphatase activity, mineralisation capability or gene expression profiles of bone-specific markers. Further issues relating to the determination of material-cell interactions concentrate on proliferation, morphology, adhesion, migration or angiogenesis [73, 74]. Apart from specific tests, the choice of adequate osteoblastic cells is a main factor. The choice is between primary cells from different species or cell lines. Each of these has their own advantages and disadvantages. Osteoblastic cell lines, much like SaOs-cells, MG-63 or MC3T3-E1, are immortal; the number of cells is unlimited and no complex isolation procedure is required. Moreover, their phenotype is mainly homogenous and there are no interspecies differences for human osteoblastic cell lines. However, cell-lines do not represent the whole range of osteoblastic phenotypes. For this purpose, primary human osteoblasts (hOBs) have been selected for the *in vitro* examinations. Cell isolation occurred out of bone specimens acquired during surgery. Even if their accessibility is limited and despite heterogeneous phenotypes, they are the first choice. They reflect the whole osteoblastic characteristics and the results are more relevant for translation into clinical processes [75, 76, 77, 78, 79, 80].

The development from pre-osteoblasts to mature osteoblasts lies in the focus of *in vitro* examinations. Fig. 1.6 displays the osteoblastic development from stem cells up to osteocytes. Numerous studies have performed their experiments with preliminary stages, mostly with mesenchymal stem cells (MSCs), to test whether their transformation into pre-osteoblasts and mature osteoblasts can be accelerated [81].

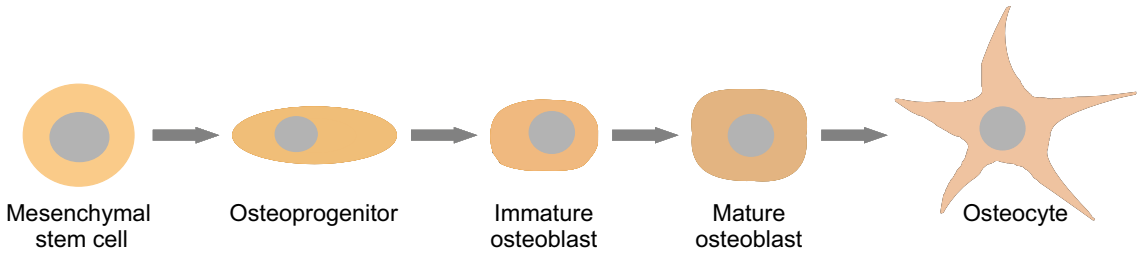

Fig. 1.6: Different stages of osteoblast development. The figure was created with Corel Draw according to Wu et al. [82].

Enhancement or support of osteoblast differentiation for bone regeneration is only one part. Most implants fail due to lack of vascularisation and therefore their effects on endothelial cells and angiogenesis will be evaluated as well. Collagen gels serve as an ideal matrix for three-dimensional experiments. Besides assisting in cell-cell-interactions, they facilitate tube formation out of cell spheroids for determining any angiogenic potential [74, 83, 84] . That is why human umbilical vein endothelial cells (HUVECs) have been examined in mono- as well as co-culture conditions with hOBs.

Several osteoblastic and endothelial genes are in the focus of gene expression analyses. Important factors for osteoblast differentiation are runt-related transcription factor-2 (RUNX2) as well as osterix (SP7); they are also known as master genes for osteoblast differentiation

[85]. Osterix acts downstream from RUNX2 and inhibits chondrogenesis, but promotes osteogenesis [86, 87, 88, 89, 90, 91]. Alkaline phosphatase (ALP) is an early osteoblast differentiation marker - it increases the local concentration of phosphate ions which, in turn, initiates mineral growth [92]. Another member of the small integrin-binding ligand N-linked glycoprotein (SIBLING) family is osteopontin (OPN), which acts as an inhibitor towards irregular formulation of mineral crystals [93]. The collagen 1 (Col1) expression is high in the initial phase and decreases during the later phase [94]. Glycoprotein osteonectin (SPARC) initiates the mineralisation processes. SPARC is expressed uniformly, except for its rise in the differentiation and mineralisation phase [95]. As endothelial markers serve adhesion molecules, such as platelet endothelial cell adhesion molecule-1 (PECAM) and melanoma cell adhesion molecule (MCAM), the von Willebrand factor (vWF) and kinase insert domain receptor (KDR), which is also known as vascular endothelial growth factor (VEGF) receptor 2.

1.4.2 *In vivo* models

Even if *in vitro* experiments can gain indications for effects on cytocompatibility and cell behaviour (proliferation, adhesion, migration, differentiation) as well as for determining angiogenic potential in more complex three-dimensional environments, they are limited compared to physiological conditions *in vivo*.

There exist numerous *in vivo* models for bone regeneration and evaluation of biomaterial-bone interactions [96, 97]. In general, they are categorised into heterotopic and orthotopic models. This classification takes place on the basis of their proximity to endogenous bone tissue. In case of heterotopic models, biomaterials are implanted or injected into subcutaneous, intramuscular or intraperitoneal pouches to assess biocompatibility and osteoinductive potential. By contrast, intraosseous defects have the benefit to reflect on physiological processes and therefore orthotopic models are more translational. The calvarial model is a standard model for testing whether biomaterials facilitate bone regeneration [97, 98, 99]. This model focuses on desmal ossification, where MSCs are differentiated into osteoblasts for direct bone formation [100]. Calvarial models are frequently associated with the term *critical size defect*. This is a defect defined as 'an orthotopic defect that will not heal without intervention'. This definition has been adjusted from the classical description, where a placed defect will not heal during the animal's lifetime. At present, the size is evaluated due to determined endpoints [98, 101]. Common critical-defect sizes for rodents are 5 mm for mice and 8 mm for rats [102]. Here two 2.7 mm defects were placed in mice calvaria. This size had earlier been evaluated by Jens Hertweck [103, 104] and Marc Eberhardt (publication in progress). The calvarial model is reproducible and a versatile tool for screening and material evaluation [98, 101, 102]. Nevertheless, it is a non-load bearing model [99] and thus, the femoral condyle defect model has been chosen additionally. Apart from load bearing, this model reflects another way of ossification. By endochondral ossification, MSCs convert into chondrocytes, which can be differentiated into a non-proliferative hypertrophic state. Subsequently, osteoblast progenitors, osteoclasts, endothelial cells and hematopoietic cells infiltrate the cartilage, followed by resorption of car-

tilage and formation of bone [100, 105, 106, 107]. Both models, taken together, can provide a comprehensive overview of the effects of BSP-functionalised materials on bone regeneration. For the choice of a suitable animal model, the individual characteristics of the animal should be considered [108]. Even though larger animal models, such as rabbit, sheep or pig, are closer to humans in terms of physiology, rodents are often chosen for research purposes. Mice and rats are suitable and reproducible animal models in short term for screening and evaluation experiments [99].

2 Aim of This Work

The aim of this work was to evaluate BSP-functionalised biomaterials for applications in orthopaedics and trauma surgery. Several experiments - *in vitro* as well as *in vivo* - were conducted to determine the effect of BSP-coating. A short overview in Fig. 2.1 summarises the different parts of this work.

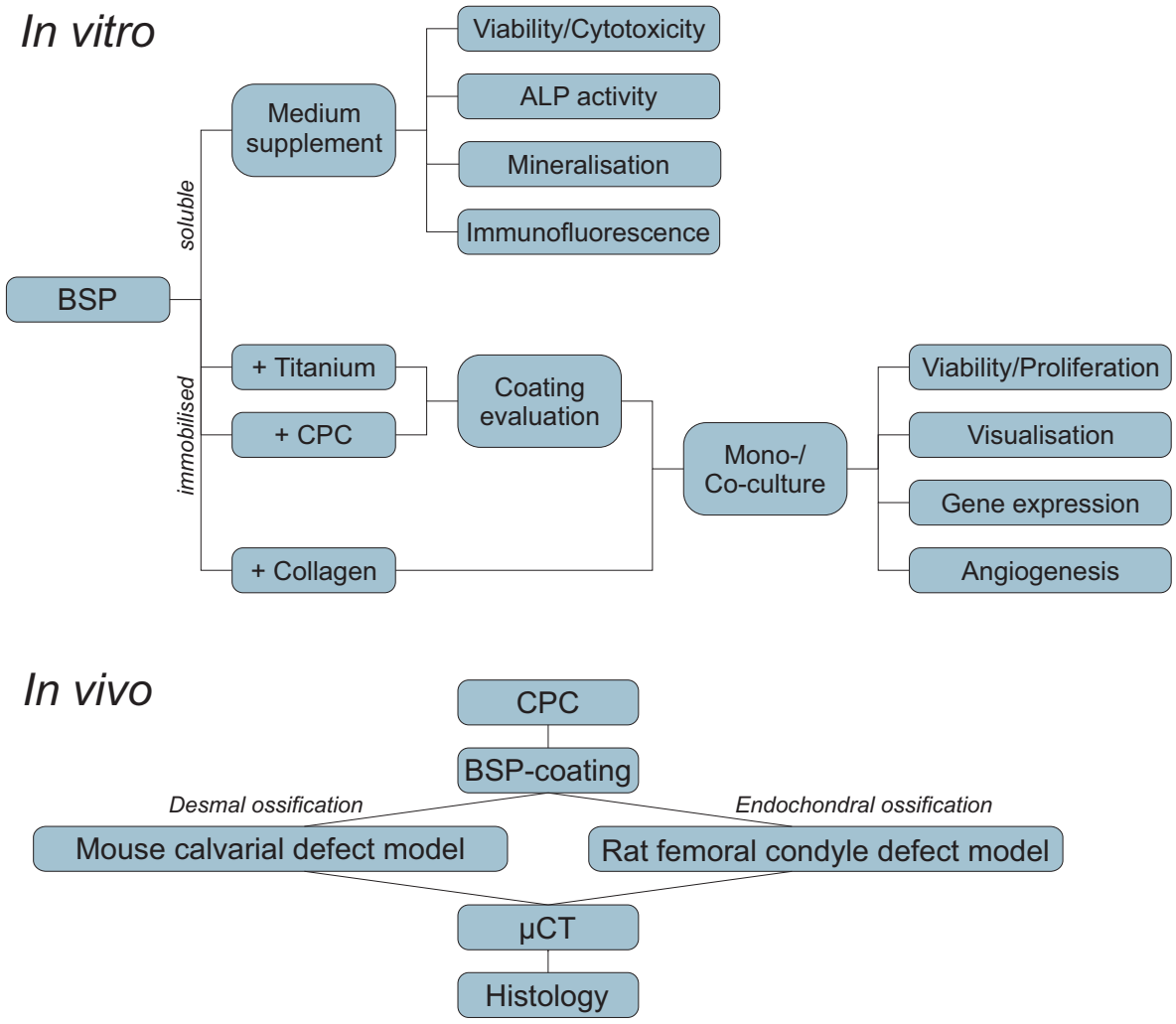

Fig. 2.1: Experimental overview.

First, the recombinant manufactured BSP has to be analysed to exclude cytotoxic reactions and screen out the BSP effect on osteoblast differentiation verified via ALP activity, mineralisation capability and immunfluorescence staining. Further, *in vitro* experiments focus on BSP-functionalisation of three different biomaterials - titanium, calcium phosphate cements and collagen. It is supposed to establish a suitable and reproducible coating method for titanium and CPCs. Experiments with primary human osteoblasts with special attention on cell viability, visualisation and differentiation will follow to evaluate different coating methods. For collagen gels, no extra coating method is required due to the direct addition of BSP during gel preparation. The objective of collagen gel puts the focus on cell-cell interactions due to

co-culturing of osteoblasts with endothelial cells and to determine BSP effects on angiogenesis - this is an essential step for vascularisation and integration of biomaterials. Building on this, two different animal experiments will serve as proof of concept. Each experimental model reflects a different ossification way: the calvarial defect model works as a model for desmal ossification and the femoral borehole defect model for endochondral ossification. On the basis of the results, the osteogenic role of BSP will be defined.

3 Materials and Methods

3.1 Materials

Titanium discs

Titanium discs (pure Grade IV) were kindly provided by Medartis® Company (Basel, Switzerland). The various sizes are displayed in Fig. 3.1 A.

Calcium phosphate cements

In *in vitro* as well as *in vivo* experiments, 3D-printed calcium phosphate cements (CPCs) were used. This enabled the production of scaffolds with different sizes and varying porosities (see Fig. 3.1 B). Compact discs without pores were used *in vitro* (B - 1, 2). This is in contrast to *in vivo* experiments where scaffolds with interconnecting pores were employed (B - 3, 4). The CPCs were manufactured by Innotere (Radebeul, Germany). A paste of CPC-powder (eight parts) and carrier liquid (two parts) was used for printing. The CPC-powder is composed of 60 % α - tricalcium phosphate (TCP), 26 % dicalcium phosphate (DCP) anhydride, 10 % calcium carbonate and 4 % precipitated HA [109, 110].

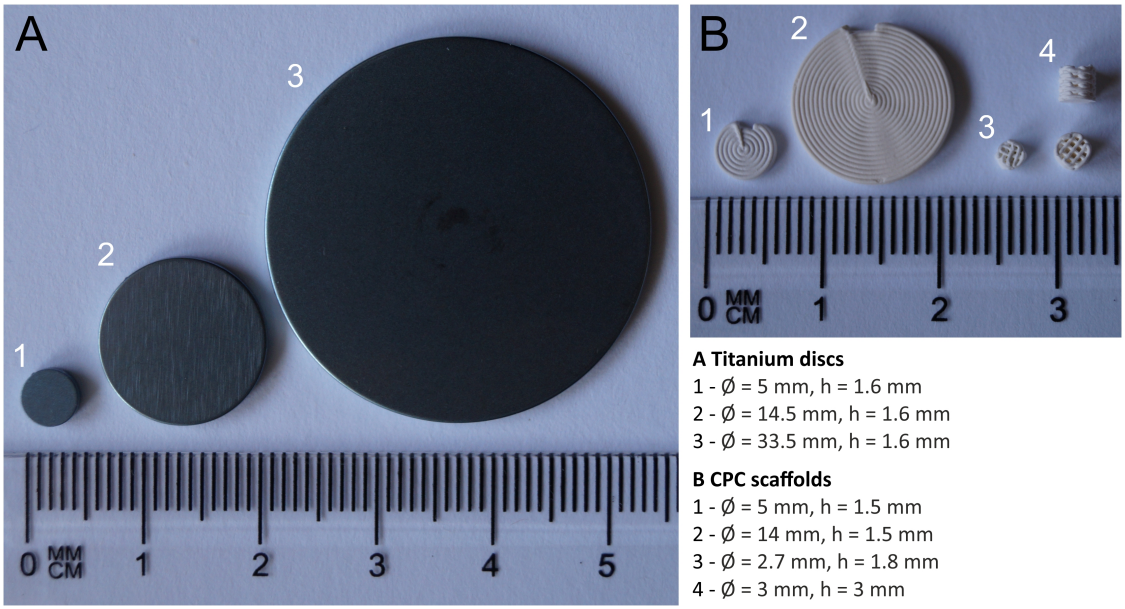

Fig. 3.1: Overview of titanium discs (A) and CPC scaffolds (B) used in the experiments.

Bone sialoprotein

Human recombinant BSP, produced by the stable Chinese hamster ovary (CHO) cell line, was provided by Immundiagnostik AG (Bensheim, Germany).

All other used materials, devices and programmes are listed in Appendix 5.

3.2 Coating methods and experimental verification

For titanium discs, a short overview of the BSP-coating process and further procedure is shown in Fig. 3.2.

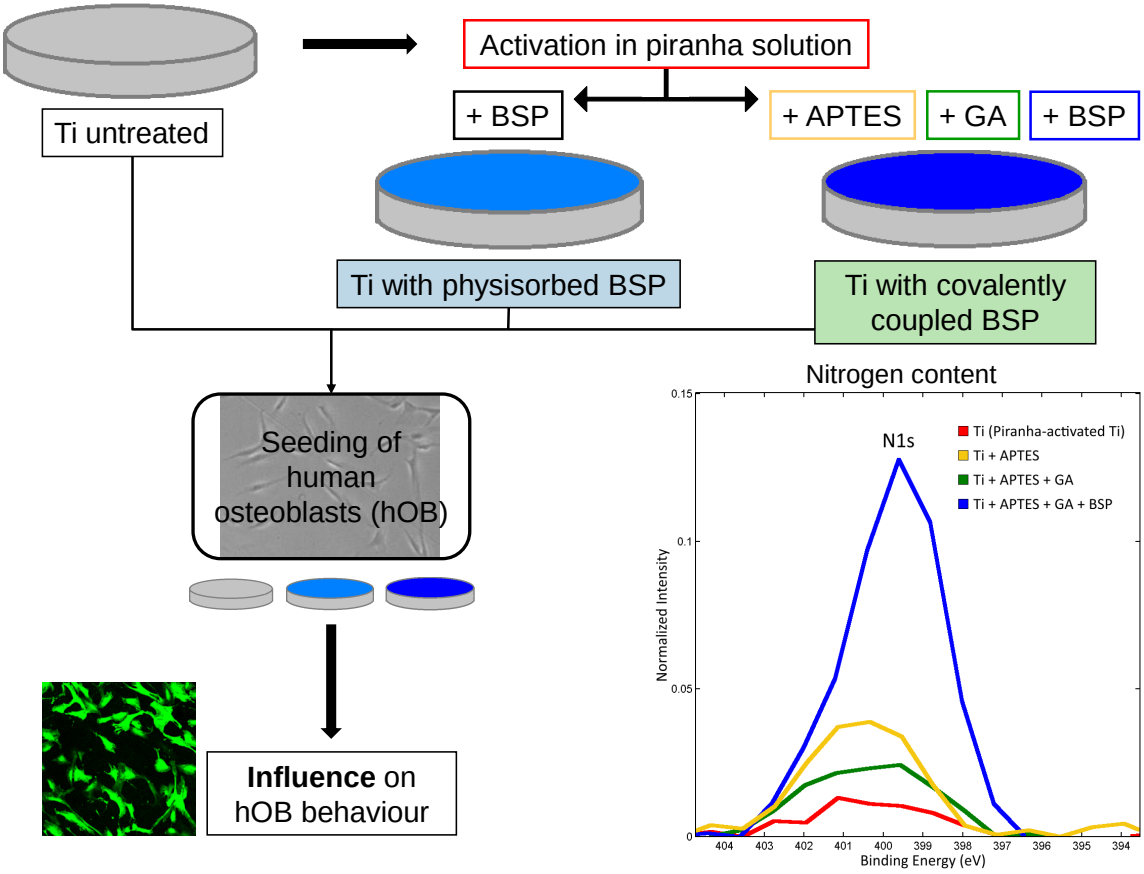

Fig. 3.2: Overview of the titanium coupling process with BSP and further procedure.

3.2.1 Surface activation with piranha solution

Prior to covalent coupling and physisorption processes, the titanium surfaces were activated overnight in piranha solution (a mixture of one part 30 % hydrogen peroxide (H_2O_2) and four parts concentrated sulfuric acid (H_2SO_4)). Next, the discs were washed with sterile water.

3.2.2 Covalent coupling via silane linkers

For covalent coupling, three steps are required: a) addition of a coupling agent to the titanium surfaces (see Fig. 3.3, A), b) linker coupling (see Fig. 3.3, B) and c) linking of the desired protein (see Fig. 3.3, C).

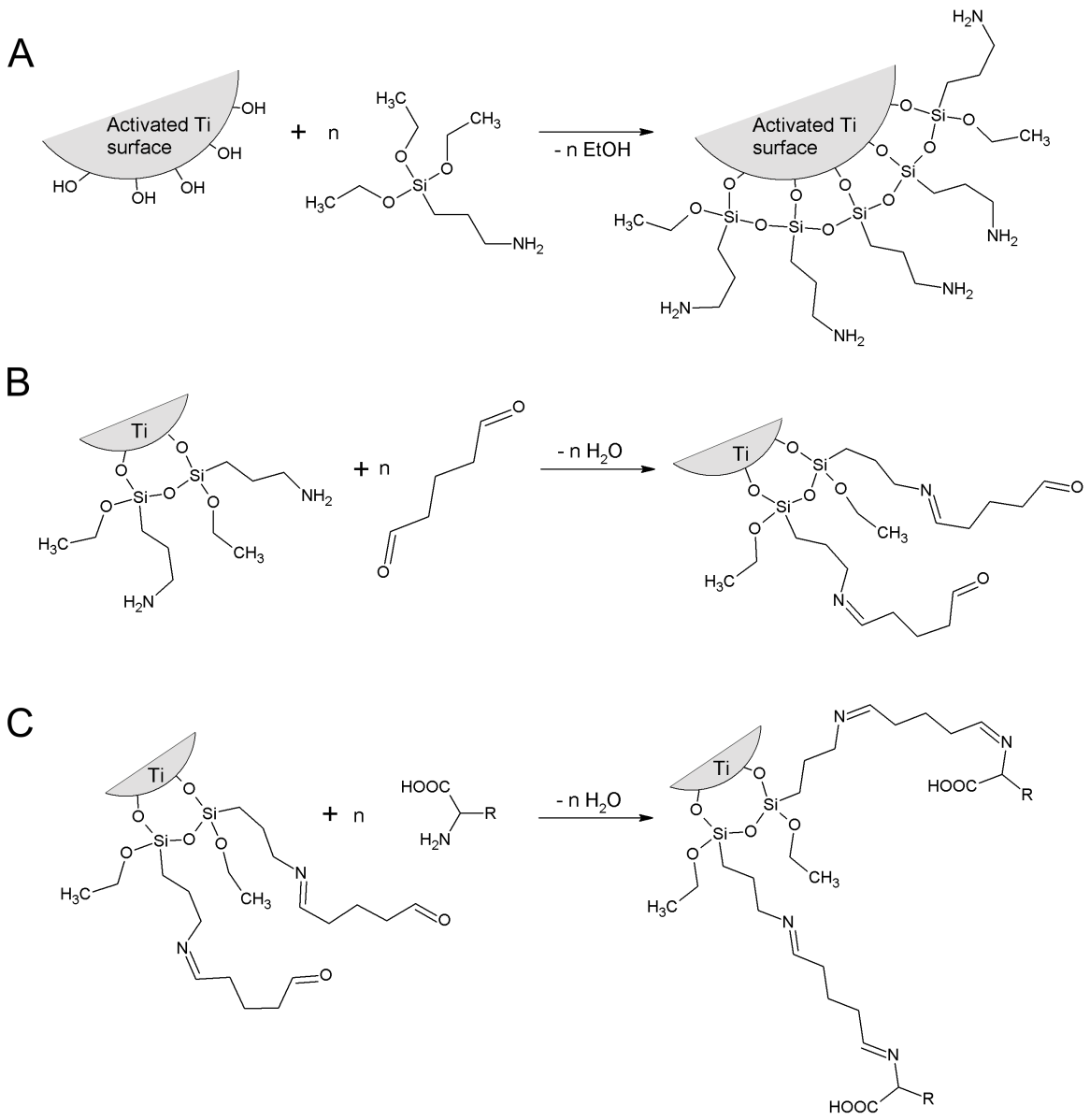

Fig. 3.3: Covalent coupling process: A - Silanisation of the titanium surface with APTES, B - Addition of the linker glutaraldehyde, C - Final step with protein (e.g. BSP) coupling. The chemical structures were drawn with ChemSketch according to Dettin et al. [111]. Part A was first published in PlosONE [112].

Aminosilanes, particularly 3-aminopropyltriethoxysilane (APTES), are often used as coupling agents to bind proteins on various surfaces. For coupling APTES to a surface, an incubation step for 30 min in 1 % APTES solution in water is required. Prior to this step, the polymerisation ability of APTES was tested with 1 N NaOH. NaOH was added to the fresh prepared 1 % APTES solution, followed by incubation for 20 min under mechanical stirring. Thereafter, the building of small silane polymers was controlled and the solution was filtered with a 0.22 µm filter. Then, with the filtered APTES solution the 30 min incubation step started, followed by cleaning with sterile water. This step is followed by incubation with 5 % glutaraldehyde (GA) solution in phosphate-buffered saline (PBS) for 1 h. GA acts as linker between the aminosilane and the protein. After another washing step with water, incubation with BSP solution is fol-

lowed for 1 h. In PBS diluted BSP solutions with different concentrations (30 µg/ml, 50 µg/ml, 150 µg/ml and 280 µg/ml) were used for coupling. Subsequent to the coupling processes, the discs were washed two times with PBS and stored in PBS until cell seeding.

3.2.3 Coating via physisorption

Titanium discs
Physisorption without surface activation led to unsatisfactory results in pilot experiments (data not shown). Consequently, it was necessary to activate the surface with piranha solution, followed by a rinsing step in water and incubation in BSP solution for 1 h.

CPC scaffolds
CPC scaffolds were incubated in Dulbecco's modified eagle medium (DMEM)/F-12 medium (no supplements) at 37 °C for 24 hours. After two washing steps with PBS, incubation with PBS diluted BSP solutions (25 µg/ml, 50 µg/ml, 100 µg/ml and 200 µg/ml BSP or only PBS) for 24 hours at 8 °C under continuous shaking were followed. Finally, after two washing steps with PBS, the scaffolds were stored temporarily in PBS until cell seeding or in case of *in vivo* experiments they were dried under laminar air flow, transferred into a 24-well plate and stored at 8 °C until scaffold implantation.

3.2.4 Verification of material coating

Surface analysis with x-ray photoelectron spectroscopy (XPS)
X-ray treatment of samples (e.g. titanium) results in ejection of photoelectrons. The kinetic energy of these photoelectrons is measured with a detector. Due to the relation between kinetic energy and atomic binding energy, conclusions can be drawn about the elemental composition of outer surface layers [113]. For XPS measurements, the titanium discs were rinsed with sterile water instead of PBS. Titanium samples from every intermediate step of the coating process were taken for measurements. The elemental composition of the surface (focusing on nitrogen (N), carbon (C), oxygen (O) and silicon (Si)) was analysed using the PHI 5600-CI XPS system.

Enzyme-linked immunosorbent assay (ELISA)
BSP coating was quantified by measuring the free BSP amount after several washing steps using a BSP-ELISA. After BSP coating with 25 µl solution / titanium implant (ø 14.5 mm; covalent or coating via physisorption) or 250 µl BSP solution / CPC disc (ø 14 mm), no final washing steps were performed. The solutions were changed at 0 h, 1 h, 2 h, 24 h, 48 h and 72 h for titanium samples and at 0 min, 1 h, 2 h, 4 h, 12 h, 24 h and 48 h for CPC discs. Fresh PBS solution (250 µl) was added to the samples. The used solutions were transferred to Eppendorf vessels and stored at 8 °C until the ELISA assay was performed according to the manufacturer's instructions.

Qualitative analysis of BSP coating with fluorescein

The efficacy of BSP physisorption was analysed qualitatively by fluorescence microscopy after linking fluorescein to BSP (Fig. 3.4).

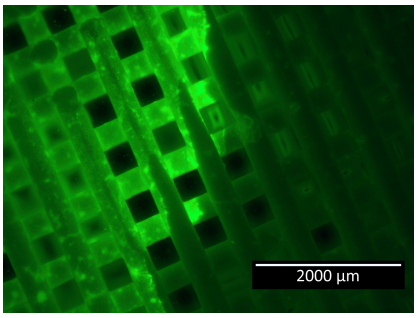

Fig. 3.4: Unilateral BSP coating of CPC. BSP was linked to fluorescein prior to the coating procedure.

For linking BSP to fluorescein, a free carboxy group (−COOH) is required. Therefore, this method is only possible for BSP physisorption.

Fluorescein was linked to BSP using a Lightnink-Link® conjugation system according to the manufacturer's instructions. In brief, 540 µl BSP solution (stock solution: 280 µg/ml) was mixed with 54 µl LL-Modifier and then transferred to LL-Fluorescein. After an incubation period of minimum 3 h, 54 µl LL-Quencher was added. As described above, titanium discs or CPC scaffolds were coated with this fluorescein-marked BSP solution. Two washing steps followed the physisorption process to remove unbound fluorescein-coupled BSP. Fluorescence microscopy was used to visualise remained to the surface-bound fluorescein-coupled BSP.

3.3 Cell culture

3.3.1 General cell culture conditions

All experiments were performed under laminar air flow. For ensuring aseptic conditions, all materials and solutions were either bought sterile from the manufacturer (e.g. consumables, cell media), autoclaved by 121 °C for 20 min (e.g. instruments), heat-sterilised by 180 °C for 2 h (e.g. Pasteur pipettes, glass equipment) or sterile-filtered with a 22 µm filter (e.g. prepared solutions, in case autoclaving was impossible).

3.3.2 Isolation of primary human osteoblasts

Primary hOBs were isolated according to a previously described protocol [114, 115]. Human bone specimens were obtained during hip or knee joint replacement surgeries. The use of residual materials was approved by the ethics committee of the Landesärztekammer Rheinland-Pfalz in accordance with the principles expressed in the Declaration of Helsinki and the ICH Guidelines for GCP. All patients provided written consent.

Cancellous bone fragments were removed with bone rongeurs from bone specimens (Fig. 3.5 B, C, D). The isolated fragments were washed several times with PBS (E, F) until a clear supernatant was achieved (G). The supernatant was discarded and 15 ml collagenase type I solution (1 mg/ml in medium 199; H, I) were added. Collagenase digestion was carried out under mechanical stirring in a water bath at 37 °C (J). After 45 min, the fragments were

washed again several times with PBS (K). The washed bone pieces were transferred into 6-well tissue culture plates with sterile forceps (L), followed by addition of DMEM/F-12 medium supplemented with 20 % foetal calf serum (FCS) and 1 % penicillin/streptomycin (PS) (M).

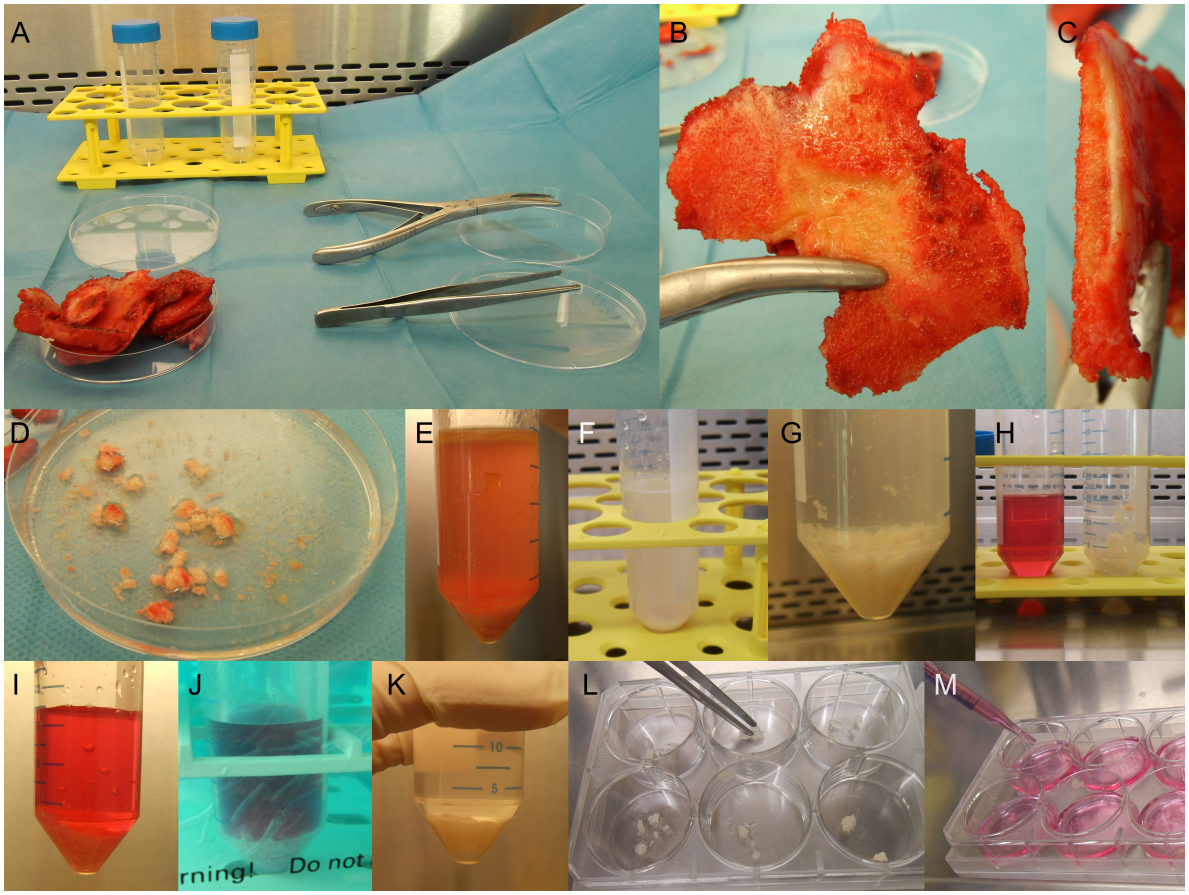

Fig. 3.5: Human osteoblast isolation procedure. A - Material overview. B - Bone fragment used for isolation. C - Lateral view of a bone fragment. D - Isolated bone pieces in PBS. EFG - Washing step with PBS (E - prior, F - during, G - final step). HI - Addition of collagenase I for digestion. J - Incubation in water bath at 37 °C. K - Washing step with PBS. L - Distribution of bone pieces. M - Addition of cell culture medium.

Outgrowth of hOBs from cultured bone pieces appeared several days later (Fig. 3.6). After the first passage, hOBs were cultured in DMEM/F-12 medium supplemented with 10 % FCS and 1 % PS. The medium was changed twice a week. For osteoblast differentiation, the medium was supplemented with 10 nM dexamethasone, 3.5 mM β-glycerophosphate, and 50 µg/ml ascorbic acid.

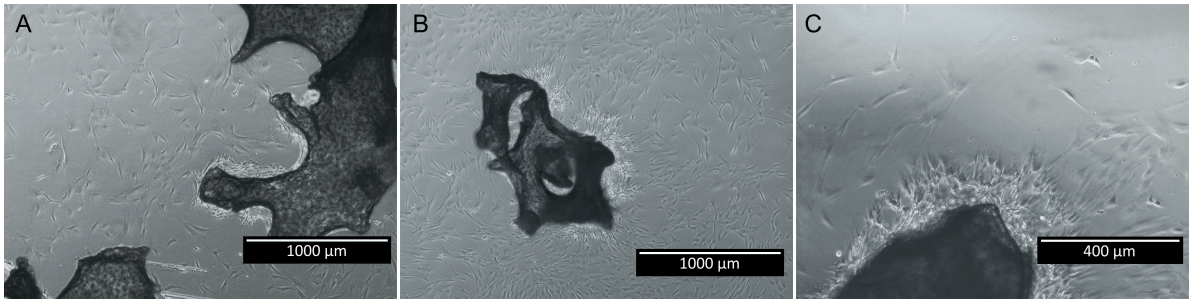

Fig. 3.6: Outgrowth of human osteoblasts from isolated bone pieces.

3.3.3 Handling of cells

Cells and media composition

Besides hOBs, L929 mouse fibroblasts and HUVECs were used in the experiments. L929 fibroblasts were cultured in minimal essential medium (MEM) with Earle's salts and supplemented with 10 % FCS and 1 % PS. They were utilised in the MTT assay and served as negative control for alkaline phosphatase (ALP)-staining. HUVECs were cultured in endothelial cell basal medium (EBM)-2 medium with 2 % FCS, 1 % PS and provided supplements (ascorbic acid, hydrocortisone, heparin, gentamicin, amphotericin B, VEGF, epidermal growth factor (EGF), insulin-like growth factor (IGF), fibroblast growth factor (FGF)). All cells were cultured at 37 °C in a humidified atmosphere containing 5 % CO_2. The medium was changed twice a week for hOBs and L929 fibroblasts; in case of HUVECs, it was changed three times a week.

Cell passaging

When cell density reached 75 % - 90 %, cells were sub-cultivated. Cells were then washed with PBS prior to incubation with accutase® solution for cell detachment at 37 °C. For inactivation of proteases, the detached cells were collected in complete medium containing FCS and centrifuged (1,400 revolutions per minute (rpm), 5 min). The cell pellet was re-suspended and split in a ratio of 1:3 or 1:4, re-seeded in cell culture flasks and further incubated at 37 °C.

Freezing and thawing of cells

For cryopreservation, the cell suspension was centrifuged (1,400 rpm, 5 min) and the pellet re-suspended in FCS containing 10 % dimethylsulfoxide (DMSO). This solution was transferred in cryo-tubes and placed in a cryo-box for slow cooling processes. After one day at -80 °C, the cryo-tubes were transferred into a N_2-tank (-196 °C). For further use, cells were thawed at room temperature (rt), diluted 1:10 with medium and finally, centrifuged (1,400 rpm, 5 min). The cell pellet was re-suspended in medium and transferred into cell culture flasks.

Cell counting

The cell suspension was mixed 1:2 with trypan blue solution (0.4 %). After transferring 10 µl of this mixture in a cell counting slide, the cell number was measured using the LUNA™ Automated Cell Counter. The desired number of cells (assay-depended) was seeded in well plates for further experiments.

3.3.4 Labelling of cells

Labelling with Cell Tracker™ Green or Red

Cells were washed two times with serum-free medium, followed by incubation for 30 min with 5 µM Cell Tracker™ in serum-free medium (stock solution 10 mM, dilution 1:2000). Another washing step with serum-free medium was followed by an incubation step (30 min) with serum-containing medium. Finally, another washing step succeeded. Labelling was controlled using

fluorescence microscopy (Fig. 3.7).

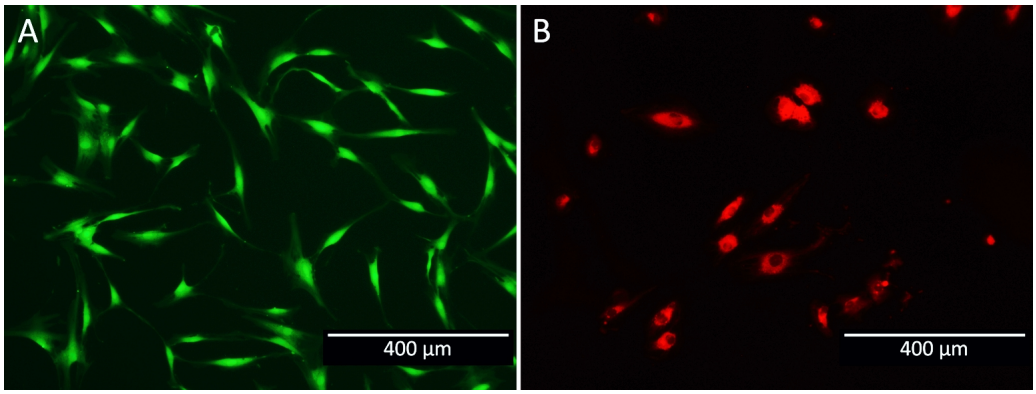

Fig. 3.7: hOBs labelled with Cell Tracker™ Green (A) and HUVECs with Cell Tracker™ Red (B).

Labelling with CalceinAM
hOBs were washed two times with serum-free medium, followed by incubation for 15 min with 1 µl CalceinAM per ml serum-free medium (stock solution 1 mg/ml, dilution 1:1000). Two more washing steps with serum-free medium followed. Fluorescence microscopy was used for the control of cell labelling.

Lentiviral transduction
For long-term labelling, hOBs were transducted with enhanced green fluorescent protein (GFP) according to a standard protocol [116, 117]. One day prior to lentiviral transduction, $2x10^4$ cells were seeded in 24-well plates. Medium was removed and replaced by medium containing 5 µg/ml protaminsulfate (enhance gene transfer efficiency). Subsequently, 20 µl of a 1:10 in medium diluted virus suspension were pipetted into each well. After 6 h, medium was changed and medium containing 20 % FCS was added. Transduction efficiency - which was above 90 % - was determined by flow cytometry.

3.4 Assessment of *in vitro* effects of BSP

Prior to investigation of BSP-coated materials, the effect of dissolved BSP had to be analysed. For this purpose, the MTT-assay, examinations of ALP activity and mineralisation capability were performed with BSP dissolved in cell culture medium. Viability assays and gene expression analyses were performed with hOBs seeded on titanium as well as on CPCs.

3.4.1 MTT assay

A standardized assay for cytotoxicity is the colorimetric 3-(4,5-dimethylthiazol-2-yl)-2,5-diphenyltetrazolium bromide (MTT) assay, according to the DIN ISO 10993–5:2009. L929 fibroblasts were seeded into 96-well plates ($1x10^4$ cells/well) and incubated for 24 h. The medium was removed and replaced by medium with different BSP concentrations (1 µg/ml,

2.5 µg/ml, 5 µg/ml, 7.5 µg/ml, 10 µg/ml, 15 µg/ml, 20 µg/ml). Cells without treatment served as internal controls. Polyurethane films with zinc diethyldithiocarbamate (ZDEC) and zinc dibutyldithiocarbamate (ZDBC) are cytotoxic; they were used as negative control for cell viability. After incubation for 24 h, the medium was removed, 50 µl of 1 mg/ml MTT solution were added to each well and the cells were incubated for 2 h at 37 °C. Thereafter, the MTT solution was discarded, the dye dissolved with 100 µl isopropyl alcohol (IPA) and the absorption measured at 570 nm (reference 650 nm) using a spectrophotometer. Cell viability was evaluated compared to the untreated control (100 %).

3.4.2 Alkaline phosphatase assay and staining

hOBs were seeded in 24-well plates (1x10^4 cells/well). Subsequent to cell adhesion, medium was replaced by medium with varied supplements (standard medium, differentiation medium and medium with 1 µg/ml, 5 µg/ml and 10 µg/ml supplemented BSP) and incubated for four and seven days, respectively. The ALP activity level was determined via the conversion from p-nitrophenylphosphate (pNPP) into p-nitrophenyl (pNP) - this is caused by alkaline phosphatase. Prior to starting the assay, a washing step with PBS was required. First, 250 µl/well 0.1 % Triton-X were added for a 30 min incubation period while shaking with 200 rpm at rt. This was followed by addition of 200 µl pNPP/well and a 30 min incubation step at 37 °C. The reaction was stopped with 50 µl 3 N NaOH and 4x 100 µl were transferred into a 96-well plate. Absorption was measured at 405 nm (reference wavelength 700 nm). ALP-activity was calculated via a pNP standard curve. For staining after four and seven days, cells were washed with PBS and fixed with methanol for 10 min. Next, the cells were stained with SIGMA-FAST™-5-bromo-4-chloro-3-indolyl phosphate (BCIP)/nitro blue tetrazolium (NBT) solution for 20 min, followed by several washing steps with PBS. Then, the cells were embedded with Aqua polymount and covered with glasses. Images were acquired via microscope with a 10-fold objective.

3.4.3 Alizarin red S staining

hOBs were seeded in 24-well plates and treated either with 1 µg/ml or 10 µg/ml BSP or 100 ng/ml bone morphogenetic protein-7 (BMP-7). Cells incubated in differentiation medium served as positive control for mineralisation. After 21 days, the cells were washed with PBS, fixed with Roti® Histofix for 15 min, followed by several washing steps with PBS. Afterwards, the cells were stained for 20 min with Alizarin red S solution (pH 4.0) and washed with sterile water. Alizarin red-stained cells were photographed with a microscope (10-fold objective). For quantification, the images were converted into a binary image using ImageJ [118].

3.4.4 AlamarBlue viability assay

The alamarBlue® assay is a method to analyse cell viability. Alamar blue is non-cytotoxic and in contrast to the MTT assay, repeated measurements of the same cell population are feasible [119, 120]. Therefore, this assay was used to analyse cell proliferation over a defined period of time.

Titanium discs
Titanium discs (ø 14.5 mm) were coated with BSP (30 µg/ml, 50 µg/ml, 150 µg/ml, 280 µg/ml) via covalent coupling or physisorption. Untreated titanium (Ti) discs served as control. The discs were placed in 24-well ultra-low-attachment plates (ULAPs) and 1.5x10^4 hOBs were seeded per disc. After 1, 4, 7, 10, 12 and 14 days, the assay was performed.

CPC scaffolds
hOBs (5x10^4) were seeded on uncoated and BSP-coated (50 µg/ml and 200 µg/ml) CPC discs placed in ULAPs. CPCs incubated in medium without cells were used as negative control. The alamarBlue® assay was carried out on days 3, 5, 7 and 10.

For the *alamarBlue® assay*, medium was removed and replaced with 500 µl of a 10 % alamar Blue® solution in standard cell culture medium and incubated at 37 °C for 4 h. Subsequently, 3x 100 µl of the medium was transferred into 96-well plates and the fluorescence intensity was measured with the Glomax®-Multi Detection System (filter with 525 nm extinction and 580–640 nm emission). The residual medium was removed, while 1 ml of fresh medium was added. This was followed by incubation until next measurement. Incubation medium without cells served as blank value. A standard curve was used for cell number calculation.

3.4.5 Analysis of gene expression

Titanium discs
Titanium discs (ø 33.5 mm) were coated with BSP (30 µg/ml or 280 µg/ml) via covalent coupling and physisorption. Untreated, piranha-activated and with BMP-7 (100 ng/ml) physisorped Ti discs served as controls. hOBs (2x10^5 cells/disc for day 1, 1x10^5 cells/disc for day 4 and 7.5x10^4 cells/disc for day 7) were seeded on the various modified Ti discs, which were placed in 6-well ULAPs. After 1, 4 and 7 days, respectively, the cells were harvested with accutase®, centrifuged and the cell pellet was stored at -80 °C until ribonucleic acid (RNA) isolation. RNA was isolated with the Qiagen RNeasy Mini or Micro Kit (depends on the amount of cell material) according to the manufacturer's instructions. Digestion with DNAse was performed and RNA was eluted with 30 µl (Mini Kit) or 14 µl (Micro Kit). RNA concentration and purity were measured via absorbance at 260 nm and 280 nm using a spectrophotometer. The 260 nm/280 nm ratio of pure RNA range from 1.9 to 2.1. An optimal amount of 2 µg of total RNA was used for reverse transcription. In case of lower RNA contents, the RNA amount

for reverse transcription and cDNA dilution for later real-time quantitative polymerase chain reaction (qPCR) was adapted.

Reverse transcription Mix I			**Reverse transcription Mix II**		
	2 µg	RNA		8 µl	5x Buffer
+	2 µl	Random hexamer primers	+	2 µl	DTT
+	2 µl	dNTPs	+	1 µl	Superscript RT III
ad	20 µl	with RNAse-free water	+	9 µl	RNAse-free water

Mix I was prepared for each sample, followed by the first thermocycler step:

1)	65 °C	5 min

Upon completion of this step, Mix II was added to each sample and it was continued with the next steps:

2)	25 °C	10 min
3)	50 °C	60 min
4)	70 °C	15 min

For qPCR, 5 µl of 1:10 diluted cDNA were transferred into 96-well plates and completed with 15 µl qPCR Mix. Triplicate measurements were performed for each sample.

qPCR Mix		
	2 µl	Primer
+	3 µl	RNAse-free water
+	10 µl	SYBR® Green PCR Master Mix

Gene expression was examined with QuantiTect® primers for 18S, ALP, SP7, Col1, RUNX2, OPN, and SPARC using the following *thermal cycling profile*:

1)	1 step	50 °C	2 min
2)	1 step	95 °C	10 min
3)	40 cycles	95 °C	15 sec
		55 °C	30 sec
		72 °C	35 sec

A dissociation step was added at the end of thermal cycling as control for the absence of primer-dimers. The results were calculated using the well-established $2^{-\Delta\Delta C_t}$ method [121]. They were presented as the expression levels relative to gene expression of hOBs seeded on untreated titanium.

CPC scaffolds

hOBs ($5x10^4$/scaffold) were seeded on the prepared bone substitutes (untreated, coated with 50 µg/ml and 200 µg/ml BSP), placed in a 24-well ULAP and incubated for 14 days. Cells were harvested with accutase®, followed by RNA isolation, reverse transcription and qPCR.

The procedure was the same as for titanium discs, except that the SYBR ® Select Master Mix was used for qPCR. Therefore, the *thermal cycling profile* was adapted:

1)	1 step	50 °C	2 min
2)	1 step	95 °C	2 min
3)	40 cycles	95 °C	15 sec
		55 °C	20 sec
		72 °C	55 sec

3.5 Visualisation methods

3.5.1 Light microscopy

Light microscopy was used as control for cell confluence or outgrowth of hOBs during hOB isolation and particularly for observation of histological slices, Alizarin red S and ALP staining.

3.5.2 Fluorescence microscopy

Evaluation of cell labelling (e.g. after staining with Calcein-AM, Cell Tracker™ Green or Red) and cell visualisation were performed with fluorescence microscopy. Three different fluorescence channels (blue, green and red) can be visualised separately or combined via merged images (Fig. 3.8).

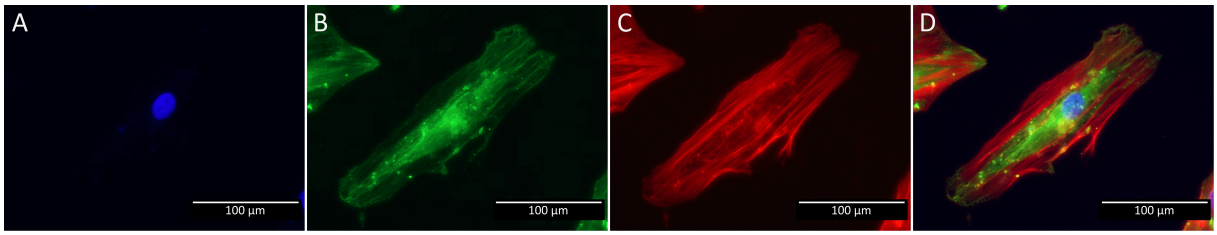

Fig. 3.8: Overview of the blue, green and red channel and their merged image. This is an immune fluorescence example with hOBs and their ALP-expression after four days of incubation with differentiation medium. A - Hoechst nucleus staining, B - Alkaline phosphatase, C - F-Actin staining, D - Merged image.

3.5.3 Confocal laser scanning microscopy

On titanium surfaces seeded eGFP-transduced hOBs were visualised with a confocal laser scanning microscope (CLSM). A water immersion objective (20-fold magnification) was used to retain the seeded cells in medium during microscopy. Images were acquired using an argon-krypton laser (excitation at 488 nm, detection at 500-550 nm).

3.5.4 Immunofluorescence

Cells were seeded into tissue culture plates. After cell adhesion, the medium was changed and replaced by medium with various supplements (cell culture medium with and without addition of BSP, differentiation medium). After 4 days of incubation, the procedure shown in Fig. 3.9 was conducted.

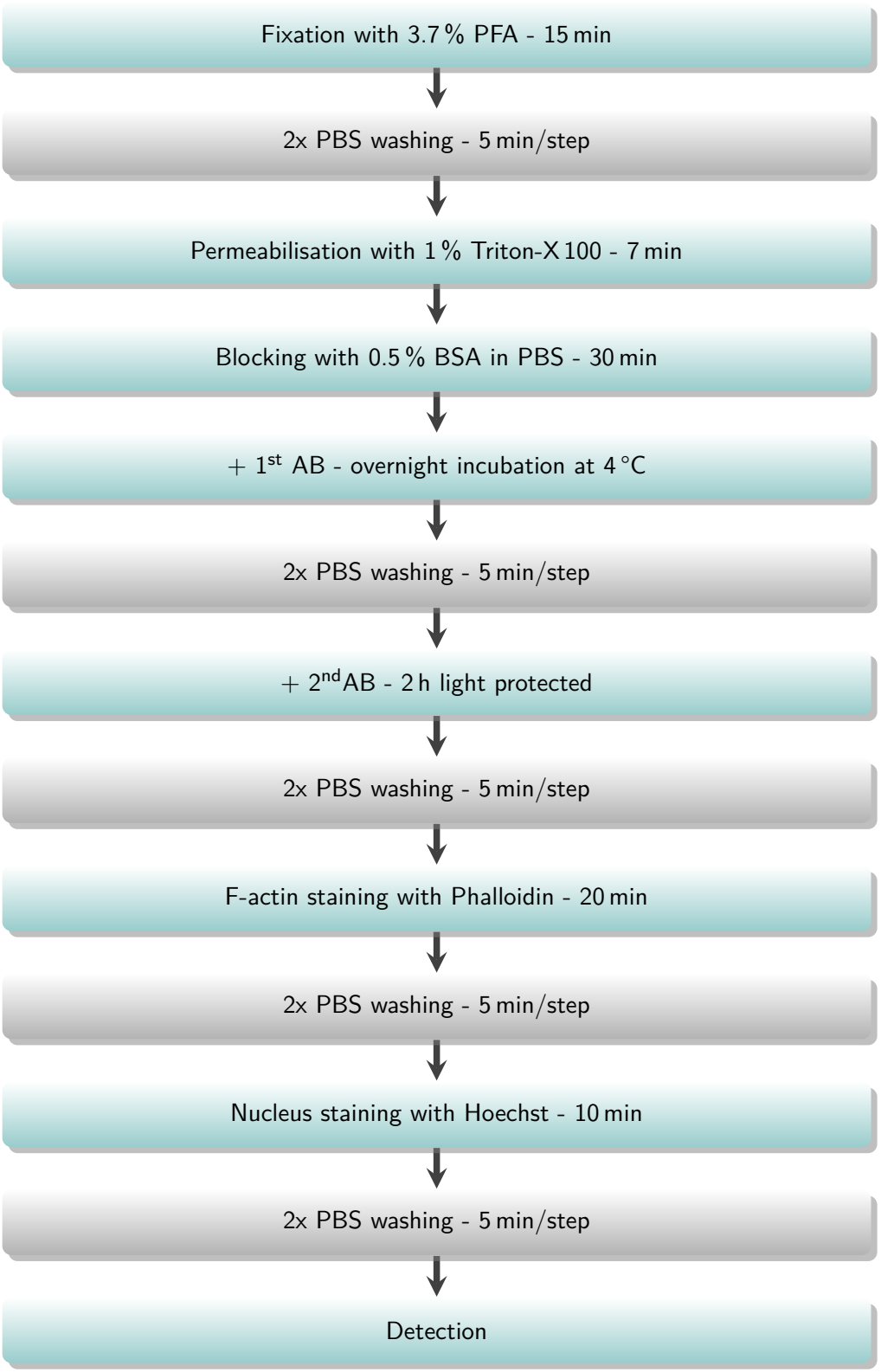

Fig. 3.9: Immunofluorescence staining procedure.

All steps were performed at room temperature (rt) unless indicated otherwise. Antibodies (AB) and fluorescence dyes were diluted with PBS containing 0.5 % bovine serum albumin (BSA) as indicated in Tab. 3.1. Finally, the cells were visualised by fluorescence microscopy.

Tab. 3.1: Dilutions for antibodies and fluorescence dyes.

Antibody or dye	Description	Dilution
ALP	1st antibody	1:100
RUNX2	1st antibody	1:100
Alexa Fluor 488	2nd antibody	1:200
Phalloidin Alexa Fluor 568	F-actin staining	1:50
Hoechst	nucleus staining	1:250

3.5.5 Scanning electron microscopy

Microstructure analyses of CPC scaffolds (untreated) were performed with a scanning-electron microscope (SEM), set at 20.0 kV, 0.8 or 1.20 mbar and a large field detector (LFD).

3.6 *In vitro* 3D experiments

3.6.1 Preparation of collagen gels

Substances have to be kept on ice as well as the prepared collagen gels. Under the influence of higher temperatures, the gel turns from the liquid into the solid form. For collagen gel preparation, the following pre-cooled substances were gently mixed:

	1.5 ml	M199 10x
+	450 µl	$NaHCO_3$ (7.5 %)
+	172 µl	NaOH (1 N)
+	6 ml	Aqua dest.

Then, collagen was added to receive a final concentration of 1.5 mg/ml:

+	6.9 ml	Collagen I (3.59 mg/ml)

BSP was added directly into the gels (1 µg/ml, 5 µg/ml or 10 µg/ml BSP) and therefore the amount of Aqua was adjusted. Meanwhile, the cells were removed from cell culture flasks, counted and then, the desired number of cells was transferred into a tube and centrifuged.

Cell type	Final cell concentration
hOB mono-culture	5x10^5 cells/ml
HUVEC mono-culture	5x10^5 cells/ml
hOB + HUVEC co-culture	each 2.5x10^5 cells/ml

The cell pellets were dissolved in 1.5 ml medium (with added FCS), mixed gently with the prepared gel and seeded into 24-well plates (300 µl/well corresponding to 1.5x10^5 cells). For gelation, an incubation period of 30 min at 37 °C followed. After this step, 1 ml medium with or without BSP-supplementation (1 µg/ml, 5 µg/ml or 10 µg/ml BSP) was added per well to the solid gel. Cells were incubated at 37 °C and 5 % CO_2 until the desired assay was performed.

3.6.2 Viability assay

Cell viability of HUVEC and hOB mono- as well as co-cultures in prepared collagen gels (see above, 0 µg/ml, 1 µg/ml and 5 µg/ml BSP) was analysed on days 1, 2, 4, 7 and 10. Collagen gels without cells and supplements served as a control. The medium was gently removed from the gels. As much as 500 µl of 1:10 diluted alamarBlue® in medium were added and the gels incubated for 4 hours at 37 °C. Finally, 3x 100 µl were transferred into 96-well plates and fluorescence intensity was measured with the Glomax® -Multi Detection System (Ex 525 nm Em 580-640 nm). The residual medium was removed and 1 ml fresh medium added, followed by incubation until next measurement.

3.6.3 Examination of gene expression in collagen gels

According to the viability assay, collagen gels without and with BSP supplementation (1 µg/ml, 5 µg/ml and 10 µg/ml) were prepared. For gene expression analyses, the gels were prepared in 6-well plates. The cell number was adapted to 1x10^6 cells/well (co-culture: 5x10^5 cells/well for each cell type). Cells were re-suspended in 1 ml collagen gel and seeded into 6-wells, they were incubated for gelation and thereafter 2 ml medium ± BSP was added per well. Standard osteoblast medium (DMEM/F-12 medium + 10 % FCS + PS) was used for hOB mono-culture. HUVEC mono-culture and hOB/HUVEC co-culture were cultivated in EBM-2 medium (without VEGF and FGF supplementation). The FCS amount was increased to 10 %. Medium was changed after four days. After one, four and seven days, the gels were washed with PBS, followed by collagen digestion using a 1 mg/ml collagenase I/dispase solution. Upon completion of collagen dissolving, the cell suspensions were transferred into tubes and centrifuged at 1,400 rpm for 5 min. The supernatant was discharged and the cell pellet was stored at -80 °C until RNA isolation.

RNA isolation

Isolation of RNA was conducted with the PeqGold Total RNA Micro Kit. The procedure was performed according to manufacturer's instruction. Optional DNA-digestion was carried out and the RNA was eluted with 30 µl of RNAse-free water. RNA content and quality were examined with a spectrophotometer. In addition, RNA quality was evaluated via agarose gel electrophoresis. Therefore, the RNA was diluted with loading buffer, followed by heat denaturation for 5 min at 65 °C. An amount of 100 ng RNA (10 µl) was loaded on a 1.5 % agarose gel containing SYBR-safe in TRIS - acetic acid - EDTA (TAE) buffer. Electrophoresis was conducted at 150 V for 1 h, followed by gel visualisation with UV-light. Sharp 28S and 18S rRNA bands indicate pure and intact RNA.

Reverse transcription

An optimal amount of 2 µg of total RNA was used for reverse transcription. For lower RNA contents, the procedure was adapted.

Reverse transcription Mix I			**Reverse transcription Mix II**		
	2 µg	RNA		1 µl	Maxima H Minus RT
+	1 µl	Random hexamer primer	+	4 µl	5x RT buffer
+	1 µl	dNTPs			
ad	20 µl	with RNAse-free water			

Mix I was prepared for each sample, followed by start of the first thermocycler step:

1)	65 °C	5 min

Upon completion of this step, Mix II was added to each sample and then the next steps continued:

2)	25 °C	10 min
3)	50 °C	30 min
4)	85 °C	5 min

Quantitative PCR

For qPCR, 5 µl of 1:10 diluted cDNA were transferred in 96-well plates and completed with 15 µl qPCR Mix. Triplicate measurements were performed for each sample.

qPCR Mix

	0.1 µl	Forward primer
+	0.1 µl	Reverse primer
+	4.8 µl	RNAse-free water
+	10 µl	PowerUp™ SYBR® Green Master Mix

Gene expression of ALP, OPN, SP7, RUNX2 and SPARC was examined in hOB mono-cultures, in contrast to PECAM, MCAM, KDR and vWF expression in HUVEC mono-cultures. In default of suitable pure RNA from HUVEC mono-cultures after 7 days, gene expression examinations were only conducted for days 1 and 4. In co-cultures, the expression of all genes was investigated. The following *thermal cycling profile* was then used:

1)	1 step	50 °C	2 min
2)	1 step	95 °C	2 min
3)	40 cycles	95 °C	15 sec
		60 °C	15 sec
		72 °C	1 min

A dissociation step was added at the end of thermal cycling as control of the absence of primer-dimers. The results were calculated using the well-established $2^{-\Delta\Delta C_t}$ method [121]; they presented the expression levels relative to gene expression of cells seeded into untreated collagen gels.

Prior to expression analyses of the mentioned genes, suitable reference genes were evaluated. Six references genes (18S, glyceraldehyde-3-phosphate dehydrogenase (GAPDH), β-actin (BACT), β-2-microglobulin (B2M), hydroxymethylbilane synthase (HMBS), hypoxanthine phosphoribosyl-transferase 1 (HPRT-1)) were evaluated via GeNorm [122], Normfinder [123], Bestkeeper [124] and the comparative Ct method [125] according to Chen et al. [126]. B2M and GAPDH turned out to be suitable reference genes. More details of this evaluation have been listed in the appendix 5.

3.6.4 Angiogenesis assay with spheroids

Spheroid preparation

Spheroid preparation was performed according to Augustin and Korff [83, 127].

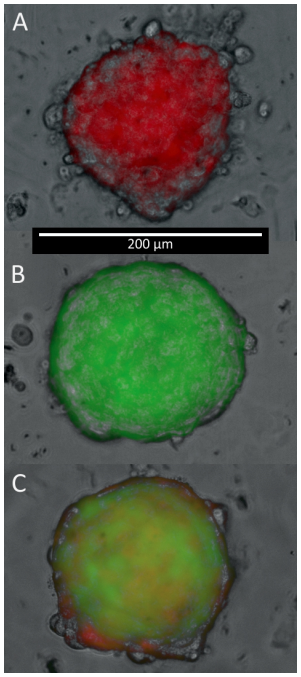

Fig. 3.10: Mono-culture (A - HUVEC, B - hOB) **and hOB-HUVEC co-culture** (C) **spheroids formed after one day incubation in 96-well plates with U-bottom.**

First, a methocel solution was prepared. A magnetic stirrer and 6 g Methocel were autoclaved at 121 °C for 20 min in a 500 ml Schott® bottle. Medium 199 was separated in two parts (each with 250 ml). One part (no supplements) was preheated at 60 °C, then added to the bottle containing methocel, and finally, stirred for 20 min at 60 °C. After cooling to room temperature, the second part of the M199 medium (with the following supplements: + 5 ml L-glut, + 5 ml PS + 50 ml FCS) was added. The combined solution was stirred over-night at 4 °C. On the next day, the solution was distributed in 50 ml tubes and centrifuged at 3,500 g for 3 h. Meanwhile, the cells were labelled with Cell Tracker™ (hOBs with Cell Tracker™ Green and HUVECs with Cell Tracker™ Red, see section 3.3.4 as well as Fig. 3.10 for mono- and co-culture spheroids of HUVECs and hOBs).

One part of the methocel solution (2.4 ml/96-well plate) was diluted with four parts medium (9.6 ml/96-well plate) and the cell suspension (for 1x 96-well: $6x10^4$ cells per mono-culture or $3x10^4$ of each cell type per co-culture) was added. After gently mixing the cells, they were seeded in a 96-well plate with U-bottom (100 µl/well corresponding to 500 cells/well) and incubated overnight. On the next day, the spheroids should have formed (Fig. 3.10).

Angiogenesis assay

For angiogenesis assays, the spheroids were embedded in collagen gels. Each experimental group (1st HUVEC mono-culture, 2nd hOB mono-culture and 3rd HUVEC hOB co-culture) was divided into four groups, depending on the added supplement (Tab 3.2).

According to Heiss et al [83] the gel is composed of 8 parts of collagen, 1 part of M199 10x and nearly 1 part of NaOH.

Heiss et al. [83]	
8 parts	Collagen I (2 mg/ml)
1 part	M199 10x
1 part	NaOH(0.2 N)

Collagen gel preparation	
3590 µl	Collagen Type I (3.12 mg/ml)
2010 µl	Aqua ad inject.
700 µl	M199 10 x
700 µl	NaOH (0.2 N)

Spheroids from each 96-well plate were collected with a 1,000 µl pipette tip (nearly 2 mm from the tip were cut with a sterile scissor), transferred in a 50 ml tube and then, centrifuged at 300 g for 3 min. The supernatant was discarded and the spheroids were gently re-suspended in 1 ml medium M199 + 20 % FCS + 0.5 % methylcellulose [6 ml methocel solution + 600 µl FCS + 7,8 ml M199 (include 20 % FCS)]. The same volume of the collagen gel (1:1) was added and very gently mixed for avoiding air bubbles. Next, 1 ml of this mixture was plated in one well of a 24-well plate (one 96-well plate resulted in two 24-wells). Supplements were added to the gels (1 ml medium ± supplements per well, see table 3.2) after 30 mins of pre-incubation at 37 °C. Images were taken via fluorescence microscopy after 1 h and 24 h. Quantification of sprout length was performed with Image J [118].

Tab. 3.2: Groups for angiogenesis assay.

Group	Name	Supplements after 30 min	Dilution
1	control	no supplements	
2	positive control	VEGF 25 ng/ml	50 ng/ml
3	BSP-low	BSP 5 µg/ml	10 µg/ml
4	BSP-high	BSP 50 µg/ml	100 µg/ml

3.7 *In vivo* experiments

National regulations for the care and use of laboratory animals were respected all time. All experiments were approved by the Landesuntersuchungsamt Rheinland-Pfalz (calvarial defect model G 15-1-050, femoral condyle defect model G 15-1-093).

3.7.1 Calvarial defect model

The calvarial model was performed with C57BL/6NRj (six weeks old, female) mice from Janvier Labs.

Surgical procedure
One day in advance of surgery, the drinking water was supplemented with tramadol (1 mg/ml) as precautionary pain management. Prior to the surgical procedure, the mice were anaesthetised with medetomidin, fentanyl and midazolam (Tab. 3.3).

Tab. 3.3: Dosage for mice anaesthesia.

Substance	Stock solution	Concentration for anaesthesia
Midazolam	5 mg/ml	5 mg/kg body weight
Medetomidin	1 mg/ml	500 µg/kg body weight
Fentanyl	50 µg/ml	50 µg/kg body weight

The operation table and the heating plate were disinfected. Next, these were covered with sterile surgical drapes. All materials (pre-sterilised instruments, sterile consumables, disinfected drill) were placed ready to hand. Several minutes after the intra-peritoneal injection, the anaesthetic depth was checked via palpebral and toe-pinch reflexes. Losing the palpebral reflex may lead to cornea dehydration. Therefore, the eyes were secured with Bepanthen ointment. The operation started with scalp disinfection using Braunol®. A mid-sagitally skin incision (1 to 1.5 cm) was set with a scalpel. The parietal bone was uncovered by anatomical tweezers. Scalp dehydration was prevented with saline rinsing. Two bone defects were carefully set with a hollow drill (ø 2.7 mm) with parallel saline washing. The bone discs were removed and the condition of the dura mater was checked. Depending on the group the mouse belonged to, it became no treatment (Group 1) or different treated bone substitutes were implanted (Group 2, 3 and 4); (see Tab. 3.4).

Tab. 3.4: Classification of the calvarial defect model.

Gr.	Shortname	Description	n (animals)
1	no CPC	negative control, no treatment	15
2	CPC	implantation of CPC-scaffolds	15
3	CPC + BSP	implantation of BSP-coated scaffolds (200 µg/ml)	15
4	CPC + BMP-7	implantation of BMP-7-coated scaffolds (10 µg/ml)	15

The prepared bone substitutes (see section 3.2) were rinsed with saline, followed by implantation in the borehole defects (Fig. 3.11). Finally, the wound was sutured with a simple interrupted stitch and disinfected. As postoperative pain management, tramadol was supplemented to their drinking water (final concentration 1 mg/ml) for 5 - 7 days. The duration depended on mice behaviour, which was controlled daily after the surgical intervention. A more detailed description of the surgical method can be found in the thesis of Jens Hertweck [103].

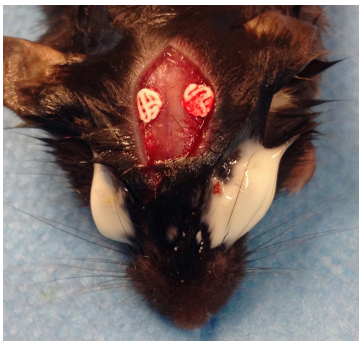

Fig. 3.11: Fresh implanted BSP-coated bone substitutes in mice parietal bone.

Post-mortem procedure

After an eight-week observation period, the mice were killed by CO_2-intoxication. First, the fur in the head and neck region was removed by using a depilatory cream. Around the upper cervical spine, the skull was decapitated. Afterwards the head was fixed with 4.5 % formaldehyde solution for a minimum of 3 days. Final preparation for micro-computed tomography (µCT) measurements includes the removal of residual cervical vertebras and for better sample arrangement, horizontal skull splitting, besides separation of the nose for length reduction.

3.7.2 Femoral condyle defect model

The femoral condyle model was performed with seven week old male Wistar rats from Janvier Labs.

Surgical procedure
Tramadol supplemented in drinking water (1 mg/ml) was used as precautionary pain management. Rats were anaesthetised with medetomidin, fentanyl and midazolam (Tab. 3.5). For better subcutaneous injections, the rats were shortly pre-anaesthetised with isoflurane.

Tab. 3.5: Dosage for rat anaesthesia.

Substance	Stock solution	Concentration for anaesthesia
Midazolam	5 mg/ml	2 mg/kg body weight
Medetomidin	1 mg/ml	150 µg/kg body weight
Fentanyl	50 µg/ml	5 µg/kg body weight

The preparations were conducted according to them in the calvarial model (see above), except for the fact that Corneregel® was used for eye protection. The fur in the operation area was trimmed, followed by skin disinfection with Braunol®. After a 1.5 - 2 cm skin incision, the femoral condyle was opened via anatomical tweezers and with the help of a spreader. Bone dehydration was prevented with saline rinsing. A borehole defect was set with a drill (ø 2.5 mm) in the femoral condyle. This was followed by washing with sterile saline and drilling manually (with a ø 3.0 mm drill). Residual bone fragments were removed to prevent ossification. Depending on the group the rats belong to, there was either no treatment (Group 1) or different treated bone substitutes were implanted (Groups 2, 3 and 4); see Tab. 3.4.

Tab. 3.6: Classification of the femoral condyle defect model.

Gr.	Shortname	Description	n (animals)
1	no CPC	negative control, no treatment	10
2	CPC	implantation of CPC-scaffolds	10
3	CPC + BSP	implantation of BSP-coated scaffolds (200 µg/ml)	10
4	CPC + BMP-7	implantation of BMP-7-coated scaffolds (10 µg/ml)	10

The prepared bone substitutes (section 3.2) were rinsed with saline and implanted in the borehole defect (Fig. 3.12 A and B). Finally, the wound was sutured subcutaneously - for better muscle fixation and stability - (Fig. 3.12 C) and cutaneous with a simple interrupted stitch, followed by disinfection. Then, the same operation procedure was performed on the other side. As postoperative pain management, tramadol was supplemented in their drinking water (final concentration 1 mg/ml) for nearly 3 - 5 days.

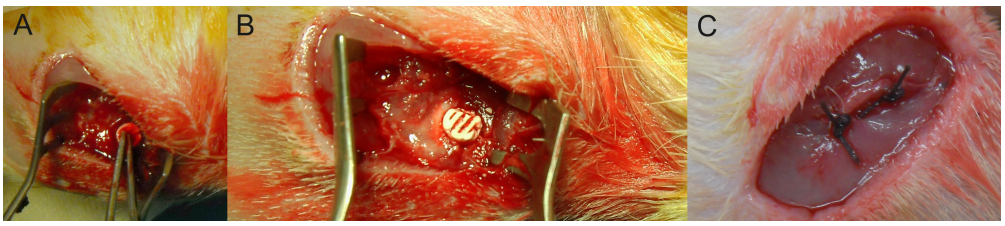

Fig. 3.12: Surgical procedure of the femoral condyle defect model. A - Implantation of the substitute B- Defect with bone substitute C - Subcutaneously sutured wound.

Post-mortem procedure

The rats were killed by CO_2-intoxication after an observation period of four weeks. Both legs were separated from the body and parts of the muscles were removed, followed by fixation with 4.5 % formaldehyde solution. Final preparation for µCT measurements includes the removal of lower legs and muscles as well as femur-shortening for length reduction.

3.7.3 µCT measurements

µCT analyses were performed with 70 kV and 114 µAmp. For calvaria samples, the voxxel size was set to 30 µm compared to 20 µm for femoral condyle samples. Furthermore, radiographs were taken from the femoral condyles.

Analysis of µCT data

µCT data were analysed with ImageJ [118, 128, 129]. In short, two different thresholds were set to gain binary images of bone + material and the material alone. The material was removed from bone via image subtraction. Next, the image stack was re-orientated with the AlignmentPlugin. A substack with a defined thickness (calvaria: 75 slices, femoral condyle: 155 slices) and the region of interest around the implant (calvaria: ø 3 mm to 5 mm, femurcondyle: ø 2.9 mm) was created for specific evaluation. Finally, the boneJ Plugin [130] was used for calculating the Bone Volume/Total Volume Fraction.
A more detailed explanation can be found in Appendix 5.

3.7.4 Histology

For histological examinations, formaldehyde-fixed samples were either de-calcified, followed by embedding in paraffin or directly embedded in Technovit®.

Paraffin embedding

The samples returned in Histofix® after µCT-measurements. For further histologic preparations cuttable tissue is required. For this reason, the probes were decalcified in a 10 % tris(hydroxymethyl)aminomethane (TRIS)-buffered ethylenediaminetetraacetic acid (EDTA) solution for three weeks, with daily changes. Subsequently, the samples were rinsed with water and the tissue was cut close to the region of interest. The probes were transferred in tissue embedding cassettes and in Histofix®. Sample infiltration with paraffin was carried out by

different washing and dehydrating steps with the autotechnicon. Paraffin-infiltrated samples were embedded in paraffin blocks with a view to correct positioning. Tissues were sectioned in series with a microtome. The cutting thickness between the sections was set to 10 µm at the start, in contrast to 5 µm in the area of interest. The sections were transferred onto an object slide, followed by different staining procedures.

Technovit® embedding

Prepared samples were dehydrated in an upward alcohol series, in each bottom 2-3 days:

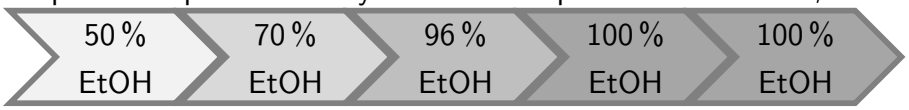

Afterwards the Technovit® (T) proportion (diluted in ethanol (EtOH)) was increased gradually under vacuum and agitation with an automated dehydration and infiltration system:

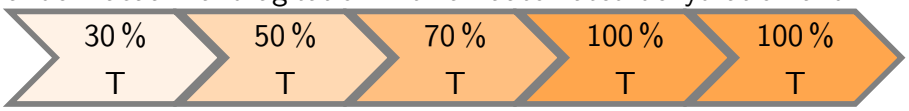

The infiltrated samples were placed in embedding moulds. Particularly, the fixation adhesive Technovit® 7230 VLC was used to hold samples in place during the embedding process with Technovit® 7200 VLC. Polymerisation was carried out in two stages in a light polymerisation unit. In the first stage, the embedding medium was polymerised at low light intensity in contrast to polymerisation of in samples infiltrated embedding medium at high light intensity. Embedded samples were separated with a saw in individual blocks, followed by preparation of histologic sections according to Donath [131].

Staining

Prior to any staining procedure, paraffin-embedded slices had to be deparaffined with xylene, followed by rehydration with a downward alcohol series with IPA (Fig. 3.13 A, green arrow). Subsequent to the selected staining procedure (B, C or D), the sections were dehydrated in an upward alcohol series and xylene (Fig. 3.13 A, blue arrow). The stained sections were coverslipped with Cytoseal™ and examined via light microscopy.

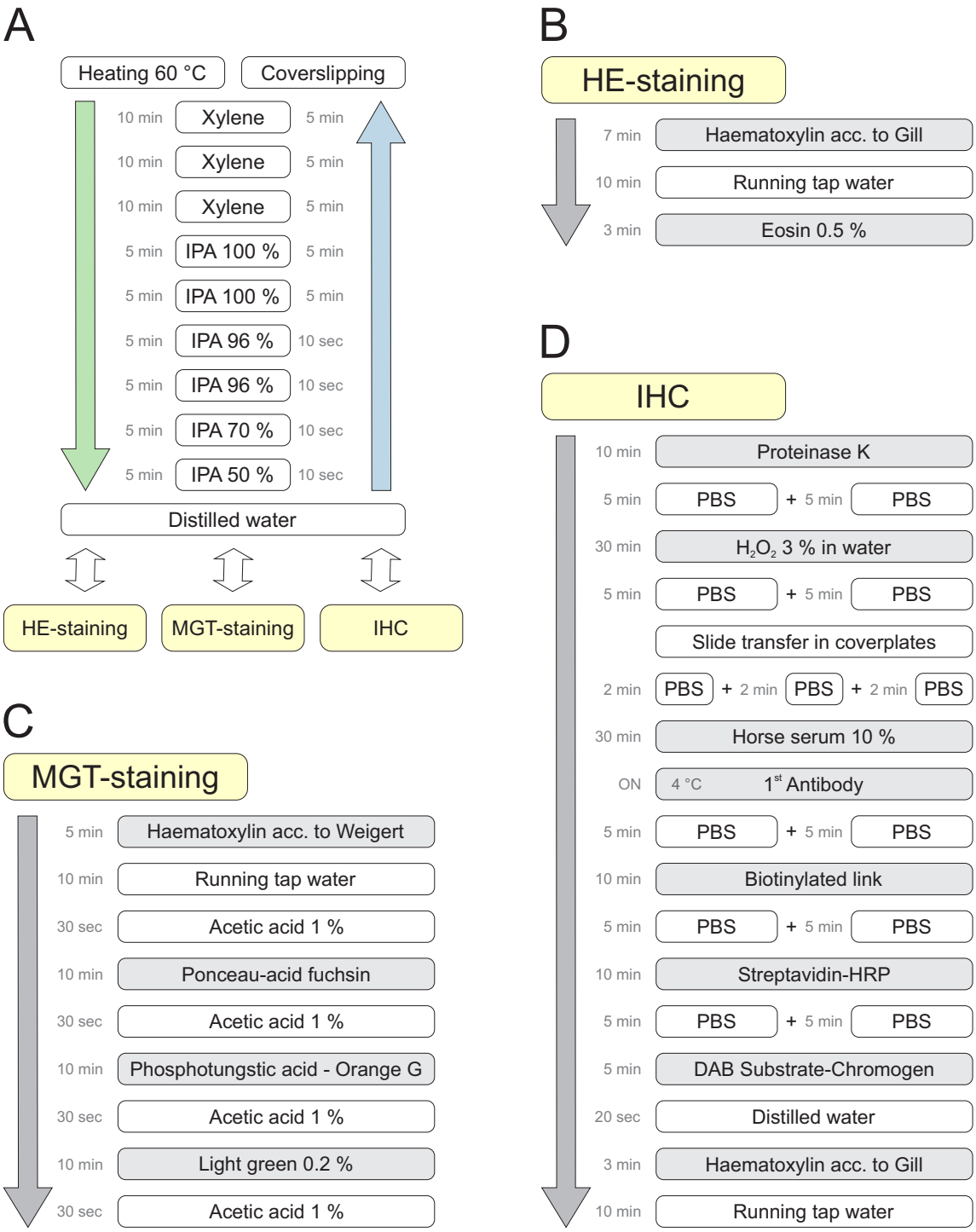

Fig. 3.13: Staining procedure of paraffin-embedded sections.

Every fifth section of each sample was stained with haematoxylin-eosin (HE), as seen in Fig. 3.13 B. HE-stained sections were used to gain an overview and select appropriate sections for Masson-Goldner trichrome (MGT) staining (staining procedure in Fig. 3.13 C) or immunohistochemistry (IHC).

Fig. 3.13 D demonstrates the detailed IHC procedure. During fixation with formaldehyde, proteins were cross-linked via methylene bridges. Therefore, the first step, enzymatic antigen retrieval with proteinase K, is mandatory to break those methylene bridges. Prior to incuba-

tion with the first antibody, endogenous peroxidases were blocked with 3 % hydrogen peroxide and unspecific antibody binding was prevented with 10 % horse serum. The sections were incubated with specific first antibodies (diluted in PBS containing 1 % BSA as indicated in Tab. 3.7) overnight at 4 °C. Negative controls were incubated only with PBS containing 1 % BSA. Detection was performed enzymatically via the labelled streptavidin-biotin method. A biotinylated link serves as second antibody. Streptavidin - conjugated to horseradish peroxidase (HRP) - binds to the biotinylated link [132]. HRP convert DAB into a brown-coloured precipitate. Finally, the sections were counterstained with haematoxylin.

Tab. 3.7: Antibody dilutions for IHC.

Antibody	Dilution
OPN	1:100
PECAM-1	1: 50
vWF	1:100

Technovit®-embedded sections were stained with toluidine blue (TB). First, the sections were incubated in 0.1 % formic acid for 10 min. Then, they were rinsed in distilled water and wiped with acetone:alcohol (1:1). This was followed by agitation in 30 % hydrogen peroxide for 20 min. After rinsing in tap water, the sections were stained with TB for 20 min. Another rinsing step in tap water was followed by differentiation with acetone:alcohol (1:1) and coverslipping with Canada balsam.

3.8 Statistical analyses

Statistical analyses were performed using the SPSS software (Version 23). The results are presented as medians and quartiles or as means $\pm$ standard deviation. Measurements were carried out in triplicates, except for ELISA measurements (duplicate). Cell-based experiments were independently repeated three times with different osteoblast preparations. Normally distributed data were analysed by one-way ANOVA. Depending on Levene's test for equality of variances, pairwise comparisons were conducted either by a Tuckey-HSD or Games-Howell post hoc test. In contrast, non-normally distributed data were evaluated with the Kruskal-Wallis test. For pairwise comparisons, the Mann-Whitney-U test was used. p-values < 0.05 were considered statistically significant (* $p<0.05$, ** $p<0.01$, *** $p<0.001$). Due to multiple testing, the p-values were adjusted via the method of Bonferroni-Holm.

4 Results and Discussion

4.1 Preliminary tests to determine the effect of supplemented BSP

Prior to any experiments with BSP-coated materials, it is required to analyse how the recombinant manufactured BSP solution affects cytocompatibility, cytotoxicity and viability of cells. This section examines the cytotoxic behaviour of BSP as well as its effect on essential osteoblast regulation factors, like alkaline phosphatase activity and mineralisation capability.

4.1.1 Cell viability and cytotoxicity

Bio- or rather cytocompatibility is a mandatory property for further applications. Therefore, the question as to whether BSP acts in a cytotoxic way or not should be answered first by means of the MTT-assay according to the DIN-ISO 10993-5:2009 norm.

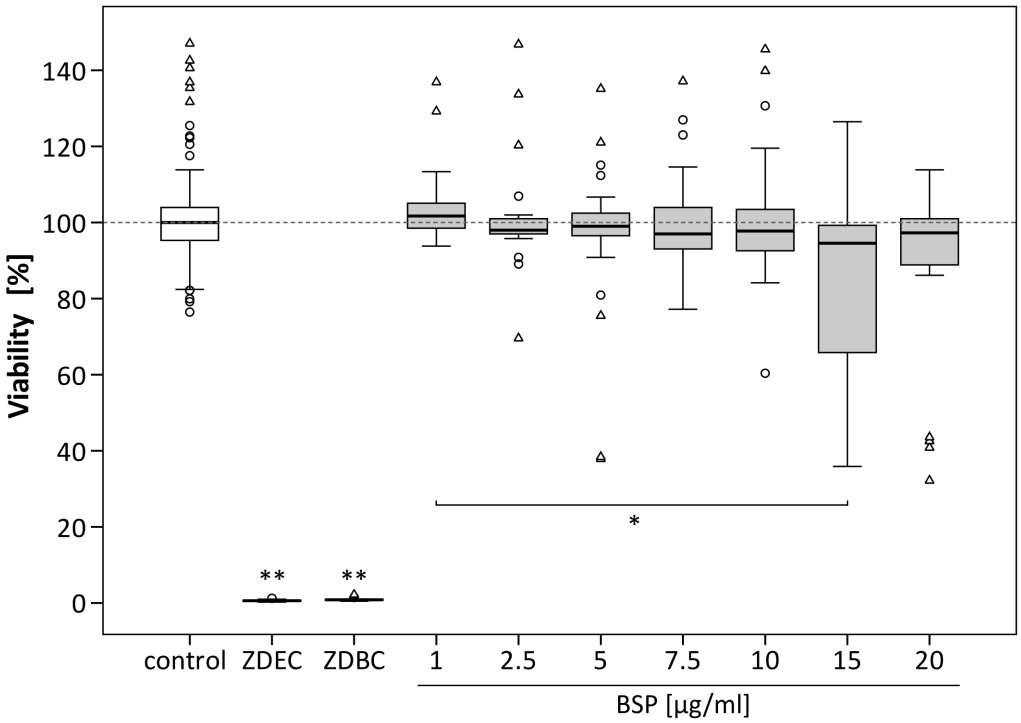

Fig. 4.1: Effect of different BSP concentrations on L929 viability. Zinc diethyldithiocarbamate (ZDEC) and zinc dibutyldithiocarbamate (ZDBC) served as negative controls. Results are expressed as medians and quartiles (n = 25; ZDEC and ZDBC n = 14). Mann-Whitney-U tests revealed significant differences (*p<0.05, **p<0.01).

L929 fibroblasts are routinely used for cytotoxic analyses. They were seeded in 96-well plates and incubated for 24 hours. The medium was removed and replaced by medium containing different BSP concentrations ranging from 1 to 20 µg/ml. Subsequent to a further 24-hour incubation period, the MTT assay was performed. The polyurethane films ZDEC and ZDBC,

known to act in a cytotoxic way, served as negative controls for cell viability.
As depicted in Fig. 4.1, no significant differences in cell viability were observed between the untreated control (median set as 100 %) and BSP-supplemented medium. An increase in cell viability was shown in the group with 1 µg/ml BSP (101.8 %). This group showed significant differences compared with addition of 15 µg/ml BSP (94.6 %). The polyurethane films ZDEC and ZDBC reduced cell viability below 1 % (ZDEC 0.6 % and ZDBC 0.85 %). In compliance with the DIN ISO 10993-5:2009, reagents are defined as cytotoxic if cell viability decreases below 70 %. All BSP groups showed medians higher than 90 % compared with the control. Therefore, BSP itself is not cytotoxic in the tested concentrations.

4.1.2 Alkaline phosphatase activity

Alkaline phosphatase, known as an early marker for bone development, was measured quantitatively via conversion of pNPP into pNP as well as qualitatively via visualisation after BCIP/NBT staining. In both methods, human osteoblasts were treated with diverse medium supplements (differentiation supplements as well as 1 µg/ml, 5 µg/ml and 10 µg/ml BSP, besides standard cell culture media as control) and incubated for a period of four and seven days. For ALP staining the cells were fixed, stained with BCIP/NBT and visualised with light microscopy. L929 fibroblasts served as negative control (see Fig. 4.2).

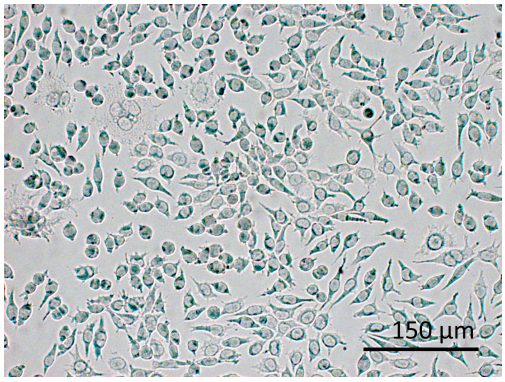

Fig. 4.2: L929 fibroblasts showed no positive ALP staining.

Standard culture medium showed the lowest intensity of ALP staining (Fig. 4.3 A, F). In contrast, the highest intensity was detected in the positive control treated with differentiation medium (E, J), quite independent of incubation days. Supplementation of 5 µg/ml (C) and 10 µg/ml BSP (D) resulted in a stronger staining after four days compared with the control with standard medium (A). After seven days, their staining (5 µg/ml H, 10 µg/ml I) was only slightly stronger than the control (F) or treatment with 1 µg/ml BSP (G).

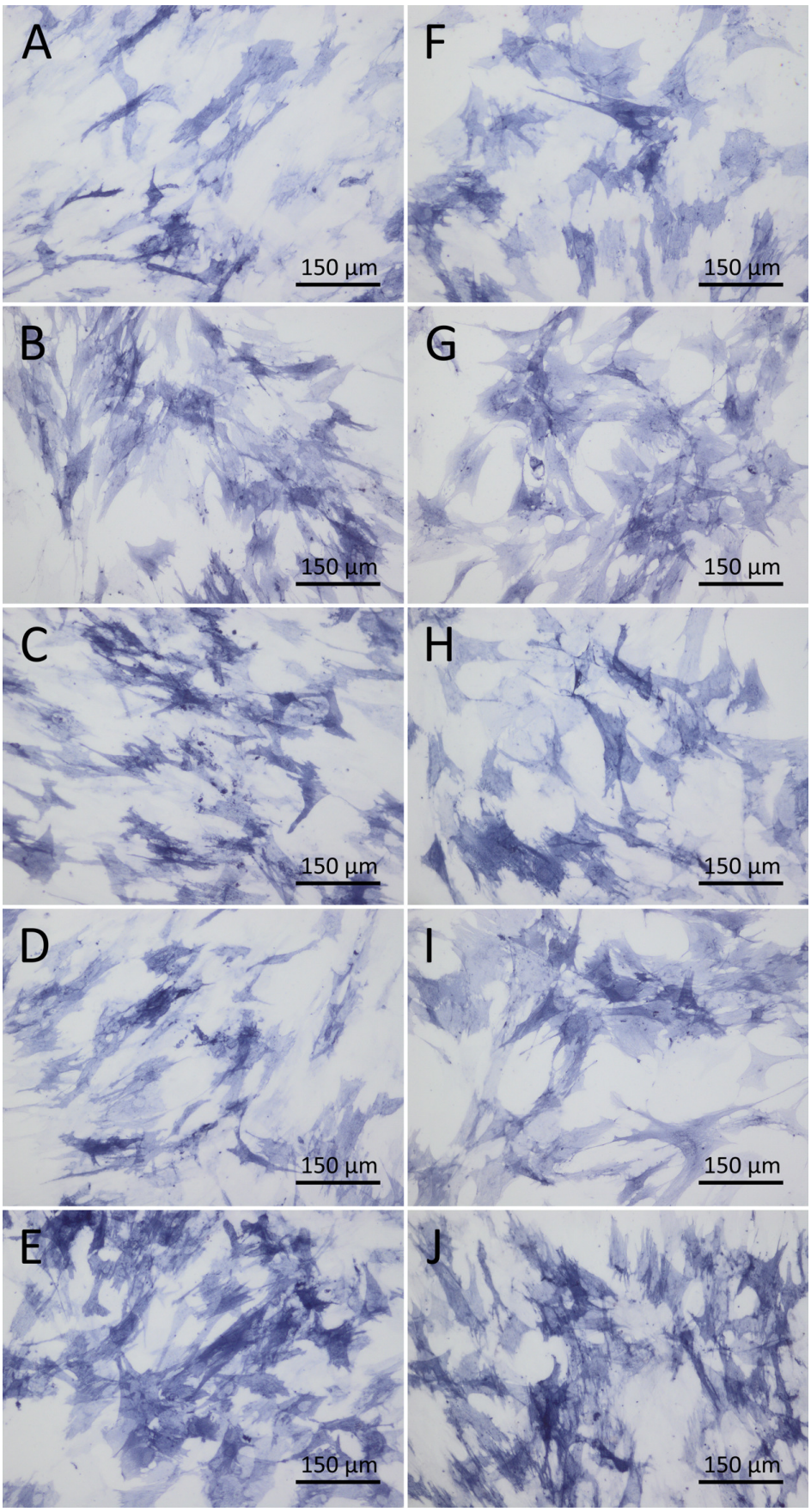

Fig. 4.3: Alkaline phosphatase staining of different treated human osteoblasts after four (A-E) **and seven** (F-J) **days.** hOBs were incubated in standard cell culture medium (A, F) as well as supplemented with 1 µg/ml BSP (B, G), 5 µg/ml BSP (C, H) and 10 µg/ml BSP (D, I). Addition of differentiation supplements (E, J) served as positive control.

Conversion of pNPP into pNP is carried out by alkaline phosphatase. Fig. 4.4 represents the quantitative analyses of ALP activity, normalised to 20,000 hOBs.

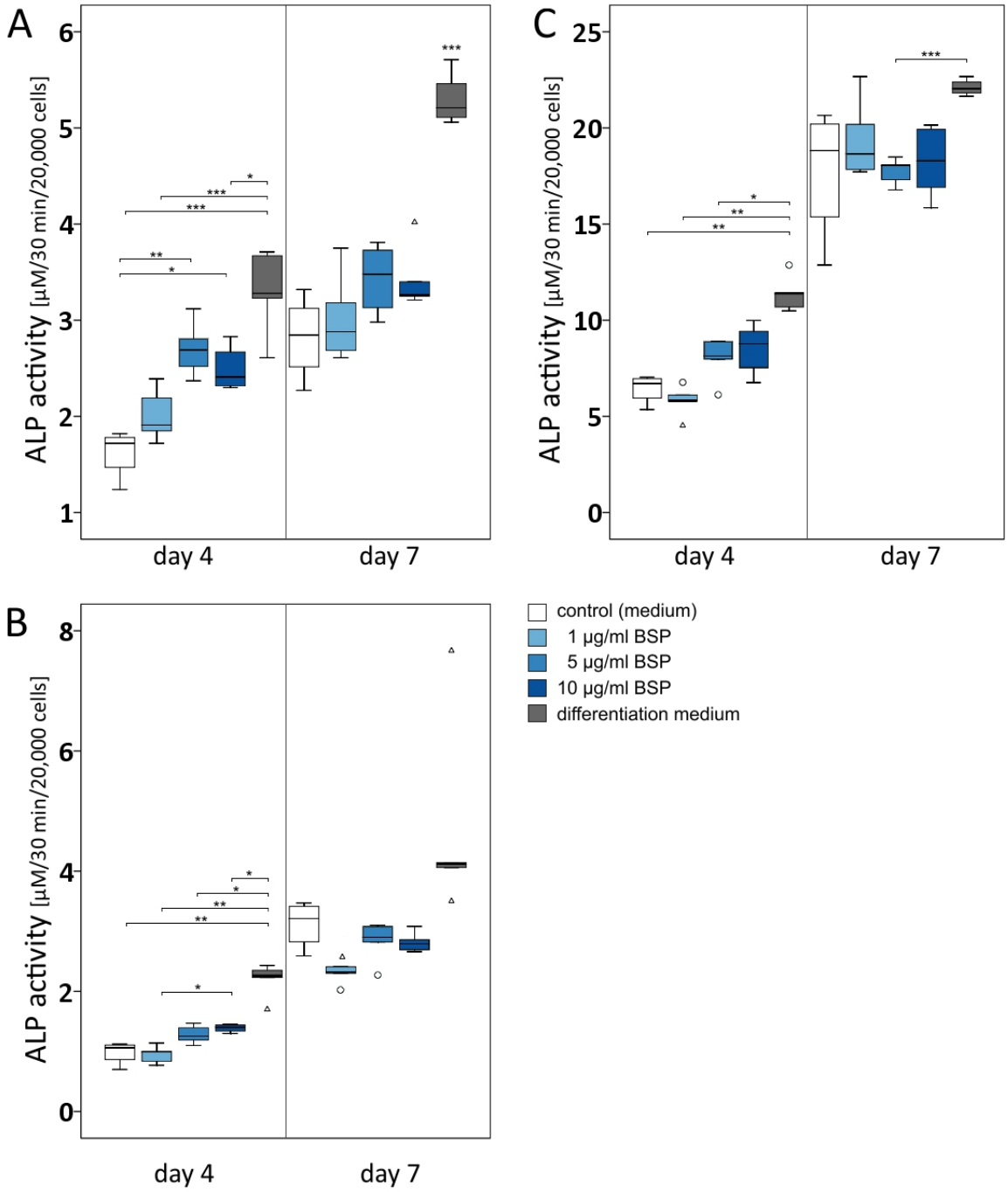

Fig. 4.4: Effect of BSP supplementation on alkaline phosphatase activity. A, B and C represent the ALP activity of human osteoblasts on days 4 and 7 of three independent experiments. Results are expressed as median and quartiles (n = 5, control n = 4). Mann-Whitney-U tests revealed significant differences (*p<0.05, **p<0.01, ***p<0.001).

Addition of differentiation supplements resulted in the highest ALP activity compared with BSP-supplementation as well as to no supplementation (see A, B and C; differences were mainly significant). Both experiments A and B showed significant differences on day 4, independent of the positive control (A - between no supplements and BSP-supplementation, B - between 1 and 10 µg/ml BSP-supplementation). All experiments (A, B and C) demonstrated

no differences between BSP-supplementation and the control (no supplements) after seven days. On day 7, significant differences existed only compared with the positive control (A, C). In general, treatment with 5 µg/ml BSP resulted in a slightly higher effect on ALP activity than the other concentrations. Nevertheless, 10 µg/ml BSP caused higher ALP activity levels than 1 µg/ml BSP.

These results reflected the findings of Gordon et al., who found that supplementation of 2 µg/ml BSP to primary rat calvaria osteoblasts showed a significant increase in ALP activity after three and five days compared with untreated osteoblast cultures. After 10 days, no significant differences were observed [133]. Additionally, Zhou et al. detected a significant ALP increase five days after seeding of MC3T3-E1 cells onto BSP-coated dishes compared with cells seeded onto uncoated dishes [134]. Division of the results into the individual experiments takes place due to usage of primary cells from different donors. As explained in the introduction, primary cells are morphologically heterogenous. Moreover, dependent on age and other factors, they are also heterogenous regarding functionality [73, 135]. This explains the huge discrepancies of ALP activity between A, B and C. The results suggested a BSP effect on ALP activity of primary hOBs only in the first few days, which ought to be enough to promote mineralisation, as seen in the following section.

4.1.3 Mineralisation

Mineralisation is an essential step during bone formation. For this purpose, the capability whether BSP facilitates the mineralisation process was examined. The rate of calcium deposition was analysed with Alizarin red staining. Areas of red stained calcium, visualised via microscopic images (see Fig. 4.5 A), were transferred into a binary picture for quantitative analysis of calcium deposits (see Fig. 4.5 B).

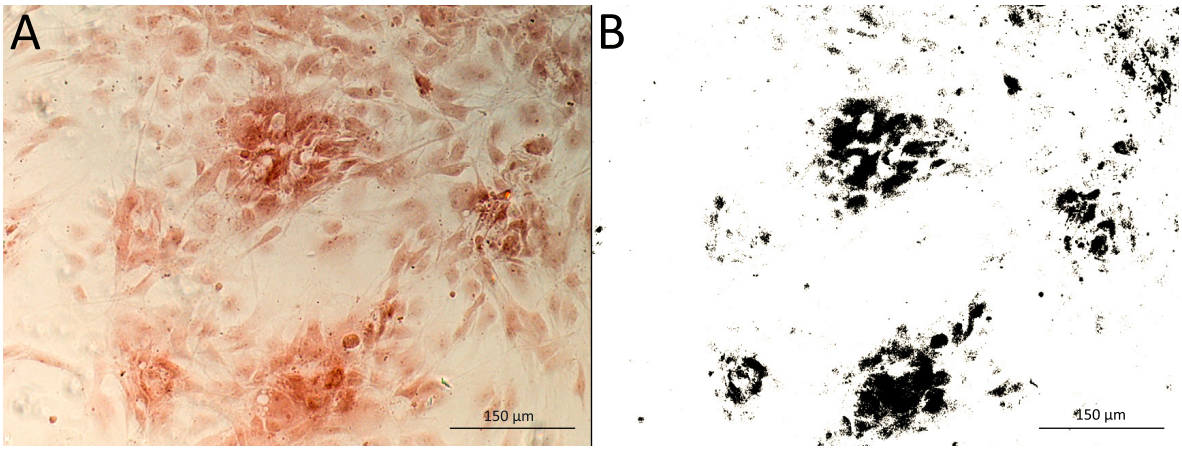

Fig. 4.5: Alizarin red staining of human osteoblasts treated with differentiation medium. Figure A shows the microscope image of Alizarin red staining, while Figure B shows the respective binary picture with calcium deposition depicted as black pixels.

Addition of dexamethasone, β-glycerolphosphate and ascorbic acid (supplements for osteoblast differentiation) resulted in the highest calcium deposition with 7.9 % (see Fig. 4.6). Differences

to all other groups were significant. Supplementation of BSP (1 µg/ml and 10 µg/ml) as well as BMP-7 (100 ng/ml) resulted in a higher calcium deposition compared with the group with no supplements. However, addition of 1 µg/ml BSP showed with 3.9 % a significant difference to the control with 1.7 % as well as to the higher BSP concentration (10 µg/ml) with 2.5 % calcium deposition. Hence, lower BSP concentrations may have a higher impact on calcium deposition.

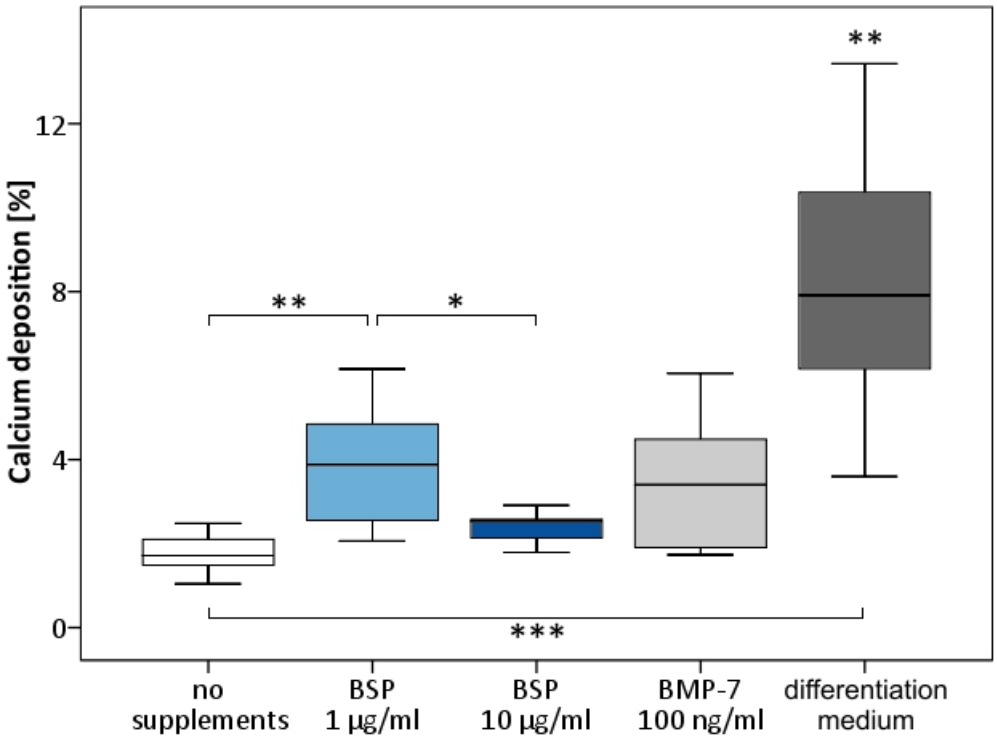

Fig. 4.6: Quantitative analysis of Alizarin red staining. Human osteoblasts were treated with different supplements and stained after 21 days with Alizarin red S. Results are represented as medians and quartiles (n = 7-15). The Games-Howell post-hoc test revealed significant differences (*p<0.05, **p<0.01, ***p<0.001).

Tye et al. examined the impact of different BSP concentrations on HA nucleation - an essential step for the mineralisation process. Minimum required concentrations for nucleation varied between nature and recombinant BSP (prokaryotic). Nature BSP showed an effect by 0.087 µg/ml BSP, while the recombinant BSP required higher concentrations (1.7 - 3.4 µg/ml) for an induction of HA nucleation [64]. In the presented results (Fig. 4.6), supplementation of 1 µg/ml recombinant BSP - a concentration within the range of the experiments performed by Tye et al. - showed promising results. However, it was not tested whether lower BSP concentrations influence mineralisation. An increase in bone nodule formation was observed in calvaria cells isolated from BSP overexpressing transgenic mice (CMV-BSP) by Valverde et al. [136]. After a two-week incubation period in osteogenic media, calvaria cells of transgenic mice showed a 2.6-fold higher number of bone nodules compared with cells isolated from wild-type mice [136]. Human MSCs seeded onto titanium surfaces with either 1 µg/ml or 10 µg/ml immobilised BSP showed an enhanced mineral bone nodule formation compared with cells seeded onto untreated titanium surfaces. Between both concentrations, no significant

differences were observed even if 10 µg/ml inclined to a higher mineralisation rate [137].

4.1.4 Immunofluorescence staining

Besides ALP activity and bone nodule formation, the effect on osteoblast markers is another way for characterising the potential of BSP supplementation. RUNX2 is an essential transcription factor involved in osteoblast differentiation. A first impression of changes in expression patterns could be achieved using immunofluorescence staining. hOBs were supplemented with BSP (1 µg/ml and 10 µg/ml) and differentiation medium. After an incubation period of 4 days, the cells were fixed, incubated with specific antibodies for antigen visualisation and dyed with Hoechst for nucleus staining.

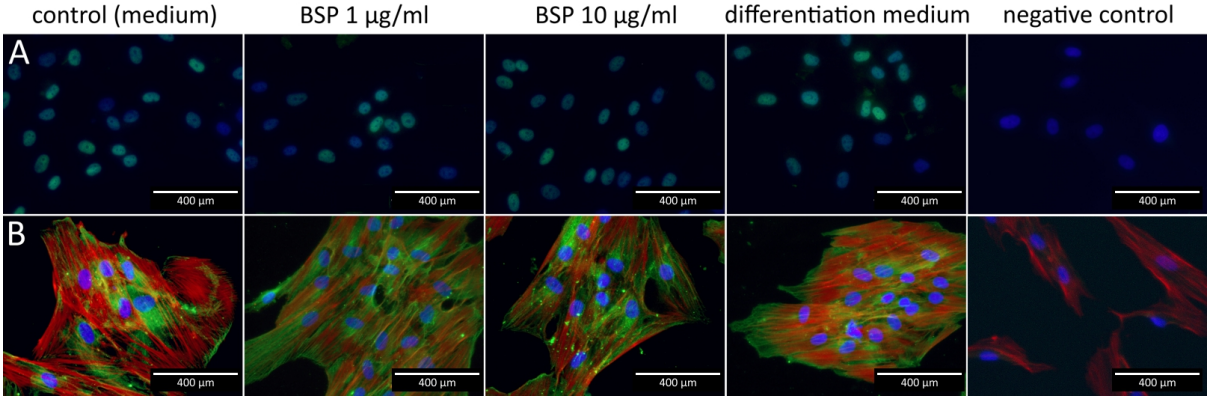

Fig. 4.7: Immunofluorescence staining of RUNX2 (A) **and ALP** (B) **after 4 days**. Merged images of nucleus staining with Hoechst (blue, A and B), RUNX2 labelling (green, A) or Alkaline phosphatase staining (green, B) and F-actin (red, B).

Fig. 4.7 represents the immunofluorescence results after a 4-day incubation period. RUNX2 (A) and ALP (B) were expressed in all four groups (control, BSP supplementation and differentiation media). As expected, the transcription factor RUNX2 was only detected in the cell nuclei, while ALP occurred in the cytoplasm located near the nuclei. No differences could be observed between the groups. However, RUNX2 expression differed from one nucleus to another. Several nuclei had a higher intensity compared with nuclei with less RUNX2 expression. Quantitative PCR analyses are required for a more accurate investigation of the marker expression at the gene level.

4.1.5 Conclusion

BSP supplementation of final concentrations in medium from 1 µg/ml to 20 µg/ml showed no cytotoxic effects. An influence on ALP expression was detectable after a 4-day incubation period with BSP-containing medium rather than the standard medium. On day 7, the effect of added BSP on ALP decreased, no significant differences were observed. Examinations of calcium deposition after three weeks showed an enhanced mineralisation caused by BSP-supplemented media. To conclude, BSP influences ALP activity in the first few days and enhances the process of mineralisation. Immunofluorescence staining with RUNX2 showed a

similar expression in both, standard and BSP-supplemented media. To specify any enhancement or decrease in hOB gene expression more precise analyses via qPCR are required. These examinations are described in the sections 4.3.3 and 4.4.3. However, previous to any experiments with BSP-coupled materials (titanium as well as CPC scaffolds), it is important to answer the following question: How to immobilise BSP onto titanium and CPCs surfaces? The next chapter will focus on this topic.

4.2 BSP functionalisation of titanium and calcium phosphate cements

First of all, the question how to immobilise BSP onto implant surfaces should be solved. Simple protein adsorption or layer-by-layer techniques are well-established methods [138, 139, 140] and are described for titanium [141, 142, 143] as well as for CPCs [144, 145, 146]. Preliminary titanium-coating experiments via BSP adsorption had shown no promising results, since most BSP amounts were released after two hours (data not shown). In contrast, the method of BSP adsorption worked in pre-tests with CPC scaffolds quite well (as seen in Fig. 3.4). Particularly, for titanium implants, another method for surface functionalisation is required. As a first step, surface activation via piranha solution was chosen, followed either by a covalent coupling technique via silanes or by a simple adsorption method.

4.2.1 Surface activation via piranha solution

Titanium implants were incubated in piranha solution - a mixture of H_2SO_4 and H_2O_2 - overnight. Implant surface modifications caused by piranha treatment were examined via XPS, in addition to light microscopy. Untreated titanium implants are coloured silver-light grey (Fig 4.8 A, B) in contrast to blue-grey coloured piranha-activated implants (E, F). Higher magnifications pointed to a more rough surface for activated Ti (G,H) compared with untreated Ti implants (C, D). However, the main surface structure remained unaffected, line hatching was detected in both implants (A-H). The colour change from grey to blue was caused by oxidation of titanium. Other studies reported this blue colour as well [147, 148]. Whether and how far changes in surface roughness infect cell behaviour should be examined in further studies (like chapter 4.3). Nevertheless, in several studies, cells seeded onto rough surfaces showed enhanced cell attachment as well as cell proliferation when compared to seeding onto smooth surfaces [149, 150, 151, 152].

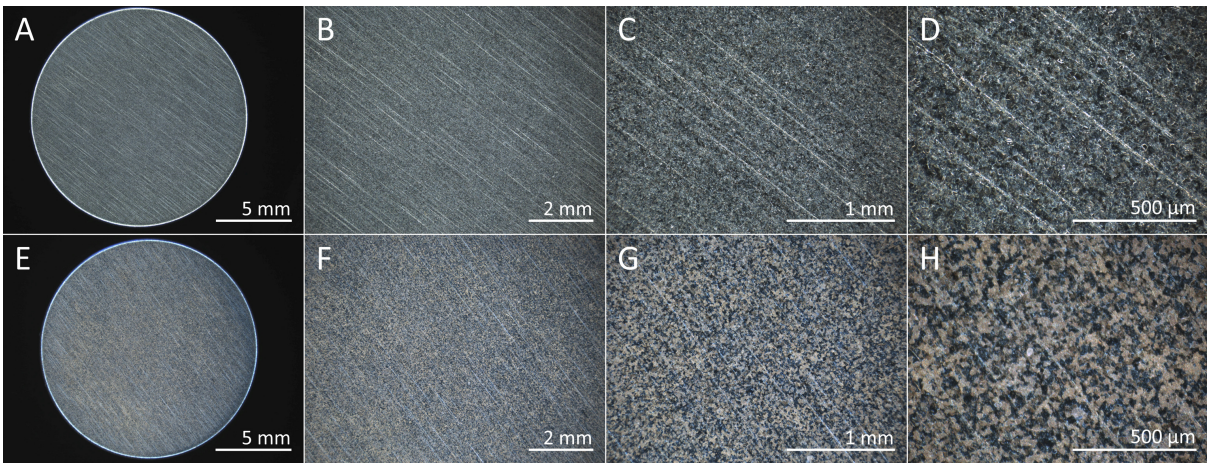

Fig. 4.8: Comparison of untreated (A-D) **and piranha-activated** (E-H) **titanium discs.** Images were acquired via light microscopy.

Table 4.1 displays the influence of piranha activation on the elemental composition of the

surface. Prior to this step, only 0.9 % titanium was detectable, besides a high carbon content (67.0 %). After surface activation, the titanium amount was increased up to 18.2 % and carbon decreased up to 25.6 %. In addition, oxygen increased from 31.1 % up to 52.3 % during this step. This could be explained by oxidation of the titanium surface. Surface contaminations with carbon, as detected by several studies [147, 111, 153], were particularly caused by organic hydrocarbon [44]. During piranha treatment, a large amount of this contamination was reduced (decrease to 25.6 %). However, carbon contamination is present on every surface [153]. Fig. 4.9 indicates the contaminations with carbon more clearly. Prior to piranha treatment, no typical titanium signal (two peaks) was visible.

Tab. 4.1: Elemental surface composition.

	Ti [%]	**C** [%]	**N** [%]	**O** [%]
Ti untreated	0.9	67.0	0.5	31.1
Ti Piranha-activated	18.2	25.6	1.1	52.3

Calculation of the Ti to O ratio resulted for untreated Ti in a ratio of 1:34.5. After piranha activation, the ratio decreased to 1:2.9, closer to the expected ratio of 1:2 for TiO_2. Nanci et al. reported a similar ratio after piranha treatment (1:3.4) [44]. Explanations for the higher than expected ratio might be adsorption of atmospheric oxygen and physisorbed water [44] as well as OH-groups [111]. The results demonstrate that piranha treatment is a crucial pre-step in order to decrease carbon contamination and activate the titanium surface. Moreover, surface activation with piranha solution facilitates controlled oxidation, an essential step for further treatments [44, 154].

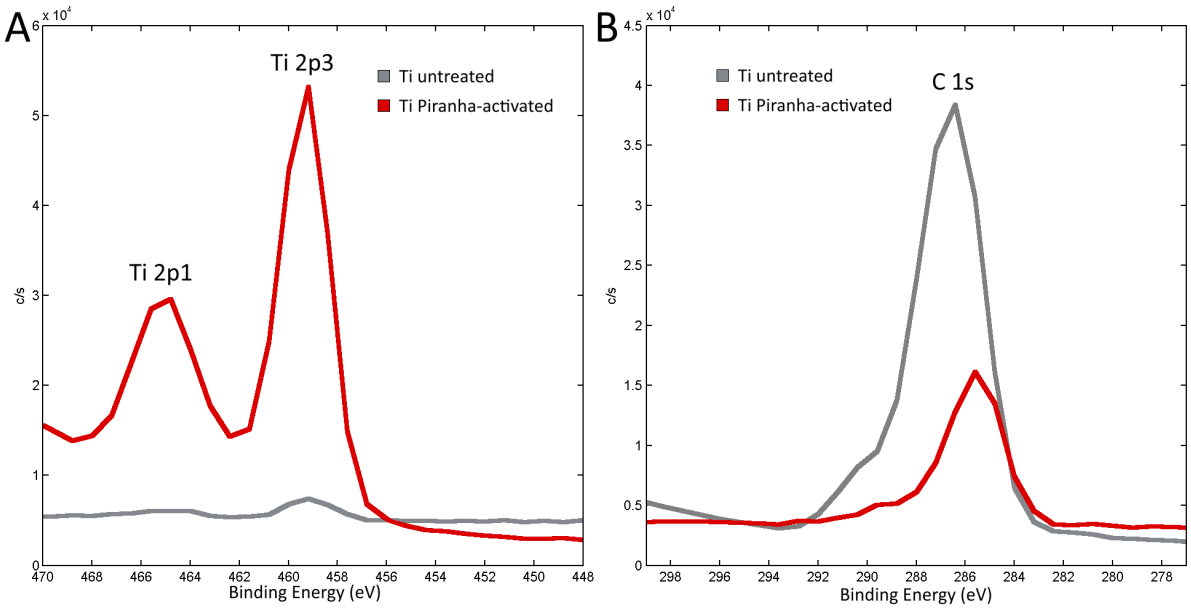

Fig. 4.9: Piranha activation changes the elemental surface composition of carbon and titanium.

4.2.2 BSP functionalisation of titanium implants

BSP functionalisation was carried out after piranha activation via simple adsorption as well as more complex covalent coupling techniques. Three different covalent coupling techniques - via APTS (3-aminopropyltrimethoxysilane), APTES and phosphate (2-aminoethyldihydrogen-phosphate) - were evaluated (data not shown). Coupling with APTES resulted in the best coating efficiency. Consequently, this method was selected for the experiments.

Qualitative examination

For qualitative evaluation of BSP coating, the N-terminal amino group of BSP was coupled with fluorescein. This method was not accomplished for covalent-coupled BSP because the free amino group is required for linking BSP to GA. Piranha activated titanium implants were coated with four different Fluorescein-marked BSP solutions (30 µg/ml, 50 µg/ml, 150 µg/ml and 230 µg/ml, respectively). Coating with the highest BSP solution (280 µg/ml) was impracticable. A decrease from 280 µg/ml to 230 µg/ml occurred due to addition of required substances for fluorescein labelling (see chapter 3). After several washing steps the residual BSP amount on the implants' surface was visualised via fluorescence microscopy. Fig. 4.10 demonstrates clearly that coating with higher BSP concentrations leads to higher fluorescence intensity. BSP coating after piranha activation showed a consistent BSP distribution on the surface. However, the surface was not completely covered with BSP (green), this may depend on the implants' surface roughness.

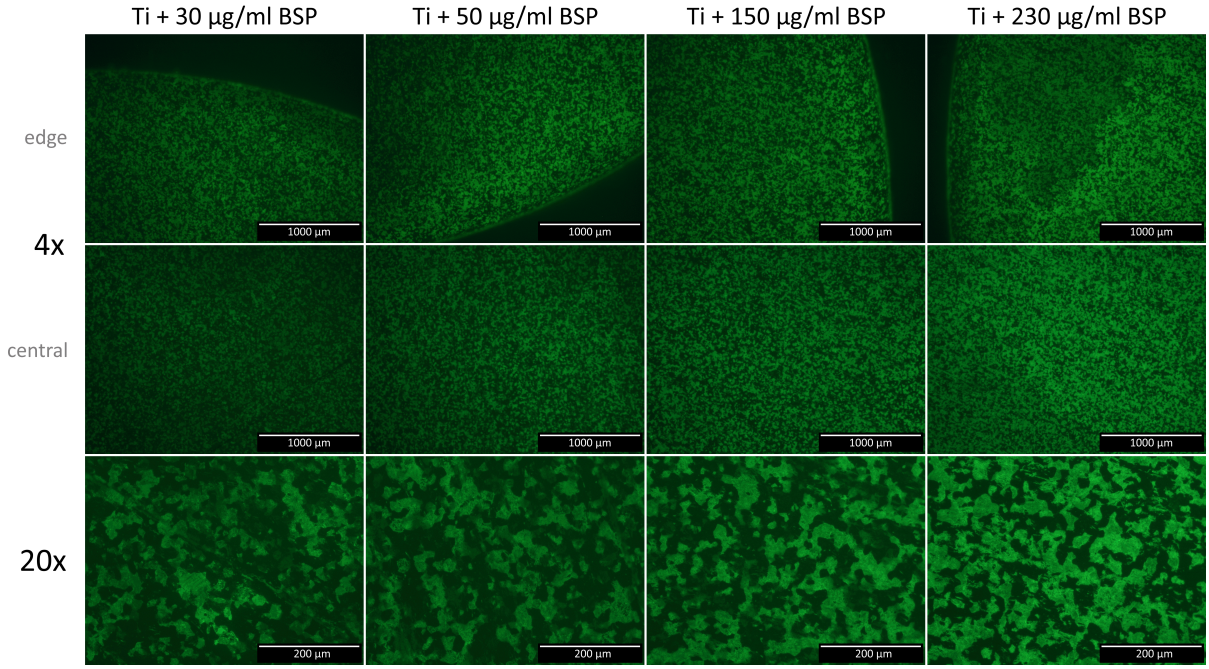

Fig. 4.10: Qualitative evaluation of fluorescein-coupled BSP coated on titanium. Activated titanium discs were incubated for 1 h with different concentrated BSP solutions, prior linked to fluorescein (green). Images were acquired with different objective magnifications (4x, 20x) via fluorescence microscopy.

Quantitative examination

Evaluation of BSP functionalisation after physisorption and covalent coupling was performed via ELISAs and XPS analyses. BSP release was calculated via ELISA measurements after every washing step (0 h, 1 h, 2 h, 24 h, 48 h and 72 h). Main BSP amounts were released during the first two steps (0 h, 1 h) caused by unbound BSP. In the following steps (2 h, 24 h, 48 h and 72 h), BSP was detected only in small quantities (data not shown). Fig. 4.11 represents the cumulative BSP release over three days. Physisorbed BSP showed a higher cumulative release compared to covalent coupled BSP. Consequently, covalent coupling resulted in higher BSP amounts remaining on the surface. However, in the groups with covalent-coupled BSP, a BSP release was detected as well. This may result from additional BSP physisorption processes, in addition to covalent coupling. Similar findings were reported by Im et al., who measured a higher amount of BSP and fibronectin on titanium surfaces coated via silanisation compared to adsorption [137]. In relation of the BSP amount used for immobilisation, coating with higher concentrations (280 µg/ml) showed less BSP release, leading to higher BSP amounts remaining on the surface compared with lower concentrations (30 µg/ml and 50 µg/ml).

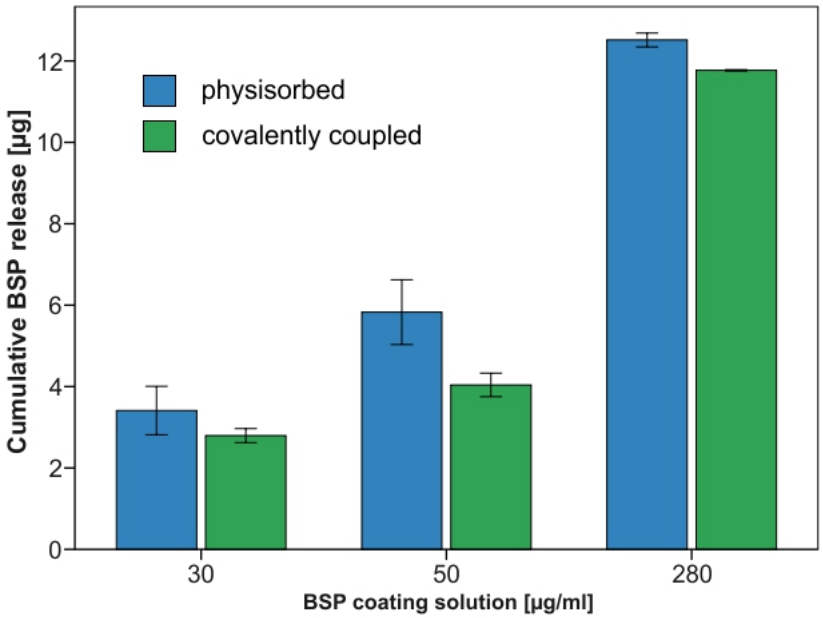

Fig. 4.11: Cumulative BSP release of BSP-functionalised titanium implants after 72 hours. Functionalisation of titanium implants was followed by several washing steps. The amount of the released BSP was measured via an ELISA. Results are expressed as mean ± SD (n = 3).

Investigations via XPS provide more information about the elemental surface composition from the outer surface. Therefore, every step of the coating process was examined for changes of the outer surface of titanium implants with special focus on the elements N, C, O, Si and Ti.

Tab. 4.2: Elemental surface composition.

	Ti [%]	**C** [%]	**N** [%]	**O** [%]	**Si** [%]
Physisorption (Ti + BSP)	12.1	41.9	3.4	40.3	1.0
Ti + APTES	10.6	42.9	2.9	38.2	4.5
Ti + APTES + GA	8.2	46.2	3.4	36.4	4.0
Ti + APTES + GA + BSP	5.8	51.9	7.1	31.3	2.9

Table 4.2 displays changes in the elemental surface composition after three coating steps, respectively and after BSP physisorption following piranha treatment. From step 1 (Ti + APTES) over to step 2 (+ GA) to step 3 (+ BSP), the Ti, O and Si amounts decrease, while C and N increase. The relative increase in atomic concentrations of C and N was used for evaluation of protein immobilising [137], whereas the N amount plays a more essential role for the quantification [155]. BSP physisorption led to an increase in N to 3.4 % (after piranha treatment 1.1 %, see Tab. 4.1) and C (41.9 % compared to 25.6 %). Figure 4.12 depicts the change in normalised nitrogen intensity during the coupling process. The lowest N intensity was detected after piranha treatment. Silanisation with APTES increases N due to its terminal amino group (see Fig. 3.3). GA contains no nitrogen and thus, the N amount of the outer surface decreases by GA linking. Finally, BSP addition resulted in a marked increase of nitrogen, indicating that protein remained on the surfaces.

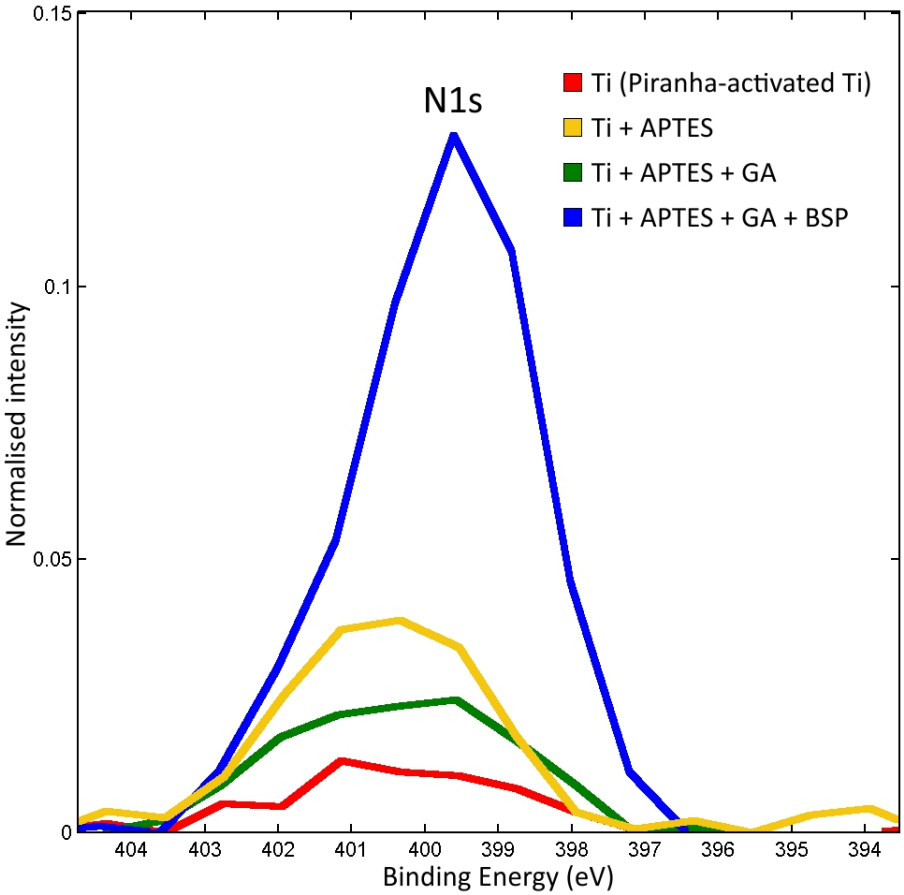

Fig. 4.12: Development of the nitrogen amount during individual steps of covalent coupling.

Calculation of N/Ti and C/Ti ratios for physisorbed (N/Ti: 0.28, C/Ti: 3.46) as well as for covalent-coupled (N/Ti: 1.2, C/Ti: 8.95) BSP reflected the findings of the quantitative evaluation via ELISA measurements. Covalent BSP functionalisation results in a greater BSP amount on the titanium surface. BSP coating of titanium implants was performed with suitable methods. However, there still remained questions regarding the protein activity after covalent coupling or storage stability. Zhou et al. tested the activity of BSP - heated (100 °C) and alkylated BSP as well as BSP free of sialic acid. The modifications showed biologic activity, thus indicating a remarkably stable structure for BSP [134]. Furthermore, the effect of immobilised BSP on hOB behaviour will be covered in section 4.3.

4.2.3 BSP functionalisation of calcium phosphate cements

In contrast to titanium implants, BSP coating via physisorption worked quite well for calcium phosphate cement scaffolds. They were incubated for 24 hours in medium without any supplements, followed by another 24-hour incubation period with BSP solution (either 50 µg/ml or 200 µg/ml). BSP physisorption was examined qualitatively as well as quantitatively.

SEM visualisation

Prior to any coating procedures, the pure scaffolds were analysed with an SEM. A detailed impression of the scaffolds microstructure was gained with magnifications from 100- to 80,000-fold, as seen in Fig. 4.13 and Fig. 4.14. Lower magnifications reflected the scaffolds' arrangement. *In vitro* discs were ordered in concentric circles. In contrast, the material for *in vivo* was arranged as a raster with interconnecting pores (see Fig. 4.13 x 100, x 250). Regions with more and less compact areas were represented in higher magnifications (x 1000, x 10,000). A further rise in magnification depicted these areas more clearly. These areas consist of small spicules between 100 and 200 nanometres in size and compact granules (see Fig. 4.14 x 50,000, x 80,000). SEM examinations of CDHA and β-TCP scaffolds by Ritz et al. detected for CDHA similar spicules, in contrast to ceramic granules reported on the β-TCP surface [156]. Ginebra et al. investigated the micro-structure during the hardening process of two α-TCP powders (Cement C and Cement F) converting into CDHA at different time points [157]. A comparison of their SEM images after 8 hours with the 10,000-fold magnifications lead to the conclusion that α-TCP particles were not yet completely transferred into CDHA during the setting in saline for 28 days. Reasons for still existing compact granules may be the initial particle size and the composition of cement powder as well as a setting time that is too short. XRD-analyses by the manufacturer (in publication) reveals the quantitative composition of CPC scaffolds. They are composed of 78 % CDHA, 12 % α-TCP, 9 % DCP and under 1 % calcium carbonate. A prolonged setting reaction may decrease the number of residual granules and lead to an increased micro-porosity; nevertheless, this might result in a reduced level of macro-porosity [110, 158]. Several studies have demonstrated enhanced protein adsorption and cell adhesion on nano-structured surfaces in contrast to micro-structures [157, 159, 160]. In addition, higher specific surface areas enhance osteoinduction [161, 162]. Nevertheless, macropores ranging

from 100 µm to 200 µm [5] are required for bone as well as vascular ingrowth [161]. Proceeding examinations will determine how far the present structure affects protein adsorption, cell behaviour and bone ingrowth.

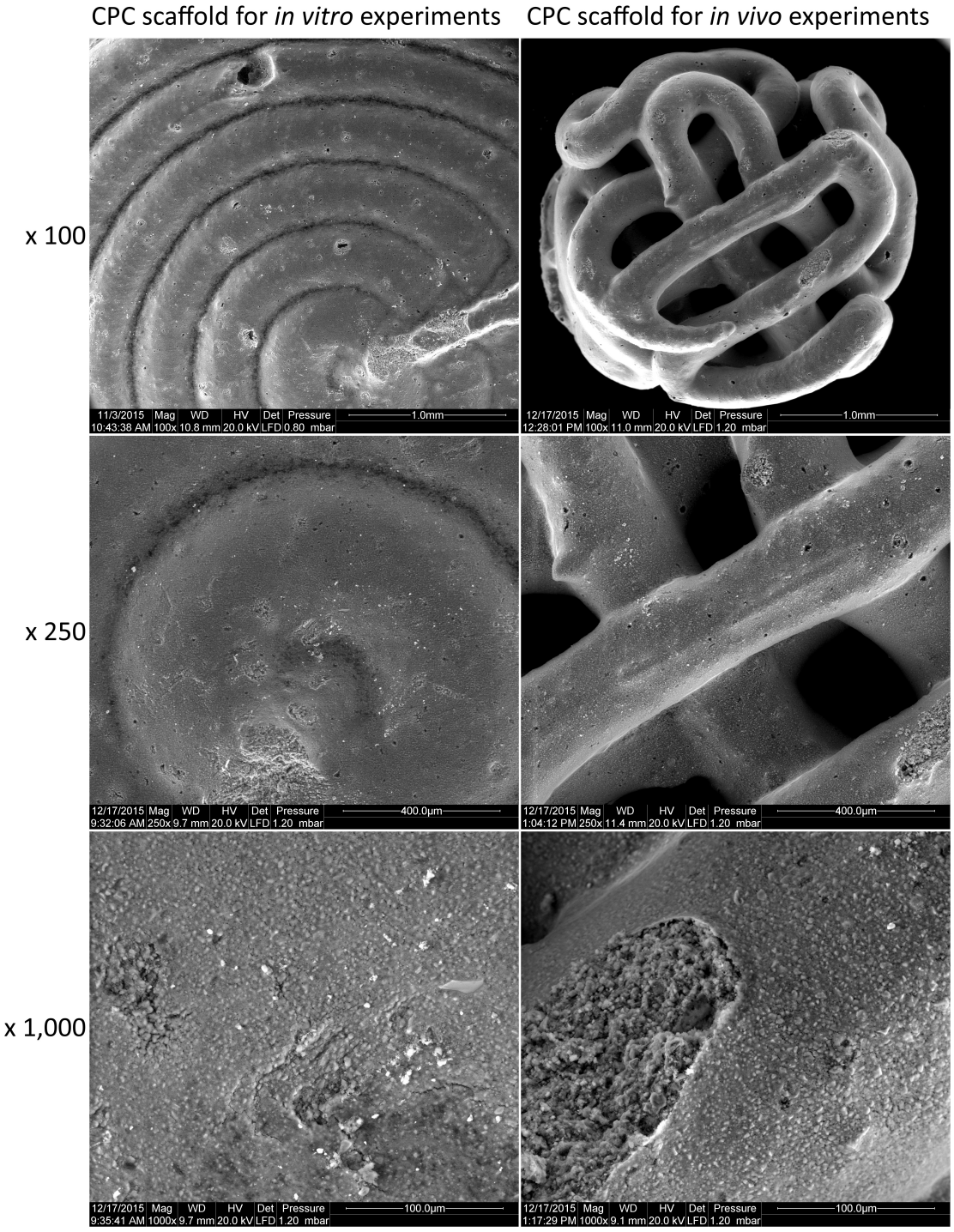

Fig. 4.13: SEM images of CPCs for *in vitro* and *in vivo* experiments with magnifications ranging from 100 x to 1000 x.

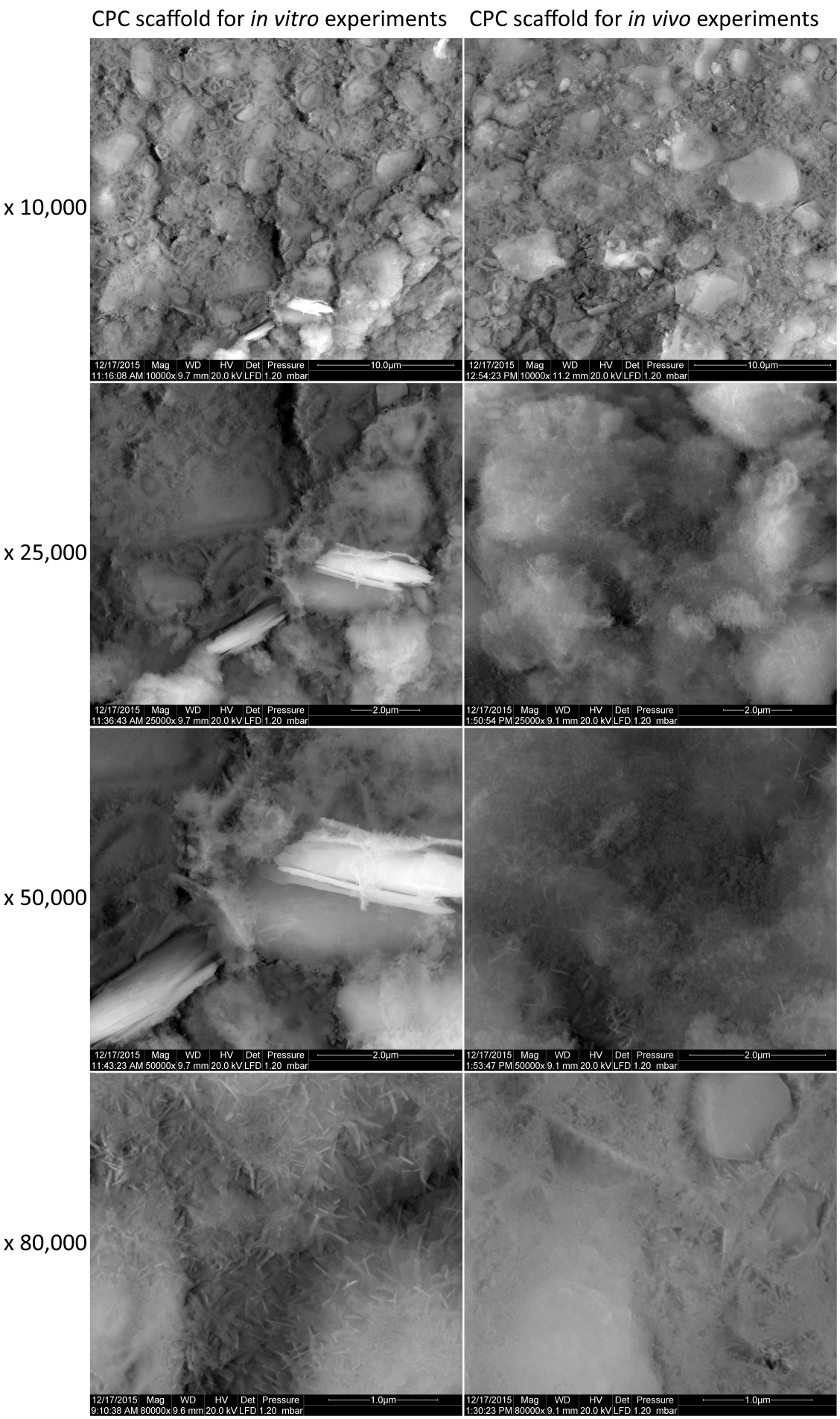

Fig. 4.14: SEM images of CPCs for *in vitro* and *in vivo* experiments with magnifications ranging from 10,000 x to 80,000 x.

Qualitative and quantitative evaluation of BSP physisorption

Qualitative evaluation of BSP physisorption occurred analogous to the qualitative adjustment of titanium implants. The bone substitutes were coated with fluorescein-linked BSP (50 µg/ml, 100 µg/ml and 200 µg/ml, respectively) for 24 hours, washed two times and visualised via fluorescence microscopy. As shown in Fig. 4.15, coating with higher BSP concentrations leads to more residual BSP amounts on the surface after several washing steps. Differences between coating with 50 µg/ml and 100 µg/ml were higher than those between using 100 µg/ml and 200 µg/ml BSP solution.

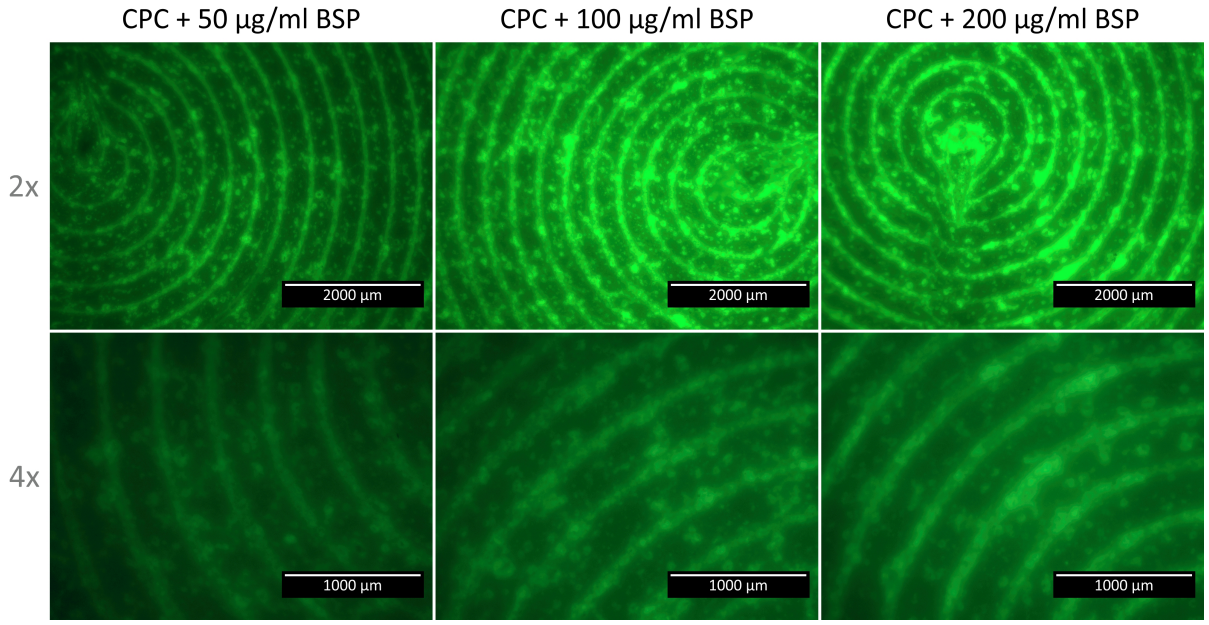

Fig. 4.15: Qualitative evaluation of fluorescein-coupled BSP coated on CPCs. CPCs were coated with different concentrated BSP solutions, prior linked to fluorescein (green). Images were acquired with different objective magnifications (2x, 4x) via fluorescence microscopy.

For quantitative coating evaluation, the scaffolds were coated with different BSP solutions (25 µg/ml, 50 µg/ml, 100 µg/ml and 200 µg/ml, respectively), followed by medium changes after several time points (0 min, 5 min, 1 h, 2 h, 4 h, 12 h, 24 h and 48 h). Desorbed BSP in the supernatant was quantified by ELISA. As shown in Fig. 4.16 A, the cumulative BSP release ranged from 0.8 µg to 28 µg. The BSP release was nearly tripled from 25 µg/ml (0.8 µg cumulative BSP release) to the 50 µg/ml group (2.5 µg), followed by a doubling to the 100 µg/ml group (4.8 µg). However, the discrepancy in the last step from 100 µg/ml to 200 µg/ml is nearly six-fold. The gradual BSP release (Fig. 4.16 B) was higher and depended on the coating concentration during the first four hours. Thereafter, the gradual BSP release was similar irrespective of the coating concentration.

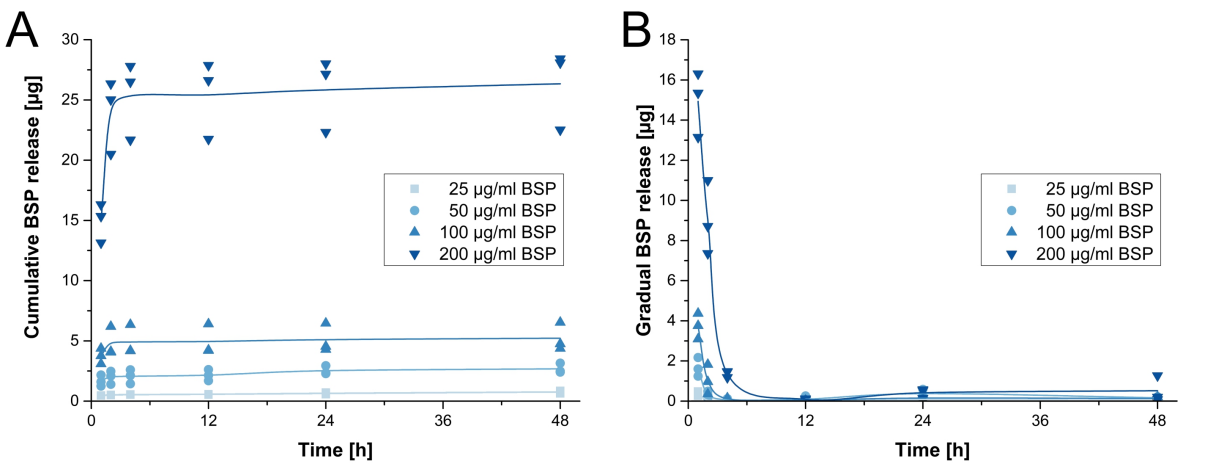

Fig. 4.16: BSP release of CPC scaffolds after BSP physisorption. Cumulative (A) and gradual (B) BSP release over 48 hours was determined via an ELISA. Results are expressed as mean (line graph) with individual data points (n = 3).

Protein coating via the simple adsorption method is one possibility for functionalisation of CPCs. Uncontrolled release and an initial burst are limitations of this method [163]. The gradual release rates during the first four hours, which were concentration dependent, indicate the release of unbound or excessive BSP. In contrast, the similar BSP release irrespective of the coating concentration demonstrates a continuous release. The nearly six-fold higher cumulative release from 100 µg/ml to 200 µg/ml might imply saturation conditions. BSA adsorption as well as incorporation into calcium phosphates resulted by Wernike et al. in a release of 55-60 % BSA and by Akkineni et al. even to a burst of 72 % BSA during 48 hours [163, 109]. A possible explanation for the continuous BSP release following the initial burst may lie by BSP itself. BSP contains polyglutamic acid sequences, which are responsible for its HA-binding capability [64, 164]. Hence, this certain property may occur in improved adsorption rather than the adsorption of proteins without HA-binding affinity. Overall, qualitative and quantitative investigations postulated physisorption as an appropriate method for BSP coating of CPC scaffolds.

4.2.4 Conclusion

Effective methods for BSP immobilisation of the two materials were presented in this chapter. BSP functionalisation of titanium implants and CPC scaffolds is feasible. Titanium implants require a surface activation via piranha solution prior to the coating procedure. BSP immobilisation on titanium was achieved via simple protein adsorption and covalent coupling via silanes. The latter method resulted in higher BSP amounts remaining on the surface. Physisorption displayed satisfactory results for BSP functionalisation of CPCs, and consequently, there was no need to implement another coating procedure. Independent of methods and materials, coating with higher concentrated BSP solutions demonstrated a better outcome. The question dealing with to what extent BSP-functionalised materials effect hOB behaviour is covered in the next two chapters.

4.3 Evaluation of BSP-modified titanium implants

This section focuses on BSP modification of titanium, which, as explained in the introduction, is one of the most used implant materials in orthopaedics and trauma surgery [5, 15, 20]. The effects of additional BSP modification were examined via cell viability, morphology and differentiation analyses.

4.3.1 Cell viability

Cell viability of hOBs on titanium with different BSP concentrations was examined with the alamarBlue® viability assay. Measurements were performed on days 1, 4, 7, 10, 12 and 14 to indicate the influence of BSP functionalisation on cell proliferation over a period of two weeks.

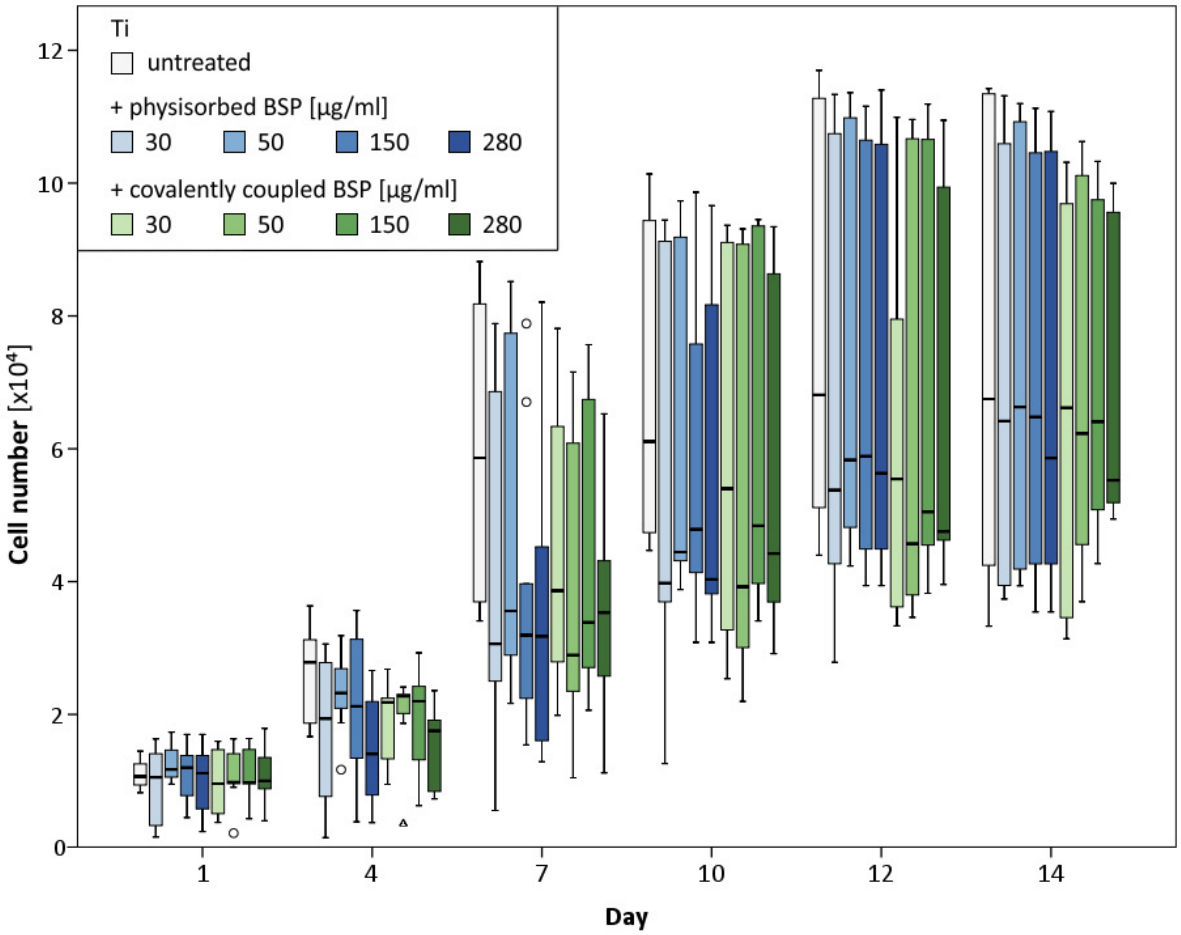

Fig. 4.17: Cell viability of hOBs seeded onto various modified titanium surfaces for 14 days. Results are expressed as medians and quartiles (n = 9).

Cell viability analyses revealed no significant differences between hOBs seeded onto untreated titanium and BSP-functionalised titanium (Fig. 4.17). However, despite nearly equal cell numbers of roundabout 1x10^4, hOBs proliferate faster on untreated titanium surfaces. Since day 4, the median was higher compared with those of BSP-modified surfaces. The greatest discrepancy occurred on day 7, when the median of untreated titanium was minimum 35 % (30 µg/ml covalent coupled BSP) and maximum 50 % (50 µg/ml covalent coupled BSP) higher.

After 14 days, this tendency was nearly equalised. Between various used BSP concentrations no obvious tendencies were observed - only after 14 days, the highest concentrations (280 µg/ml) lagged slightly behind. Considering the equal cell numbers on day 1, cytotoxic effects of BSP can be excluded. This was confirmed by other cytototoxic and viability analyses concerning BSP in supplemented form (described in section 4.1.1) or BSP immobilised onto titanium implants [112]. Therefore, the delayed cell proliferation compared to untreated titanium may be caused by an effect of BSP on cell differentiation. This correlates with examinations of Valverde et al. using calvaria cells isolated from BSP overexpressing mice. They had a lower proliferation rate than cells isolated from wild-type mice over eight days - this is in contrast to an enhancement in cell differentiation [136]. Authors of several studies have demonstrated that any increase in osteogenic activity is correlated to a decrease in cell proliferation [165, 166, 143]

4.3.2 Cell visualisation

Besides cell viability examinations, the effect on hOB cell morphology and cell attachment, caused by different modified titanium discs, provides more information about biocompatibility. Therefore, eGFP-transduced hOBs were seeded onto untreated, piranha-activated and BSP-functionalised (via physisorption as well as covalent coupled) titanium surfaces. Cell morphology was visualised with a CLSM after one, three and five days.
On day 1, more osteoblasts were attached in groups without BSP (Ti untreated, Ti piranha activated). Surface functionalisation with BSP resulted in less cell attachment. Comparing both methods, surfaces with physisorbed BSP led to better hOB adhesion than surfaces with covalent-coupled BSP. As shown in Fig. 4.18, more hOBs on covalent-coupled BSP surfaces showed a spherical shape compared with the other groups. Cell confluence increased in all groups from day 1 till day 5. However, cell confluence was reduced on BSP- modified surfaces. Previous examinations of cell adhesion onto BSP-modified titanium implants reflected these findings. Osteoblast adhesion was reduced on BSP-functionalised surfaces. Moreover, surfaces with covalent-coupled BSP showed significantly lower cell adhesion during the first few hours [112]. Chan et al. modified polymers with BSP. MC3T3-E1 cells, which were seeded onto those BSP-functionalised polymers, showed no effects on cell proliferation [167]. These results correlate well with the ones described above (see section 4.3.1). However, their findings regarding cell attachment and cell spreading contradict the results in Fig. 4.18. MC3T3-E1 cells seeded onto BSP-modified polymers showed a significantly increased cell attachment compared with unmodified as well as albumin-modified polymers. Furthermore, these cells showed already after two hours spreading cells on BSP-modified surfaces, in contrast to rounded and minimal spreading cells on unmodified polymers [167]. Albeit, primary human osteoblasts were used for this examination, these contradictory findings cannot be explained using different cell types. On the contrary, these findings may depend on the material or the coating procedure. Byzoza et al. blocked cell adhesion mainly by adding an RGD-containing peptide [168]. Therefore, the decreased cell attachment could be explained by BSP released from the titanium surface. Both physisorption and covalent coupling showed a BSP release over

three days (see section 4.2.2), while coating via physisorption resulted in a higher release. However, this could not explain why covalent-coupled BSP resulted in less cell attachment and more rounded morphology compared with hOBs on implants with physisorbed BSP. A probable explanation for this difference might be the shielding effect caused by the alkyl silane layer [44, 169].

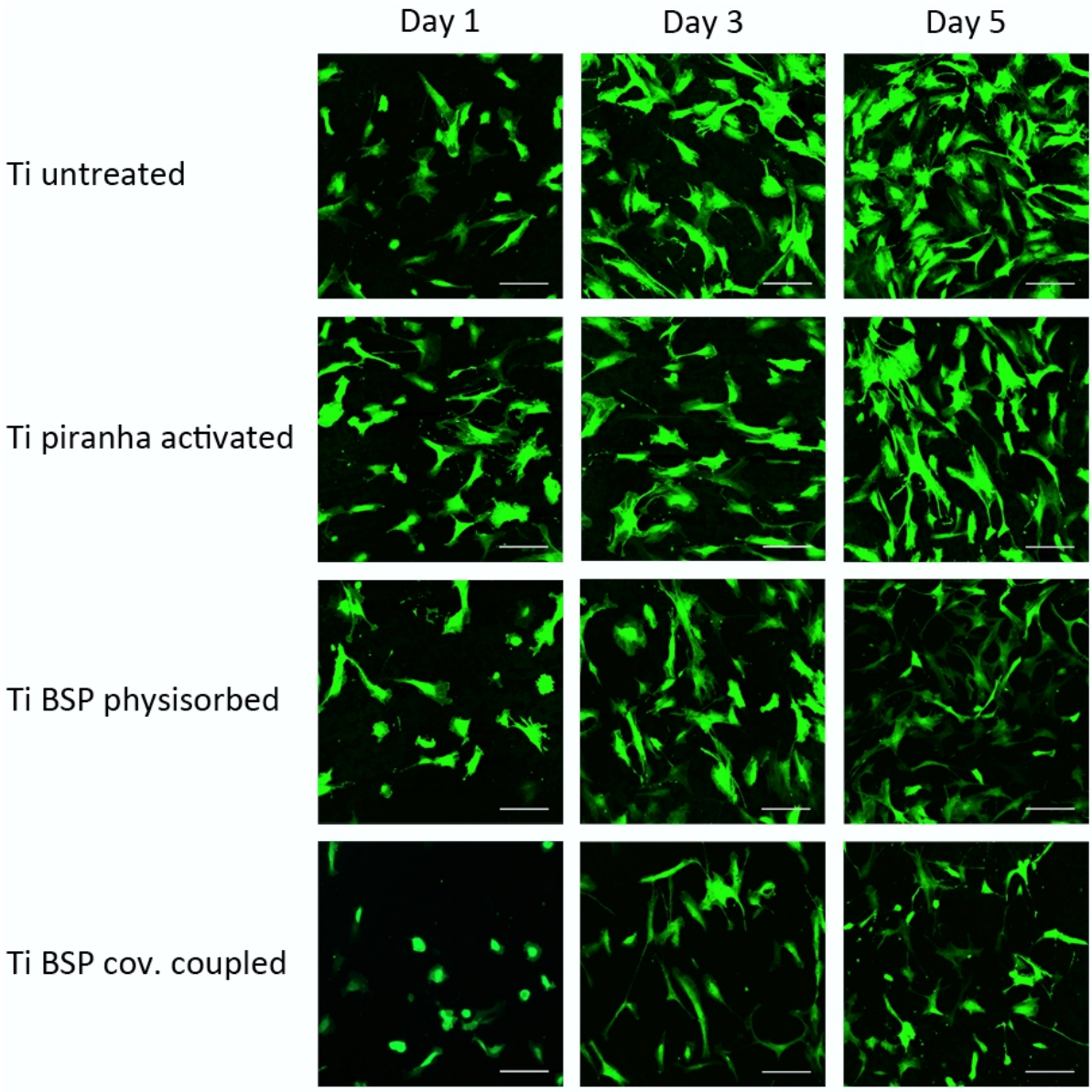

Fig. 4.18: Cell morphology of primary human osteoblasts seeded on different modified titanium discs after one, three and five days (scale bars = 150 µm). This figure was first published in PlosONE [112].

4.3.3 Gene expression analyses

Effect on hOB gene marker expression due to BSP functionalisation was examined by qPCR. Human osteoblasts were seeded onto different modified titanium surfaces, followed by cell harvesting after one, four and seven days of incubation. RNA was isolated, transcribed into cDNA and the expression rates of ALP, Col1, OPN, RUNX2, SP7 and SPARC were calculated via qPCR. For evaluation, the expression rates were compared with untreated titanium (relative expression of untreated titanium = 1). Besides untreated titanium, piranha-activated titanium implants and implants with physisorbed BMP-7 (100 ng/ml) were used as controls.

On day 1, hOBs seeded onto BSP- and BMP-7-functionalised titanium surfaces displayed no significant differences in **ALP** expression compared with untreated titanium (Fig. 4.19 A). Both covalent-coupled BSP-groups (30 µg/ml and 280 µg/ml) as well as the group with physisorbed BMP-7 showed a significant decrease on day 4 and day 7. However, osteoblasts seeded onto titanium with 30 µg/ml physisorbed BSP resulted only on day 4 in a significant decrease of ALP mRNA expression. Both physisorbed BSP-groups showed on day 7 a reduced, though not significant, median compared to the untreated control. No differences occurred in gene expression of cells seeded onto piranha-activated surfaces compared with seeding onto untreated titanium surfaces despite a trend of higher medians.

The **collagen** expression was significantly reduced in all BSP-groups as well as in the group with physisorbed BMP-7 on day 1 (Fig. 4.19 B). During the observation period of seven days, no changes were observed in the BMP-7 group. This contrasts with BSP-modified titanium surfaces, which resulted, with one exception, in a similar hOB gene expression compared with those seeded on untreated titanium after day 4 and day 7. The only exception is a significant decrease in Col1 expression of osteoblasts seeded on titanium with 30 µg/ml physisorbed BSP after seven days.

The mRNA expression of **SPARC** was significantly reduced in the group with physisorbed BMP-7 on days 4 and 7 (Fig. 4.19 C). No significant differences were observed with BSP-functionalised surfaces compared to untreated titanium. On day 1 all BSP-groups resulted in a lower median; it was the same on day 4; and finally, in the groups with covalent-coupled BSP an increased median on day 7 was found compared to untreated titanium.

In general reflection of **SP7**, **RUNX2** and **OPN** expressions, BSP-functionalisation, led besides a decrease after one day, to an increased gene expression after day 4 and day 7, respectively. The latter increase was not as high as observed after day 4 (Fig. 4.20). The transcription factors RUNX2 and osterix (SP7) are mainly involved in osteoblast differentiation. Despite the general trend, significant differences were observed in SP7 after day 1 and day 4. On day 1, the SP7 expression was significantly reduced in the groups with physisorbed BMP-7 and BSP physisorption with the high concentration, in contrast to a 1.5-fold expression in the group with covalently-coupled BSP (high concentration) after four days (Fig. 4.20 A).

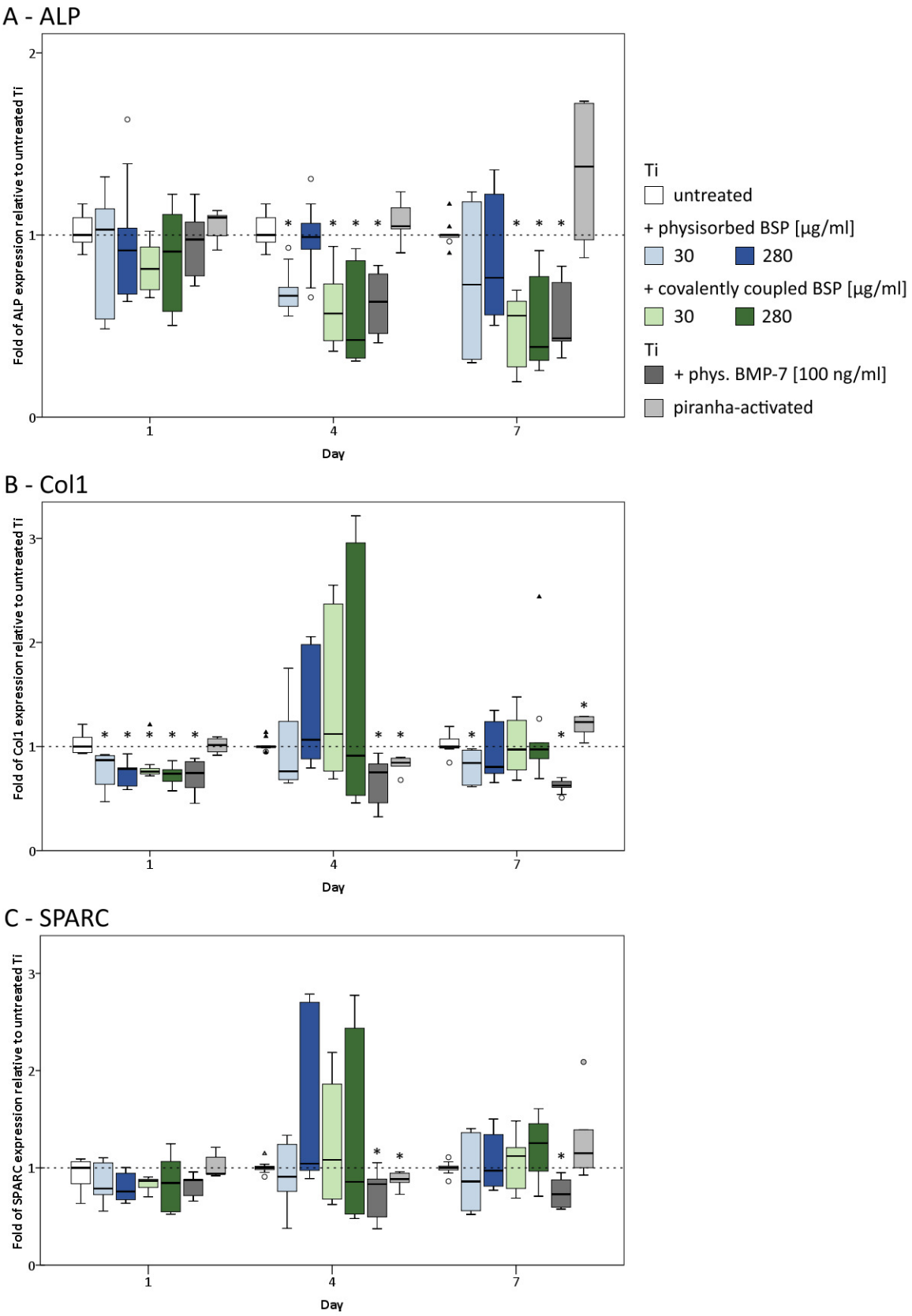

Fig. 4.19: Relative alkaline phosphatase (A)**, collagen 1** (B) **and osteonectin** (C) **expression of hOBs seeded onto different modified titanium implants.** Gene expression rates were compared with untreated titanium discs (gene expression = 1). Results are expressed as median and quartiles (n = 9, Ti piranha-activated n = 6). Mann-Whitney-U tests revealed significant differences (*p<0.05).

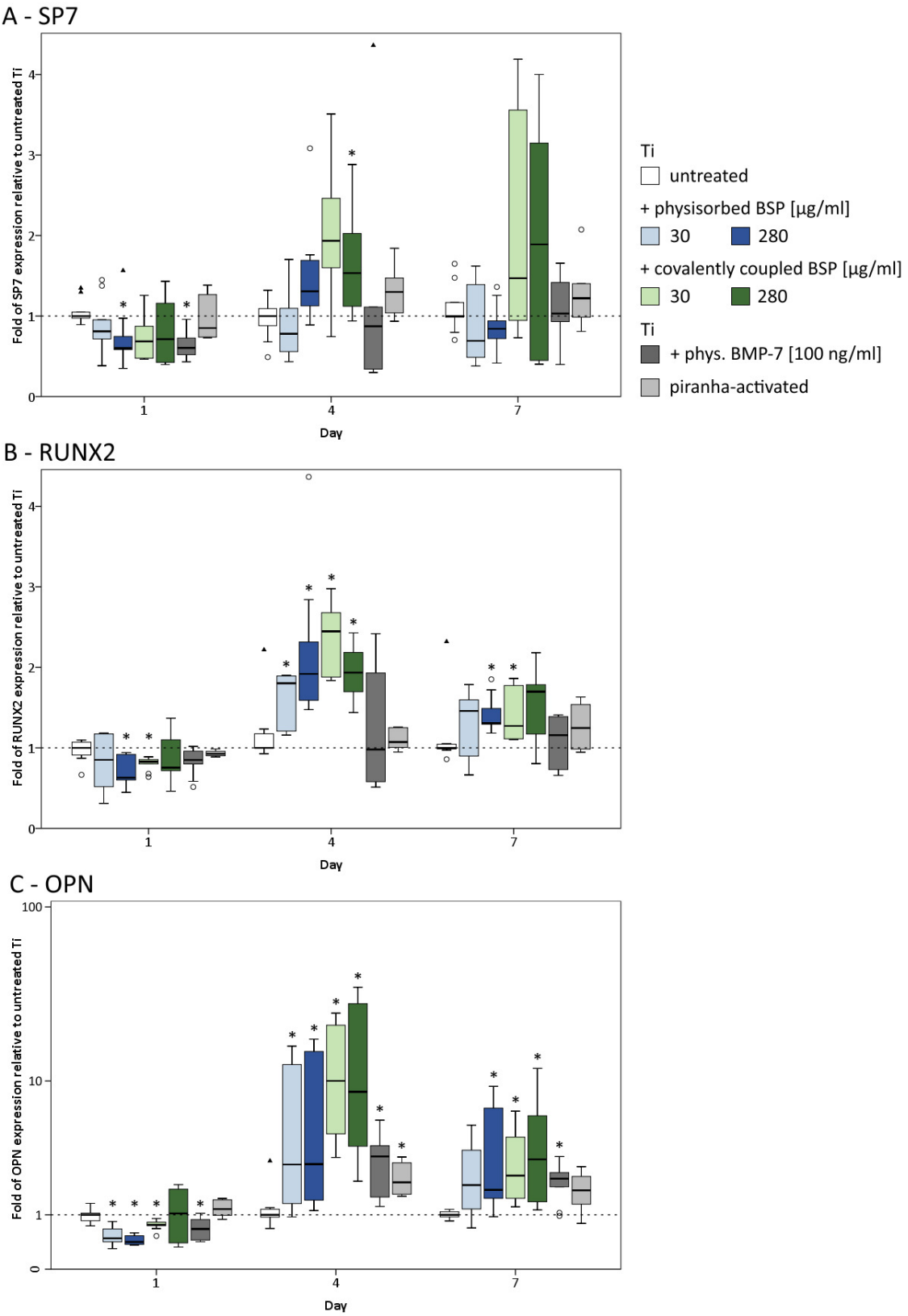

Fig. 4.20: Relative osterix (A)**, RUNX2** (B) **and osteopontin** (C) **expression of hOBs seeded onto different modified titanium implants.** Gene expression rates were compared with untreated titanium discs (gene expression = 1). Results are expressed as median and quartiles (n = 9, Ti piranha-activated n = 6). Mann-Whitney-U tests revealed significant differences (*$p<0.05$).

In particular, the general trend was statistically significant in RUNX2 expression of osteoblasts seeded on two BSP-modified implants (Ti + 280 µg/ml physisorbed BSP; Ti + 30 µg/ml covalently coupled BSP). The reduced gene expression on day 1, was followed by an enhanced relative expression on day 4 (1.9-fold; 2.5-fold) and day 7 (1.3-fold; 1.3-fold). The other BSP-functionalised groups (Ti + 30 µg/ml physisorbed BSP; Ti + 280 µg/ml covalently coupled BSP) resulted in a significantly increased RUNX2 expression on day 4 (Fig. 4.20 B) as well. Osteoblasts seeded onto BSP- (except Ti + 280 µg/ml covalently coupled BSP) and BMP-7-modified surfaces showed a significant decrease in OPN gene expression on day 1. A significant increase in OPN expression was observed after four days as well as after seven days in mostly all BSP- and BMP-7 modified groups. As shown in Fig. 4.20 C, the maximum effect on hOB gene expression was detectable on day 4, with nearly a 10-fold increase in OPN expression.
Particularly, the decrease in gene marker expression in BSP-modified groups on day 1 (Col1, OPN, RUNX2, SP7, SPARC) could be explained by lower cell attachment caused by BSP (as shown in section 4.3.2) - this may have resulted in less cell interactions. Titanium, on its own, increased, for example, RUNX2 and SP7 gene expression [170]. These initial differences were compensated until day 4. Enhancement of RUNX2 and SP7 gene expression caused by BSP contributed to several findings in the literature [133, 137, 171]. The observation of higher RUNX2 and SP7 levels on day 4 compared with those on day 7 are consistent with the findings of Gordon et al. [133]. Supplementation of 2 µg/ml BSP to primary rat calvaria osteoblasts showed a significant increase in SP7 and RUNX2 gene expression after day 3 and day 5 compared with those in untreated osteoblast cultures (more than eight-fold on day 5). After 10 days, no significant differences were observed [133]. In addition, enhanced relative RUNX2 and SP7 mRNA expression was detected in human MSCs seeded onto Ti surfaces functionalised with BSP by Im et al. [137]. A peak in RUNX2 expression was detected on day 10 (more than a five-fold increase) in contrast to a continuous increase of SP7 expression from day 1 to day 28 (increase more than 20-fold) [137]. These studies showed a higher x-fold increase in RUNX2 and SP7 gene expression (more than five-, eight- or 20-fold) compared to the highest relative mRNA expression above (2.5-fold for RUNX2). Reasons for the lower influence on relative gene expression could be explained by using primary osteoblasts instead of MSCs, as used by Im et al. [137]. Moreover, Gordon et al. as well as Im et al. boosted cell differentiation by adding supplements like ascorbic acid, β-glycerol phosphate and dexamethasone. Finally, they calculated their gene expressions relative to the control on the first day [133, 137]. Here the gene expression was referred to the mRNA expression on untreated titanium at the same day. Overall, BSP coating of titanium implants via physisorption as well as covalent coupling techniques, increased osteoblastic differentiation, particularly after four days. Covalent-modified surfaces displayed a greater effect on osteoblast differentiation compared to implants with physisorbed BSP. Effects, depending on different concentrations, were observed for physisorbed BSP only on day 4. Coating with a 280 µg/ml BSP solution displayed higher gene expression rates of ALP, Col1, SPARC, RUNX2 and SP7 compared with those of the lower concentration. However, no tendencies were observed after

seven days. Modification via covalent coupling showed on day 4 a tendency for the lower BSP concentration (particularly for ALP, RUNX2 and SP7 mRNA expression). This contrasts with the findings on day 7, which indicate a higher effect by coating with 280 µg/ml BSP (RUNX2, SP7, SPARC).

4.3.4 Conclusion

Both covalent coupling and physisorption of BSP are suitable coating procedures for titanium implants, resulting in similar effects on hOB behaviour. BSP functionalisation of titanium implants displayed for seeded hOBs a trend to slower cell proliferation as well as reduced cell spreading and cell attachment. Significant enhancement of osteoblast gene expression was observed for OPN and RUNX2 on day 4 and day 7 respectively. In addition, an increase in SP7 mRNA expression was observed without significance. Titanium implants with physisorbed BSP resulted in better cell spreading and hOB attachment. In contrast, covalently modified surfaces showed a greater impact on mRNA expression. Since physisorption is a simpler and cheaper method with similar effects on gene expression, it represents the preferential coating method.

4.4 Evaluation of BSP-modified calcium phosphate cements

Biomaterials constitute one approach solving the disadvantages of autogenous bone grafting. A suitable bone substitute material requires osteoconductive as well as osteoinductive properties. The following section presents the effects of BSP-functionalised calcium phosphate cement scaffolds on osteoblast behaviour.

4.4.1 Cell viability

Primary hOBs ($5x10^4$) were seeded onto uncoated as well as BSP-coated (50 µg/ml and 200 µg/ml) scaffolds. On days 3, 5, 7 and 10, cell viability was measured by the alamarBlue® assay. The number of viable cells was calculated via fluorescence intensity and a standard curve.

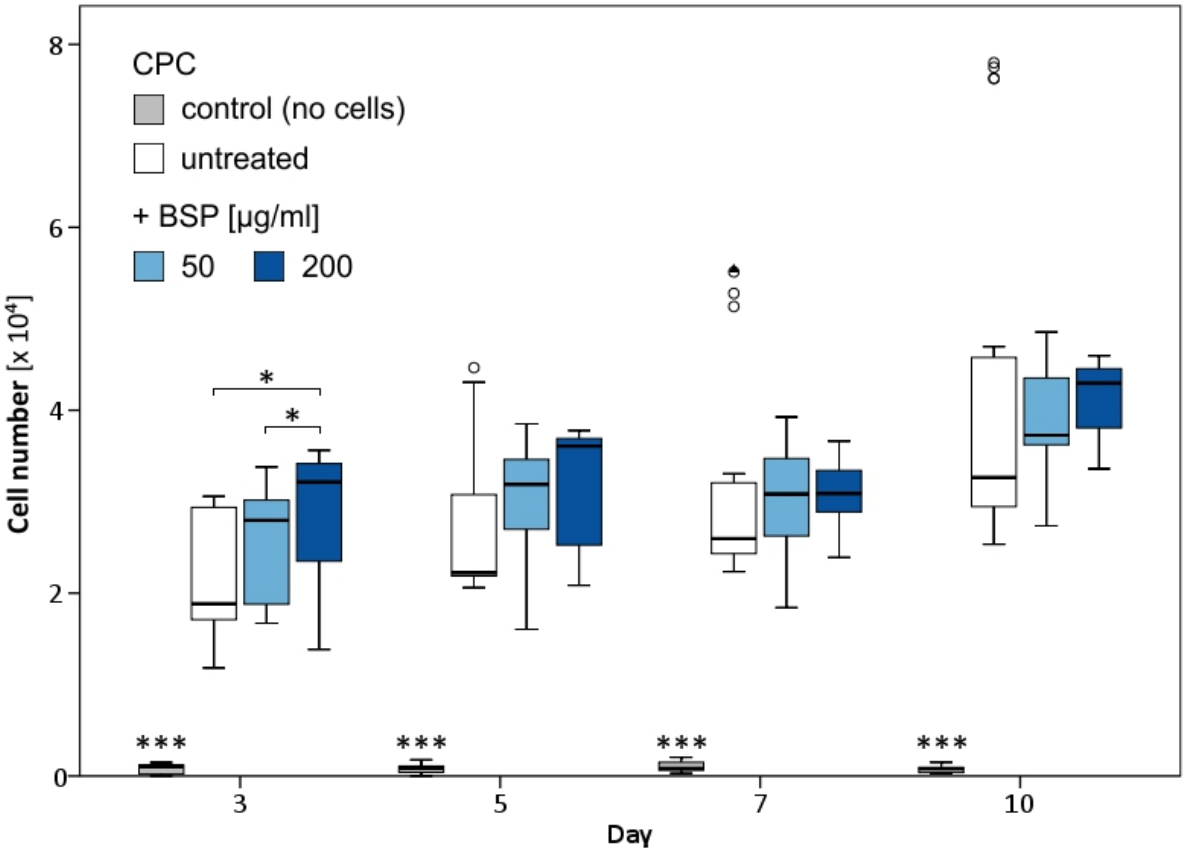

Fig. 4.21: Cell viability assay of human osteoblasts. Human osteoblasts were seeded onto uncoated and BSP-coated (50 µg/ml and 200 µg/ml BSP-solution) scaffolds. Analysis of cell viability was performed on days 3, 5, 7 and 10 with the alamarBlue® assay. Untreated scaffolds without cells served as negative control. Results are expressed as median and quartiles (n = 20). Mann-Whitney-U tests revealed significant differences (*$p<0.05$, ***$p<0.001$).

As depicted in Fig. 4.21, only a slight increase in cell proliferation was detectable between day 3 and day 10 in all groups. A higher cell number on BSP-coated scaffolds than on uncoated scaffolds was shown on all the days. Moreover, coating with the higher BSP concentration

resulted in a higher cell number compared to the lower concentration. However, significant differences between those groups existed only on day 3. After five days of incubation, the differences were equalised and showed no significant differences. Cell numbers of the control (pure scaffold, no seeded cells) is close to zero. Therefore, an interference of CPC itself along with the alamarBlue® solution can be excluded. Having a closer look at cell numbers during the 10-day observation period, the marginal cell number ranged from nearly $2x10^4$ to $4x10^4$ cells. Considering the initial number of seeded cells ($5x10^4$), the seeding efficiency was poor. These results are in accordance with Lode et al., who reported, after seeding hMSCs on equivalent scaffolds, a prolonged lag phase until 14 days [110]. Several studies have described a delayed cell proliferation during the first few days after seeding cells on similar scaffolds [172, 173]. In accordance with the results for titanium implants (see section 4.3.1), BSP coating showed no positive influence on cell proliferation - this was also confirmed in other studies [112, 136]. Since the low proliferation rate in our study could be observed independently from BSP coating, the material itself may have caused the above-mentioned effects. This leads to two questions: First, why does the material itself cause delayed cell proliferation? And second, as BSP alone indicates no positive effect on cell proliferation, why did we see significantly higher cell numbers dependent on BSP concentration on day 3? Besides an increase in cell differentiation [165, 173], possible explanations for the delayed proliferation may be the rough surface of the material [174, 175, 176] or the removal of calcium ions out of cell culture medium due to calcium-deficient materials [110, 173, 177]. The latter explanation may be only relevant *in vitro* due to small medium volumes. Besides cell growth and proliferation, the calcium content is further essential for cell attachment, which is mediated over integrins or cadherines. Low calcium conditions lead to a loss of cadherine functions [177], which may be, besides surface roughness, accountable for the modest initial cell numbers. This could answer the second question as well. BSP coating may compensate the effects of the material surface and may lead due to its RGD-domain to a raised cell attachment via integrins.

4.4.2 Cell visualisation

Osteoblasts were seeded on different modified CPCs stained with Calcein AM after one or rather 14 days, followed by visualisation with fluorescence microscopy. Seeding on uncoated and BSP-coated scaffolds showed no differences in cell confluence after 14 days (Fig. 4.22 B). Cells seeded on standard tissue culture plates displayed confluent cells and the beginning of bone nodule formation can be observed. These results are in accordance with the viability assay mentioned above. Increased cell numbers on BSP-treated surfaces at the beginning were normalised throughout the observation period. The huge differences between cells seeded onto CPC scaffolds and culture plates resulted from CPC surface properties - this caused poor seeding efficiency and low cell proliferation rates (see section 4.4.1). Seeding of $1x10^5$ hOBs per disc resulted after one day in differences concerning cell morphology. Cells seeded on uncoated CPCs are more spherical, in contrast to more polygonal and spread hOBs on BSP-coated CPCs (Fig. 4.22 A). Moreover, the occupied cell area was higher on BSP-coated surfaces than on

untreated CPC. These results contrast with cell morphology analyses after one day on titanium (see section 4.3.2). Cells on BSP-coated titanium showed more a spherical shape compared with polygonal cells on untreated titanium. A possible explanation for this discrepancy may be the material itself. Untreated titanium itself has very good cell adhesion characteristics, while the seeding efficiency of CPCs is poor. BSP-coating of CPCs may improve cell attachment due to its integrin binding capacity.

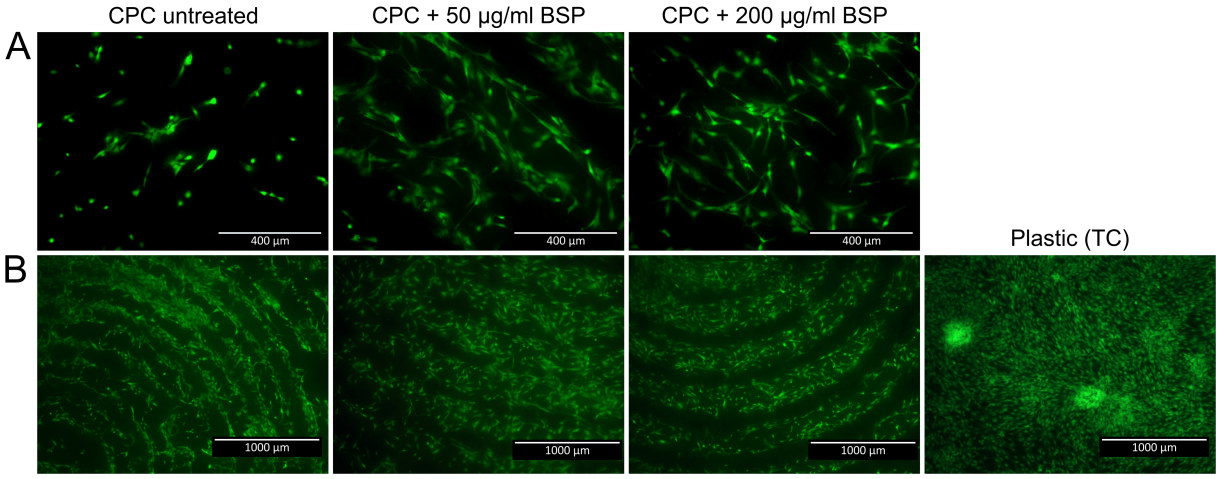

Fig. 4.22: Cell morphology of hOBs seeded onto modified CPCs. A - Cell adhesion and morphology one day after cell seeding (10x objective magnification), B - Cell visualisation 14 days after cell seeding (4x objective magnification).

4.4.3 Gene expression analyses

Differentiation of osteoblasts is associated with the expression of specific genes. For gene expression analyses, hOBs were seeded on untreated and BSP-modified scaffolds. After a 14-day incubation period, the cells were harvested, followed by RNA isolation, reverse transcription and qPCR analysis of important osteoblast markers (ALP, OPN, SP7, RUNX2 and SPARC). Gene marker expression was calculated with reference to the expression on untreated CPCs.
As shown in Fig. 4.23, the effect on osteoblast gene expression seems to be dependent on BSP concentration. Scaffold coating with a lower BSP concentration (50 µg/ml) resulted in a similar expression level of OPN and RUNX2, while the expression of SP7, SPARC and ALP decreased compared to hOB gene expression on uncoated scaffolds. The latter two were significantly downregulated. In contrast, hOBs seeded on scaffolds coated with the higher BSP concentration (200 µg/ml) showed, compared to the control, an increase in SP7, SPARC, OPN and RUNX2 expression, albeit not with significant differences. Expression of alkaline phosphatase is similar to the expression on uncoated CPCs.
Investigations by Ritz et al. demonstrated an enhanced ALP and RUNX2 mRNA expression of primary human osteoblasts seeded on CDHA bioceramics [156]. This reflects that the material on its own effects hOB gene expression. Lower BSP concentrations may be incapable to compensate this effect, particularly after 14 days. As SP7 increased over 28 days [137], this marker showed the highest median on hOB expression (over three-fold increase); followed by nearly a two-fold increase in SPARC expression. SPARC is involved in bone mineralisation

[178], which explained the increase in gene expression after 14 days compared with only a minimal increase after seven days in the titanium experiments. Gordon et al. reported similar results. Treatment of osteoblastic cells with 2 µg/ml eukaryotic rBSP resulted in a significant increase in SP7 and RUNX2 expression on day 3 and day 5. However, no significant differences were detected after 10 days [133]. Performing expression analyses on earlier points in time may show a more clearer BSP effect on osteoblast differentiation. But this was, with regard of the poor seeding efficiency and low proliferation rate, not feasible with CPC.

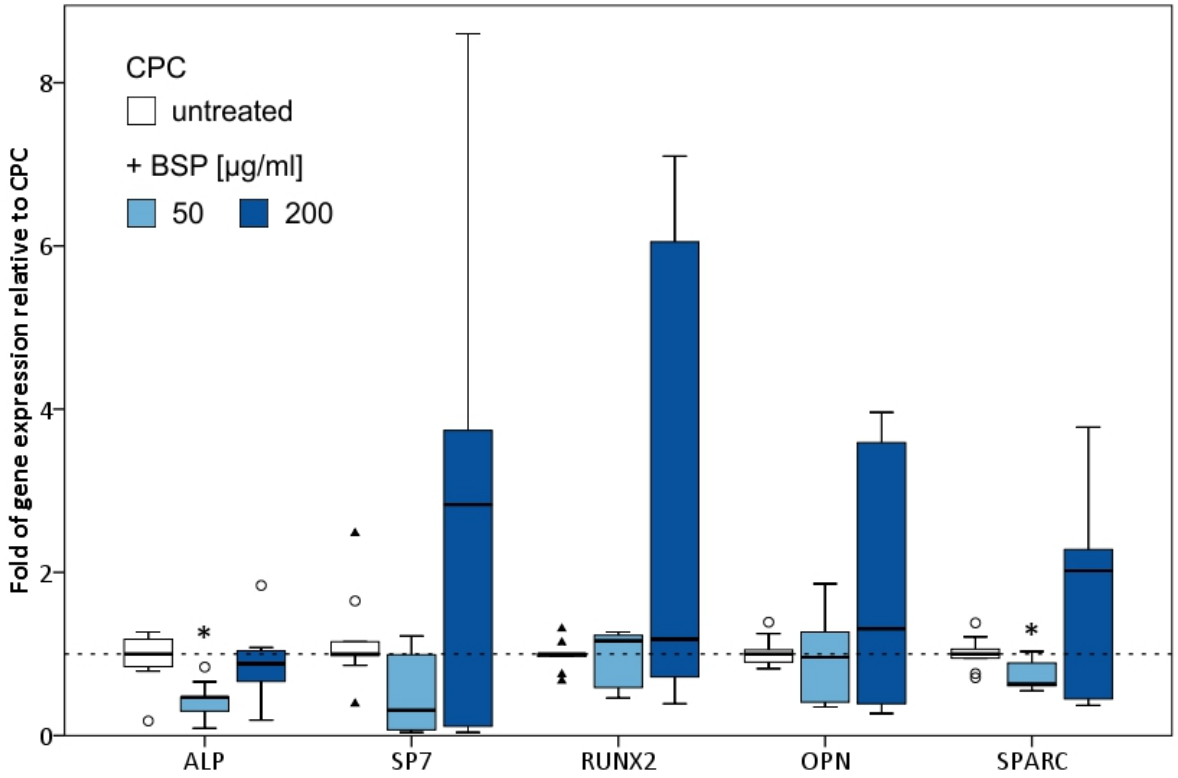

Fig. 4.23: Relative gene expression of human osteoblasts seeded onto BSP-modified scaffolds compared with seeding on untreated CPCs. hOB gene expression of the control (untreated CPC) marked as an interrupted line. Results are expressed as medians and quartiles (n = 9). Mann-Whitney-U tests revealed significant differences (*p<0.05).

Even if no significant differences exist in gene marker expression, the tendency towards enhanced cell differentiation of hOBs seeded on CPCs functionalised with the high BSP concentration (200 µg/ml) led to the decision to use the high BSP concentration in further *in vivo* experiments. This decision was assisted by a previous study with BSP-coated biomaterials. Coating with low concentrations of 1 µg/ml and 10 µg/ml BSP showed no influence on hMSC differentiation *in vitro* as well as *in vivo* [179]. Furthermore, higher concentrations are often needed for *in vivo* investigations compared with those concentrations used for *in vitro* assays.

4.4.4 Conclusion

Human osteoblasts seeded on CPCs showed poor seeding efficiency and low proliferation rates. BSP functionalisation increased the cell numbers, particularly after three days. Morphology

analyses revealed on BSP-coated CPCs polygonal and spreaded hOBs compared to more spherical cells on uncoated CPCs. Gene expression analyses revealed concentration-dependent effects of BSP-functionalised scaffolds. Lower concentrations decreased or had no effect on hOB marker gene expression, while higher BSP concentrations displayed tendencies towards an increased marker expression. Therefore, the high concentration (200 µg/ml) was selected for further *in vivo* tests. Prior to *in vivo* experiments, the effect of BSP on endothelial cells and on angiogenesis - which is important for biomaterial vascularisation - was examined as well. The next chapter deals with these issues.

4.5 *In vitro* 3D experiments with BSP-modified collagen gels

Examination of cell-cell interactions, particularly in a three-dimensional environment, is feasible in collagen gels. These gels represent conditions comparable to the ECM and neovascularisation can be measured by angiogenesis assays with different cells (hOBs and HUVECs) cultured in spheroids [83, 127, 180].

4.5.1 Cell viability

Human osteoblasts and HUVECs were seeded as mono- or co-cultures in differently modified collagen gels (0, 1 and 5 µg/ml BSP). Cell viability was measured with the alamarBlue® assay on days 1, 2, 4, 7 and 10.
Collagen gels containing 1 µg/ml BSP showed significant enhanced cell viability and proliferation rates in both mono- and co-cultures compared with the other groups (Fig. 4.24).

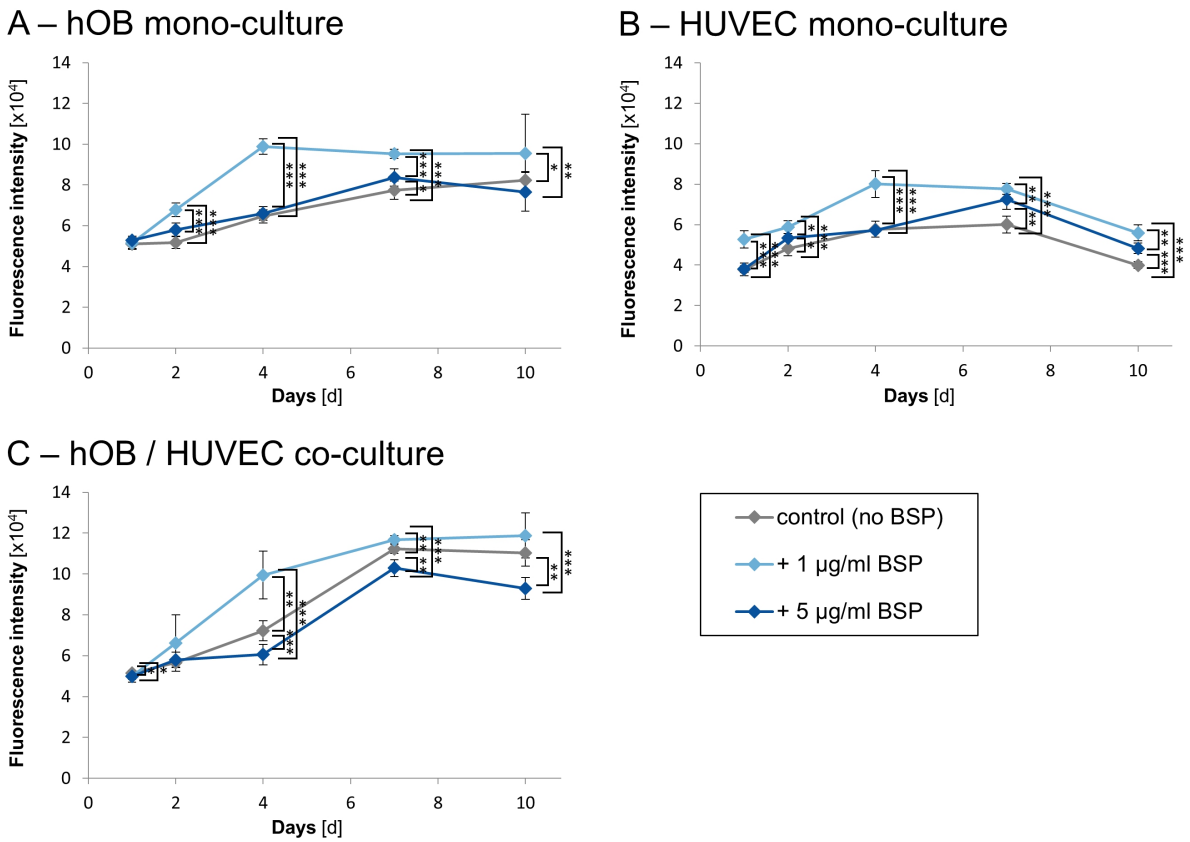

Fig. 4.24: Cell viability of hOBs and HUVECs in collagen gels with immobilised BSP. Results are expressed as mean ± SD (n = 9). Games-Howell or Tukey-HSD post-hoc tests (dependent on Levene's test) revealed significant differences (*p<0.05, **p<0.01, ***p<0.001).

Cells seeded in collagen gels containing 5 µg/ml BSP led in HUVEC mono-culture after six days to a significant enhancement and in hOB mono-culture they led to a similar situation compared with the control. In co-culture conditions after day 2 they showed a significant decrease in cell

proliferation compared with the control and the low BSP concentration group. The increase in cell proliferation over 10 days was stronger in co-culture conditions than in both mono-cultures, whereby in the HUVEC mono-culture the viability decreased after seven days. As described by several authors, endothelial cells and osteoblasts influence proliferation and differentiation of each other due to growth factor release [181, 182, 183, 184, 185]. Particularly, the VEGF release of osteoblasts may enhance endothelial cell survival in co-culture conditions [181].

4.5.2 Gene expression analyses

The effect of BSP on gene expression of hOBs and HUVECs was carried out via qPCR. Cells were seeded as mono- and as co-cultures in differently modified collagen gels (0 µg/ml BSP, 1 µg/ml BSP, 5 µg/ml BSP and 10 µg/ml BSP). After days 1, 4 and 7, the cells were harvested, followed by RNA-isolation, reverse transcription and qPCR analysis. ALP, OPN, RUNX2, SP7 and SPARC were evaluated as markers of osteoblast differentiation. PECAM, MCAM, KDR and vWF were utilised for HUVEC characterisation.
Prior to reverse transcription, the RNA quality was verified via spectrophotometry as well as agarose gel electrophoresis. Fig. 4.25 shows a representative RNA agarose gel. All RNA samples displayed sharp 28S and 18S rRNA bands, indicating pure and intact RNA.

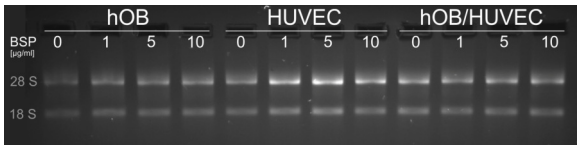

Fig. 4.25: Representative image of an RNA agarose gel for evaluation of RNA quality.

Gene expression analyses of hOB mono-cultures revealed the general trend of a decreased or consistent expression after one and seven days, whereas an increase in gene expression was only observed after four days (Fig. 4.26). The ALP expression of hOBs was significantly downregulated in collagen gels containing 5 and 10 µg/ml BSP after one day as well as in gels with 1 µg/ml BSP after four days. OPN expression was decreased in all BSP groups after day 1. In contrast, it was enhanced in highly concentrated BSP gels and downregulated in gels with 5 µg/ml after 4 days. The SPARC expression was significantly reduced in low concentrated BSP-collagen gel after one and four days, respectively. After four days, the key factors of osteoblastic differentiation showed an upregulation for SP7 in all BSP groups and for RUNX2 in high concentrated BSP gels. HUVEC mono-cultures displayed the general tendency of enhanced gene expression after one day and a decrease after four days (Fig. 4.27). Significant enhancement was only detected in PECAM expression of HUVECs seeded in low concentrated BSP-collagen gels after one day. On day 4, significant downregulations were observed in low concentrated BSP gels for vWF and KDR as well as in all BSP gels for MCAM. In co-cultures, the trend of osteogenic markers was similar to those of hOB mono-cultures. Significant changes occurred merely after four days of culture. ALP (by 10 µg/ml BSP) and SPARC (1 and 10 µg/ml BSP) expression decreased, whereas OPN (1 and 5 µg/ml BSP) as well as RUNX2 (5 µg/ml) expression increased.

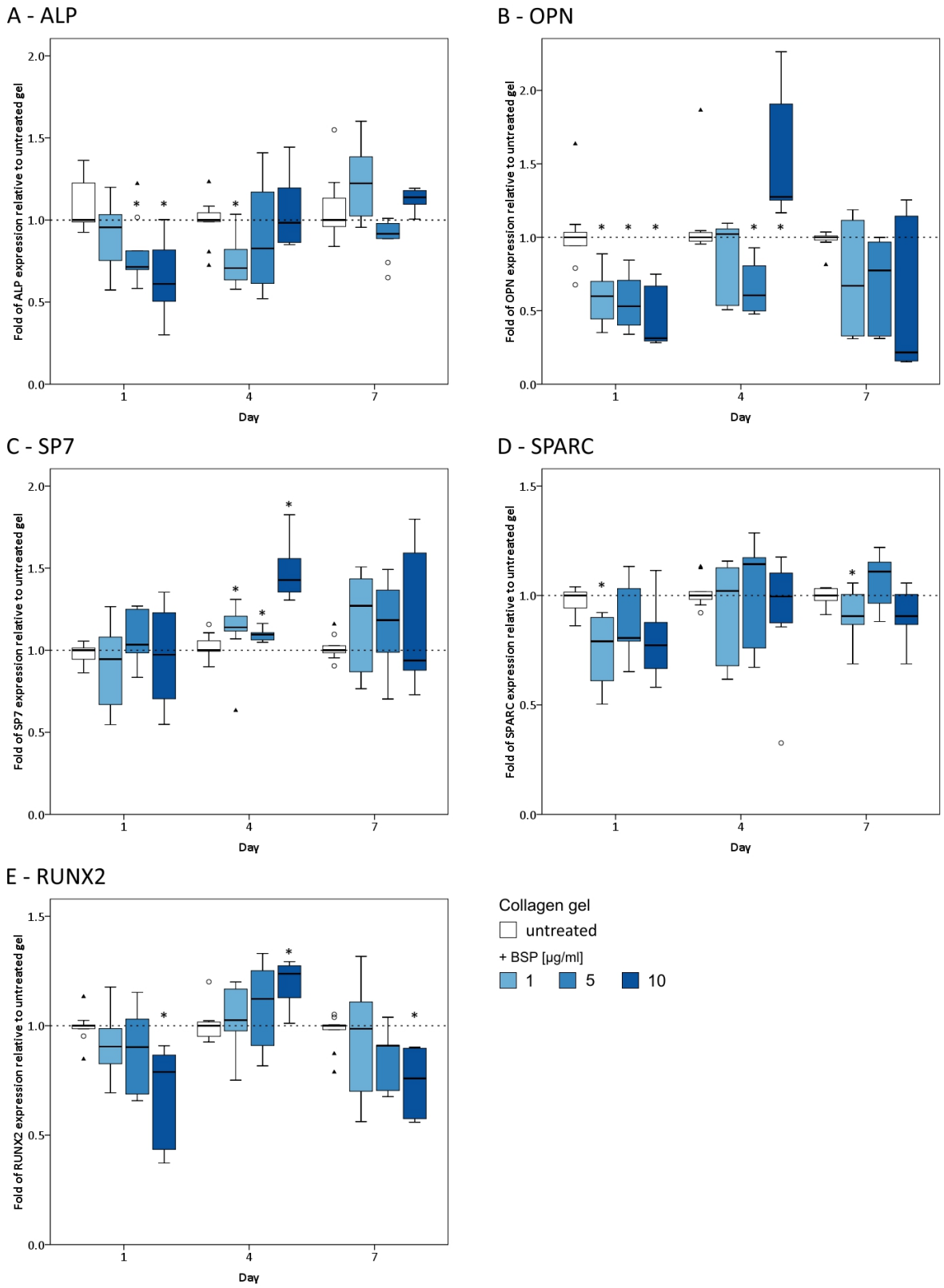

Fig. 4.26: Effect of BSP encapsulation in collagen gels on hOB mono-cultures. Relative alkaline phosphatase (A), osteopontin (B), osterix (C), osteonectin (D) and RUNX2 (E) expression of hOBs seeded in different modified collagen gels were compared with untreated collagen gels (gene expression = 1). Results are expressed as median and quartiles (n = 9). Mann-Whitney-U tests revealed significant differences (*$p<0.05$).

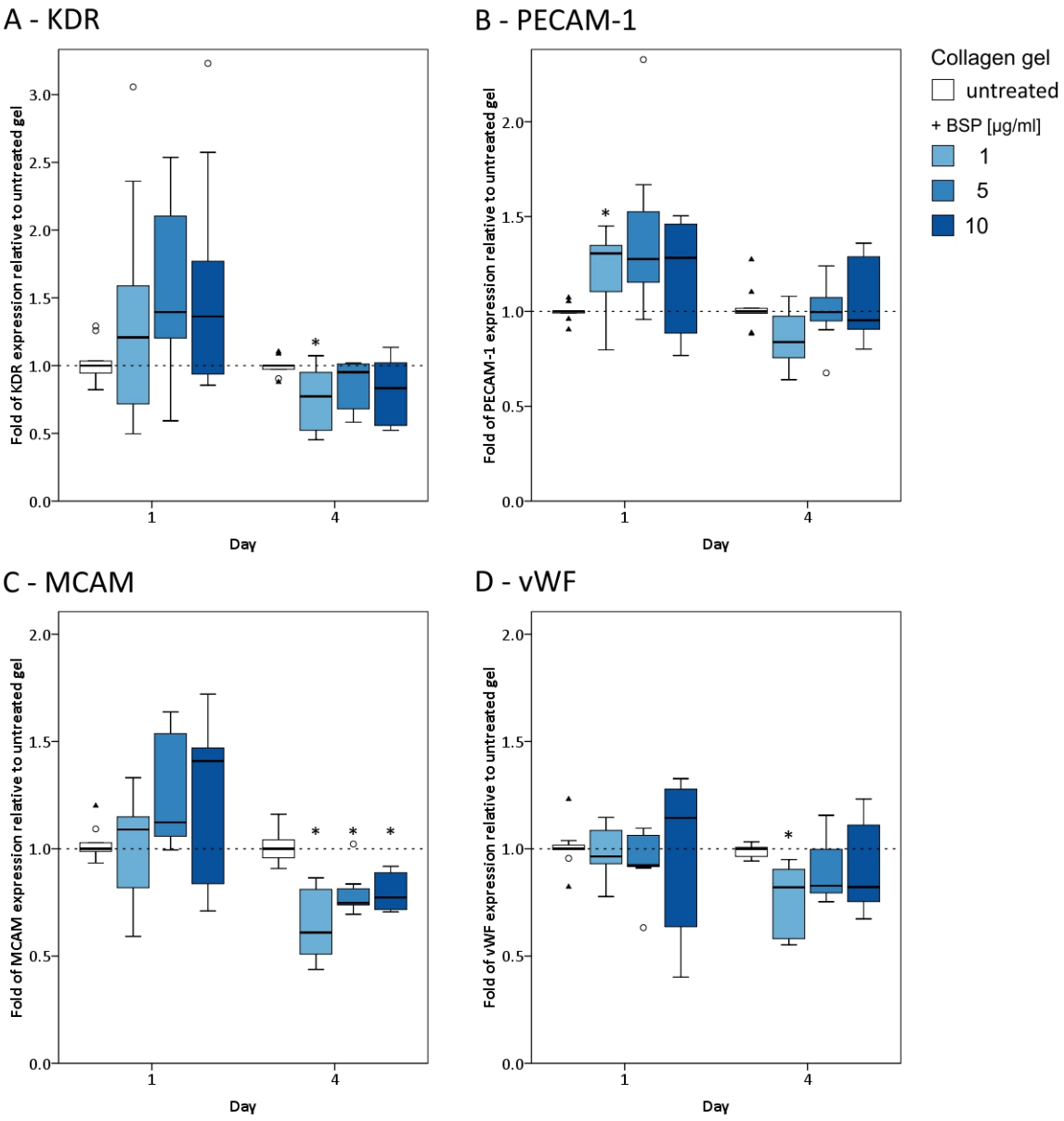

Fig. 4.27: Effect of BSP encapsulation in collagen gels on HUVEC mono-cultures. Relative KDR (A), PECAM (B), MCAM (C) and vWF (D) expression of HUVECs seeded in different modified collagen gels were compared with untreated collagen gels (gene expression = 1). Results are expressed as median and quartiles (n = 9). Mann-Whitney-U tests revealed significant differences (*$p<0.05$).

In co-culture examinations, the SP7 expression was not affected by BSP supplementation in contrast to a significant up regulation by all three BSP concentrations in hOB mono-cultures. Endothelial markers were primarily downregulated after one and four days in co-culture collagen gels. After seven days, the expression rates were similar to those of untreated cells.

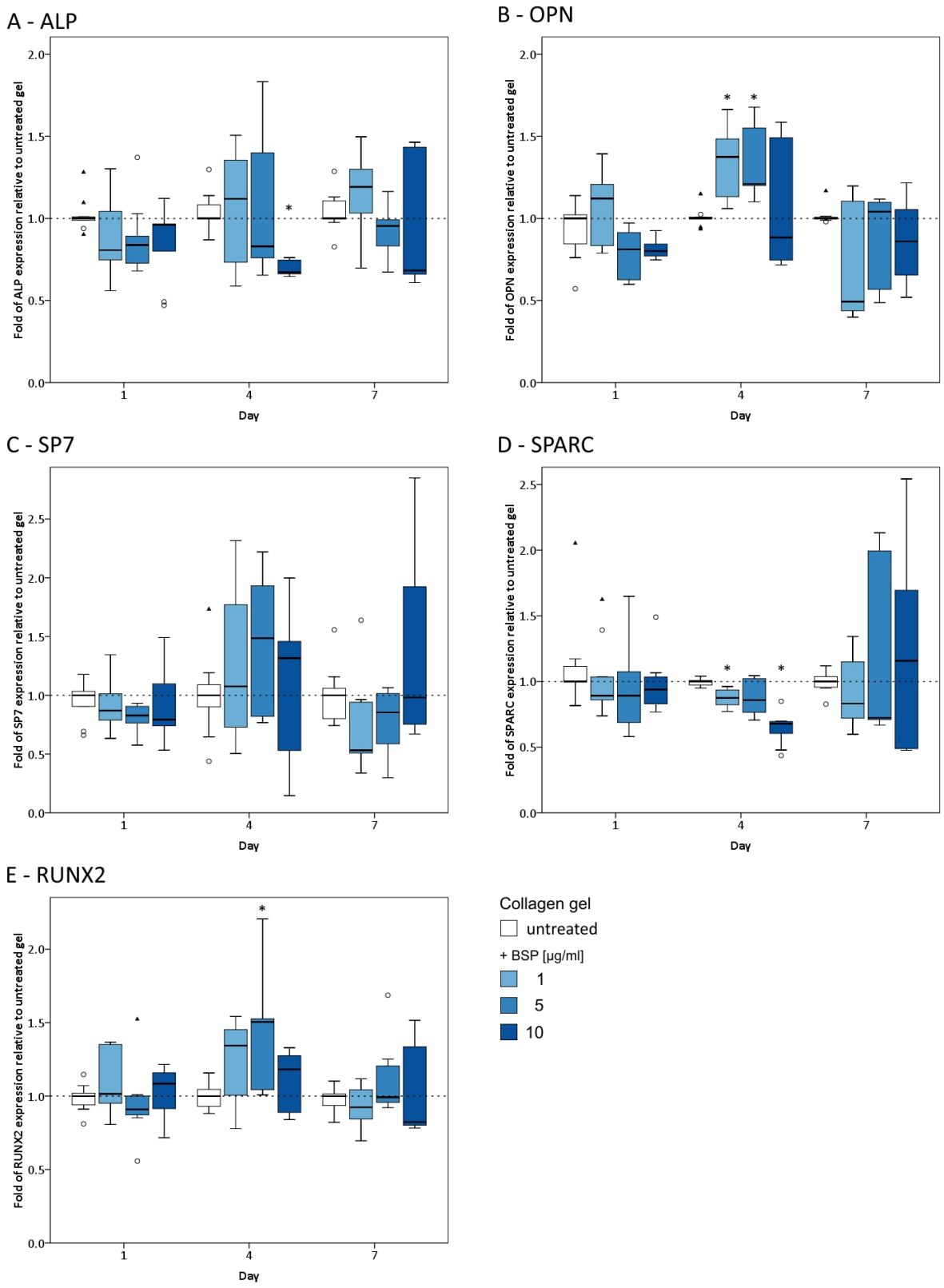

Fig. 4.28: Effect of BSP encapsulation in collagen gels on hOB/HUVEC co-cultures. Relative alkaline phosphatase (A), osteopontin (B), osterix (C), osteonectin (D) and RUNX2 (E) expression of hOB HUVEC co-cultures seeded in different modified collagen gels were compared with untreated collagen gels (gene expression = 1). Results are expressed as median and quartiles (n = 9). Mann-Whitney-U tests revealed significant differences (*$p<0.05$).

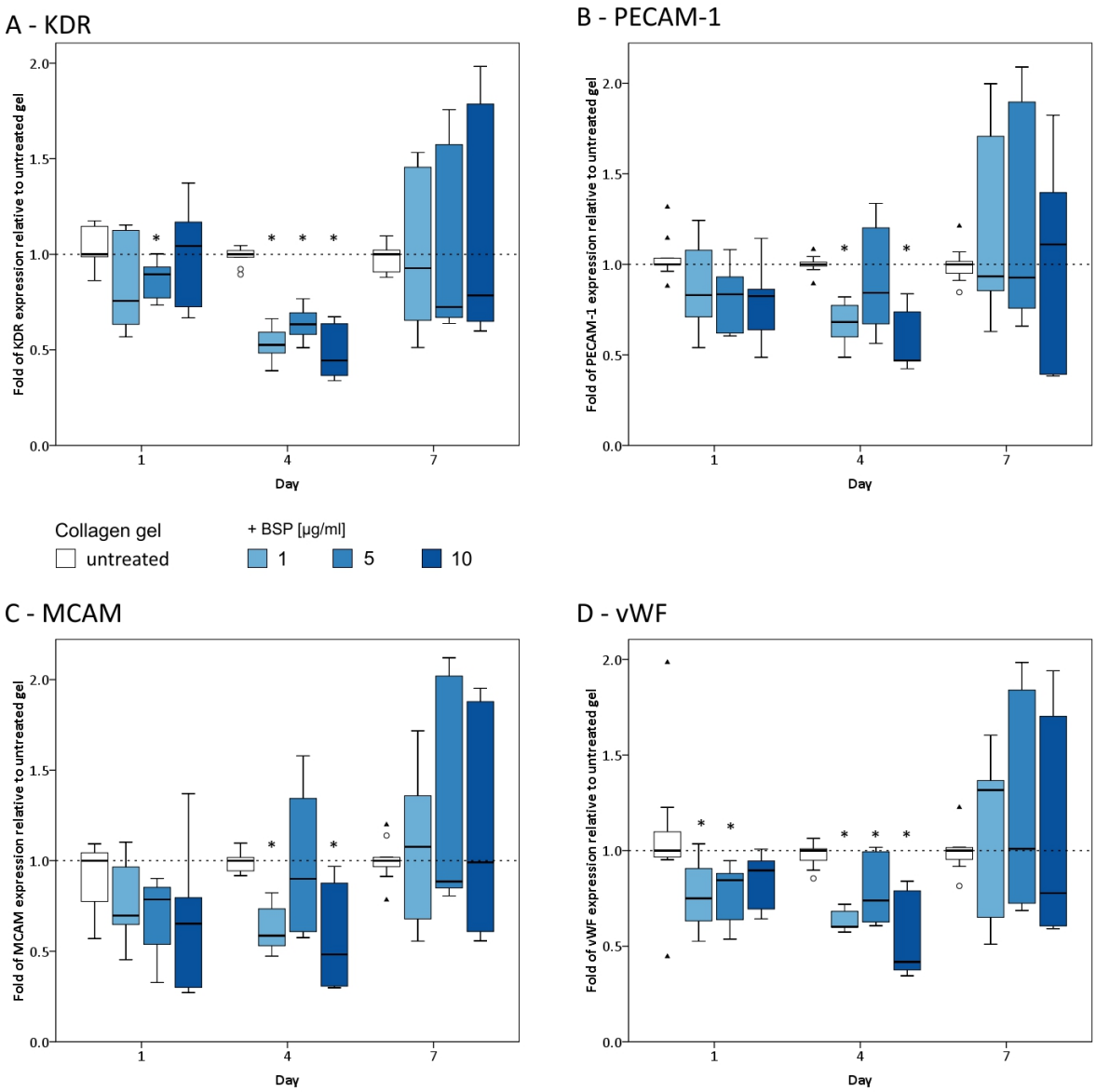

Fig. 4.29: Effect of BSP encapsulation in collagen gels on hOB/HUVEC co-cultures. Relative KDR (A), PECAM (B), MCAM (C) and vWF (D) expression of hOB HUVEC co-cultures seeded in different modified collagen gels were compared with untreated collagen gels (gene expression = 1). Results are expressed as median and quartiles (n = 9). Mann-Whitney-U tests revealed significant differences (*$p<0.05$).

The effect of BSP on osteogenic markers - e.g. OPN, SP7 and RUNX2 - was already discussed in chapters 4.3 and 4.4. HUVEC mono-cultures tend to a slightly increased expression of KDR, MCAM and PECAM-1. This tendency may be caused by interactions of BSP with integrins. The decrease on day 4 may depend on a limited or negative effect of BSP as well as on gradually dying cells. Particularly, HUVEC mono-cultures underwent apoptosis during seven days in culture. The reasons may be the lack of VEGF and basic FGF, which are essential factors for endothelial differentiation [186]. Both HUVEC mono- and co-culture with hOB were treated identically. The factors were omitted because they influence on osteoblast differentiation as well [187]. Survival of HUVECs in co-culture could be explained by VEGF expressed from osteoblasts [188, 181, 185, 182, 183]. A possible explanation for the decrease of endothelial

markers during the first four days, might be an overwhelming effect of osteoblasts, which was coped until day 7. BSP treatment may support this and lead to competition for $\alpha_v\beta_3$ integrins. PECAM-1 [189], vWF [190, 191] and OPN [191] interact like BSP with this integrin. Regarding the effect of different BSP concentrations, a trend can hardly be determined because of varying results. Highest BSP concentrations (10 µg/ml) seemed to have the greatest effect on hOB mono-cultures after four days as well as on HUVEC mono-cultures after one day. Co-cultures were mainly influenced by middle BSP concentration (5 µg/ml) after four days. Nevertheless, alterations in relative gene expression were rather low - they varied between 0.5- and 1.5-fold. In general, gene expression rates below half or more than double are considered biologically relevant. In certain cases, lower effects may be more desirable than exaggerated effects, such as excessive bone growth by BMPs. Whether these low modifications influence bone and vessel formation *in vivo* will be determined in further studies.

4.5.3 Angiogenesis assay

Angiogenesis is one key factor for the success or failure of biomaterials [188, 192, 193]. Mono- as well as co-culture spheroids of hOBs and HUVECs were seeded in different modified collagen gels. After 24 hours, sprouting was visualised. Representative images of mono-culture spheroids are shown in Fig. 4.30 for endothelial cells and in Fig. 4.31 for human osteoblasts. Co-culture spheroids after 1 hour as well as after 24 hours are represented in Fig. 4.32 and Fig. 4.33. Images acquired after 1 h served as control for intact spheroids without any obvious sprouting. No obvious differences were observed by HUVEC as well as hOB mono-culture spheroids between the individual groups. Instead of sprout formation, single HUVEC cells started to move away from the spheroid in all directions during 24 hours (Fig. 4.30). In contrast, numerous sprouts were detectable in hOB mono-culture spheroids after 24 hours (Fig. 4.31). In co-culture spheroids, more HUVECs are located on the outer surface, as seen in Fig. 4.32. During 24 hours, multiple sprouts grew out of the spheroids. In contrast to numerous hOB-mono sprouts displayed in all groups, the number of sprouts comprising both cell types varied in the groups. Therefore, the formed sprouts were quantified regarding the numbers per spheroid, individual sprout length, cumulative sprout length and sprout diameter. The results of the quantitative evaluation are shown in Fig. 4.34.

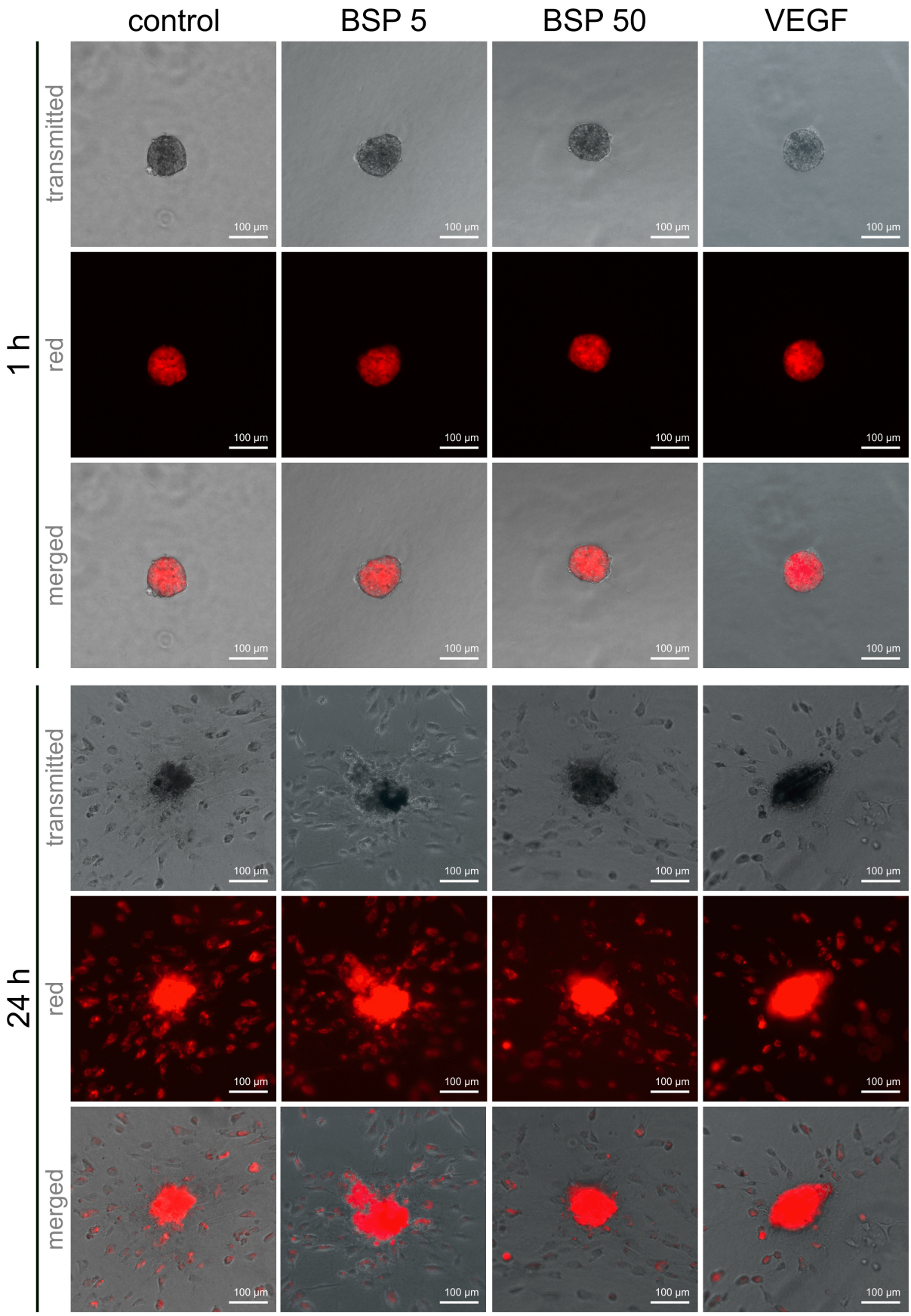

Fig. 4.30: Representative images of HUVEC mono-culture spheroids after one and 24 hours in different treated collagen gels. HUVECs were stained prior with Cell-Tracker™ red.

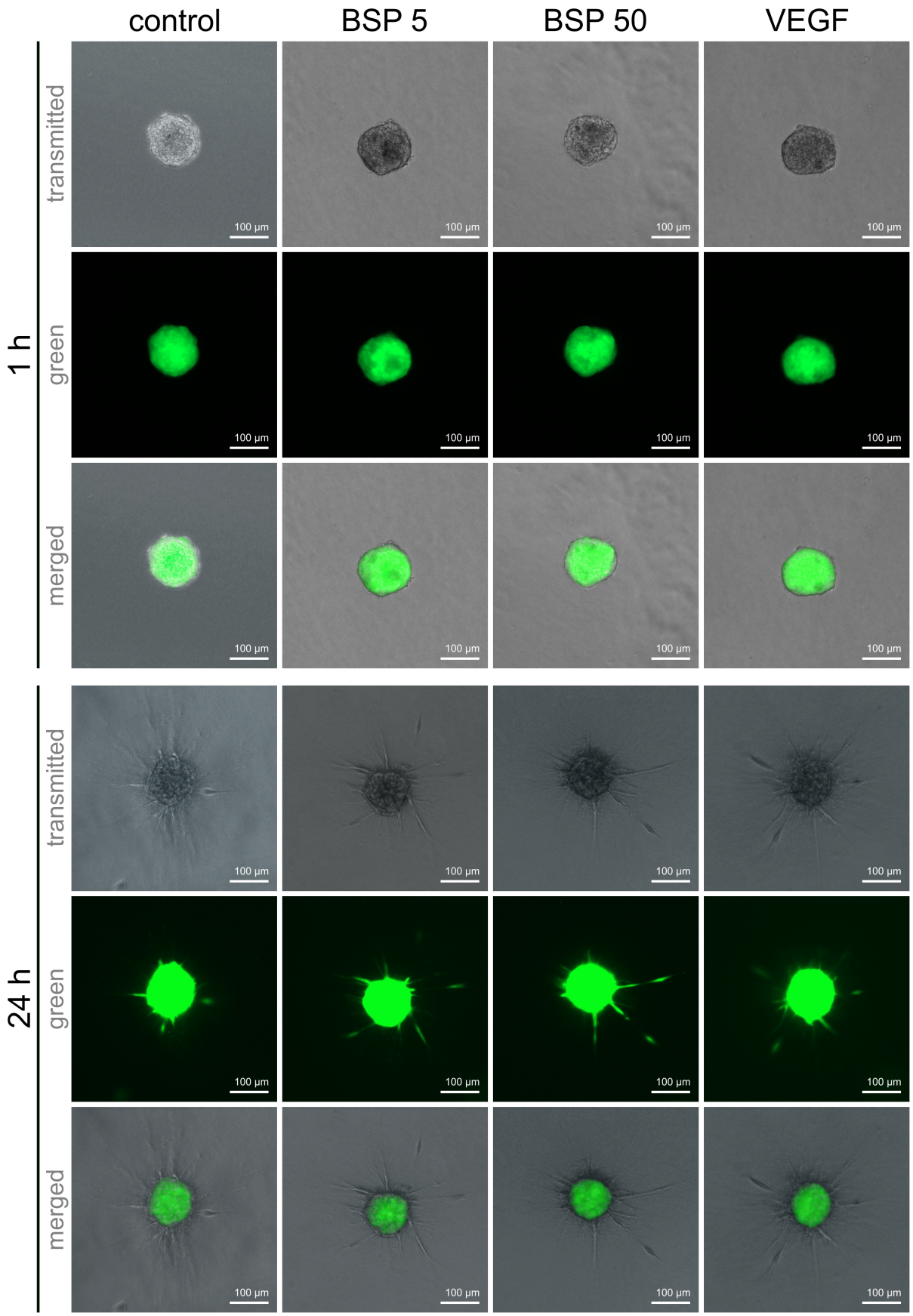

Fig. 4.31: Representative images of hOB mono-culture spheroids after one and 24 hours in different treated collagen gels. hOBs were stained prior with Cell-Tracker™ green.

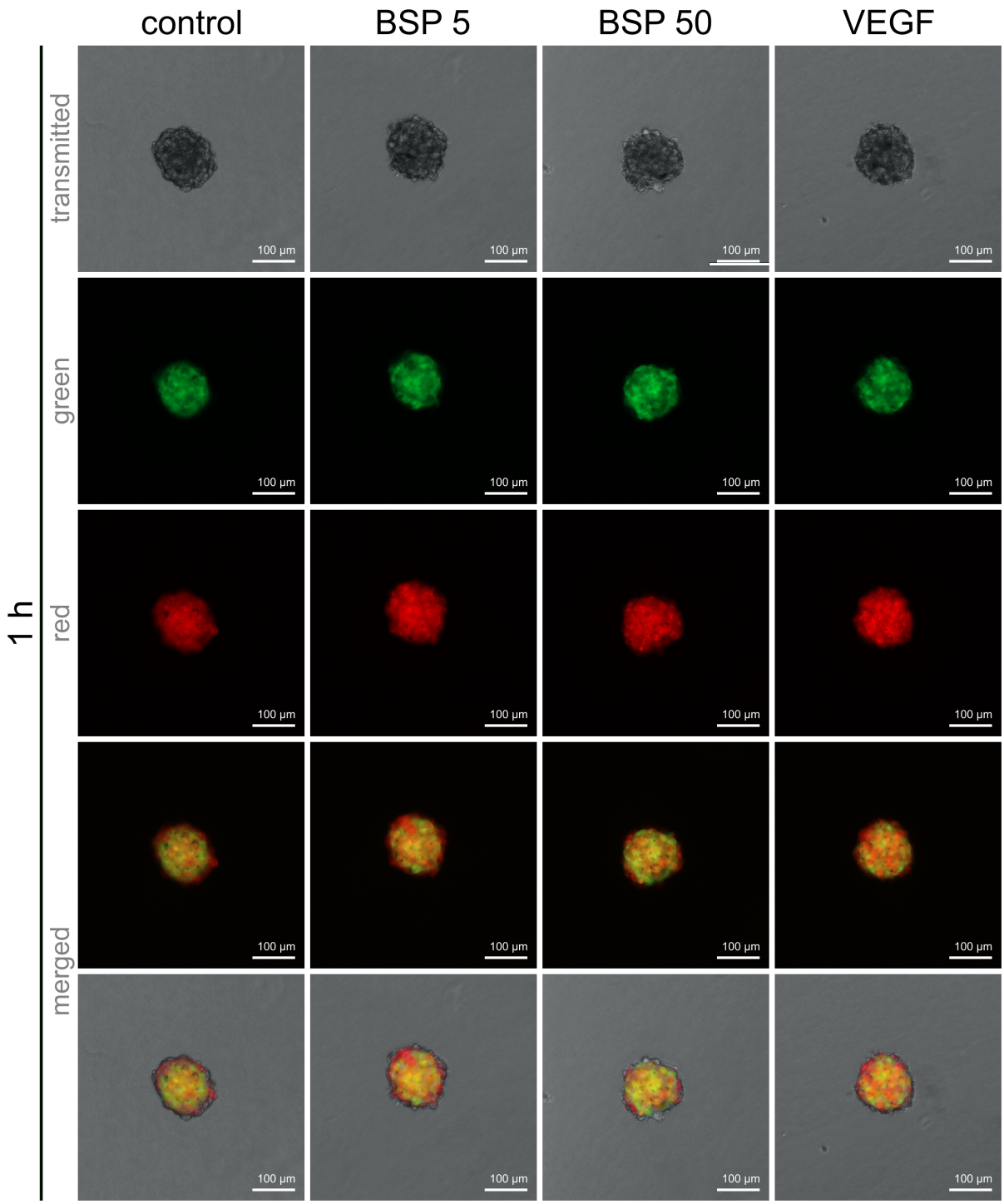

Fig. 4.32: Representative images of hOB/HUVEC co-culture spheroids after one hour in different treated collagen gels. hOBs were stained prior with Cell-Tracker™ green and HUVECs with Cell-Tracker™ red.

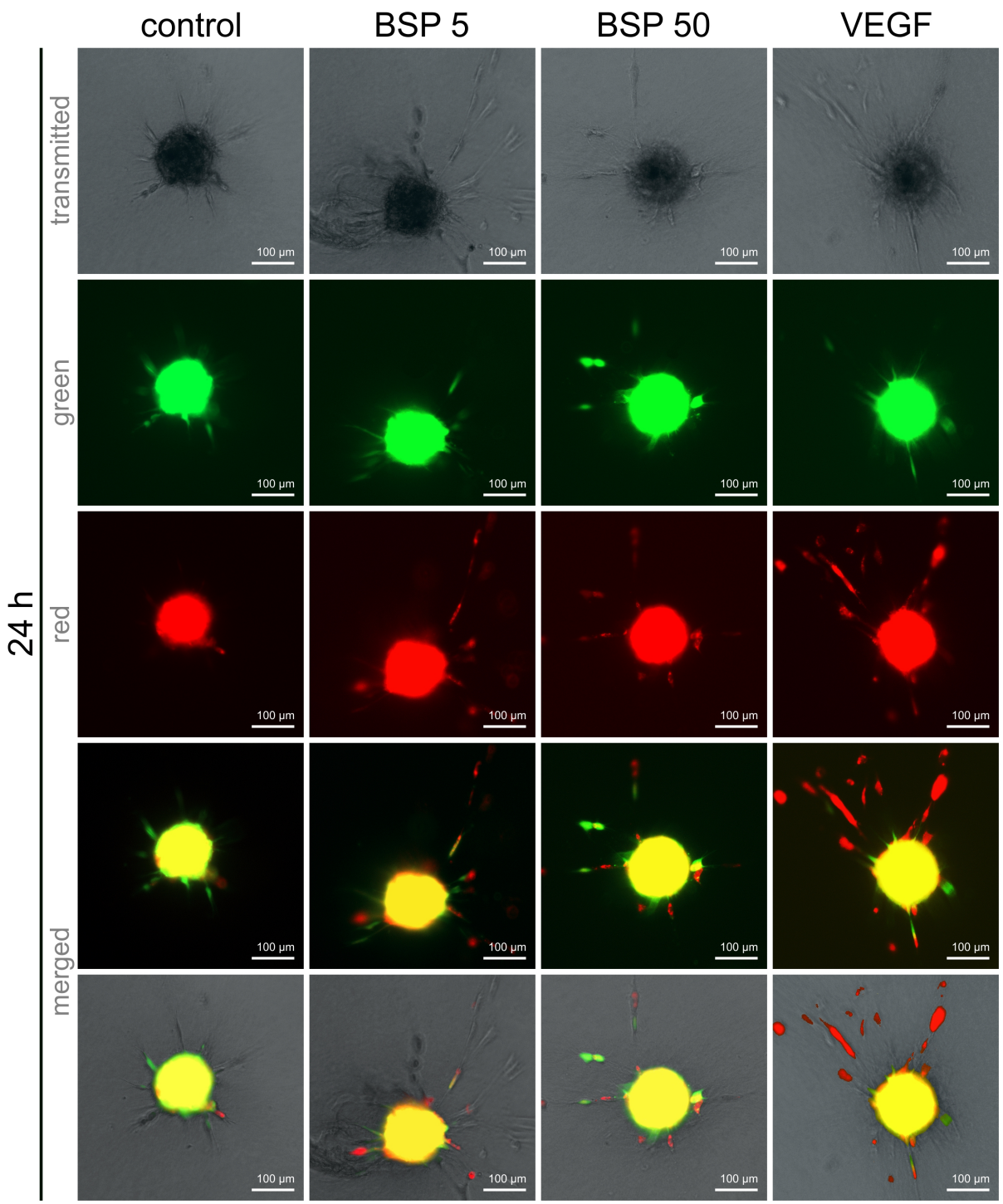

Fig. 4.33: Representative images of hOB/HUVEC co-culture spheroids after 24 hours in different treated collagen gels. hOBs were stained prior with Cell-Tracker™ green and HUVECs with Cell-Tracker™ red.

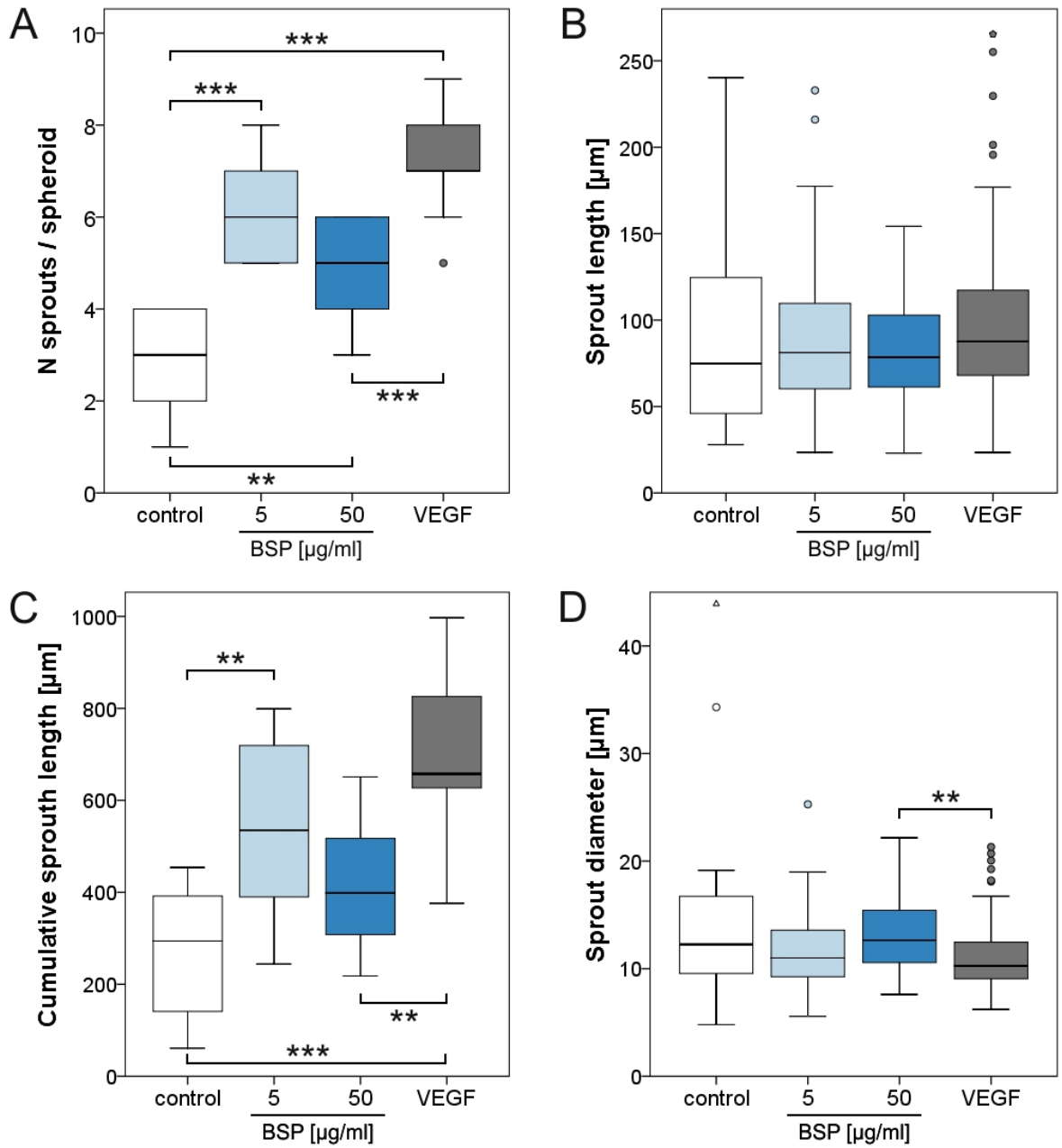

Fig. 4.34: Effect of BSP encapsulation in collagen gels on hOB/HUVEC co-culture spheroids. The number of sprouts per spheroid (A), sprout length (B), cumulative sprout length (C) and sprout diameter (D) was examined after 24 hours. Results are expressed as median and quartiles (n = 10). Tukey-HSD post-hoc tests (A, C) and Mann-Whitney-U tests (B, D) revealed significant differences (**$p<0.01$, ***$p<0.001$).

No differences were observed in individual sprout lengths (B). Sprout diameters differ only between VEGF and the high BSP concentration (D). In contrast, the number of sprouts per spheroid was obvious different. The lowest number was three in the control group, followed by nearly five in the high BSP concentration group, six by low BSP concentration and finally the positive control with VEGF with roundabout seven sprouts per spheroid. All three groups (BSP low, BSP high, VEGF) differ significantly from the control group. In addition, the VEGF group showed significantly enhanced number of sprouts per spheroid to the high BSP concentration group, but it was not compared with the low concentration group. The same was

visible for calculation of cumulative sprout length.
In contrast to several authors, no sprout formation was observed in HUVECs mono-culture spheroids [83, 194]. The reasons for the release of single cells may be the collagen gel itself - e.g. composition or strength. Moreover, it may depend on the cells. Culture conditions, the number of passages, cell density and proliferation can affect HUVEC behaviour [83]. Considering that the form and appearance of sprouts from hOB mono-culture as well as from co-culture are similar to those presented by Wenger et al., the second explanation may be the more probable one. The HUVEC assembling on the outer surface in co-culture spheroids was detected by Wenger et al. as well [194]. Quantitative examinations of the cumulative sprouting length (CSL) by Heiss et al. revealed similar results. The CSL of sprouts which grew out of HUVEC spheroids was roundabout 50 µm. VEGF stimulation increased CSL up to nearly 750 µm [83]. Wenger et al. examined further HUVEC mono- and HUVEC hOB co-culture spheroids. The CSL baseline laid by nearly 300 µm for HUVEC mono-spheroids and by approximately 560 µm for co-culture spheroids. VEGF stimulation enhanced the CSL of HUVEC mono-spheroids significantly up to 780 µm. The increase of 20 µm up to 580 µm CSL by co-culture spheroids was not significant [194]. As shown in Fig. 4.34 stimulation with the same VEGF-concentration (25 ng/ml) resulted in a significant CSL increase from 300 µm up to 650 µm. In opposite to Wenger et al., only sprouts comprising both cell types were included for sprout quantification. Sprout-like outgrowths from hOBs alone were not included. This may explain the discrepancies and more closely results to those of HUVEC mono-spheroids. BSP supplementation enhanced significantly the CSL or the number of sprouts per spheroid. Bellahence et al. were the first authors who discovered that BSP facilitates angiogenesis. Besides the enhancement of HUVEC cell attachment and migration, BSP displayed angiogenetic potential in the CAM-Assay (chorio-allantoic membrane) [195]. Due to this angiogenetic effect, BSP functionalisation of biomaterials may be a step to overcome the limitations of biomaterial vascularisation.

4.5.4 Conclusion

Cell viability examinations revealed significant enhanced cell viability and cell proliferation in low-concentrated (1 µg/ml) BSP collagen gels. Supplementation of 5 µg/ml BSP to collagen gels resulted in a similar or decreased cell proliferation regarding osteoblasts, in contrast to enhanced HUVEC proliferation after four days. hOBs seeded in collagen gels with BSP showed enhanced mRNA expression of osteogenic markers (RUNX2, SP7, OPN) after four days. The same effect was observed in the co-culture with HUVEC in collagen gels. BSP supplementation decreased the expression of endothelial markers in co-culture gels during the first four days. Nevertheless, BSP treatment led to an enhanced angiogenesis in the sprouting assay. To what extent these effects may benefit the *in vivo* bone formation is one remaining question, which is covered in the next chapter.

4.6 *In vivo* experiments

Bone formation is a very complex process with multiple factors involved. *In vitro* experiments provided only a first impression, but cannot be directly transferred to *in vivo* conditions. Therefore, *in vivo* tests are required to confirm previous results. As explained in the introduction, there are two ways of bone formation. The effect of BSP coating was evaluated in a calvarial defect model - for desmal ossification - as well as in a femoral condyle defect model for endochondral ossification.

4.6.1 Calvarial borehole defect model

In mice, 2.7 mm thick critical size defects (CSDs) were generated. Uncoated, BSP-coated and BMP-7-coated CPC scaffolds were implanted in those CSD defects. No treatment served as internal control. After an eight-week observation period, µCT examinations were carried out. In Fig. 4.35, representative 3D images were displayed. Even after eight weeks no bone formation was detectable in the negative control (A). In the other groups (B - uncoated CPC, C - BSP coated CPC, D - BMP-7 coated CPC), the implanted scaffolds are largely connected to bone. Quantitative analyses via the bone-implant contact (BIC) and the bone volume/total volume (BV/TV) were required to show the differences more clearly.

Fig. 4.35: 3D visualisation of mice calvaria gained via µCT examinations. A) negative control: no scaffold was inserted after setting the CSD defect. B) uncoated CPCs, C) BSP-coated CPCs and D) BMP-7 coated CPCs.

Evaluation of BIC and BV/TV via µCT

A closer look at the bone-implant interface gains a first impression on bone regeneration. Fig. 4.36 shows representative images of the bone-implant contact (BIC) for a qualitative impression. Calvarial bone has a common thickness of around 260 µm (A, see also Fig. 4.37). All groups treated with different modified CPCs increased the bone thickness (B, C, D). In addition, bone ingrowth into the scaffolds was observed.

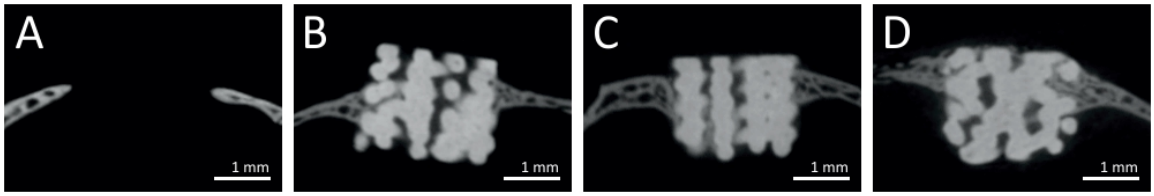

Fig. 4.36: Representative images of bone-implant contact. A) negative control, B) uncoated CPCs, C) BSP- coated and D) BMP7 coated CPCs.

Quantitative investigations displayed these effects more clearly (Fig. 4.37). Therefore, the BIC was calculated at four different points of each scaffold. The highest bone thickness at the bone-implant interface was detected in the group with BMP-7-coated scaffolds (679 µm ± 287 µm). BSP-coated scaffolds followed directly with a BIC of 676 µm ± 250 µm. Uncoated CPCs led to an increase to 566 µm ± 162 µm thickness. However, no significant differences were observed between the three implant groups. Significant differences were only detected compared with negative control.

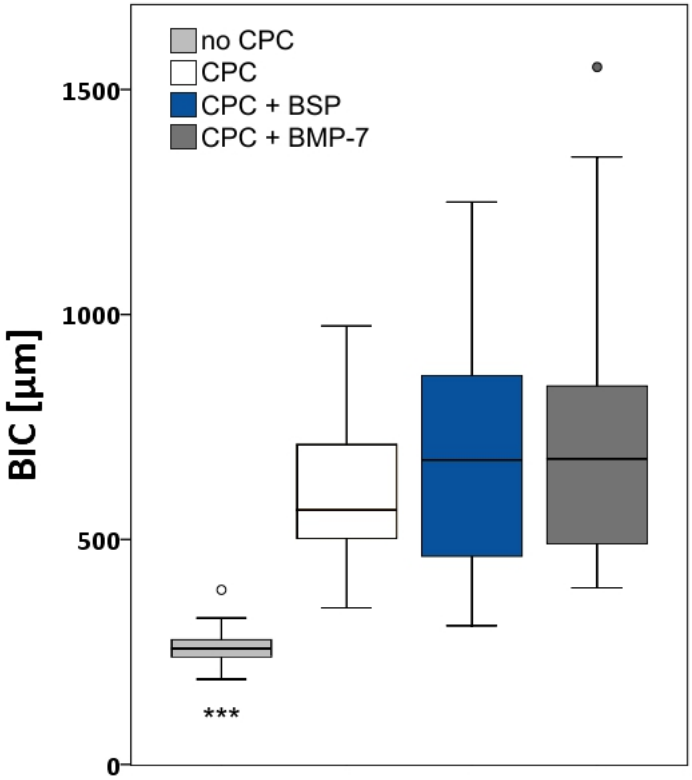

Fig. 4.37: Bone-implant contact measurements after an eight week observation period. Results are expressed as median and quartiles (n = 28 - 40). Mann-Whitney-U tests revealed significant differences (***$p<0.001$).

Furthermore, an even better impression of bone growth throughout the entire defect will be received with the evaluation of the BV/TV. This method allows the quantification of new bone (bone volume) in a defined total volume set as virtual cylinder. The BIC results showed a greater bone thickness, besides the implants compared to their usual thickness. For such reasons, several diameters were chosen for the cylindrical total volume (3 mm, 4 mm, 4.5 mm and 5 mm). In contrast to the BIC results (see Fig. 4.37), implants coated with BSP showed

the highest bone volume (see Fig. 4.38), followed by BMP-7-coated and uncoated scaffolds, which showed an equal ratio. Significant differences were only detectable compared with the negative control. As shown in Fig. 4.38, the same trends were observed for all diameters.

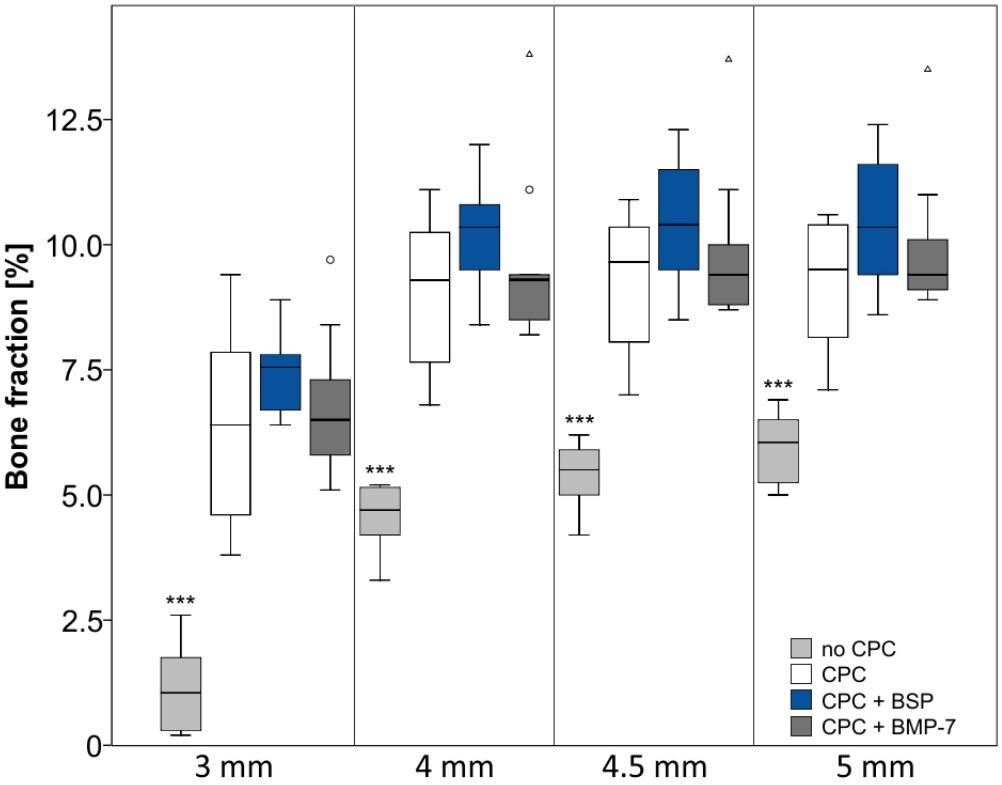

Fig. 4.38: Bone volume/total volume ratio for calculation of newly formed bone. Results are expressed as median and quartiles (n = 8 - 10). Mann-Whitney-U tests revealed significant differences (***p<0.001).

Histological examinations

Samples were de-calcified in EDTA solution over three weeks, followed by embedding in paraffin. Slices accomplished via microtome were stained with MGT staining. No bone formation was observed in the negative control (no CPC). The defect was covered with connective tissue (see Fig. 4.39). In the groups with implanted CPCs, new bone formation (grey arrows) was detectable. BSP-coated scaffolds tend towards more bone formation compared with the uncoated scaffolds. This was recognized qualitatively by a higher amount of osteoid areas (orange-stained). Moreover, blood vessels were detected. The stained slices confirm the quantitative results gained by µCT examination.

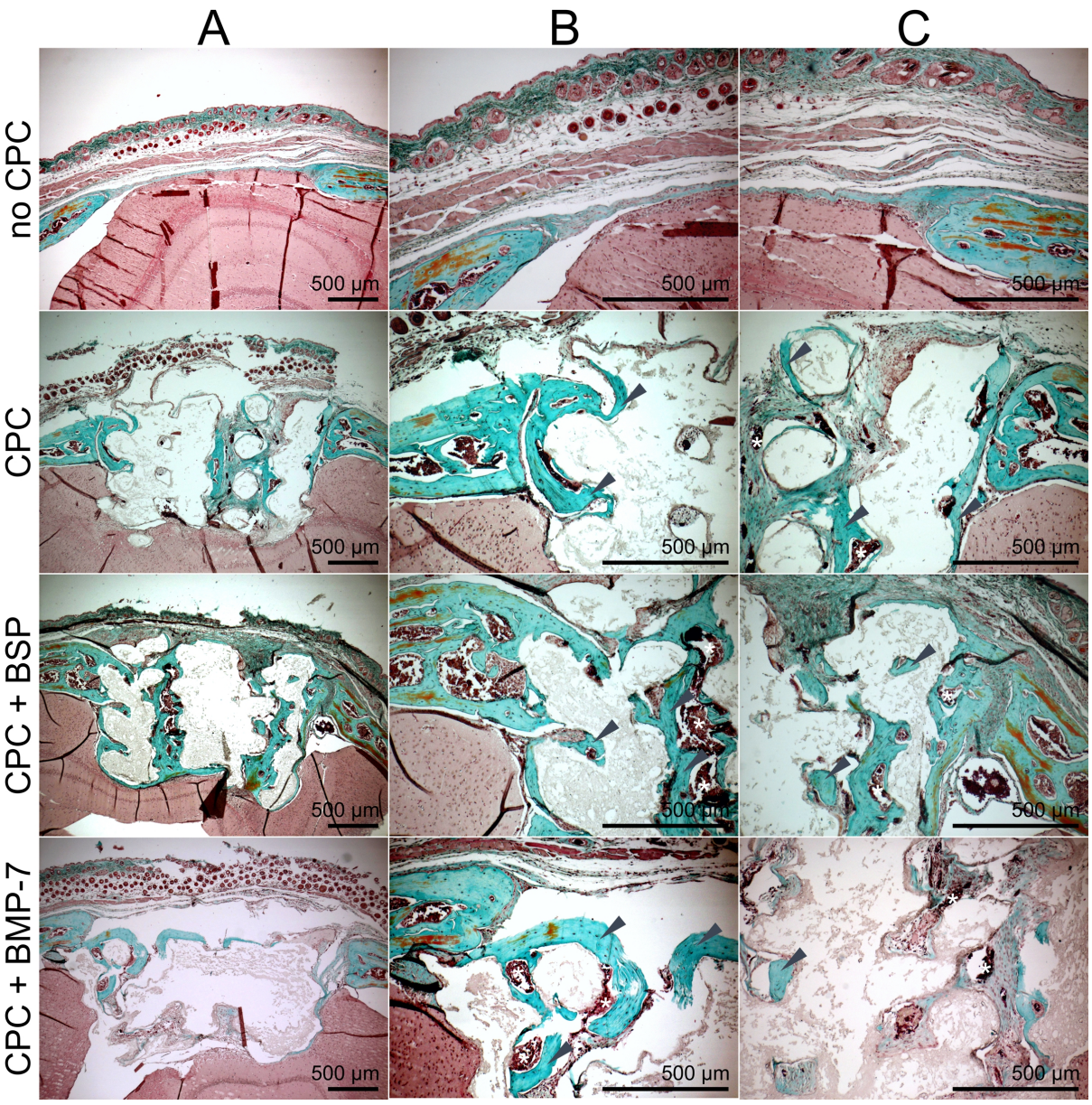

Fig. 4.39: Masson-Goldner trichrome staining. A) Overview of the defect (40-fold magnification), B) and C) a detailed view (100-fold magnification). Areas of new formed bone are indicated with grey arrows.

Immunohistological staining for OPN, PECAM and vWF are presented in Fig. 4.40. Brown-coloured areas display positive staining. In the negative control (NC), no brown- coloured areas were detected. In the group with no scaffold implantation, weak brown-coloured areas were visible, restricted to the borders of the defect. In contrast, the representative images of all other groups (CPC, CPC + BSP, CPC + BMP-7) showed brown-stained areas in the middle of the placed defect. Brown areas were displayed mostly at the borders of newly formed bone.

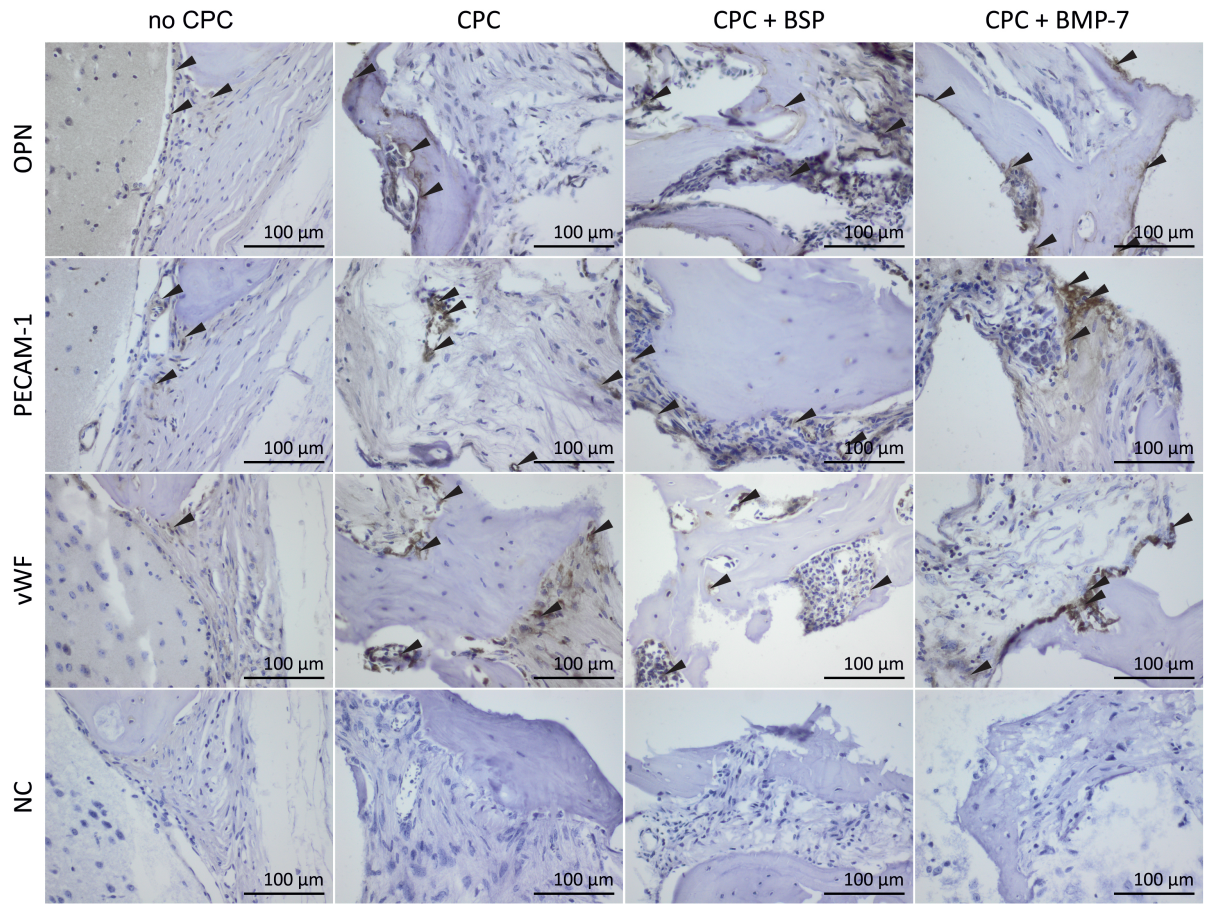

Fig. 4.40: Representative images of immunohistology. Expression of Osteopontin, PECAM-1 and vWF is indicated with black arrows. As negative control (NC) served sections incubated with PBS instead of a first antibody.

First indications that BSP could influence desmal bone formation were shown in earlier *in vitro* experiments with calvarial cells [133, 196]. Here no significant differences were observed in bone regeneration by BSP-coated CPCs compared with uncoated scaffolds. However, a tendency towards a greater bone volume was detected. In the groups with BSP-coated scaffolds, more bone formation was detected in the centre of the defect. Bone formation on the edge of defect is similar to the formation by untreated scaffolds (Fig. 4.39). Considering the enhanced bone formation in the middle of the defect, BSP may initially boost bone formation or accelerate the whole process. These results are similar to the findings of Choi et al. [197], who prepared a collagen-binding peptide (CB-peptide) on the basis of the sequence of the collagen-binding region of BSP. Choi et al. implanted a hydroxyapatite (HA) scaffold without or with absorbed CB-peptide in an 8 mm calvarial defect of rats. After two weeks, the group with HA-scaffold and CB-peptide showed a significant higher area of newly formed bone compared with HA alone. In addition, besides bone growth at the bony borders, bone growth was also detected at the centre of the calvarial defect [197]. Xu et al. observed fibrous tissue at the centre of a CSD in rats treated with collagen or gelatine alone. In contrast, new bone formation was shown in the middle by treating with BSP-gelatine or BSP-collagen after four weeks [198]. Examinations on varied time points within 30 days after implantation of BSP-collagen implants into rat calvarial defects as well as thoracic subcutaneous pouches

revealed mineral deposition and bone formation only in calvarial defects [171]. These studies focused on the first four weeks. After eight weeks, bone formation at the centre of the defect was further detected in the control group with an uncoated CPC scaffold. Therefore, more investigations are required on earlier time points (e.g. two and four weeks) to confirm the early effect of BSP on bone formation as well as on later time points (e.g. four months, six months) to examine whether differences caused by the initial boost effect of BSP would result in a different or a similar quality of bone.

4.6.2 Femoral condyle borehole defect model

A 3 mm thick borehole defect was placed in the lateral femur condyle on each side. Uncoated, BSP-coated and BMP-7-coated CPC scaffolds were implanted in those defects. No treatment served as internal control. After a four-week observation period, µCT examinations were carried out for the quantification of the BV/TV ratio.

Evaluation of BV/TV via µCT

Fig. 4.41 displays radiographs and µCT images as well as the results of BV/TV analyses. Between the CPC modified groups, no obvious differences were detected: all implants were integrated into bone (A). It is, therefore, required to perform quantitative examinations for more clear results. In the control group with no CPC implantation, the defect was closed only marginally after four weeks. Notches were visible on the side where the defect was set (C).

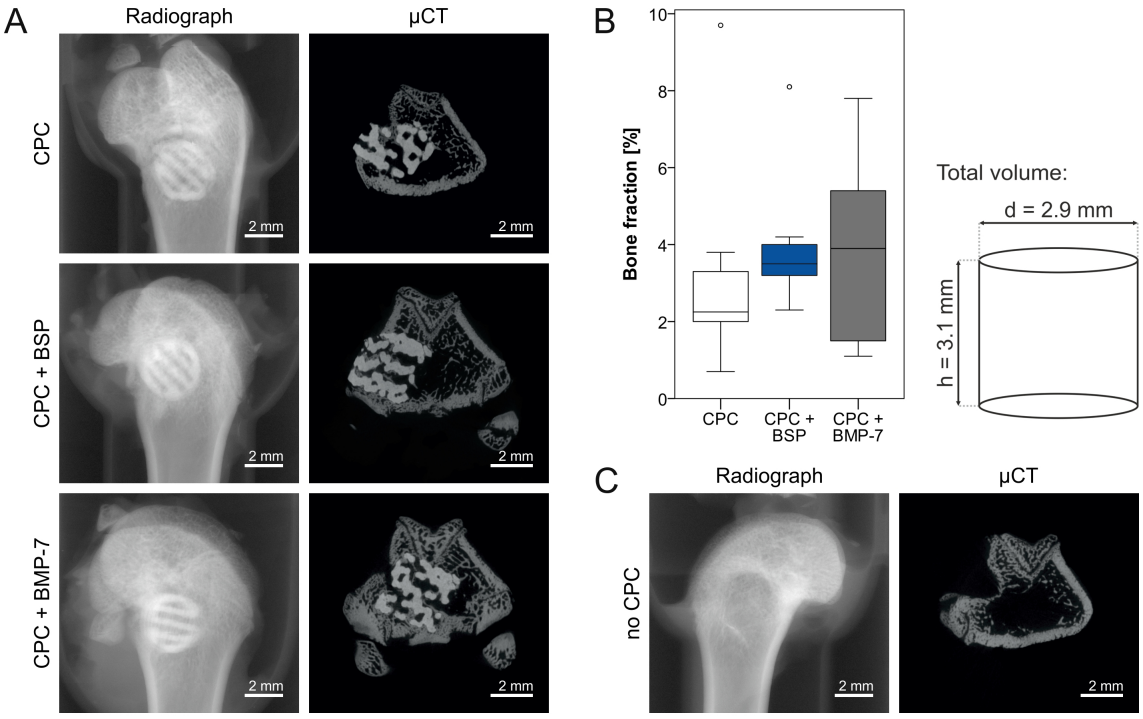

Fig. 4.41: Results of the femoral condyle defect model. Part A shows representative radiographs and µCT images four weeks after setting a 3 mm borehole defect. B displays the bone fraction due to bone volume/total volume examinations. Results are expressed as medians and quartiles (n=10). C displays representative images from the control with no scaffold implantation (no CPC).

Evaluation of the BV/TV ratio showed the highest amount of bone in the group with BMP-7-coated scaffolds (3.9 %), followed by BSP-coated scaffolds (3.5 %). The lowest bone fraction (2.3 %) was detected in the group with uncoated scaffolds. However, no significant differences were shown between the various groups.

Histological examinations

Staining of histological sections with TB and HE showed after four weeks in the control connective tissue on the edge of the defect. Particularly, a still existing gap was visible in the highest magnification. Groups with implanted materials showed in bone integrated scaffolds. Moreover, bone formation was detectable inside the scaffolds, as shown in Fig. 4.42 (areas are indicated by white arrows).

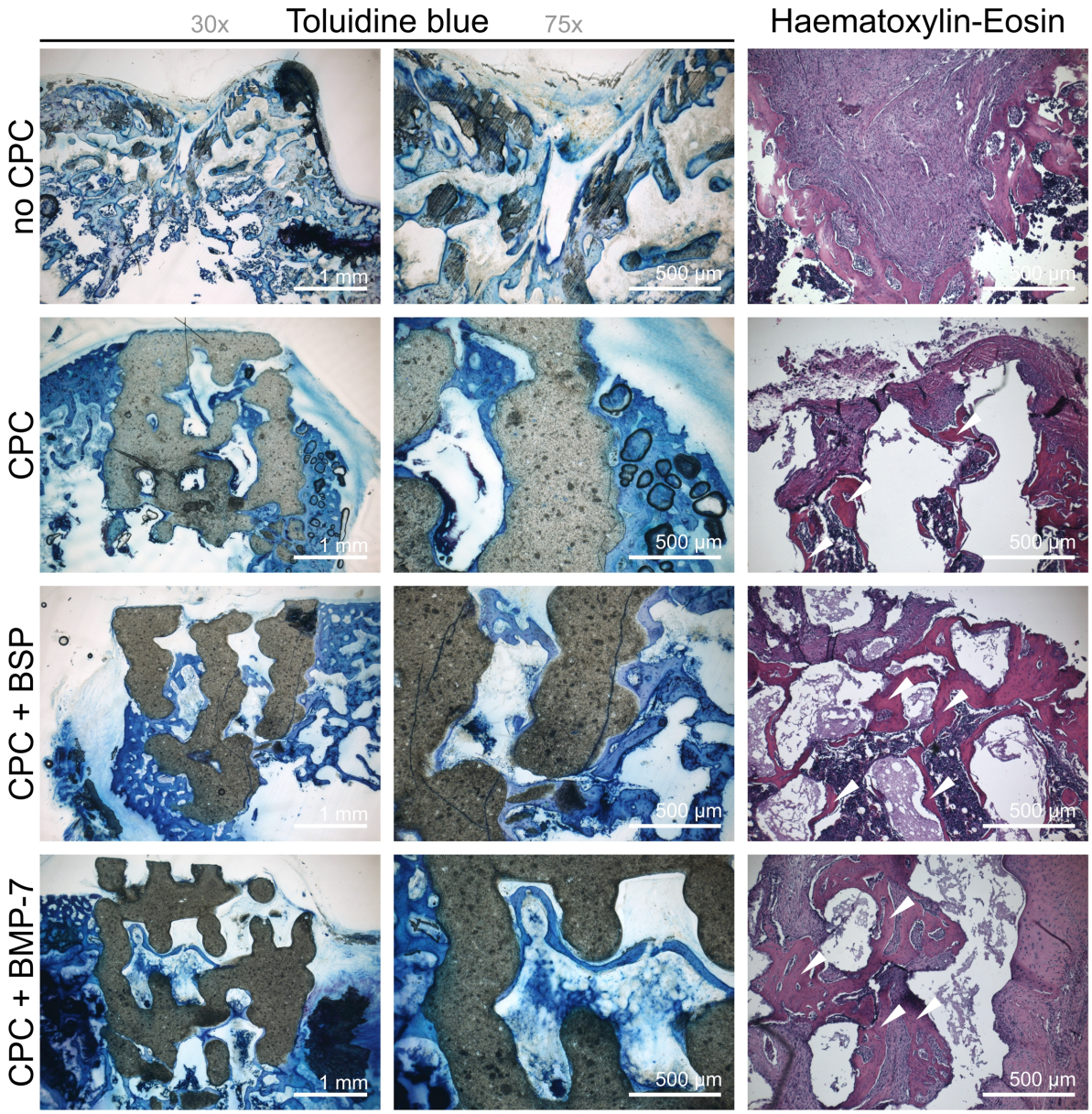

Fig. 4.42: Histological examinations of bone regeneration in femoral condyle defects after four weeks via toluidine blue and HE staining.

Although no significant differences were observed between the varied modified implants after four weeks, BSP coating of CPC bone substitutes indicate more bone formation than the uncoated scaffolds. A study by Holm et al. demonstrated a potential role of BSP in endochondral ossification. BSP knock-out mice showed delayed mineral deposition and less femur bone growth compared to wild-type mice [199]. Similar studies with BSP knock-out mice [65, 200, 67] underline the essential role of BSP in bone formation. $BSP^{-/-}$ mice had shorter bones, which were further hypomineralised [65] and showed declined cortical defect repair [67]. In addition, O'Toole et al. performed pull-out tests of BSP coated titanium implanted in rat femurs. Addition of BSP displayed in histologically examinations a higher number of osteoblasts and parts with neovascularisation even if no effect of BSP on the pull-out strength was detected [201]. As mentioned in section 4.6.1, further analyses are required to figure out the whole potential of BSP-coated biomaterials. Nevertheless, examinations focusing on possible initiations of further problems - for example BSP is known as a key factor of osteoarthritis [202] - should not be neglected.

4.6.3 Conclusion

Implantation of BSP-coated CPC scaffolds displayed a trend of enhanced bone formation in calvarial and femoral condyle defects in comparison with untreated scaffolds. Although no significant differences were detected, this trend pointed out a possible role of BSP in bone formation. Particularly, histological analyses displayed in calvarial defects more bone ingrowth into the centre of the defect. However, further studies are required to confirm this trend.

4.7 Discussion

4.7.1 Final discussion of the *in vitro* part

Regarding the overall *in vitro* results, BSP effects osteogenic differentiation. Gene expression of RUNX2, SP7 and OPN was enhanced, mainly significant, after four days. This applied for BSP-functionalised titanium implants as well as for collagen gels. In light of the poor seeding efficiency of hOBs on CPCs, gene expression analyses could only be conducted after 14 days. Nevertheless, the same markers (SP7, RUNX2 and OPN) displayed by highly concentrated BSP coating solutions a trend of enhanced expression rates when compared to no BSP coating. Those results - significant enhanced gene expression after four days as well as a not-significant trend after 14 days - are congruent with other *in vitro* data, where BSP was supplemented directly to cell culture medium [133]. Nevertheless, a consistent BSP release via cytomegalovirus-mediated adenoviral BSP overexpressing cells led to a significant enhancement even after 10 days in their study [133]. This leads to the assumption that continuous BSP release may better support gene expression and bone formation. Therefore, drug-delivery-systems [203, 204], which release BSP in a continuous and stable way, may be one option for further studies. One focus of this work lies in the aim to find a suitable and practicable coating method for BSP. Both physisorption and covalent coupling were feasible. Limitations of the performed release kinetics are the short duration (two or three days) as well as not determining saturation conditions. Another aspect, which should be taken into consideration, is the discrepancy between BSP concentrations for direct addition or for coating procedures. Supplementation of soluble BSP or its incorporation in collagen gels operated with lower concentrations (1 - 10 µg/ml), whereas obvious higher concentrations were used for BSP functionalisation (up to 280 µg/ml). Optimisation concerning BSP concentrations, release kinetics over weeks as well as other coupling agents (e.g. carbodiimides) or other drug-delivery systems should be performed or evaluated in ongoing studies.
Another point of criticism could be that large deviations were observed in most experiments. Probably these variations resulted from the use of primary human osteoblasts. As explained in the introduction (see 1.4.1), primary cells may have inhomogeneous phenotypes, particularly when the respective experiments were performed with cells from three different donors. Osteoblast preparations from ten different donors - age ranged between 51 and 90 - were used for the experiments. However, this fact can also be seen as an advantage as it enables to screen or evaluate the potential of BSP functionalisation independent of individual characteristics. Overall, the *in vitro* results showed that higher concentrations generally promote osteogenic differentiation, while lower concentrations have a better effect on mineralisation and angiogenetic potential.

4.7.2 Final discussion of the *in vivo* part

Bone formation and regeneration require mineralisation, osteogenic differentiation and angiogenesis processes [192]. The choice to test only one high concentration *in vivo* was owed to concentration-dependent effects on the gene expression results of CPCs and moreover, on previous studies where lower concentrations (10 µg/ml) of equal recombinant BSP showed no effects *in vivo* [179]. Adoptions to other concentrations are reserved for further studies in case of appropriate results.

Limitations of the calvarial model existed by the positive control - CPCs coated with BMP-7. On the basis of BSP coating, the same procedure of functionalisation was carried out with BMP-7. The strategy was to treat all samples identically. Unfortunately, in case of BMP-7, this resulted in non-active BMP-7 on the scaffolds' surface probably due to protein instability. This assumption was concluded as no substantial differences existed compared with the pure scaffold. Moreover, in another proof-of-concept study, where BMP-7 immobilised in collagen gels was used as positive control, enormous bone formation was observed and the defect was closed completely after six weeks [103, 104]. Considering these facts, the assumption that BSP might be in-active cannot be excluded. Fortunately, this is extremely implausible. Significant effects were shown after BSP functionalisation *in vitro* and a study by Zhou et al. examined the stability of BSP. Heated (up to 100 °) or alkylated BSP was still able to increase ALP activity [134]. Changes in the scaffolds' treatment on part of the manufacturer for the second *in vivo* model might explain the better outcome of BMP-7-coated CPCs in the femoral condyle defect model. Due to convincing studies, the manufacturer changed his protocol and stored the scaffolds in stimulated body fluid. This change in procedure might result in slightly better BMP-7 functionality after the coating procedure.

Another problem occurred due to the fitting precision of the scaffolds. On the one hand, they were much higher than the calvaria itself and on the other hand, not all scaffolds fitted perfectly in the defect by diameter. The greater implant height might affect the dura. The dura itself can support bone regeneration [101, 205, 206], that is why utmost care was taken not to injure the dura during surgery. However, a study by Cooper et al. demonstrated that this influence is negligible [101]. Greater effects were accomplished due to vibrations of the drill resulting in marginal greater defects than the implants' diameter. Tight bone implant contact may promote bone formation on a better way. To prevent those double standards, only samples with direct bone implant contact were included in BIC as well as BV/TV analyses.

This problem was circumvented in the second model. A smaller drill was used to set a marginal smaller defect, which was extended to the desired size by manual drilling. However, in this model, the greatest challenge was to create the defects directly in the femoral condyle. This was obtained with the help of x-ray. Nevertheless, after the observation period, some defects shifted proximal.

In both *in vivo* models, no significant differences were observed. Results of histological staining of the calvarial model are of particular interest. Almost complete bone structures were formed vertically in the middle of the defect in the BSP group. Lateral pores allowed cell ingrowth.

But sufficient space for new bone formation existed only in the greater pores in the middle. The scaffold itself hindered new bone formation. Therefore, one option for further studies may be a material which serves at the beginning as leading structure and degrades with time.
The effects of BSP functionalisation are clear for *in vitro* experiments. BSP effects differentiation of osteoblasts and supports angiogenesis, both essential properties for bone formation and regeneration. *In vivo* experiments displayed no significant results. In conformity with other studies where BSP displayed significant effects on earlier time points [198], a presumption is that BSP unfolds its effects on earlier time points. The osteoinductive effect of BSP may boost or accelerate bone formation. Nevertheless, this assumption has to be verified in further studies. In case of the verification of such a boost effect, there is still the question as to whether this effect would lead to a decisive therapeutic benefit. BSP functionalisation might be a promising strategy in cases of load-stability on earlier time points or formation of qualitative physiological bone. In addition, comprehensive studies concerning negative side effects should be conducted as well.
In case of the evaluated material, BSP functionalisation of CPC scaffolds is not worth considering. Defect treatment with the uncoated material resulted in bone ingrowth. The bone formation does not certainly proceeded as in the case of BSP coating, but the discrepancy is acceptable. Enhancement due to additional BSP coating may be negligible compared with the additional effort. However, for biomaterials without osteoinductive properties, BSP functionalisation may be one possible option.

5 Conclusion and Outlook

In this work, BSP functionalisation of different biomaterials was evaluated for applications in orthopaedics and trauma surgery. *In vitro* as well as *in vivo* experiments served as the basis for verification of the achieved effects due to BSP coating. Examination of BSP functions without any carrier material displayed no cytotoxicity, but an enhanced osteoblast mineralisation and alkaline phosphatase activity. For titanium and calcium phosphate cements, appropriate coating methods were established. Physisorption proved to be a suitable coating method for CPCs due to the BSP-binding capability of HA. In contrast, titanium implants required, prior to any coating procedures, surface activation with piranha solution. Thereafter, successful coating procedures via physisorption as well as covalent coupling with silanes are practised to immobilise BSP onto titanium. Both methods resulted in similar effects on hOB behaviour. Physisorption is the simpler and cheaper method, but covalent coupling leads to stronger and controlled BSP functionalisation. Here covalent-modified surfaces showed a greater impact on mRNA expression. Whether this difference is also notable *in vivo* can only be discovered in ongoing experiments. Notwithstanding the biomaterial used for evaluation, BSP functionalisation influenced osteogenic differentiation markers. In general, ALP, Col1 and SPARC displayed no changes or in some cases, a decreased gene expression activity. Greatest effects - which are mainly significant - occurred after four days in RUNX2, SP7 and OPN gene expression. Besides the effect on the key markers of osteoblast differentiation, revealed BSP angiogenetic potential in the angiogenesis assay. Regarding BSP concentrations, higher concentrations seem to result in more enhancement on gene expression, while lower concentrations seem to cause more angiogenetic behaviour. With the help of animal models regarding different ossification ways - the calvarial defect model for desmal ossification and the femoral condyle defect model for endochondral ossification - those *in vitro* effects were verified *in vivo*. No significant differences were observed in new bone formation. BSP-functionalised scaffolds seemed to be better than uncoated materials by trend. To conclude, significant *in vitro* effects on osteoblast differentiation and angiogenesis could not be transferred to *in vivo* conditions. BSP coating of CPCs is by no means worse than the uncoated scaffolds. But the implantation of pure CPC scaffolds resulted in partial bone ingrowth and in bone-integrated materials. Therefore, BSP coating of those materials may not be a realistic option. Nevertheless, histological images from the calvarial defect increases the chance to adopt the option of using BSP in further applications. Consequently, BSP coating of other biomaterials without osteoinductive properties, may be a possible option. Future studies will be necessary to evaluate the potential of BSP irrespective of CPCs. Feasible alternatives as carrier material for BSP may be collagen or with focus on drug-delivery systems, a composite with PLGA.

Bibliography

[1] Vert M, Doi Y, Hellwich KH, Hess M, Hodge P, Kubisa P, Rinaudo M and Schué F (2012). Terminology for biorelated polymers and applications (IUPAC Recommendations 2012). *Pure and Applied Chemistry* **84**, 377–410.

[2] Williams DF (1999). The Williams dictionary of biomaterials (Liverpool: Liverpool University Press).

[3] Ratner BD and Bryant SJ (2004). Biomaterials: where we have been and where we are going. *Annual Review of Biomedical Engineering* **6**, 41–75.

[4] Statistisches Bundesamt. Fallpauschalenbezogene Krankenhausstatistik (DRG-Statistik): Operationen und Prozeduren der vollstationären Patientinnen und Patienten der Krankenhäuser (4-Steller).

[5] Geetha M, Singh AK, Asokamani R and Gogia AK (2009). Ti based biomaterials, the ultimate choice for orthopaedic implants – A review. *Progress in Materials Science* **54**, 397–425.

[6] Frohlich M, Grayson W, Wan L, Marolt D, Drobnic M and Vunjak-Novakovic G (2008). Tissue engineered bone grafts: Biological requirements, tissue culture and clinical relevance. *Current Stem Cell Research & Therapy* **3**, 254–264.

[7] Bauer TW and Muschler GF (2000). Bone graft materials: An overview of the basic science. *Clinical Orthopaedics and Related Research* **371**.

[8] Verrier S, Alini M, Alsberg E, Buchman SR, Kelly D, Laschke MW, Menger MD, Murphy WL, Stegemann JP, Schutz M, Miclau T, Stoddart MJ and Evans C (2016). Tissue engineering and regenerative approaches to improving the healing of large bone defects. *European Cells & Materials* **32**, 87–110.

[9] Charnley J (1960). Surgery of the hip-joint. *British Medical Journal* **1**, 821–826.

[10] Charnley J (1961). Arthroplasty of the hip: A new operation. *The Lancet* **277**, 1129–1132.

[11] Dohan Ehrenfest DM, Coelho PG, Kang BS, Sul YT and Albrektsson T (2010). Classification of osseointegrated implant surfaces: Materials, chemistry and topography. *Trends in Biotechnology* **28**, 198–206.

[12] Epple M (2003). Biomaterialien und Biomineralisation: Eine Einführung für Naturwissenschaftler, Mediziner und Ingenieure. Teubner-Studienbücher : Chemie, 1. edition (Stuttgart and Leipzig and Wiesbaden: Teubner).

[13] Parida P, Behera A and Mishra SC (2012). Classification of biomaterials used in medicine. *International Journal of Advances in Applied Sciences* **1**, 31–35.

[14] Bolle T, Meyer F, Walcher F, Lohmann C, Jockenhovel S, Gries T and Hoffmann W (2017). Werkstoffe/Biomaterialien in der interventionellen und operativen Medizin - eine kurze Uebersicht und aktuelle Trends. *Zentralblatt fuer Chirurgie* **142**, 216–225.

[15] Navarro M, Michiardi A, Castano O and Planell JA (2008). Biomaterials in orthopaedics. *Journal of the Royal Society* **5**, 1137–1158.

[16] Hench LL and Polak JM (2002). Third-generation biomedical materials. *Science* **295**, 1014–1017.

[17] Roach P, Eglin D, Rohde K and Perry CC (2007). Modern biomaterials: A review—bulk properties and implications of surface modifications. *Journal of Materials Science: Materials in Medicine* **18**, 1263–1277.

[18] Williams DF (2008). On the mechanisms of biocompatibility. *Biomaterials* **29**, 2941–2953.

[19] Geetha M, Singh AK, Asokamani R and Gogia AK (2009). Ti based biomaterials, the ultimate choice for orthopaedic implants – A review. *Progress in Materials Science* **54**, 397–425.

[20] Pohler OE (2000). Unalloyed titanium for implants in bone surgery. *Injury* **31**, D7–D13.

[21] Albrektsson T, Brånemark PI, Hansson HA and Lindström J (2009). Osseointegrated titanium implants: Requirements for ensuring a long-lasting, direct bone-to-implant anchorage in man. *Acta Orthopaedica Scandinavica* **52**, 155–170.

[22] Salgado PC, Sathler PC, Castro HC, Alves GG, Oliveira AMd, Oliveira RCd, Maia MDC, Rodrigues CR, Coelh PG, Fuly A, Cabral LM and Granjeiro JM (2011). Bone remodeling, biomaterials and technological applications: Revisiting basic concepts. *Journal of Biomaterials and Nanobiotechnology* **02**, 318–328.

[23] Kolk A, Handschel J, Drescher W, Rothamel D, Kloss F, Blessmann M, Heiland M, Wolff KD and Smeets R (2012). Current trends and future perspectives of bone substitute materials - from space holders to innovative biomaterials. *Journal of Cranio-Maxillo-Facial Surgery* **40**, 706–718.

[24] Farack J, Wolf-Brandstetter C, Glorius S, Nies B, Standke G, Quadbeck P, Worch H and Scharnweber D (2011). The effect of perfusion culture on proliferation and differentiation of human mesenchymal stem cells on biocorrodible bone replacement material. *Materials Science and Engineering: B* **176**, 1767–1772.

[25] García-Gareta E, Coathup MJ and Blunn GW (2015). Osteoinduction of bone grafting materials for bone repair and regeneration. *Bone* **81**, 112–121.

[26] Wennerberg A and Albrektsson T (2009). Effects of titanium surface topography on bone integration: A systematic review. *Clinical Oral Implants Research* **20 Suppl 4**, 172–184.

[27] Liu X, Chu P and Ding C (2004). Surface modification of titanium, titanium alloys, and related materials for biomedical applications. *Materials Science and Engineering: R: Reports* **47**, 49–121.

[28] Zhang J, Liu W, Schnitzler V, Tancret F and Bouler JM (2014). Calcium phosphate cements for bone substitution: Chemistry, handling and mechanical properties. *Acta Biomaterialia* **10**, 1035–1049.

[29] Eliaz N, Metoki N and Laquerriere P (2017). Calcium phosphate bioceramics: A review of their history, structure, properties, coating technologies and biomedical applications. *Materials* **10**, 334.

[30] Bose S and Tarafder S (2012). Calcium phosphate ceramic systems in growth factor and drug delivery for bone tissue engineering: A review. *Acta Biomaterialia* **8**, 1401–1421.

[31] LeGeros RZ (2008). Calcium phosphate-based osteoinductive materials. *Chemical Reviews* **108**, 4742–4753.

[32] Ginebra MP, Canal C, Espanol M, Pastorino D and Montufar EB (2012). Calcium phosphate cements as drug delivery materials. *Advanced Drug Delivery Reviews* **64**, 1090–1110.

[33] Trombetta R, Inzana JA, Schwarz EM, Kates SL and Awad HA (2017). 3D printing of calcium phosphate ceramics for bone tissue engineering and drug delivery. *Annals of Biomedical Engineering* **45**, 23–44.

[34] Miyata T, Taira T and Noishiki Y (1992). Collagen engineering for biomaterial use. *Clinical Materials* **9**, 139–148.

[35] Parenteau-Bareil R, Gauvin R and Berthod F (2010). Collagen-based biomaterials for tissue engineering applications. *Materials* **3**, 1863–1887.

[36] Friess W (1998). Collagen – biomaterial for drug delivery. *European Journal of Pharmaceutics and Biopharmaceutics* **45**, 113–136.

[37] Lee CH, Singla A and Lee Y (2001). Biomedical applications of collagen. *International Journal of Pharmaceutics* **221**, 1–22.

[38] Chattopadhyay S and Raines RT (2014). Review collagen-based biomaterials for wound healing. *Biopolymers* **101**, 821–833.

[39] Cen L, Liu W, Cui L, Zhang W and Cao Y (2008). Collagen tissue engineering: Development of novel biomaterials and applications. *Pediatric Research* **63**, 492–496.

[40] Roach P, Farrar D and Perry CC (2006). Surface tailoring for controlled protein adsorption: effect of topography at the nanometer scale and chemistry. *Journal of the American Chemical Society* **128**, 3939–3945.

[41] Williams DF (1987). Tissue-biomaterial interactions. *Journal of Materials Science* **22**, 3421–3445.

[42] Vroman L (1962). Effect of adsorbed proteins on the wettability of hydrophilic and hydrophobic solids. *Nature* **196**, 476 EP.

[43] Leonard EF and Vroman L (1992). Is the Vroman effect of importance in the interaction of blood with artificial materials? *Journal of Biomaterials Science, Polymer Edition* **3**, 95–107.

[44] Nanci A, Wuest JD, Peru L, Brunet P, Sharma V, Zalzal S and McKee MD (1998). Chemical modification of titanium surfaces for covalent attachment of biological molecules. *Journal of Biomedical Materials Research* **40**, 324–335.

[45] Maia FR, Bidarra SJ, Granja PL and Barrias CC (2013). Functionalization of biomaterials with small osteoinductive moieties. *Acta Biomaterialia* **9**, 8773–8789.

[46] Puleo D and Nanci A (1999). Understanding and controlling the bone–implant interface. *Biomaterials* **20**, 2311–2321.

[47] Hlady V and Buijs J (1996). Protein adsorption on solid surfaces. *Current Opinion in Biotechnology* **7**, 72–77.

[48] Nakanishi K, Sakiyama T and Imamura K (2001). On the adsorption of proteins on solid surfaces, a common but very complicated phenomenon. *Journal of Bioscience and Bioengineering* **91**, 233–244.

[49] Liu SQ, Ito Y and Imanishi Y (1992). Cell growth on immobilized cell-growth factor; 4: Interaction of fibroblast cells with insulin immobilized on poly(memthyl methacyrlate) membrane. *Journal of Biochemical and Biophysical Methods* **25**, 139–148.

[50] Liu SQ, Ito Y and Imanishi Y (1993). Cell growth on immobilized cell growth factor: 5. Interaction of immobilized transferrin with fibroblast cells. *International Journal of Biological Macromolecules* **15**, 221–226.

[51] Kuhl PR and Griffith-Cima LG (1996). Tethered epidermal growth factor as a paradigm for growth factor–induced stimulation from the solid phase. *Nature Medicine* **2**, 1022 EP.

[52] Puleo DA (1999). Release and retention of biomolecules in collagen deposited on orthopedic biomaterials. *Artificial Cells, Blood Substitutes, and Biotechnology* **27**, 65–75.

[53] Compston JE (2001). Sex steroids and bone. *Physiological Reviews* **81**, 419–447.

[54] Florencio-Silva R, Sasso GRdS, Sasso-Cerri E, Simoes MJ and Cerri PS (2015). Biology of bone tissue: Structure, function, and factors that influence bone cells. *BioMed Research International* **2015**, 421746.

[55] Vincent K and Durrant MC (2013). A structural and functional model for human bone sialoprotein. *Journal of Molecular Graphics & Modelling* **39**, 108–117.

[56] Staines KA, MacRae VE and Farquharson C (2012). The importance of the SIBLING family of proteins on skeletal mineralisation and bone remodelling. *The Journal of Endocrinology* **214**, 241–255.

[57] Ross FP, Chappel J, Alvarez JI, Sander D, Butler WT, Farach-Carson MC, Mintz KA, Robey PG, Teitelbaum SL and Cheresh DA (1993). Interactions between the bone matrix proteins osteopontin and bone sialoprotein and the osteoclast integrin alpha v beta 3 potentiate bone resorption. *Journal of Biological Chemistry* **268**, 9901–9907.

[58] Rapuano BE, Wu C and MacDonald DE (2004). Osteoblast-like cell adhesion to bone sialoprotein peptides. *Journal of Orthopaedic Research* **22**, 353–361.

[59] Chatakun P, Nunez-Toldra R, Diaz Lopez EJ, Gil-Recio C, Martinez-Sarra E, Hernandez-Alfaro F, Ferres-Padro E, Giner-Tarrida L and Atari M (2014). The effect of five proteins on stem cells used for osteoblast differentiation and proliferation: A current review of the literature. *Cellular and Molecular Life Sciences : CMLS* **71**, 113–142.

[60] Siebers MC, ter Brugge PJ, Walboomers XF and Jansen JA (2005). Integrins as linker proteins between osteoblasts and bone replacing materials. A critical review. *Biomaterials* **26**, 137–146.

[61] Gordon JAR, Hunter GK and Goldberg HA (2009). Activation of the mitogen-activated protein kinase pathway by bone sialoprotein regulates osteoblast differentiation. *Cells Tissues Organs* **189**, 138–143.

[62] Ogata Y (2008). Bone sialoprotein and its transcriptional regulatory mechanism. *Journal of Periodontal Research* **43**, 127–135.

[63] Yang Y, Mkhonto D, Cui Q and Sahai N (2011). Theoretical study of bone sialoprotein in bone biomineralization. *Cells Tissues Organs* **194**, 182–187.

[64] Tye CE, Rattray KR, Warner KJ, Gordon JAR, Sodek J, Hunter GK and Goldberg HA (2003). Delineation of the hydroxyapatite-nucleating domains of bone sialoprotein. *The Journal of Biological Chemistry* **278**, 7949–7955.

[65] Malaval L, Wade-Gueye NM, Boudiffa M, Fei J, Zirngibl R, Chen F, Laroche N, Roux JP, Burt-Pichat B, Duboeuf F, Boivin G, Jurdic P, Lafage-Proust MH, Amedee J, Vico L, Rossant J and Aubin JE (2008). Bone sialoprotein plays a functional role in bone

formation and osteoclastogenesis. *The Journal of Experimental Medicine* **205**, 1145–1153.

[66] Boudiffa M, Wade-Gueye NM, Guignandon A, Vanden-Bossche A, Sabido O, Aubin JE, Jurdic P, Vico L, Lafage-Proust MH and Malaval L (2010). Bone sialoprotein deficiency impairs osteoclastogenesis and mineral resorption in vitro. *Journal of Bone and Mineral Research* **25**, 2669–2679.

[67] Monfoulet L, Malaval L, Aubin JE, Rittling SR, Gadeau AP, Fricain JC and Chassande O (2010). Bone sialoprotein, but not osteopontin, deficiency impairs the mineralization of regenerating bone during cortical defect healing. *Bone* **46**, 447–452.

[68] Bouleftour W, Juignet L, Bouet G, Granito RN, Vanden-Bossche A, Laroche N, Aubin JE, Lafage-Proust MH, Vico L and Malaval L (2016). The role of the SIBLING, Bone sialoprotein in skeletal biology - Contribution of mouse experimental genetics. *Matrix Biology* **52-54**, 60–77.

[69] Marsell R and Einhorn TA (2011). The biology of fracture healing. *Injury* **42**, 551–555.

[70] Nakahama KI (2010). Cellular communications in bone homeostasis and repair. *Cellular and Molecular Life Sciences : CMLS* **67**, 4001–4009.

[71] Schindeler A, McDonald MM, Bokko P and Little DG (2008). Bone remodeling during fracture repair: The cellular picture. *Seminars in Cell & Developmental Biology* **19**, 459–466.

[72] Marks SC JR and Popoff SN (1988). Bone cell biology: The regulation of development, structure, and function in the skeleton. *The American Journal of Anatomy* **183**, 1–44.

[73] Hoemann CD, El-Gabalawy H and McKee MD (2009). In vitro osteogenesis assays: Influence of the primary cell source on alkaline phosphatase activity and mineralization. *Pathologie-Biologie* **57**, 318–323.

[74] Liu WC, Chen S, Zheng L and Qin L (2017). Angiogenesis assays for the evaluation of angiogenic properties of orthopaedic biomaterials – A general review. *Advanced Healthcare Materials* **6**, 1600434–n/a.

[75] Czekanska EM, Stoddart MJ, Richards RG and Hayes JS (2012). In search of an osteoblast cell model for in vitro research. *European Cells & Materials* **24**, 1–17.

[76] Boskey AL and Roy R (2008). Cell culture systems for studies of bone and tooth mineralization. *Chemical Reviews* **108**, 4716–4733.

[77] Declercq H, van den Vreken N, Maeyer ED, Verbeeck R, Schacht E, Ridder LD and Cornelissen M (2004). Isolation, proliferation and differentiation of osteoblastic cells to study cell/biomaterial interactions: Comparison of different isolation techniques and source. *Biomaterials* **25**, 757–768.

[78] Jonsson KB, Frost A, Nilsson O, Ljunghall S and Ljunggren Ö (1999). Three isolation techniques for primary culture of human osteoblast-like cells: A comparison. *Acta Orthopaedica Scandinavica* **70**, 365–373.

[79] Kartsogiannis V and Ng KW (2004). Cell lines and primary cell cultures in the study of bone cell biology. *Molecular and Cellular Endocrinology* **228**, 79–102.

[80] Katzburg S, Lieberherr M, Ornoy A, Klein BY, Hendel D and Somjen D (1999). Isolation and hormonal responsiveness of primary cultures of human bone-derived cells: Gender and age differences. *Bone* **25**, 667–673.

[81] Yorukoglu AC, Kiter AE, Akkaya S, Satiroglu-Tufan NL and Tufan AC (2017). A concise review on the use of mesenchymal stem cells in cell sheet-based tissue engineering with special emphasis on bone tissue Regeneration. *Stem Cells International* , doi.org/10.1155/2017/2374161.

[82] Wu M, Chen G and Li YP (2016). TGF and BMP signaling in osteoblast, skeletal development, and bone formation, homeostasis and disease. *Bone Research* **4**, 16009 EP.

[83] Heiss M, Hellstrom M, Kalen M, May T, Weber H, Hecker M, Augustin HG and Korff T (2015). Endothelial cell spheroids as a versatile tool to study angiogenesis in vitro. *FASEB Journal* **29**, 3076–3084.

[84] Richards J, Larson L, Yang J, Guzman R, Tomooka Y, Osborn R, Imagawa W and Nandi S (1983). Method for culturing mammary epithelial cells in a rat tail collagen gel matrix. *Journal of Tissue Culture Methods* **8**, 31–36.

[85] Prince M, Banerjee C, Javed A, Green J, Lian JB, Stein GS, Bodine PV and Komm BS (2001). Expression and regulation of Runx2/Cbfa1 and osteoblast phenotypic markers during the growth and differentiation of human osteoblasts. *Journal of Cellular Biochemistry* **80**, 424–440.

[86] Marie PJ (2008). Transcription factors controlling osteoblastogenesis. *Archives of Biochemistry and Biophysics* **473**, 98–105.

[87] Kundu M, Javed A, Jeon JP, Horner A, Shum L, Eckhaus M, Muenke M, Lian JB, Yang Y, Nuckolls GH, Stein GS and Liu PP (2002). Cbfbeta interacts with Runx2 and has a critical role in bone development. *Nature Genetics* **32**, 639–644.

[88] Komori T (2006). Regulation of osteoblast differentiation by transcription factors. *Journal of Cellular Biochemistry* **99**, 1233–1239.

[89] Amorim BR, Okamura H, Yoshida K, Qiu L, Morimoto H and Haneji T (2007). The transcriptional factor Osterix directly interacts with RNA helicase A. *Biochemical and Biophysical Research Communications* **355**, 347–351.

[90] Kaback LA, Soung DY, Naik A, Smith N, Schwarz EM, O'Keefe RJ and Drissi H (2008). Osterix/Sp7 regulates mesenchymal stem cell mediated endochondral ossification. *Journal of Cellular Physiology* **214**, 173–182.

[91] Nakashima K, Zhou X, Kunkel G, Zhang Z, Deng JM, Behringer RR and de Crombrugghe B (2002). The novel zinc finger-containing transcription factor osterix is required for osteoblast differentiation and bone formation. *Cell* **108**, 17–29.

[92] Samavedi S, Whittington AR and Goldstein AS (2013). Calcium phosphate ceramics in bone tissue engineering: A review of properties and their influence on cell behavior. *Acta Biomaterialia* **9**, 8037–8045.

[93] Sodek J, Ganss B and McKee MD (2000). Osteopontin. *Critical Reviews in Oral Biology & Medicine* **11**, 279–303.

[94] Aubin JE, Liu F, Malaval L and Gupta AK (1995). Osteoblast and chondroblast differentiation. *Bone* **17**, S77–S83.

[95] Kulterer B, Friedl G, Jandrositz A, Sanchez-Cabo F, Prokesch A, Paar C, Scheideler M, Windhager R, Preisegger KH and Trajanoski Z (2007). Gene expression profiling of human mesenchymal stem cells derived from bone marrow during expansion and osteoblast differentiation. *BMC Genomics* **8**, 70.

[96] O'Connor JP (1998). Animal models of heterotopic ossification. *Clinical Orthopaedics and Related Research* **346**, 71–80.

[97] Schindeler A, Mills RJ, Bobyn JD and Little DG (2017). Preclinical models for orthopedic research and bone tissue engineering. *Journal of Orthopaedic Research* **2017**.

[98] Spicer PP, Kretlow JD, Young S, Jansen JA, Kasper FK and Mikos AG (2012). Evaluation of bone regeneration using the rat critical size calvarial defect. *Nature Protocols* **7**, 1918–1929.

[99] Gomes PS and Fernandes MH (2011). Rodent models in bone-related research: The relevance of calvarial defects in the assessment of bone regeneration strategies. *Laboratory Animals* **45**, 14–24.

[100] Berendsen AD and Olsen BR (2015). Bone development. *Bone* **80**, 14–18.

[101] Cooper GM, Mooney MP, Gosain AK, Campbell PG, Losee JE and Huard J (2010). Testing the critical size in calvarial bone defects: revisiting the concept of a critical-size defect. *Plastic and Reconstructive Surgery* **125**, 1685–1692.

[102] Vajgel A, Mardas N, Farias BC, Petrie A, Cimões R and Donos N (2014). A systematic review on the critical size defect model. *Clinical Oral Implants Research* **25**, 879–893.

[103] Hertweck J (2016). In vivo Untersuchung prävaskularisierter Knochenersatzkonstrukte. Dissertation, Johannes Gutenberg-Universität Mainz, Mainz.

[104] Hertweck J, Ritz U, Götz H, Schottel PC, Rommens PM and Hofmann A (2017). CD34(+) cells seeded in collagen scaffolds promote bone formation in a mouse calvarial defect model. *Journal of Biomedical Materials Research Part B, Applied Biomaterials* , 10.1002/jbm.b.33956.

[105] Nishimura R, Hata K, Ono K, Amano K, Takigawa Y, Wakabayashi M, Takashima R and Yoneda T (2012). Regulation of endochondral ossification by transcription factors. *Frontiers in Bioscience* **17**, 2657–2666.

[106] Mackie EJ, Ahmed YA, Tatarczuch L, Chen KS and Mirams M (2008). Endochondral ossification: How cartilage is converted into bone in the developing skeleton. *The International Journal of Biochemistry & Cell Biology* **40**, 46–62.

[107] Hata K, Takahata Y, Murakami T and Nishimura R (2017). Transcriptional network controlling endochondral ossification. *Journal of Bone Metabolism* **24**, 75–82.

[108] Pearce AI, Richards RG, Milz S, Schneider E and Pearce SG (2007). Animal models for implant biomaterial research in bone: a review. *European Cells & Materials* **13**, 1–10.

[109] Akkineni AR, Luo Y, Schumacher M, Nies B, Lode A and Gelinsky M (2015). 3D plotting of growth factor loaded calcium phosphate cement scaffolds. *Acta Biomaterialia* **27**, 264–274.

[110] Lode A, Meissner K, Luo Y, Sonntag F, Glorius S, Nies B, Vater C, Despang F, Hanke T and Gelinsky M (2014). Fabrication of porous scaffolds by three-dimensional plotting of a pasty calcium phosphate bone cement under mild conditions. *Journal of Tissue Engineering and Regenerative Medicine* **8**, 682–693.

[111] Dettin M, Bagno A, Gambaretto R, Iucci G, Conconi MT, Tuccitto N, Menti AM, Grandi C, Di Bello C, Licciardello A and Polzonetti G (2009). Covalent surface modification of titanium oxide with different adhesive peptides: surface characterization and osteoblast-like cell adhesion. *Journal of Biomedical Materials Research Part A* **90**, 35–45.

[112] Baranowski A, Klein A, Ritz U, Ackermann A, Anthonissen J, Kaufmann KB, Brendel C, Gotz H, Rommens PM and Hofmann A (2016). Surface functionalization of orthopedic titanium implants with bone sialoprotein. *PloS One* **11**, e0153978.

[113] Watts JF (1994). X-ray photoelectron spectroscopy. *Vacuum* **45**, 653–671.

[114] Hofmann A, Ritz U, Hessmann MH, Schmid C, Tresch A, Rompe JD, Meurer A and Rommens PM (2008). Cell viability, osteoblast differentiation, and gene expression are altered in human osteoblasts from hypertrophic fracture non-unions. *Bone* **42**, 894–906.

[115] Hofmann A, Ritz U, Verrier S, Eglin D, Alini M, Fuchs S, Kirkpatrick CJ and Rommens PM (2008). The effect of human osteoblasts on proliferation and neo-vessel formation of human umbilical vein endothelial cells in a long-term 3D co-culture on polyurethane scaffolds. *Biomaterials* **29**, 4217–4226.

[116] Brendel C, Muller-Kuller U, Schultze-Strasser S, Stein S, Chen-Wichmann L, Krattenmacher A, Kunkel H, Dillmann A, Antoniou MN and Grez M (2012). Physiological regulation of transgene expression by a lentiviral vector containing the A2UCOE linked to a myeloid promoter. *Gene Therapy* **19**, 1018–1029.

[117] Kuhn S, Kroth J, Ritz U, Hofmann A, Brendel C, Muller LP, Forch R and Rommens PM (2014). Reduced fibroblast adhesion and proliferation on plasma-modified titanium surfaces. *Journal of Materials Science Materials in Medicine* **25**, 2549–2560.

[118] Schneider CA, Rasband WS and Eliceiri KW (2012). NIH Image to ImageJ: 25 years of image analysis. *Nature Methods* **9**, 671–675.

[119] O'Brien J, Wilson I, Orton T and Pognan F (2000). Investigation of the Alamar Blue (resazurin) fluorescent dye for the assessment of mammalian cell cytotoxicity. *European Journal of Biochemistry* **267**, 5421–5426.

[120] Bopp SK and Lettieri T (2008). Comparison of four different colorimetric and fluorometric cytotoxicity assays in a zebrafish liver cell line. *BMC Pharmacology* **8**, 8.

[121] Livak KJ and Schmittgen TD (2001). Analysis of relative gene expression data using real-time quantitative PCR and the 2(-Delta Delta C(T)) Method. *Methods* **25**, 402–408.

[122] Vandesompele J, de Preter K, Pattyn F, Poppe B, van Roy N, de Paepe A and Speleman F (2002). Accurate normalization of real-time quantitative RT-PCR data by geometric averaging of multiple internal control genes. *Genome Biology* **3**, research0034.1.

[123] Andersen CL, Jensen JL and Orntoft TF (2004). Normalization of real-time quantitative reverse transcription-PCR data: a model-based variance estimation approach to identify genes suited for normalization, applied to bladder and colon cancer data sets. *Cancer Research* **64**, 5245–5250.

[124] Pfaffl MW, Tichopad A, Prgomet C and Neuvians TP (2004). Determination of stable housekeeping genes, differentially regulated target genes and sample integrity: Best-Keeper – Excel-based tool using pair-wise correlations. *Biotechnology Letters* **26**, 509–515.

[125] Silver N, Best S, Jiang J and Thein SL (2006). Selection of housekeeping genes for gene expression studies in human reticulocytes using real-time PCR. *BMC Molecular Biology* **7**, 33.

[126] Chen G, Zhao L, Feng J, You G, Sun Q, Li P, Han D and Zhou H (2013). Validation of reliable reference genes for real-time PCR in human umbilical vein endothelial cells on substrates with different stiffness. *PloS One* **8**, e67360.

[127] Korff T and Augustin HG (1998). Integration of endothelial cells in multicellular spheroids prevents apoptosis and induces differentiation. *The Journal of Cell Biology* **143**, 1341–1352.

[128] Schindelin J, Rueden CT, Hiner MC and Eliceiri KW (2015). The ImageJ ecosystem: An open platform for biomedical image analysis. *Molecular Reproduction and Development* **82**, 518–529.

[129] Cardona A, Schmid B, Rueden C, White DJ, Frise E, Arganda-Carreras I, Tinevez JY, Schindelin J, Eliceiri K, Longair M, Tomancak P, Preibisch S, Saalfeld S, Pietzsch T, Kaynig V and Hartenstein V (2012). Fiji: An open-source platform for biological-image analysis. *Nature Methods* **9**, 676.

[130] Doube M, Klosowski MM, Arganda-Carreras I, Cordelieres FP, Dougherty RP, Jackson JS, Schmid B, Hutchinson JR and Shefelbine SJ (2010). BoneJ: Free and extensible bone image analysis in ImageJ. *Bone* **47**, 1076–1079.

[131] Donath K (1995). Preparation of histologic sections: by the cutting-grinding technique for hard tissue and other material not suitable to be sectioned by routine methods: - Equipment and methodical performance -. *EXAKT-Kulzer-Publicaton* .

[132] Guesdon JL, Ternynck T and Avrameas S (1979). The use of avidin-biotin interaction in immunoenzymatic techniques. *The Journal of Histochemistry and Cytochemistry* **27**, 1131–1139.

[133] Gordon JAR, Tye CE, Sampaio AV, Underhill TM, Hunter GK and Goldberg HA (2007). Bone sialoprotein expression enhances osteoblast differentiation and matrix mineralization in vitro. *Bone* **41**, 462–473.

[134] Zhou HY, Takita H, Fujisawa R, Mizuno M and Kuboki Y (1995). Stimulation by bone sialoprotein of calcification in osteoblast-like MC3T3-E1 cells. *Calcified Tissue International* **56**, 403–407.

[135] Phinney DG, Kopen G, Righter W, Webster S, Tremain N and Prockop DJ (1999). Donor variation in the growth properties and osteogenic potential of human marrow stromal cells. *Journal of Cellular Biochemistry* **75**, 424–436.

[136] Valverde P, Zhang J, Fix A, Zhu J, Ma W, Tu Q and Chen J (2008). Overexpression of bone sialoprotein leads to an uncoupling of bone formation and bone resorption in mice. *Journal of Bone and Mineral Research* **23**, 1775–1788.

[137] Im BJ, Lee SC, Lee MH, Leesungbok R, Ahn SJ, Kang YG, Lee DY, Yoon JH and Lee SW (2016). Promotion of osteoblastic differentiation and osteogenic transcription factor expression on a microgroove titanium surface with immobilized fibronectin or bone sialoprotein II. *Biomedical Materials* **11**, 035020.

[138] Tang Z, Wang Y, Podsiadlo P and Kotov NA (2006). Biomedical applications of layer-by-layer assembly: From biomimetics to tissue engineering. *Advanced Materials* **18**, 3203–3224.

[139] Cai K, Rechtenbach A, Hao J, Bossert J and Jandt KD (2005). Polysaccharide-protein surface modification of titanium via a layer-by-layer technique: Characterization and cell behaviour aspects. *Biomaterials* **26**, 5960–5971.

[140] Zeng H, Chittur KK and Lacefield WR (1999). Analysis of bovine serum albumin adsorption on calcium phosphate and titanium surfaces. *Biomaterials* **20**, 377–384.

[141] Graf HL, Stoeva S, Armbruster FP, Neuhaus J and Hilbig H (2008). Effect of bone sialoprotein and collagen coating on cell attachment to TICER and pure titanium implant surfaces. *International Journal of Oral and Maxillofacial Surgery* **37**, 634–640.

[142] Yang Y, Cavin R and Ong JL (2003). Protein adsorption on titanium surfaces and their effect on osteoblast attachment. *Journal of Biomedical Materials Research Part A* **67**, 344–349.

[143] Shi Z, Neoh KG, Kang ET, Poh CK and Wang W (2009). Surface functionalization of titanium with carboxymethyl chitosan and immobilized bone morphogenetic protein-2 for enhanced osseointegration. *Biomacromolecules* **10**, 1603–1611.

[144] Vater C, Lode A, Bernhardt A, Reinstorf A, Heinemann C and Gelinsky M (2010). Influence of different modifications of a calcium phosphate bone cement on adhesion, proliferation, and osteogenic differentiation of human bone marrow stromal cells. *Journal of Biomedical Materials Research Part A* **92**, 1452–1460.

[145] Zhu XD, Fan HS, Xiao YM, Li DX, Zhang HJ, Luxbacher T and Zhang XD (2009). Effect of surface structure on protein adsorption to biphasic calcium-phosphate ceramics in vitro and in vivo. *Acta Biomaterialia* **5**, 1311–1318.

[146] Rao H, Lu Z, Liu W, Wang Y, Ge H, Zou P and He H (2016). The adsorption of bone-related proteins on calcium phosphate ceramic particles with different phase composition and its adsorption kinetics. *Surface and Interface Analysis* **48**, 1048–1055.

[147] Pan J, Thierry D and Leygraf C (1994). Electrochemical and XPS studies of titanium for biomaterial applications with respect to the effect of hydrogen peroxide. *Journal of Biomedical Materials Research* **28**, 113–122.

[148] Pan J, Thierry D and Leygraf C (1996). Hydrogen peroxide toward enhanced oxide growth on titanium in PBS solution: blue coloration and clinical relevance. *Journal of Biomedical Materials Research* **30**, 393–402.

[149] Degasne I, Baslé MF, Demais V, Huré G, Lesourd M, Grolleau B, Mercier L and Chappard D (1999). Effects of roughness, fibronectin and vitronectin on attachment, spreading, and proliferation of human osteoblast-like cells (Saos-2) on titanium surfaces. *Calcified Tissue International* **64**, 499–507.

[150] Deligianni DD, Katsala ND, Koutsoukos PG and Missirlis YF (2000). Effect of surface roughness of hydroxyapatite on human bone marrow cell adhesion, proliferation, differentiation and detachment strength. *Biomaterials* **22**, 87–96.

[151] Deligianni D (2001). Effect of surface roughness of the titanium alloy Ti–6Al–4V on human bone marrow cell response and on protein adsorption. *Biomaterials* **22**, 1241–1251.

[152] Anselme K and Bigerelle M (2005). Topography effects of pure titanium substrates on human osteoblast long-term adhesion. *Acta Biomaterialia* **1**, 211–222.

[153] Dettin M, Herath T, Gambaretto R, Iucci G, Battocchio C, Bagno A, Ghezzo F, Di Bello C, Polzonetti G and Di Silvio L (2009). Assessment of novel chemical strategies for covalent attachment of adhesive peptides to rough titanium surfaces: XPS analysis and biological evaluation. *Journal of Biomedical Materials Research Part A* **91**, 463–479.

[154] Pan J, Thierry D and Leygraf C (1996). Electrochemical impedance spectroscopy study of the passive oxide film on titanium for implant application. *Electrochimica Acta* **41**, 1143–1153.

[155] Ray S and Shard AG (2011). Quantitative analysis of adsorbed proteins by X-ray photoelectron spectroscopy. *Analytical Chemistry* **83**, 8659–8666.

[156] Ritz U, Götz H, Baranowski A, Heid F, Rommens PM and Hofmann A (2017). Influence of different calcium phosphate ceramics on growth and differentiation of cells in osteoblast–endothelial co–cultures. *Journal of Biomedical Materials Research Part B: Applied Biomaterials* **105**, 1950–1962.

[157] Ginebra MP, Driessens FCM and Planell JA (2004). Effect of the particle size on the micro and nanostructural features of a calcium phosphate cement: a kinetic analysis. *Biomaterials* **25**, 3453–3462.

[158] Espanol M, Perez RA, Montufar EB, Marichal C, Sacco A and Ginebra MP (2009). Intrinsic porosity of calcium phosphate cements and its significance for drug delivery and tissue engineering applications. *Acta Biomaterialia* **5**, 2752–2762.

[159] Boyan BD, Sylvia VL, Liu Y, Sagun R, Cochran DL, Lohmann CH, Dean DD and Schwartz Z (1999). Surface roughness mediates its effects on osteoblasts via protein kinase A and phospholipase A2. *Biomaterials* **20**, 2305–2310.

[160] Webster TJ, Ergun C, Doremus RH, Siegel RW and Bizios R (2000). Specific proteins mediate enhanced osteoblast adhesion on nanophase ceramics. *Journal of Biomedical Materials Research* **51**, 475–483.

[161] Habibovic P, Sees TM, van den Doel MA, van Blitterswijk CA and de Groot K (2006). Osteoinduction by biomaterials–physicochemical and structural influences. *Journal of Biomedical Materials Research Part A* **77**, 747–762.

[162] Polak SJ, Levengood SKL, Wheeler MB, Maki AJ, Clark SG and Johnson AJW (2011). Analysis of the roles of microporosity and BMP-2 on multiple measures of bone regeneration and healing in calcium phosphate scaffolds. *Acta Biomaterialia* **7**, 1760–1771.

[163] Wernike E, Hofstetter W, Liu Y, Wu G, Sebald HJ, Wismeijer D, Hunziker EB, Siebenrock KA and Klenke FM (2010). Long-term cell-mediated protein release from calcium phosphate ceramics. *Journal of Biomedical Materials Research Part A* **92**, 463–474.

[164] Ganss B, Kim RH and Sodek J (1999). Bone sialoprotein. *Critical Reviews in Oral Biology & Medicine* **10**, 79–98.

[165] Stein GS and Lian JB (1993). Molecular mechanisms mediating proliferation/differentiation interrelationships during progressive development of the osteoblast phenotype. *Endocrine Reviews* **14**, 424–442.

[166] van der Zande M, Walboomers XF, Briest A, Springer M, Alava JI and Jansen JA (2008). The effect of combined application of TGFbeta-1, BMP-2, and COLLOSS E on the development of bone marrow derived osteoblast-like cells in vitro. *Journal of Biomedical Materials Research Part A* **86**, 788–795.

[167] Chan WD, Goldberg HA, Hunter GK, Dixon SJ and Rizkalla AS (2010). Modification of polymer networks with bone sialoprotein promotes cell attachment and spreading. *Journal of Biomedical Materials Research Part A* **94**, 945–952.

[168] Byzova TV, Kim W, Midura RJ and Plow EF (2000). Activation of integrin alpha(V)beta(3) regulates cell adhesion and migration to bone sialoprotein. *Experimental Cell Research* **254**, 299–308.

[169] Margel S, Vogler EA, Firment L, Watt T, Haynie S and Sogah DY (1993). Peptide, protein, and cellular interactions with self-assembled monolayer model surfaces. *Journal of Biomedical Materials Research* **27**, 1463–1476.

[170] Hata K, Ikebe K, Wada M and Nokubi T (2007). Osteoblast response to titanium regulates transcriptional activity of RUNX2 through MAPK pathway. *Journal of Biomedical Materials Research Part A* **81**, 446–452.

[171] Wang J, Zhou HY, Salih E, Xu L, Wunderlich L, Gu X, Hofstaetter JG, Torres M and Glimcher MJ (2006). Site-specific in vivo calcification and osteogenesis stimulated by bone sialoprotein. *Calcified Tissue International* **79**, 179–189.

[172] Knabe C, Berger G, Gildenhaar R, Meyer J, Howlett CR, Markovic B and Zreiqat H (2004). Effect of rapidly resorbable calcium phosphates and a calcium phosphate bone cement on the expression of bone-related genes and proteins in vitro. *Journal of Biomedical Materials Research Part A* **69**, 145–154.

[173] Palmer I, Nelson J, Schatton W, Dunne NJ, Buchanan FJ and Clarke SA (2016). Biocompatibility of calcium phosphate bone cement with optimized mechanical properties. *Journal of Biomedical Materials Research Part B, Applied Biomaterials* **104**, 308–315.

[174] Cook SD, Walsh KA and Haddad RJ (1985). Interface mechanics and bone growth into porous Co-Cr-Mo alloy implants. *Clinical Orthopaedics and Related Research* **193**, 271–280.

[175] Kieswetter K, Schwartz Z, Hummert TW, Cochran DL, Simpson J, Dean DD and Boyan BD (1996). Surface roughness modulates the local production of growth factors and cytokines by osteoblast-like MG-63 cells. *Journal of Biomedical Materials Research* **32**, 55–63.

[176] Leize EM, Hemmerlé J and Leize M (2000). Characterization, at the bone crystal level, of the titanium-coating/bone interfacial zone. *Clinical Oral Implants Research* **11**, 279–288.

[177] Malafaya PB and Reis RL (2009). Bilayered chitosan-based scaffolds for osteochondral tissue engineering: influence of hydroxyapatite on in vitro cytotoxicity and dynamic bioactivity studies in a specific double-chamber bioreactor. *Acta Biomaterialia* **5**, 644–660.

[178] Engel J, Taylor W, Paulsson M, Sage H and Hogan B (1987). Calcium binding domains and calcium-induced conformational transition of SPARC/BM-40/osteonectin, an extracellular glycoprotein expressed in mineralized and nonmineralized tissues. *Biochemistry* **26**, 6958–6965.

[179] Schaeren S, Jaquiery C, Wolf F, Papadimitropoulos A, Barbero A, Schultz-Thater E, Heberer M and Martin I (2010). Effect of bone sialoprotein coating of ceramic and synthetic polymer materials on in vitro osteogenic cell differentiation and in vivo bone formation. *Journal of Biomedical Materials Research Part A* **92**, 1461–1467.

[180] Saltzman WM, Parkhurst MR, Parsons-Wingerter P and Zhu WH (1992). Three-dimensional cell cultures mimic tissues. *Annals of the New York Academy of Sciences* **665**, 259–273.

[181] Unger RE, Sartoris A, Peters K, Motta A, Migliaresi C, Kunkel M, Bulnheim U, Rychly J and Kirkpatrick CJ (2007). Tissue-like self-assembly in cocultures of endothelial cells and osteoblasts and the formation of microcapillary-like structures on three-dimensional porous biomaterials. *Biomaterials* **28**, 3965–3976.

[182] Furumatsu T, Shen ZN, Kawai A, Nishida K, Manabe H, Oohashi T, Inoue H and Ninomiya Y (2003). Vascular endothelial growth factor principally acts as the main angiogenic factor in the early stage of human osteoblastogenesis. *Journal of Biochemistry* **133**, 633–639.

[183] Kaigler D, Krebsbach PH, Polverini PJ and Mooney DJ (2003). Role of vascular endothelial growth factor in bone marrow stromal cell modulation of endothelial cells. *Tissue Engineering* **9**, 95–103.

[184] von Schroeder H, Veillette C, Payandeh J, Qureshi A and Heersche J (2003). Endothelin-1 promotes osteoprogenitor proliferation and differentiation in fetal rat calvarial cell cultures. *Bone* **33**, 673–684.

[185] Deckers MML, van Bezooijen RL, van der Horst G, Hoogendam J, van der Bent C, Papapoulos SE and Löwik CWGM (2002). Bone morphogenetic proteins stimulate angiogenesis through osteoblast-derived vascular endothelial growth factor A. *Endocrinology* **143**, 1545–1553.

[186] Yang S, Graham J, Kahn JW, Schwartz EA and Gerritsen ME (1999). Functional roles for PECAM-1 (CD31) and VE-Cadherin (CD144) in tube assembly and lumen formation in three-dimensional collagen gels. *The American Journal of Pathology* **155**, 887–895.

[187] Mayr-Wohlfart U, Waltenberger J, Hausser H, Kessler S, Guenther KP, Dehio C, Puhl W and Brenner R (2002). Vascular endothelial growth factor stimulates chemotactic migration of primary human osteoblasts. *Bone* **30**, 472–477.

[188] Spector JA, Mehrara BJ, Greenwald JA, Saadeh PB, Steinbrech DS, Bouletreau PJ, Smith LP and Longaker MT (2001). Osteoblast expression of vascular endothelial growth factor is modulated by the extracellular microenvironment. *American Journal of Physiology - Cell Physiology* **280**, C72–C80.

[189] Piali L, Hammel P, Uherek C, Bachmann F, Gisler RH, Dunon D and Imhof BA (1995). CD31/PECAM-1 is a ligand for alpha v beta 3 integrin involved in adhesion of leukocytes to endothelium. *The Journal of Cell Biology* **130**, 451–460.

[190] Oldberg A, Franzén A, Heinegård D, Pierschbacher M and Ruoslahti E (1988). Identification of a bone sialoprotein receptor in osteosarcoma cells. *Journal of Biological Chemistry* **263**, 19433–19436.

[191] Saito T, Albelda SM and Brighton CT (1994). Identification of integrin receptors on cultured human bone cells. *Journal of Orthopaedic Research* **12**, 384–394.

[192] Fang TD, Salim A, Xia W, Nacamuli RP, Guccione S, Song HM, Carano RA, Filvaroff EH, Bednarski MD, Giaccia AJ and Longaker MT (2005). Angiogenesis is required for successful bone induction during distraction osteogenesis. *Journal of Bone and Mineral Research* **20**, 1114–1124.

[193] Phelps EA and García AJ (2010). Engineering more than a cell: Vascularization strategies in tissue engineering. *Current Opinion in Biotechnology* **21**, 704–709.

[194] Wenger A, Stahl A, Weber H, Finkenzeller G, Augustin HG, Stark GB and Kneser U (2004). Modulation of in vitro angiogenesis in a three-dimensional spheroidal coculture model for bone tissue engineering. *Tissue Engineering* **10**, 1536–1547.

[195] Bellahcene A, Bonjean K, Fohr B, Fedarko NS, Robey FA, Young MF, Fisher LW and Castronovo V (2000). Bone sialoprotein mediates human endothelial cell attachment and migration and promotes angiogenesis. *Circulation Research* **86**, 885–891.

[196] Bouet G, Bouleftour W, Juignet L, Linossier MT, Thomas M, Vanden-Bossche A, Aubin JE, Vico L, Marchat D and Malaval L (2015). The impairment of osteogenesis in bone sialoprotein (BSP) knockout calvaria cell cultures is cell density dependent. *PloS One* **10**, e0117402.

[197] Choi YJ, Lee JY, Chung CP and Park YJ (2013). Enhanced osteogenesis by collagen-binding peptide from bone sialoprotein in vitro and in vivo. *Journal of Biomedical Materials Research Part A* **101**, 547–554.

[198] Xu L, Anderson AL, Lu Q and Wang J (2007). Role of fibrillar structure of collagenous carrier in bone sialoprotein-mediated matrix mineralization and osteoblast differentiation. *Biomaterials* **28**, 750–761.

[199] Holm E, Aubin JE, Hunter GK, Beier F and Goldberg HA (2015). Loss of bone sialoprotein leads to impaired endochondral bone development and mineralization. *Bone* **71**, 145–154.

[200] Malaval L, Monfoulet L, Fabre T, Pothuaud L, Bareille R, Miraux S, Thiaudiere E, Raffard G, Franconi JM, Lafage-Proust MH, Aubin JE, Vico L and Amedee J (2009). Absence of bone sialoprotein (BSP) impairs cortical defect repair in mouse long bone. *Bone* **45**, 853–861.

[201] O'Toole GC, Salih E, Gallagher C, FitzPatrick D, O'Higgins N and O'Rourke SK (2004). Bone sialoprotein-coated femoral implants are osteoinductive but mechanically compromised. *Journal of Orthopaedic Research* **22**, 641–646.

[202] Pesesse L, Sanchez C, Walsh DA, Delcour JP, Baudouin C, Msika P and Henrotin Y (2014). Bone sialoprotein as a potential key factor implicated in the pathophysiology of osteoarthritis. *Osteoarthritis and Cartilage* **22**, 547–556.

[203] Jao D, Xue Y, Medina J and Hu X (2017). Protein-based drug-delivery materials. *Materials* **10**, 517.

[204] Mir M, Ahmed N and Rehman AU (2017). Recent applications of PLGA based nanostructures in drug delivery. *Colloids and Surfaces B: Biointerfaces* **159**, 217–231.

[205] Hobar PC, Schreiber JS, McCarthy JG and Thomas PA (1993). The role of the dura in cranial bone regeneration in the immature animal. *Plastic and Reconstructive Surgery* **92**, 405–410.

[206] Hobar PC, Masson JA, Wilson R and Zerwekh J (1996). The importance of the dura in craniofacial surgery. *Plastic and Reconstructive Surgery* **98**, 217–225.

[207] Koressaar T and Remm M (2007). Enhancements and modifications of primer design program Primer3. *Bioinformatics* **23**, 1289–1291.

[208] Untergasser A, Cutcutache I, Koressaar T, Ye J, Faircloth BC, Remm M and Rozen SG (2012). Primer3—new capabilities and interfaces. *Nucleic Acids Research* **40**, e115–e115.

Appendix

Materials

Chemicals

Tab. A.1: Chemicals

Substance	Provider
Acetic acid, 100 % and 96 %	Carl-Roth® GmbH, Karlsruhe, Germany
Agarose, electrophoresis grade	Invitrogen™, Carlsbad, USA
alamarBlue® stock solution	Life Technologies, Invitrogen™, Karlsruhe, Germany
Alizarin red S	Fluka -Chemie GmbH, Buchs, Switzerland
Alkaline phosphatase yellow, pNPP	Sigma-Aldrich®, Steinheim, Germany
Alzane® vet, 5 mg/ml, Atipamezol	Zoetis GmbH, Berlin, Germany
3-Aminopropyltriethoxysilane, 98 %	Sigma-Aldrich®, Steinheim, Germany
3-Aminopropyltrimethoxysilane, 97 %	Sigma-Aldrich®, Steinheim, Germany
Ampuwa®, Aqua ad. injectabila, Plastipur®	Fresenius Kabi AG, Bad Homburg, Germany
Anexate®, Flumazenil, 0.1 mg/ml	Roche Pharma AG, Grenzach-Wyhlen, Germany
Ascorbic acid	Sigma-Aldrich®, Steinheim, Germany
Aqua, Irrigation solution	B. Braun Melsungen AG, Melsungen, Germany
Aqua ad injectabila	B. Braun Melsungen AG, Melsungen, Germany
Aqua-Poly-Mount	Polysciences Inc., Warrington, USA
Bepanthen® Wund- und Heilsalbe, Dexpanthenol	Bayer Vital GmbH, Leverkusen, Germany
Biocidal ZF™	WAK-Chemie Medical GmbH, Steinbach, Germany

Continued on next page

Tab. A.1 – continued from previous page

Substance	Provider
BMP-7, 10 µg, research grade	Miltenyi Biotec GmbH, Bergisch-Gladbach, Germany
BSA, Bovines serum albumin, 30 %	PAA Laboratories GmbH, Pasching, Austria
BSP, Bone sialoprotein, 280 µg/ml Puffer	Immundiagnostik AG, Bensheim, Germany
Braunol®, 7.5 % Povidon-Jod	B. Braun Melsungen AG, Melsungen, Germany
β-Glycerophosphate	Sigma-Aldrich®, Steinheim, Germany
β-Mercaptoethanol	Applichem GmbH, Darmstadt, Germany
Canada balsam for microscopy	Merck KGaA, Darmstadt, Germany
Cell dissociation buffer	Gibco®, Life Technologies, Grand Island, USA
Collagen type I, rat tail, 3.12 mg/ml	BD Biosciences, Heidelberg, Germany
Collagen type I, rat tail, 3.59 mg/ml	Corning, Discovery Labware, Corning, USA
Cytoseal™ XYL	Richard-Allan Scientific, San Diego USA
Corneregel®, eye gel, Dexpanthenol	Bausch & Lomb, Rochester, USA
Depilatory cream	Reckitt Benckiser, Mannheim, Germany
Dexamethasone	Sigma-Aldrich®, Steinheim, Germany
Dimethyl sulfoxide (DMSO), HYBRI-MAX®	Sigma-Aldrich®, Ayrshire, UK
Dorbene vet®, Medetomidin 1 mg/ml	Zoetis Deutschland GmbH, Berlin, Germany
Dulbecco's modified Eagle medium (DMEM/F-12)(1:1) + GlutaMAX	Gibco®, Life Technologies, Grand Island, USA
Dulbecco's phosphate buffered saline, [-] $CaCl_2$, [-] $MgCl_2$	Gibco®, Life Technologies, Grand Island, USA
Dulbecco's phosphate buffered saline	Sigma-Aldrich®, Steinheim, Germany
Dulbecco's modified Eagle's medium/nutrient mixture F-12 Ham	Sigma-Aldrich®, Steinheim, Germany

Continued on next page

Tab. A.1 – continued from previous page

Substance	Provider
dNTP Mix, 10 mM	Bioron GmbH, Ludwigshafen, Germany
EBM-2, Endothelial basal medium-2	Lonza Group AG, Basel, Switzerland
EDTA disodium salt	Applichem GmbH, Darmstadt, Germany
Eosin G-solution, 0.5 %	Carl-Roth® GmbH, Karlsruhe, Germany
Ethanol abolute	Applichem GmbH, Darmstadt, Germany
FCS, Foetal calf serum	Biochrom AG, Berlin, Germany
Fentanyl-Janssen 0.1 mg/2ml	Janssen-Cilag GmbH, Neuss, Germany
Fentanyl 50 µg/ml	Hameln Pharma Plus GmbH, Hameln, Germany
Forene®, Isofluran, 100 % (V/V)	AbbVie Deutschland GmbH & Co. KG, Ludwigshafen, Germany
Glutaraldehyde solution, 25 %	Applichem GmbH, Darmstadt, Germany
Gigasept® Instru AF	Schülke & Mayr GmbH, Norderstedt, Germany
Gill's Hematoxylin solution # 3	Polysciences Europe GmbH, Eppelheim, Germany
Goldner's stain II, Phosphotungstic acid-Orange G	Carl-Roth® GmbH, Karlsruhe, Germany
Haematoxylin solution A acc. to Weigert	Carl-Roth® GmbH, Karlsruhe, Germany
Haematoxylin solution B acc. to Weigert	Carl-Roth® GmbH, Karlsruhe, Germany
Horse serum	Biochrom AG, Berlin, Germany
Hydrogen peroxide, H_2O_2, 30 % - 35 %	Merck KGaA, Darmstadt, Germany
Hydrogen peroxide, H_2O_2, $\geq$ 35 %	Sigma-Aldrich®, Steinheim, Germany
Isopropanol	Hedinger, Stuttgart, Germany
Light green SF	Chroma-Gesellschaft, Schmid GmbH, Köngen, Germany

Continued on next page

Tab. A.1 – continued from previous page

Substance	Provider
Loading buffer, 6x	PEQLAB Biotechnologie GmbH, Erlangen, Germany
MEDIUM 199 with Earle's salts, L-glutaine and $NaHCO_3$	Sigma® Life Science, Sigma-Aldrich, Steinheim, Germany
MEDIUM 199 10x	Sigma® Life Science, Sigma-Aldrich, Steinheim, Germany
MEM with Earle's salts	Biochrom AG, Berlin, Germany
MEM Earl without phenol-red	Gibco®, Life Technologies, Grand Island, USA
Methanol	Applichem GmbH, Darmstadt, Germany
Methyl cellulose, Viscosity 4,000 cP	Sigma-Aldrich®, Steinheim, Germany
Midazolam-hameln 5 mg/ml	Hameln Pharma Plus GmbH, Hameln, Germany
NaCl, 0.9 %	B. Braun Melsungen AG, Melsungen, Germany
NaOH	Merck Millipore, Darmstadt, Germany
$NaHCO_3$	Merck Millipore, Darmstadt, Germany
O-Phosphorylethanolamine	Sigma-Aldrich®, Steinheim, Germany
Paraffin, Roti®-Plast Paraffin-Pastillen	Carl-Roth® GmbH, Karlsruhe, Germany
PFA, Paraformaldehyde	Carl-Roth® GmbH, Karlsruhe, Germany
Penicillin/Streptomycin, 10,000 U/ml / 10,000 µg/ml	Gibco®, Life Technologies, Grand Island, USA
p-Nitrophenol standard solution, 10 mM	Sigma-Aldrich®, Steinheim, Germany
Ponceau S solution	Sigma-Aldrich®, Steinheim, Germany
PowerUp™ SYBR® green master mix, 2x	Applied Biosystems, Austin, USA
Protaminsulfate	Sigma-Aldrich®, Steinheim, Germany
2-Propanol Rotipuran®, $\leq 99.8\,\%$	Carl-Roth® GmbH, Karlsruhe, Germany
Random primers, 500 µg/ml, 20 µg	Promega, Madison, WI, USA

Continued on next page

Tab. A.1 – continued from previous page

Substance	Provider
RNase free water	Qiagen GmbH, Hilden, Germany
Roti® Histofix 4.5 %, acid-free, phosphate buffered	Carl-Roth® GmbH, Karlsruhe, Germany
SIGMA*FAST*™ BCIP®/NBT	Sigma-Aldrich®, Steinheim, Germany
Sulfuric acid, H_2SO_4, 95-98 %	Merck, Darmstadt, Germany
SYBR® green PCR master mix, 2x	Applied Biosystems, Austin, USA
SYBR® green select mix, 2x	Applied Biosystems, Austin, USA
SYBR® safe DNA gel stain, 10,000x concentrate	Gibco®, Invitrogen™, Carlsbad, USA
Technovit® 7200 VLC	Kulzer GmbH, Hanau, Germany
Technovit® 7210 VLC	Kulzer GmbH, Hanau, Germany
Technovit® 7230 VLC	Kulzer GmbH, Hanau, Germany
Terralin® liquid disinfection	Schülke & Mayr, Norderstedt, Germany
Thiazolyl blue tetrazolium bromide, MTT	Sigma-Aldrich®, Steinheim, Germany
Toluidine blue	Sigma-Aldrich®, Steinheim, Germany
Trypan blue stain, 0.4 %	Gibco®, Invitrogen™, Carlsbad, USA
Tramadol-ratiopharm® 100 mg/ml, drops	Ratiopharm GmbH, Ulm, Germany
Triton™ X-100	Sigma-Aldrich®, Steinheim, Germany
TRIS	Applichem GmbH, Darmstadt, Germany
VEGF, 10 µg	Biomol GmbH, Hamburg, Germany
Xylene - mixture of isomeres, p.a., Ph. Eur.	Applichem Pancreac, Darmstadt, Germany
ZDEB 0.1 % polyurethane film, Ch. B. A-131	Hatano Research Institute, Food and Drug Safety Center, Hadano, Japan
ZDEC 0.1 % polyurethane film, Ch. B. B-122 K	Hatano Research Institute, Food and Drug Safety Center, Hadano, Japan

Enzymes

Tab. A.2: Enzymes

Enzyme	Provider
Accutase® solution, A6964	Sigma-Aldrich®, Steinheim, Germany
Collagenase type I, 285 U/mg, LS004217	Worthington Biochemical Corporation, Lakewood, USA
Dispase II, 1.8 U/mg, 17105-041	Gibco®, Life Technologies, Carlsbad, USA
Proteinkinase K, ready-to-use, S3020	Dako Deutschland GmbH, Hamburg, Germany

Antibodies & dyes & primer

Tab. A.3: Antibodies

Antibodies	Provider
Alexa Fluor 488, A11001, 1:200	Invitrogen™ Molecular Probes®, Eugene, USA
ALP, ab54778, 1:100	Abcam, Cambridge, UK
OPN, ab91655, 1:100	Abcam, Cambridge, UK
PECAM-1, ab28364, 1:50	Abcam, Cambridge, UK
RUNX-2, sc-390351, 1:100	Santa Cruz Biotechnology, Dallas, USA
vWF, LS-C357440, 1:100	Life Span Biosciences Inc., Seattle, USA

Tab. A.4: Dyes

Dyes	Provider
Calcein AM, C-3099	Invitrogen™ Molecular Probes®, Eugene, USA
Cell Tracker™ Green, CMFDA, C7025	Invitrogen™ Molecular Probes®, Eugene, USA
Cell Tracker™ Red, CMTPX, C34552	Invitrogen™ Molecular Probes®, Eugene, USA
Hoechst stain solution, H6024	Sigma-Aldrich®, Steinheim, Germany

Continued on next page

Tab. A.4 – continued from previous page

Dyes	Provider
Texas Red® - X phalloidin, T7471	Invitrogen™ Molecular Probes®, Eugene, USA

Gene expression analyses of human osteoblasts seeded on titanium and calcium-phosphate cements were carried out with QuantiTect® primers from Qiagen (Hilden, Germany). Details are listed in Tab. A.5.

Tab. A.5: QuantiTect® primers

Gene	Specification
18 S	QT00199367
ALP	QT00012957
Col1	QT00037793
OPN	QT01008798
RUNX2	QT00020517
SPARC	QT00018620
SP7	QT00213514

Primers for gene expression analyses in collagen gels were carried out with primers generated via primer3output [207, 208] and manufactured from Eurofins Genomics (Ebersberg, Germany). Primers are listed in Tab. A.6.

Tab. A.6: Primer details for qPCR analyses. For each gene, sequences for forward (fw) and reverse (rv) primers, the accession number (Acc. Nr.), final product size (Pr. Size) and annealing temperature (T_A) are listed.

Gene	Sequenz	Acc. Nr.	Pr. Size	T_A
18 S	fw: ctgaggatgaggtggaacgt	X69150	153	59.4
	rv: ggtcttcacggagcttgttg			59.4
ALP	fw: gtacaacaccaatgcccagg	NM000478	182	59.4
	rv: cagatttcccagcgtccttg			59.4
BACT	fw: aaactggaacggtgaaggtg	NM001101	171	57.3
	rv: agagaagtggggtggctttt			57.3
B2M	fw: ctcacgtcatccagcagaga	NM004048	214	59.4
	rv: acggcaggcatactcatctt			57.3
GAPDH	fw: cgaccactttgtcaagctca	M33197	203	57.3

Continued on next page

Tab. A.6 – continued from previous page

Gene	Sequenz	Acc. Nr.	Pr. Size	T_A
	rv: aggggagattcagtgtggtg			59.4
HMBS	fw: acccacacacagcctacttt	NM000190	159	57.3
	rv: tcaatgttgccaccacactg			57.3
HPRT-1	fw: cctggcgtcgtgattagtga	NM000194	162	59.4
	rv: gcctcccatctccttcatca			59.4
KDR	fw: ttacttgcaggggacagagg	NM002253	170	59.4
	rv: ttcccggtagaagcacttgt			57.3
MCAM	fw: cggcaagtgaacaagaccaa	NM006500	170	57.3
	rv: gtctggtgtgagggtggtta			59.4
OPN	fw: ggtcactgattttcccacgg	NM001040058	196	59.4
	rv: ctcctcgctttccatgtgtg			59.4
PECAM-1	fw: cattggcgtgttgggaagaa	NM000442	153	57.3
	rv: gctcatgtttgcctagctcc			59.4
RUNX2	fw: ctgtggttactgtcatggcg	NM001024630	183	59.4
	rv: aggtagctacttggggagga			59.4
SPARC	fw: agtggagttggtgaatcggt	NM003118	163	57.3
	rv: aacgagttctcagcctgtga			57.3
SP7	fw: acaagcactaatgggctcct	NM001173467	196	57.3
	rv: gggtgtgtcatgtccagaga			59.4
vWF	fw: ggattcagtggatgcagcag	NM000552	161	59.4
	rv: tagggaggtcttcgattcgc			59.4

Buffer and solutions

Alizarin red S solution, pH 4.0, in Aqua dest.	Alizarin red	40 mM
Bone decalcification solution, pH 7.2, in Aqua dest.	EDTA – Na_2	10 % (m/V)
	TRIS	0.27 M
Collagenase-Dispase solution, in PBS (0.5 % BSA)	Collagenase I	0.1 % (m/V)
	Dispase II	0.1 % (m/V)
Cryo solution	DMSO	10 % (V/V)
	FCS	90 % (V/V)
Differentiation medium, in DMEM/F-12 medium (with 10 % FCS, 1 % PS)	Ascorbic acid	0.005 % (m/V)
	Dexamethasone	10 nM
	β-Glycerophosphate	3.5 mM
Methocel solution	Methylcellulose, autoclaved	6 g
	M199 medium (no supplements), 60 °C	250 ml
	M199 medium including:	250 ml
	2 % L-glut (V/V)	
	2 % PS (V/V)	
	20 % FCS (V/V)	
Piranha solution	H_2O_2	20 % (V/V)
	conc. H_2SO_4	80 % (V/V)
TAE-Buffer, 50x, in Aqua dest.	TRIS	2 M
	Acetic acid	1 M
	EDTA – Na_2, pH 8	0.05 M
TRIS-EDTA (TE) buffer, pH 8.0, in Aqua dest.	TRIS	10 mM
	EDTA – Na_2	1 mM

Cells

Tab. A.7: Cells

Cells	Provider
HUVEC, C-12200, Lot: 7062701.1	PromoCell GmbH, Heidelberg, Germany
L929 mouse fibroblasts, ACC2, Lot: 13	DSMZ Deutsche Sammlung von Mikroorganismen und Zellkulturen GmbH, Braunschweig, Germany

Tab. A.8: Details of osteoblast preparations

Designation	Source	Gender	Donor age
hOB 49	hip	female	55
hOB 50	hip	female	69
hOB 51	knee	male	62
hOB 52	hip	female	70
hOB 53	hip	male	90
hOB 54	knee	female	58
hOB 55	hip	male	51
hOB 56	knee	male	60
hOB 57	hip	female	65
hOB 58	knee	male	62

Kits

Tab. A.9: Kits

Kit & Composition	Provider
BD Accuri™ C6 Flow Cytometer Fluid Kit	BD, Heidelberg, Germany
Bacteriostatic concentrate solution	
Cleaning concentrate solution	
Decontamination concentrate solution	
Extended flow cell clean solution 06-0769	
BSP ELISA Kit	Immundiagnostik AG, Bensheim,
Conjugate (Mouse-anti-BSP, peroxidase-labelled)	Germany

Continued on next page

Tab. A.9 – continued from previous page

Kit & Composition	Provider
Controls	
Microtiter plate (precoated)	
Sample dilution buffer	
Standards	
Stop solution	
TMB (Tetramethylbenzidine) substrate	
WASHbuffer concentrate	
Dako LSAB2 System-HRP	Dako, Carpinteria, USA
Biotinylated link	
DAB chromogen	
DAB substrate buffer	
Peroxidase block	
Streptavidin-HRP	
EGM™-2 BulletKit™, CC-3162	Lonza Group AG, Basel,
Ascorbic acid	Switzerland
Endothelial basal medium-2	
FBS (Foetal bovine serum), 10 ml	
hEGF	
Heparin	
hFGF-B	
Hydrocortisone	
GA-1000 (Gentamicin, Amphothericin-B)	
R^3-IGF-1	
VEGF	
Lightning-Link® Fluorescein Conjugation Kit	Innova Biosciences, Cambridge, UK
LL-Modifier reagent	
LL-Quencher FD reagent	
Lightning-Link® mix (LL-Fluorescein)	
Maxima H Minus Reverse Transcriptase	Thermo Scientific™, Waltham,
Maxima H minus RT (200 U/µl)	USA
5X RT buffer	

Continued on next page

Tab. A.9 – continued from previous page

Kit & Composition	Provider
peqGOLD MicroSpin Total RNA Kit	PEQLAB Biotechnologie GmbH,
Collection tubes (2 ml)	Erlangen, Germany
DNA removing columns	
PerfectBind MS RNA columns	
RNase-free water	
RNA lysis buffer T	
RNA wash buffer I	
RNA wash buffer II (conc.)	
RNase-free DNase Set	Qiagen GmbH, Hilden, Germany
RNase-free DNase I (lyophilized)	
Buffer RDD	
RNase-free water	
Qiagen RNeasy® Micro Kit	Qiagen GmbH, Hilden, Germany
Buffer RLT	
Buffer RPE (concentrate)	
Buffer RW1	
Carrier RNA, poly-A	
Collection tubes (1.5 ml, 2 ml)	
RNase-free water	
RNeasy MinElute® spin columns	
Qiagen RNeasy® Mini Kit	Qiagen GmbH, Hilden, Germany
Buffer RLT	
Buffer RPE (concentrate)	
Buffer RW1	
Collection tubes (1.5 ml, 2 ml)	
RNase-free water	
RNeasy mini spin columns	
Superscript® Reverse Transcriptase III	Invitrogen™, Carlsbad, USA
DTT (100 mM)	
Superscript® Reverse Transcriptase III (200 U/µl)	
5X first-strand buffer	

Consumables

Tab. A.10: Consumables

Consumables	Provider
Barrier tips, ART®, 10 µl / 1000 µl	Molecular BioProducts, Thermo Fisher Scientific Inc., Waltham, USA
BD Microlance™ needles, 0.9 x 40 mm, 20 G	Becton Dickinson S.A., Fraga, Spain
Biosphere® plus filter tips, 200 µl	Sarstedt AG, Nümbrecht, Germany
Black well-plates, 24-well / 96-well	Greiner Bio-One GmbH, Frickenhausen, Germany
Cell culture flasks, 25 cm^2 / 75 cm^2 / 175 cm^2	Greiner Bio-One GmbH, Frickenhausen, Germany
ClipTip pipette tips, 1250 µl, filter	Thermo Fisher Scientific Inc., Waltham, USA
Combitips advanced®, 1 ml / 5 ml / 10 ml, Biopur®	Eppendorf AG, Hamburg, Germany
CPC scaffolds	INNOTERE, Radebeul, Germany
Disposable hypodermic needle Sterican®, 0.45 x 25 mm, 26 G	B. Braun Melsungen AG, Melsungen, Germany
Eppendorf Safe-Lock tubes, 0.5 ml / 1.5 ml / 2.0 ml / 5.0 ml	Eppendorf AG, Hamburg, Germany
Folded filters, ø 270 mm	Whatman plc, GE Healthcare, Chalfont St Giles, UK
KIMTECH Science Kimwipes, white	Kimberly-Clark Professional, Roswell, USA
Light-Duty tissue WIPERS	VWR International, Radnor, USA
Loctite® 401	Henkel AG &Co. KGaA, Garching, Germany
Luna™ cell counting slides	Biozym Scientific GmbH, Hessisch Oldendorf, Germany
Microplates, 96-well, F-bottom	Greiner Bio-One GmbH, Frickenhausen, Germany
Microscope cover glasses, 24 x 50 mm	Marienfeld Laboratory Glassware, Lauda-Königshofen, Germany

Continued on next page

Tab. A.10 – continued from previous page

Consumables	Provider
Microscope slides, superfrost® plus, 75 x 25 x1 mm	Gerhard Menzel, Braunschweig, Germany
Microscope slides, 25 x 75 x 1.5 mm / 50 x 100 x 2 mm	RESULAB GmbH, Marburg, Germany
Microtome blades, S35	FEATHER®, Osaka, Japan
Minisart® high flow syringe filter, 0.22 µm, Polyethersulfone	Sartorius Stedim Biotec SA, Göttingen, Germany
Mini-Spike® filter	B. Braun Melsungen AG, Melsungen, Germany
Nalgene® cryogenic vials	Thermo Fisher Scientific Inc., Waltham, USA
Opsite-Essential surgical drape, 90 x 75 cm	Medline Industries, Inc., Illinois, USA
Optical adhesive covers	Applied Biosystems, Austin, USA
Pasteur capillary pipettes, 150 mm / 230 mm, glass	Carl-Roth® GmbH, Karlsruhe, Germany
Pasteur plast pipettes, 3 ml	Ratiolab®, Dreieich, Germany
PCR 8-well tube strips and caps	PEQLAB Biotechnologie GmbH, Erlangen, Germany
Petri dishes, polystyrene	Greiner Bio-One GmbH, Frickenhausen, Germany
Pipettes CELLSTAR®, 2 ml / 5 ml / 10 ml / 25 ml	Greiner Bio-One GmbH, Frickenhausen, Germany
Pipettes COSTAR®, 5 ml / 10 ml / 25 ml)	Corning Inc., Corning, USA
QIAshredder	Qiagen GmbH, Hilden, Germany
Quality pipette tips, 20 µl	Sarstedt AG, Nümbrecht, Germany
qPCR SemiSkirted 96-well PCR plates	PEQLAB Biotechnologie GmbH, Erlangen, Germany
Reagent reservoir, 100 ml	VWR International, Radnor, USA
Scalpel, disposable, No. 11 / No. 15 / No. 23	Feather® Safety Razor Co., Osaka, Japan
Set of gauze balls, 15 x15 , sterile	Fuhrmann GmbH, Much, Germany
Shandon Coverplate™ , disposable immunostaining chamber	Richard-Allan-Scientific, Thermo Scientific Inc., Kalamazoo, USA

Continued on next page

Tab. A.10 – continued from previous page

Consumables	Provider
Suspension culture microplates, 96-well, U-bottom	Greiner Bio-One GmbH, Frickenhausen, Germany
Suture material, Ethilon, 4.0, 45 cm, XN699	Ethicon®, Johnson + Johnson International, Diegen, Belgium
Suture material, Ethilon II, 5.0, 45 cm, XN698	Ethicon®, Johnson + Johnson International, Diegen, Belgium
Suture material, Vicryl™, 4.0, 70 cm,V304	Ethicon®, Johnson + Johnson International, Diegen, Belgium
Syringes Discardit™ II, 5 ml / 10 ml / 20 ml	Becton Dickinson S.A., Fraga, Spain
Syringes Injekt®-F, 1 ml / 3 ml	B. Braun Melsungen AG, Melsungen, Germany
TipOne® Tips, 1000 µl / 1000 µl XL filter tips	STARLAB GmbH, Hamburg, Germany
Tips, 100 µl	Greiner Bio-One GmbH, Frickenhausen, Germany
Tissue culture plates, Cellstar®, 6-well / 24-well / 69-well	Greiner Bio-One GmbH, Frickenhausen, Germany
Tissue-Tek®, Mega-Cassette® system	Sakura® Finetek Europe, Zoeterwoude, Netherlands
Titanium discs, pure Grade IV	Medartis®, Basel, Switzerland
Tubes, CELLSTAR®, 15 ml / 50 ml	Greiner Bio-One GmbH, Frickenhausen, Germany
ULAP, ultra-low-attachment plates, 6-well / 24-well / 69-well	Corning Inc., Corning, USA
Vliwazell® absorbent dressing pads	Lohmann & Rauscher GmbH & Co. KG, Rengsdorf, Germany

Surgical instruments

Tab. A.11: Surgical instruments

Instrument	Provider
Bone rongeur; 155 mm, 6 / 180 mm, 7	Aesculap AG & Co. KG, Tuttlingen, Germany
Delicate scissor, straight, 105 mm	Aesculap AG & Co. KG, Tuttlingen, Germany
Durotip dissecting scissor, curved, 140 mm	Aesculap AG & Co. KG, Tuttlingen, Germany
HSS twist drill set with centering spike, ø 2.5 mm / ø 3 mm	PROXXON S.A., Wecker, Luxembourg
Irrigation needle, bulb end, curved	Ernst Kratz GmbH, ACUFIRM Nadel- und Kanülentechnologie, Dreieich, Germany
Micro forceps, 0.3 mm, angled, 110 mm / 0.2 mm, curved, 115 mm	Aesculap AG & Co. KG, Tuttlingen, Germany
Microscopy forceps, angled, 100 mm	Aesculap AG & Co. KG, Tuttlingen, Germany
Needle holder, 125 mm / 130 mm	Aesculap AG & Co. KG, Tuttlingen, Germany
Ochsner double-ended dissector, 3 mm, 5 mm; 18.1 cm	Scanlan International Inc., Saint Paul, USA
Self retaining retractor, 70 mm	Aesculap AG & Co. KG, Tuttlingen, Germany
Surgical scissor, straight, blunt/blunt, 145 mm	Aesculap AG & Co. KG, Tuttlingen, Germany
Tissue forceps, 1x2 teeth, 125 mm	Aesculap AG & Co. KG, Tuttlingen, Germany
Trephines, tissue punch, ø 2.7 mm	Hager & Meisinger GmbH, Neuss, Germany

Equipment

Tab. A.12: Equipment

Equiment	Provider
Absorbance microplate reader, Tecan Sunrise™ Remote	Tecan Group Ltd., Männedorf, Switzerland
Analytical balance, DI-234	Denver Instrument, Denver, USA
Autoclave Systec DX-45	Systec GmbH Labortechnik, Wettenberg, Germany
Autotechnicon Sakura Tissue-Tek® VIP	Miles Scientific, Naperville, USA
Balances, Sartorius handy H110, Sartorius BA BA 200	Sartorius AG, Göttingen, Germany
Biophotometer	Eppendorf, Hamburg, Germany
Cell counter, Luna™ automated cell counter, L10001	Logos Biosystems, Annandale, USA
Centrifuge Heraeus BIOFUGE fresco	Kendro Laboratory Products, Langenselbold, Germany
Centrifuge Heraeus Fresco 17	Thermo Scientific, Osterode, Germany
Centrifuges, 5804 R, 5810 R, 5415 C	Eppendorf, Hamburg, Germany
Clipper, Favorita® CL	Aesculap Suhl GmbH, Suhl, Germany
Confocal laser scanning microscope, Leica TCS SP2	Leica Mikrosysteme Vertrieb GmbH, Wetzlar, Germany
Cooling - Heating thermostat, CH-100	Peqlab Biotechnologie GmbH, Erlangen, Germany
Dehydration and infiltration system, EXAKT 510	EXAKT Apparatebau GmbH, Norderstedt, Germany
Diamond band saw, EXAKT 300 CL	EXAKT Apparatebau GmbH, Norderstedt, Germany
Drying and heating chamber	WTC Binder, Tuttlingen, Germany
Electrophoresis power supply, Consort EV231	Consort bvba, Turnhout, Belgium
Electrophoresis system PerfectBlue™-horizontal Mini Gel System, 40-0911	PEQLAB Biotechnologie GmbH, Erlangen, Germany
EVOS® Digital Inverted Microscope	Life Technologies, Carlsbad, USA
Film sealing unit, polystar® 620 DSM	Rische + Herfurth GmbH, Hamburg, Germany

Continued on next page

Tab. A.12 – continued from previous page

Equipment	Provider
Flow cytometer, accuri® C6 Flow cytometer, C.Sampler®	Accuri Cytometers Inc., Ann Arbor, USA
Fluid aspiration system, BVC21 NT Vario	Vaccuubrand GmbH, Wertheim, Germany
Fume cupboard, Type 2-418, DIN 12924	Köttermann GmbH & Co. KG, Uetze-Hänigsen, Germany
Fume cupboard, Niederraum DI1200SZ	Laborbau Grittmann, A. Grittmann GmbH & Co. KG, Heidelberg, Germany
Freezing container, Cryo 1C	NUNC International, Rochester, USA
Glomax® -Multi detection system	Promega, Madison, USA
Heating and drying table, 13800	Medax Nagel GmbH, Kiel, Germany
Heating oven, Universal Oven UN30	Memmert, Schwabach, Germany
Heating plate bw03, 37 °C	Baxter Deutschland GmbH, Unterschleißheim, Germany
Ice machine, 083817	ZIEGRA Eismaschinen GmbH, Isernhagen, Germany
Imaging system, Gel logic 2200	Eastman Kodak Company, Rochester, USA
Incubating mini shaker, 444-0274	VWR International, Radnor, USA
Incubation shaker, Certomat® H, Certomat® U	B.Braun Biotech International GmbH, Melsungen, Germany
Incubator, HERAcell 240	Heraeus Holding, Hanau, Germany
Isofluran vapor	Dräger Safety AG & Co KGaA, Wiesbaden, Germany
Laminar airflow cabinet, NuAIRE™ Biological safety cabinets, NU-440-600E, class II	NuAire, Plymouth, USA
Light polymerisation, EXAKT 520	EXAKT Apparatebau GmbH, Norderstedt, Germany
Magnetic stirrer, Heidolph MR Hei-Mix-S	Heidolph Instruments, Schwabach, Germany
Magnetic stirrers, IKA RET basic, IKA RO 5 power	IKA®-Werke GmbH & Co. KG, Staufen, Germany

Continued on next page

Tab. A.12 – continued from previous page

Equipment	Provider
Micro grinder, EXAKT 400 CS	EXAKT Apparatebau GmbH, Norderstedt, Germany
Microliter pipettes, 2.5 µl / 10 µl / 200 µl / 1000 µl	Eppendorf, Hamburg, Germany
Microliter pipettes, 10 µl / 200 µl / 1000 µl	Thermo Fisher Scientific, Waltham, USA
Microscope Leica MZ16A	Leica Mikrosysteme Vertrieb GmbH, Wetzlar, Germany
Microscope camera, Leica DC480	Leica Mikrosysteme Vertrieb GmbH, Wetzlar, Germany
Microscope Wilovert®, 202888 inverted	Helmut Hund GmbH, Wetzlar, Germany
Microscope Zeiss Axioplan, 451889	Carl Zeiss AG, Jena, Germany
Microscope camera OLYMPUS XC30	Olympus Soft Imaging Solutions GmbH, Münster, Germany
Microscope Zeiss Axioskop, 451485	Carl Zeiss AG, Jena, Germany
Microscope camera Leica DFC 420C	Leica Mikrosysteme Vertrieb GmbH, Wetzlar, Germany
Microtome 2030	Reichert-Jung, Nussloch, Germany
Mini centrifuge, Spectrafuge, 3-1810	neoLab® Migge GmbH, Heidelberg, Deutschland
Mini centrifuge, Sprout®, 12V	Heathrow Scientific®, Vernon Hills, USA
Multichannel pipette, E1-ClipTip Equalizer, 6-ch, 15 µl - 1250 µl	Thermo Fisher Scientific, Waltham, USA
Multifunction tool, Dremel	TCM, Tchibo GmbH, Hamburg, Germany
Neubauer improved counting chamber	Brand GmbH & Co. KG, Wertheim, Germany
Nitrogen storage vessels, Nitrogen Container Arpege 110,	Air Liquide S.A., Paris, France
pH-meter, Sartorius PB-11	Sartorius AG, Göttingen, Germany
Pipette controller	Gilson®, Middleton, USA
Platform shaker, waving, Polymax 1040	Heidolph Instruments, Schwabach, Germany

Continued on next page

Tab. A.12 – continued from previous page

Equipment	Provider
Real time PCR system 7300	Applied Biosystems Deutschland GmbH, Darmstadt, Germany
Scanning electron microscope, Quanta™ 200 FEG,FEI	Thermo Fisher Scientific, Philips Electron Optics, Eindhoven, Netherlands
Specimen radiography system, Faxitron MX-20	Faxitron X-ray Company, Lincolnshire, USA
Stepper/ Repetitive pipette, HandyStep® electronic	BRAND GmbH & Co. KG, Wertheim, Germany
Thermal printer, DPU-414	Seiko Instruments GmbH, Neu-Isenburg, Germany
Thermocycler, PEQLAB Primus 96 advanced	PEQLAB Biotechnologie GmbH, Erlangen, Germany
Thermocycler, peqSTAR 2x Gradient	PEQLAB Biotechnologie GmbH, Erlangen, Germany
Tissue flotation bath, Type 1052	GFL® Gesellschaft für Labortechnik, Burgwedel, Germany
Tissue-Tek® TEC III embedding center, Model 4584, thermal, dispensing and cryo console	Miles Scientific, Newark, USA
Ultra low temperature freezer, U570 premium	New Brunswick Scientific, Edison, USA
Ultrasonic cleaner USC 300 T	VWR International, Leuven, Netherlands
Vacuum adhesive press, EXAKT 401	EXAKT Apparatebau GmbH, Norderstedt, Germany
Vortex mixer, IKA® MS 3 digital	IKA®-Werke GmbH & Co. KG, Staufen, Germany
Water bath, LAUDA E100	Lauda, Lauda-Königshofen, Germany
XPS system, PHI 5600-CI	Physical Electronics, Eden Prairie, USA
µCuvette G1.0	Eppendorf, Hamburg, Germany
µCT40	Scanco Medical AG, Brüttisellen, Switzerland

Software

Tab. A.13: Software

Software	Provider
BD Accuri™ C6 / CSampler™ software, Ink. 1.0.264.21	BD, Heidelberg, Germany
Citavi 5.6	Swiss Academic Software GmbH, Wädenswil, Switzerland
Chem Sketch (Freeware) 2015	Advanced Chemistry Development Inc., ACD/Labs, Toronto, Canada
Corel Draw® Graphics Suite X8	Corel Corporation, Ottawa, Canada
Corel® Photo-Paint X8	Corel Corporation, Ottawa, Canada
Faxitron SR, DCF Version 3.1.86	Faxitron X-ray Corporation, Lincolnshire, USA
FIJI (ImageJ 1.50e)	NIH (National Institutes of Health), Rockville, USA
ImageJ, Version 1.48 and 1.50i	NIH (National Institutes of Health), Rockville, USA
Microsoft Office Professional Plus 2016, Excel, Word, Powerpoint	Microsoft Corporation, Redmond, USA
Photoshop CS6, CS5	Adobe Systems Software Ireland Limited, Dublin, Ireland
Primer3web, Version 4.0.0	Whitehead Institute for Biomedical Research, Cambridge, USA
Sequence detection software, Version 1.4, AB 7300 System	Applied Biosystems, Austin, USA
Slicer 4.7.0	NIH (National Institutes of Health), Rockville, USA
SPSS, Version 23.0, 22.0	IBM Deutschland GmbH, Ehningen, Germany
Synedra View Personal 15	Synedra information technologies GmbH, Innsbruck, Austria
TexLive, Version 2015	TeX Users Group, Portland, USA
Texmaker 4.5	Free Software Foundation, Boston, USA

Reference gene evaluation

Prior to gene expression analyses of specific genes it is recommended to find reliable reference genes. Suitable Reference genes have to be unaffected from later treatment, in this case from BSP-supplementation. Therefore, gene expression of six reference genes (BACT, B2M, HMBS, HPRT-1, GAPDH, 18S) were evaluated for mono- (hOBs, HUVECs and co-cultures concerning stable expression rates irrespective of BSP addition. C_t-values were analysed via different algorithms. Analyses with the GeNorm algorithm (Fig. A.1) revealed GAPDH and 18S as best reference genes. In contrast, the other algorithms demonstrated GAPDH, B2M or 18 S as more reliable genes and HPRT-1, HMBS or BACT as less reliable reference genes. Combination of all four methods (see Tab. A.14), demonstrated GAPDH and B2M as best reference genes to analyse BSP effects on gene expression in hOB and HUVEC collagen gels.

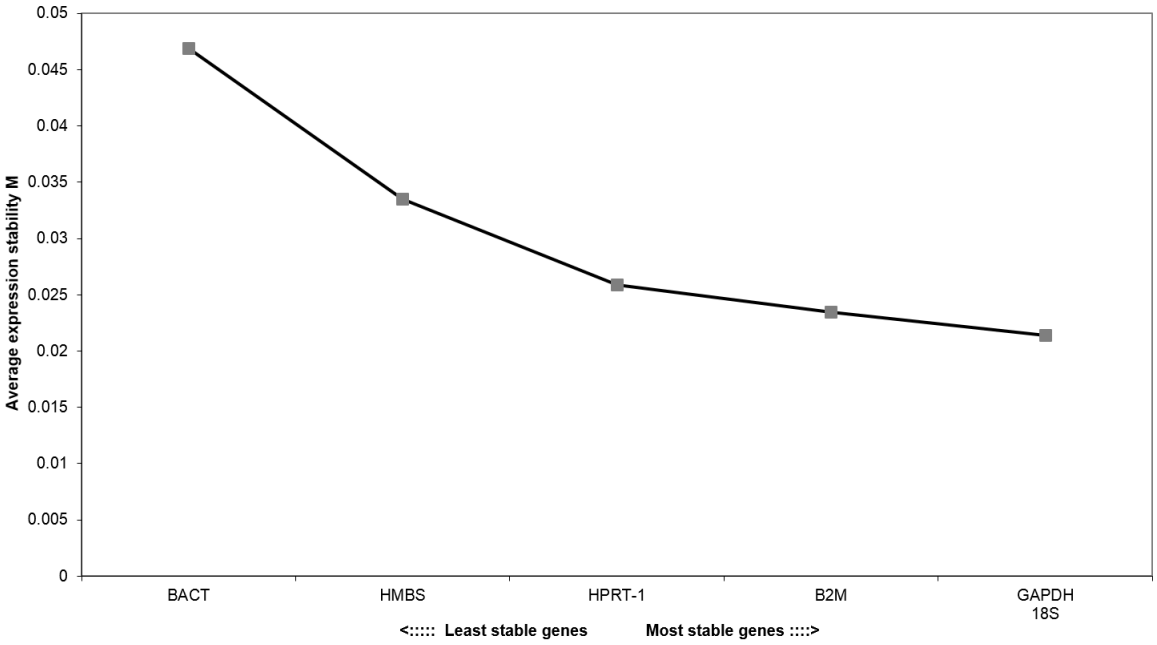

Fig. A.1: Reference gene evaluation with GeNorm. Average expression stability values of selected reference genes.

Tab. A.14: Ranking of the reference gene evaluation. Individual ranking order of all four methods are combined in the final ranking.

Rank	GeNorm	Normfinder	Bestkeeper	Ct Method	Final Ranking	
1	GAPDH	GAPDH	B2M	GAPDH	GAPDH	1.5
2	18S	HPRT1	18S	B2M	B2M	2.5
3	B2M	18 S	GAPDH	18 S	18S	2.5
4	HPRT-1	B2M	HPRT-1	HPRT-1	HPRT-1	3.5
5	HMBS	HMBS	HMBS	BACT	HMBS	5.3
6	BACT	BACT	BACT	HMBS	BACT	5.8

µCT

Analyses of µCT-Data were performed with Image J (v1.50 i; calvaria model) [118] or Fiji (Image J v1.50 e; femoral condyle model) [128, 129].

Detailed procedure for BV/TV analyses:

1) Import of µCT-Data (saved as .DICOM-files) **to ImageJ:**

File > Import > Image sequence...
Select the desired folder and the first slide. As *Sequence Options* the option 'Sort names numerically' must be set (✓).

2) Threshold setting for creation of a binary with bone + implant:

File > Adjust > Threshold...
Threshold setting is conducted in two steps. First, a threshold has to be selected for background removal and to gain a binary of bone together with the implant. For binary creation the options as seen in Fig. A.2 B have to be selected (✓Dark background, ✓Stack histogram). Pressing 'Apply' is followed by opening of the check-box 'Convert Stack to Binary' (C). All ✓have to be removed from the boxes, followed by creating the binary via 'OK'. The resulted binary (D) should be saved for later use (see step 4).

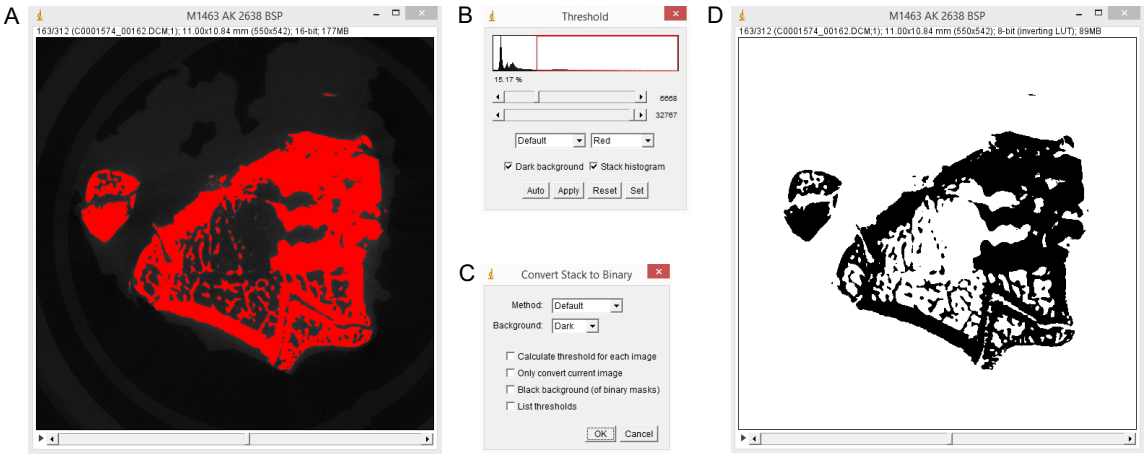

Fig. A.2: Threshold setting for binary creation. A - Threshold setting for background removing, B - Check box *Threshold*, C - Check box *Convert Stack to Binary*, D - Binary output *bone + implant*.

3) Threshold setting for creation of a binary from the implant:

File > Adjust > Threshold...

In the second step, the µCT-Data has to be re-opened (see step 1) and a threshold has to be set carefully to remove background as well as bone in order to achieve a binary from the implant (same options as in step 2). Due to the blurred boarder between implant and bone resulting from individual voxels and resolution, an implant size correction has to be implemented to minimise errors. Therefore, the option 'Dilate' has to be conducted three times (*Plugins > Process > Dilate (3D)*, see Fig. A.3.).

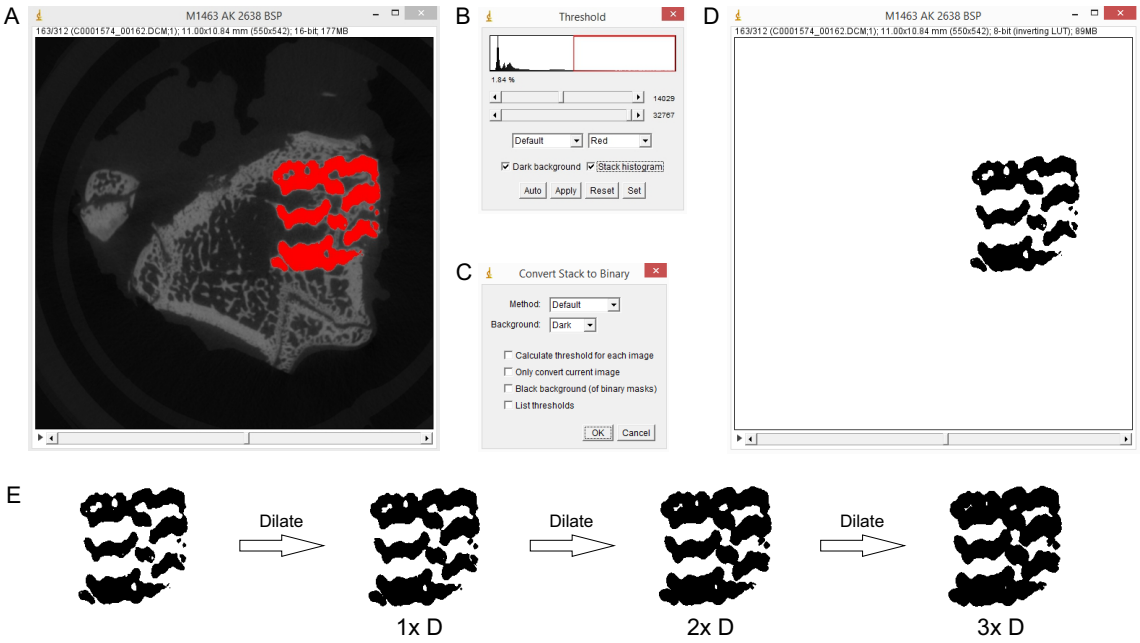

Fig. A.3: Threshold setting for binary creation. A - Threshold setting for implant extraction, B - Check box *Threshold*, C - Check box *Convert Stack to Binary*, D - Binary output *implant*, E - Modification via 'Dilate'-option

.

4) Image substraction of both binarys (step 2 + 3):

Process > Image Calculator...

With help of the 'Image Calculator', the dilated binary of the implant has to be subtracted from the combined binary (bone + implant) as seen in Fig. A.4.

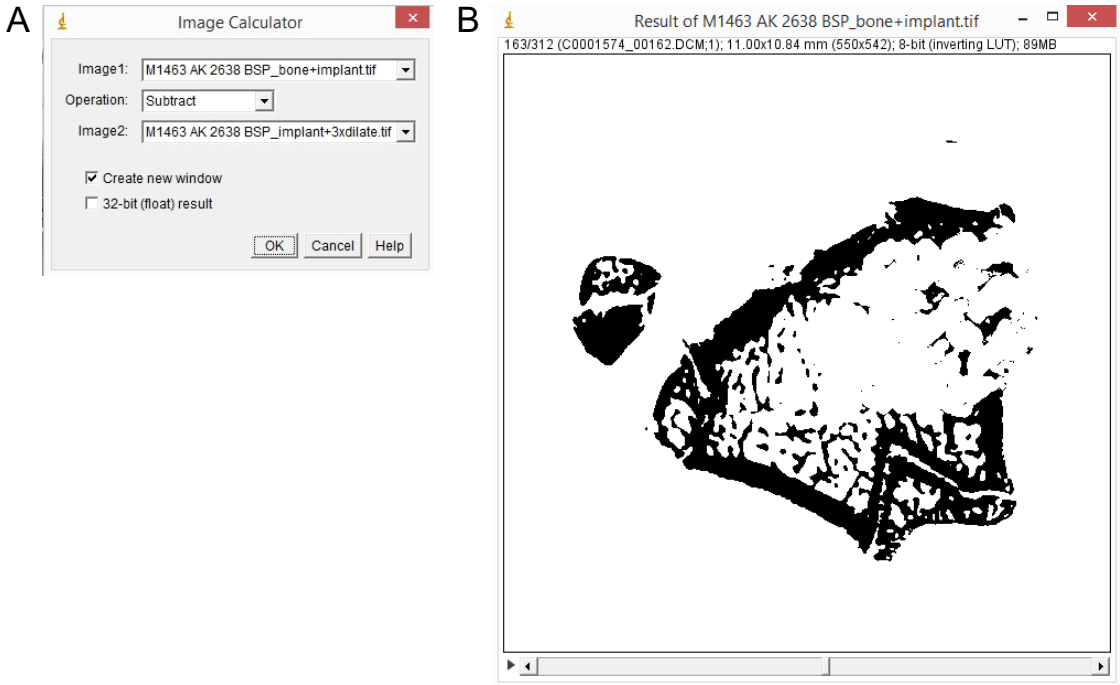

Fig. A.4: Image calculation via subtraction. A - Check box 'Image Calculator', B - Result of image subtraction.

5) Stack reorientation with Align Stacks plugin:

For reorientation the original data (see step 1) is more suitable than the created binary, as the *clearly visible* implant is helpful for alignment.

Plugins > *Align Stacks* > *Reorient3 TP*

Besides the views from different axes (axial, coronal, sagital) the control unit opens. With the button *Mouse selected view*, the point of view can be selected on the individual axes. Realignment has to be conducted with the angle tool. After different rotation steps (e.g. *Rotate axial*, Fig. A.5 A and *Rotate sagital*, B), the orientation of the scaffold has to be checked (e.g. 90° angle, C), followed by export of the top view via creation of an axial-output file (D). The same angles can be used for reorientation of the binary output file.

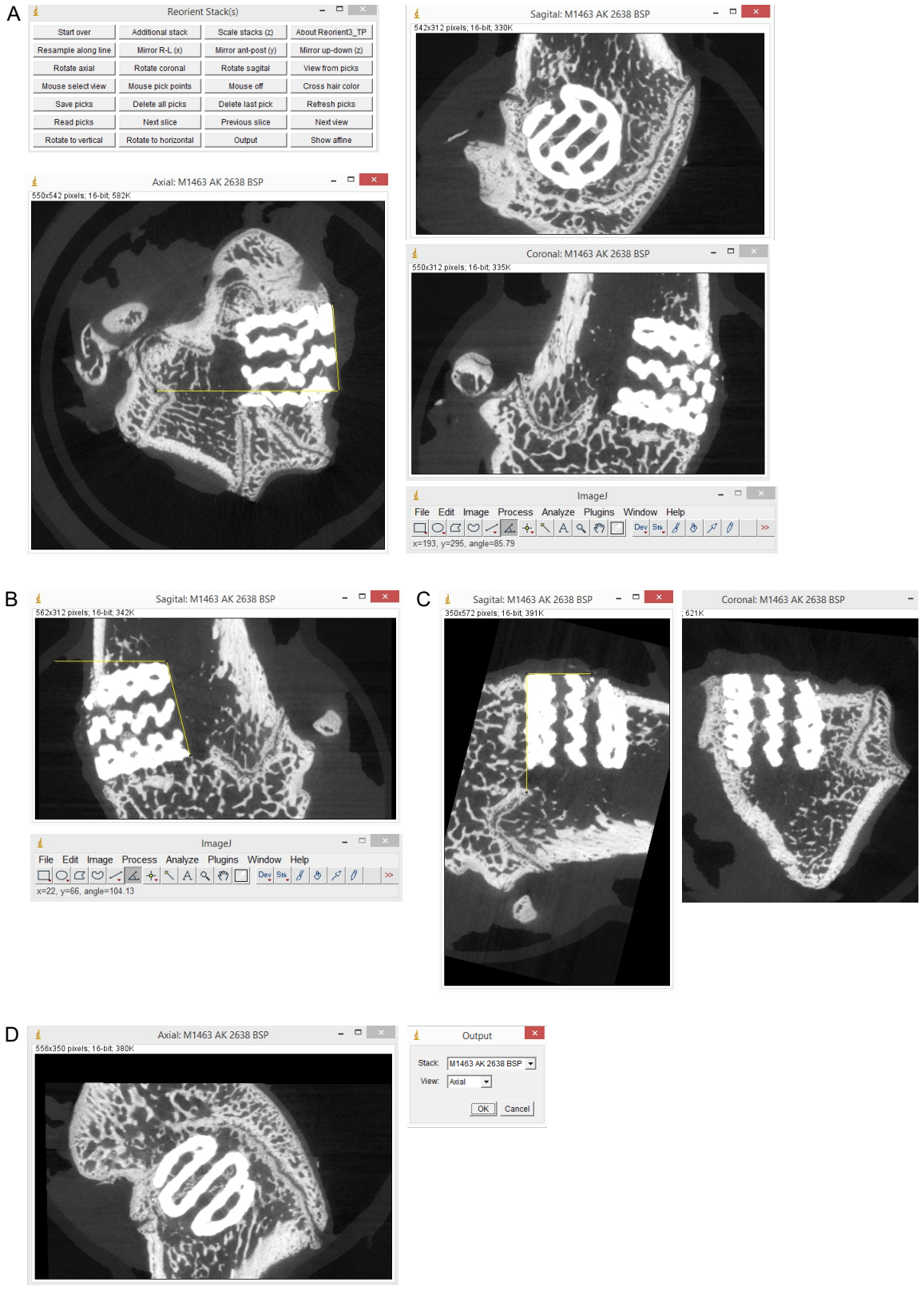

Fig. A.5: Reorientation with the Align Stacks plugin. A - Control unit and individual view from three-dimensional axes, B - Angle measurement with the angle tool, C - Control of alignment, D - Generation of an axial output file.

6) Substack creation:

Image > *Stacks* > *Tools* > *Make Substack...*

For BV/TV analyses a defined volume is required. Therefore, a new stack has to be created in the area of the implant. Depending on implants high, 155 slices are needed for the femoral condyle model (1 voxel = 20 µm, 155 slices correspond to 3.1 mm) and 75 slices for the calvaria model (1 voxel = 30 µm, 75 slices correspond to 2.25 mm).

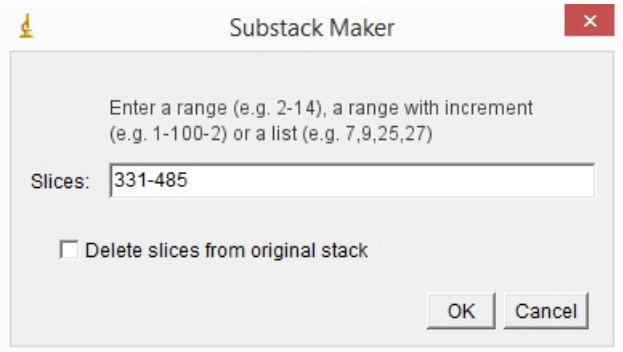

Fig. A.6: Substack maker.

7) Specify the 'region of interest (ROI)':

Edit > *Selection* > *Specify...*

Height adaption of the cylinder takes place in step 6. The area or rather, the region of interest (ROI) has to be selected with the option *Specify*. First, all boxes have to be activated (✓Oval, ✓Constrain square/circle, ✓Centered, ✓Scaled units (mm), see Fig. A.7 A). As diameters 2.9 mm has to be inserted for the femoral condyle model in contrast to 3, 4, 4.5 and 5 mm for the calvarial model (B). The same settings can be used for the binary substack (C).

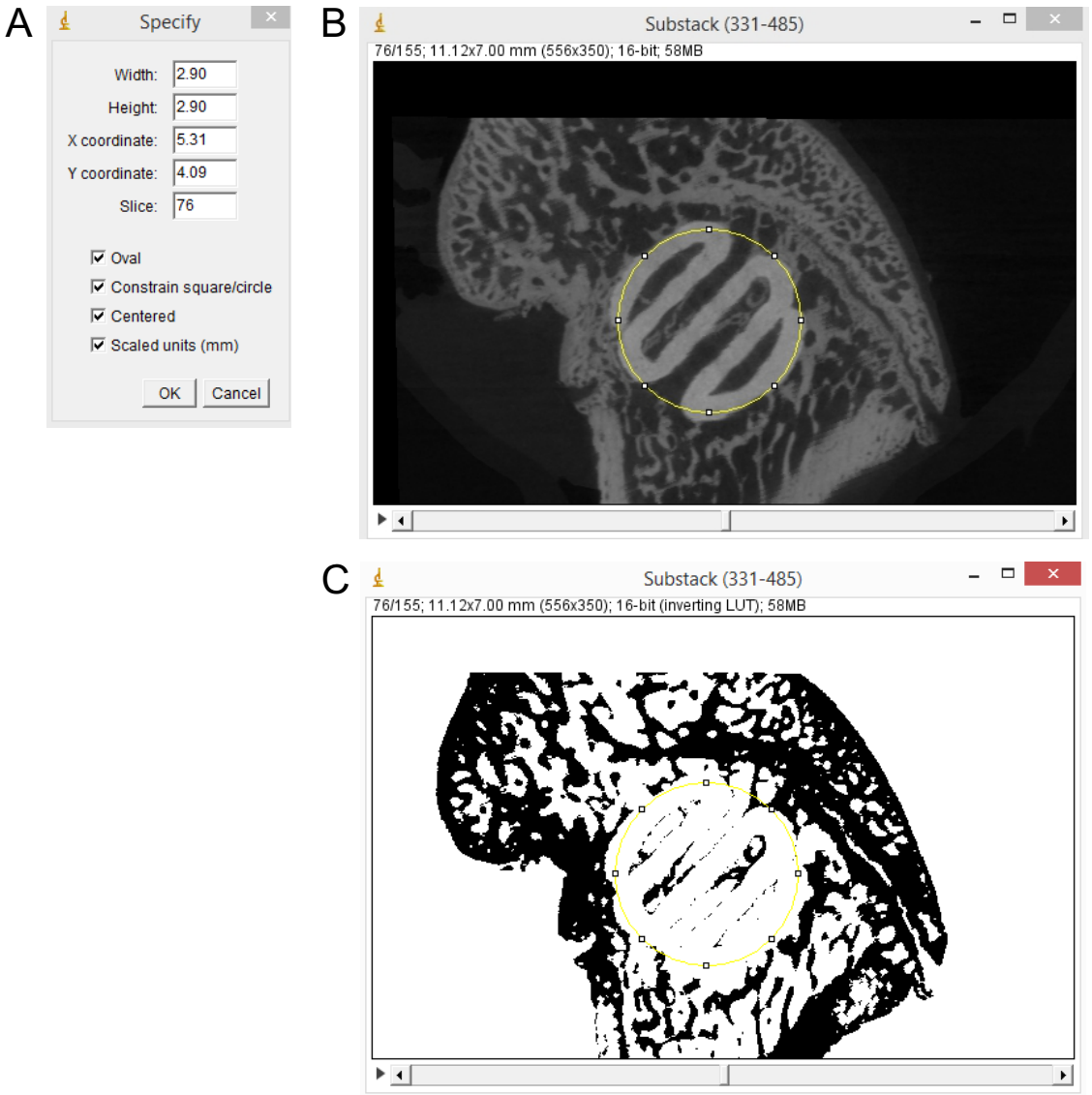

Fig. A.7: Specification of the region of interest. A - Check box *Specify*, B - ROI in the greyvalue substack, C - ROI in the binary substack.

8) Calculation of the BV/TV ratio with the BoneJ [130] plugin:

Plugins > *BoneJ* > *Volume Fraction*

For BV/TV calculation the 'Voxel' algorithm and 'ROI Manager'

(✓) have to be elevated. This is followed by setting a threshold (see Fig. A.8) for image analyses. The results have to be output in a new file.

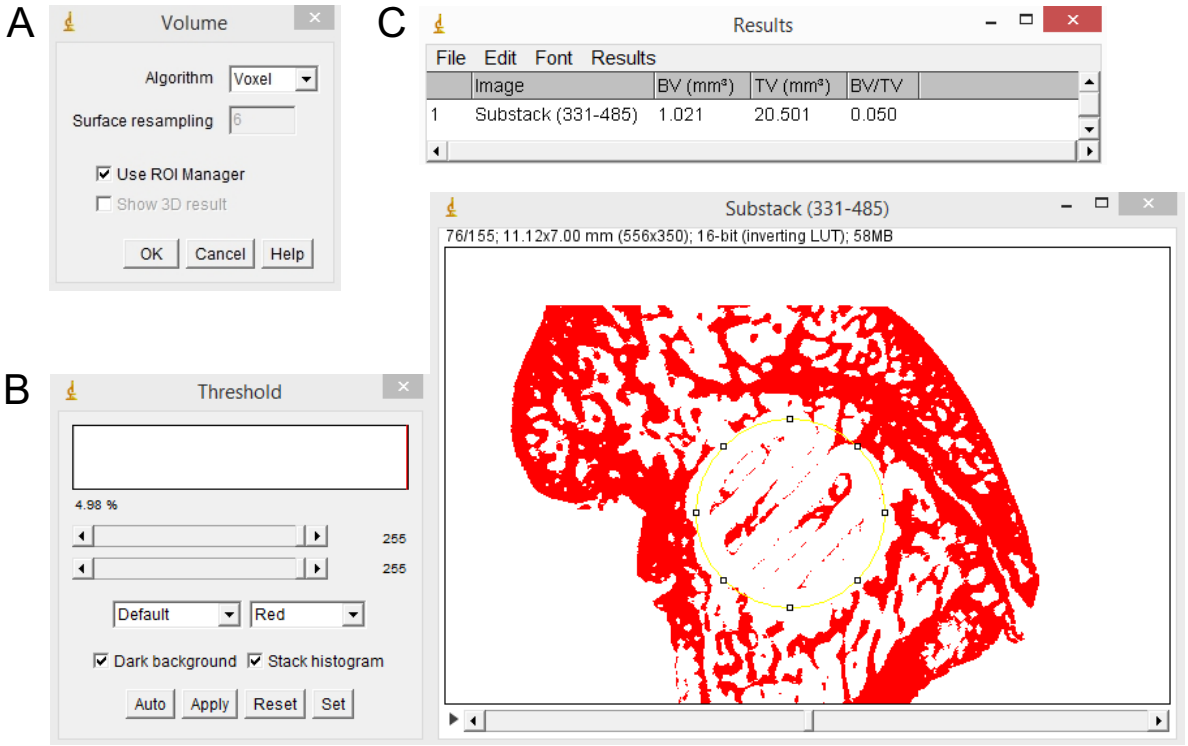

Fig. A.8: BV/TV analyses with the BoneJ plugin. A - Checkbox *Volume*, B - Threshold settings, C - Output result file.

List of Tables

List of Figures

Curriculum Vitae

Scientific Contributions

Danksagung

Declaration